DIFFRACTION BY A PENETRABLE WEDGE

A thesis
presented for the degree of
Doctor of Philosophy
in Electrical Engineering
in the
University of Canterbury,
Christchurch,
New Zealand

by

T. S. Yeo (B.Eng; M.Eng.)

1985

ABSTRACT

New approaches to the problem of diffraction by a penetrable wedge are introduced in this thesis. The motivation has been to add to the power of the Geometrical Theory of Diffraction by obtaining diffraction coefficients for corners of penetrable bodies.

It is shown that a solution due to Bates (1973 , 1980a) enables one to determine the field behaviour close to the apex of a (penetrable) wedge. Computational examples are presented demonstrating that knowledge of this field behaviour leads to marked improvements in the stability and efficiency of numerical solutions. Numerical results are presented for diffraction by penetrable wedge-cylinders (i.e. wedges terminated in cylinders with no change in slope where they join). Cut-off frequencies are calculated for circular waveguides loaded with dielectic wedges (these agree closely with measured values).

The null-field method is invoked to attack the infinite wedge problem. The approach adopted here is verified by applying it initially to totally reflecting wedges. Numerical evaluations of fields diffracted by penetrable wedges, the values of whose refractive indices are of interest in practice, are presented. Close agreement is obtained with Rawlins (1977a) and Kaminetzky and Keller (1972, 1975) under the specialised conditions which constrain these authors' analysis. The very recent results of Joo et al (1980, 1984) and Kim et al (1893) are shown to be (unfortunately) incorrect. The approach introduced here for the infinite penetrable wedge is checked (only approximately but nevertheless encouragingly) against calculations for wedge-cylinders of small apex angle and refractive index fairly close to unity.

ACKNOWLEDGEMENTS

First of all, I must thank my supervisor, Prof. R. H. T. Bates for suggesting such an interesting topic. His constant encouragement has kept me going through the endless disappointments and sleepless nights. I have also benefited enormously from all the stimulating discussions with Prof. Bates and Dr. D. J. N. Wall, my co-supervisor. Thanks also to Dr. Wall for his patience in explaining the intriguing mathematics.

I must also express my sincere gratitude to Messrs. R. Young, A. Vernon and J. Jongens for fashioning the hardware, and Messrs. D. Miyama and K. P. Tan for assisting me in the experiments reported in this thesis.

In the process of turning ten chapters of gibberish into an acceptable thesis, I must admit that I am responsible for all the white hair Prof. Bates acquired in the last six months. Therefore, I must show my deepest appreciation to Dr. K. L. Garden and Miss B. V. Nottingham for their courage, in reading and typing respectively, this manuscript.

I would also like to express my thanks to all the people whose help and companionship have made my stay in New Zealand such a wonderful time.

Finally, I would like to acknowledge the granting of a three and a half years study leave from the National University of Singapore, and a Bilateral Aid Scholarship from the Government of New Zealand.

PROLOGUE

Who is interested in scattering by a penetrable wedge?

Physicists:

Radlow wrote in 1964, "..... diffraction by a dielectric wedge. This problem - or its optical equivalent, the diffraction of light through a prism - has been of interest since the era of Newton; ....". This is indeed an understatement. The basic principle of geometrical optics, that light travels in straight lines and the breaking of the ray at reflecting and refracting surfaces was developed as early as the time of Euclid (280 BC). Ptolemy (100-170) taught the equality of the angle of incidence and reflection and experimentally found a fair approximation to the law of refraction. Aristotle (384-322 BC) was captivated by the beauty of the rainbow and Newton (1642-1727) performed the well known experiment of passing light through a prism. At about the same time, Snell (1580-1626) presented his well known law of refraction in 1621 and Descartes (1596-1650) applied the law to the theory of the rainbow. The research in this topic, though interesting and important in its own right, however, was overshadowed by the researches into the wave/particle properties of light [Newton (1642-1727), Hooke (1635-1702), Huygens (1629-1695), Young (1773-1829), Brewster (1781-1868), Franklin (1706-1790), Euler (1707-1783), Fresnel (1831-1879), Cauchy (1789-1857)]. Maxwell's (1831-1879) Treatise on Electricity and Magnetism (1872) completely dominated the stage at that time. The revival of the research interest into scattering by wedges came only near the end of the nineteenth century, when the research into perfectly conducting wedges (as a special case) once again brought the problem into the limelight.

Mathematicians:

Jones and Pidduck (1950) wrote, on diffraction by wedges, "The general theoretical problem of diffraction is that of an electric wave falling on a mass of dielectric . . . . . is intractable." However, mathematicians must be credited with the revival of research interest in scattering by wedges when they attempted and successfully solved the special case of scattering by a conducting wedge. Poincaré (1892, 1897), Macdonald (1895), Sommerfeld (1896), Bromwich (1915) and Carslaw (1920) are but a few of the early pioneers, to whom the credit of laying a strong foundation

for this subject must be given. The momentum of the research effort was kept alive throughout the years by such as Kontorowich and Lebedev (1939) who established the solution by means of an integral transform, Bouwkamp (1946) who discussed the singularities which occur at sharp edges, Jones and Pidduck (1950) who considered diffraction by metal wedges, Keller and Blank (1951) who developed the solution for an incident plane wave and Oberhettinger (1954) who solved the problem for an inident cylindrical wave. At about the same time, other variations on the general wedge diffraction problem started to appear in the literature; as the interest in the subject heightened. Wedges with one perfectly conducting face and one impedance face were considered by Karal and Karp (1958), Karal, Karp, Chu and Kouyoumjian (1961) and Chu, Kouyoumjian, Karal and Karp (1962). Absorbing or impedance wedges were considered by Felsen (1959), Karp and Karal (1959), Latz (1973) and James (1977). The dielectric half-plane was examined by Collin (1960), Rawlins (1977b) and Anderson (1979). The special case of a right-angled dielectric wedge was studied extensively throughout this period by Radlow (1964), Kuo and Plonus (1967), Kraut and Lehman (1969) and Rawlins (1977a). Attempts have also been made to solve the problem of diffraction by dielectric wedges of arbitrary angles. Meixner (1972), Balling (1973a,b) Bates (1973), Hurd (1976,1977), Andersen and Solodoukhov (1978) and Berntsen (1978,1983) contributed to the subject. Unfortunately, there is as yet no general agreement that any of these solutions are generally valid.

Engineers:

"The edge condition allows us to . . . . gain a significant improvement of the calculation . . . . ," wrote Vassallo (1976) in his paper entitled "On a direct use of edge condition in modal analysis."

The study of electromagnetic diffraction by dielectric wedges is of particular interest to engineers, as can be seen from the numerous papers produced in the last three decades. Representative publications are, in the theory of dielectric waveguide matching, James and Gallett (1972-73), Mittra (1971), Kapilevich and Simin (1976) and Takensaka and Fukumitsu (1983); in the theory of resonators, Kuriko (1968); in radio wave propagation over earth, Clemmow (1966); in dielectric antenna design, Jamwal and Dahr (1981) and Jamwal, Vakil and Dahr (1982); in the millimetre-wave power combiner, Wandinger and Nalbandian (1983); in coupling mechanism in integrated optical devices, Wang and Laybourn (1983). Furthermore, Maurer and Felsen (1967) used a ray-optical approach to study edge diffraction while King and Husting

(1971), Landstorfer (1975), Balling (1973a,b) and Kumar (1981) measured the field diffracted by the edge experimentally.

Analogous problems to that of the dielectric wedge also appear in the fields of acoustics and elasticity. See, for example, the papers by Kraut (1968), Kapustianskii (1976), Poruchikov (1976), Larsen (1980), Gautesen (1983) and Papadopoulous (1983). It should finally be noted that Yu and Ludduck (1967), Vassallo (1976), Mur (1981a) and Okuno and Yasuura (1982) studied the direct application of edge condition to engineering analysis.

CONTENTS

CHAPTER PAGE

PREFACE

The problem of penetrable wedge diffraction has a long, outstanding and controversial history. The optical equivalent of the problem, that of light refracted at the faces of a glass prism, has aroused interest since the era of Newton. To the mind of the uninitiated, the problem is nothing but trivial. Since Snell established a solution for the refraction problem as early as the eighteenth century, one might assume that there should be no problem at all in formulating a solution to the corresponding diffraction problem. After all, what one has to do is to move the light from the prism faces to the apex. Unfortunately, the problem is not as simple as it may seem. Throughout the years, it has not ceased to puzzle many of the more notable field theorists.

The interest in the penetrable wedge diffraction problem of this author is largely due to the influence of Prof. Bates. The major portion of this thesis is devoted to attempts at numerical solutions to this long standing problem. Many different approaches have been attempted. Some have failed miserably and some have had limited success. The most encouraging method presented here is the combination of a ray-optical and a modified (radial) null-field approach. The advantage of using the ray-optical field as a basis to build up a complete solution has been argued convincingly by Keller, Ufimtsev, Wu and Tsai and Vasil'ev and Solodoukhov. The viability of the modified radial null-field method, as applied to infinite body scattering, is established in this thesis. The method is shown to be analytically correct for the infinite conducting wedge diffraction problem. Results are reported in this thesis and are compared to those obtained by other authors.

In order to fully appreciate the penetrable wedge diffraction problem, understanding of analytical and numerical constraints in electromagnetic field computations is essential. This is the reason why the longest chapter in this thesis is devoted to discussing these basic concerns.

A chapter on the inverse scattering problem has also been included. The various known solutions to inverse problems stem from the knowledge acquired from studies of basic electromagnetic field diffraction concepts. The numerical work done in attempting these inverse problems also helps to lay a foundation for the more sophisticated work required in the penetrable wedge problem.

The thesis itself has been divided into three parts. The first part deals with general concepts of direct and inverse scattering problems. It consists of two chapters. Section 1.1 defines the (direct and inverse) scattering problems. The concepts of rays and reflection and refraction are introduced in Section 1.2. Section 1.3, however, deals with the wave nature of the electromagnetic field. For two-dimensional problems, which are of primary concern in this thesis, the vector wave equations of the electromagnetic field can be reduced to scalar wave equations. So, a basic scalar wave equation is derived in Section 1.3 and the associated boundary, radiation and edge conditions are introduced. Exact solutions to canonical problems are discussed in Section 1.4. The general solution to the wave equation is introduced. Analytical continuation and the Rayleigh hypotheses are also discussed. Section 1.5 is devoted to the matrix solution of scattering problems. Various different methods, like point matching, finite difference/finite element, integral equations and the null-field method, are outlined. The construction, stability and solution of matrix equations are also discussed. The last section of Chapter 1, Section 1.6, on the other hand, presents various approximations to the scattering problems. Geometrical optics, physical optics, the Rayleigh-Gans approximation, the Rytov approximation, the geometrical theory of diffraction and the physical theory of diffraction are discussed.

Chapter 2 introduces aspects of inverse scattering. The degree of coherency of an electromagnetic field, the dimensionality difficulty, and the questions of stability and uniqueness when attempting solutions to inverse scattering problems are also discussed. State of the art techniques in the solution of inverse problems are introduced in Section 2.4. Section 2.4 also contains a list of equations, from which theoretical resolution limits for inverse scattering problems can be estimated. This work was done as part of the author's doctoral research programme and has since been published (cf. Seagar et al. 1984). Sections 2.5 and 2.7 also introduce new techniques devised during the course of this research. A simple algorithm for the solution of inverse source problems is presented in Section 2.5. In Section 2.6, the possibility of extending this simple algorithm as the basis for an initial estimate for a sophisticated inverse scattering algorithm is discussed. The null-field method, which has been shown to be useful in many direct and inverse scattering problems (cf. Bates and Wall 1977), is formulated for the general inverse scattering problem in Section 2.7. The viability of the formulation is tested by considering a simple example; the reconstruction

of (conducting and penetrable) circular cylinders from computer-generated far-field scattering data.

Part 2 of this thesis is devoted to various aspects of infinite wedge problems. Section 3.2.1 describes how the Kontorowich-Lebedev transform is used to solve the perfectly conducting wedge diffraction problem. Section 3.2.2, however, points out the reasons why the same method cannot be used to solve the penetrable wedge diffraction problem, although Wall (1984) has indicated possible ways of overcoming these difficulties. In section 3.3, the viability of a modified form of null-field method called the radial null-field methods, is tested by comparing it with a standard formulation of diffraction by a conducting wedge. This new approach to scattering by infinite bodies is the basis of the major contribution reported by the author in this thesis.

Chapter 4 contains an introduction to the infinite penetrable wedge diffraction problem. General difficulties one encounters in solving penetrable wedge problems are discussed in Section 4.1. Notations and terminology which are used throughout this thesis are also introduced. The main part of this chapter is a review and general discussion of the literature relating to the penetrable wedge diffraction problem. Section 4.2 discusses field singularities which exist close to the apex of the wedge. Sections 4.3 and 4.4 briefly outline the various approaches presented in the literature for right-angled and arbitrarily-angled penetrable wedges respectively.

Chapter 5 delineates an approach devised by Bates for solving the penetrable wedge diffraction problem. Although one cannot obtain a complete solution based on this approach, nevertheless, it presents a clear picture of the field behaviour close to the apex of a wedge. The numerical benefit of this knowledge is expounded in Chapter 6, where an example is used to illustrate the enhanced computational efficiency realised by employing this knowledge.

In Chapter 6, diffraction by a wedge-cylinder is evaluated. Three methods are employed. The first method incorporates the additional knowledge mentioned in the previous paragraph. The second method uses an arbitrary field expansion. The third method, which is due to Morita (1979), makes use of two coupled integral equations, thus avoiding the need for prior knowledge of the analytic behaviour of the edge field. It is shown in Chapter 6 that the first method, using the correct field expansion, is most stable and efficient numerically.

Chapter 7 introduces two specialised solutions to the penetrable wedge diffraction problem. Special constraints (i.e. the incoming field is incident symmetrically on the wedge, and the wedge angle must be greater than $\pi/2$ and less than π), are needed. Furthermore, the difficulty of relative convergence (cf. Section 1.5.1.2) implies that these approaches are useful only when a sufficiently large computing facility is available.

In Chapter 8, the radial null-field method, which is introduced in Chapter 3 and is used there for evaluating conducting wedge diffraction, is applied to the penetrable wedge. Numerical results for the diffracted fields are generated and are shown (computationally) to be outgoing. Diffraction patterns are also evaluated and compared with those obtained by Rawlins (1977) and Kaminetzky and Keller (1975). The agreement is encouraging. The diffracted fields in the back-scattering region, of the infinite penetrable wedge and of the wedge-cylinder, are also shown to correspond usefully.

Chapter 9 reports the experimental results obtained in this research. The theoretically calculated and measured cutoff wave numbers of a circular-cylindrical cavity loaded with dielectric sectors (cf. Section 9.1) are shown to agree to about 1% in most cases and always better than 2%. A preliminary parallel-plate scattering experiment is described and possible ways of improving it are discussed in Section 9.2.

Part 3 consists only of Chapter 10. General conclusions are drawn there. Also, suggestions are made for further research into the direct/inverse scattering problem in general, and the penetrable wedge diffraction problem in particular.

Based on the results reported in this thesis, an article has already been published and another has been submitted for publication:

(i) Seagar, A, Yeo, T. S. and Bates, R. H. T. 'Full wave computed tomography Part 2: Resolution limits' IEE Part A, vol 131, pp 616-622, 1984.

(ii) Yeo, T. S., Wall, D. J. N. and Bates, R.H.T. 'Diffraction by a penetrable prism' submitted to the Journal of Optical Society of America, special issue on direct scattering problems.

Other papers which are presently being prepared for publication are:

(i) Yeo, T. S., Wall, D. J. N. and Bates, R. H. T. 'Diffraction by a penetrable prism'. To be submitted to Proc. IEE Part A.

(ii) Bates, R. H. T., Yeo, T. S. and Wall, D. J. N. 'Inverse Optics II'. To be submitted to Proc. SPIE.

(iii) Yeo, T. S., Wall, D. J. N. and Bates, R. H. T. 'Aspect of penetrable wedge scattering'. To be submitted to IEEE Transaction on Antenna Propagation.

(iv) Wall, D. J. N., Yeo, T. S. and Bates, R. H. T. 'Application of Null-field method to inverse scattering problems'. To be submitted to Wave Motion.

PART I

DIFFRACTION BY AN ISOLATED BODY

CHAPTER ONE

INTRODUCTION

1.1 THE PROBLEM

Studies of interaction between waves or wave-like motions and natural or man-made objects have long been of interest to engineers and physicists. Although the interests of individual researchers vary and their researches can be widely diversified, they are nevertheless chiefly concerned with the same underlying mathematical physics. It is therefore appropriate to begin this thesis by introducing some general ideas supported by suitable terminology and notation.

Wave - It can either be wave motion, particle beam or radiation, the mathematical physics of all of which can be reduced to a convenient canonical form:

$$\nabla^2\Psi + \Lambda\,\Psi = 0 \qquad (1.1)$$

Where $\Psi = \Psi(\rho;\ \phi,\ k)$, is a scalar function which describes the wave motion and $\Lambda = \Lambda(\rho;\ \phi,\ k)$ is called the generalised constitutive parameter by Bates (1984), who shows how the mathematical physics of the various processes can be reduced to canonical form with the aid of formulas presented in Chapter 2 of the treatise by Morse and Feshbach (1953).

Object - It can be anything that is capable of interacting with a wave. It can either be natural (e.g. a human body as in X-ray computed tomography) or man-made (e.g. an antenna in radio communication). The main concern of this thesis is with the interaction of wave and isolated object. An isolated object is defined as an object with boundary/boundaries where a jump in the general constitutive parameter occurs i.e. $\partial\Lambda/\partial\hat{n} = \infty$, where $\hat{n}$ denotes the outward normal on the boundary.

There are two general situations a researcher may encounter in the study of wave-object interaction;

(i) Direct problem:

The researcher is to determine the wave scattered by an object with known general constitutive parameter. The incident wave used to probe the object is fully under the researcher's control.

(ii) Inverse problem:

It has, by itself, two subdivisions:

(a) Inverse scattering problem:

The researcher probes an unknown object with a known incident wave, and is to determine the general constitutive parameter of the object from measured values of the scattered wave.

(b) Inverse source problem:

The researcher measures the radiated wave from a certain unknown distribution of sources and is to re-construct the distribution from measured data.

Direct problems are of interest in engineering applications like waveguide matching (cf. Mittra and Lee 1971, Section 2.2), resonators (cf. Kuriko 1968), radio wave propagation (cf. Clemmow 1966, Section 5.1), radar scattering (cf. Bates 1969c), antenna design (cf. Silver 1949) and many others. Solutions to direct problems can also be valuable in leading to a better understanding of inverse problems. Although the direct problem is usually the easier of the two to solve, there remain restrictions on the type of direct problem which can be solved arbitrarily accurately. Full analytic solutions are restricted to a few bodies having shapes so simple that they can be fully analysed straightforwardly by the method of separation of variables. Solutions for objects with complicated shapes are limited by the computer memory space available and the stability of the numerical techniques which are used. However, most surprisingly, not all problems involving objects of simple shapes have been solved either analytically or numerically. The problem of wave scattering by a wedge into which the wave motion can penetrate (this is the main concern of this thesis) has still not been solved explicitly.

Inverse problems abound in science and engineering. Typical ones are: antenna synthesis (Deschamps and Cabayan 1972), computed tomography in medical physics (Bates, Garden and Peters 1983), and profile inversion in geophysics (Backus and Gilbert 1967). Inverse source problems are encountered in, for example, astronomy (Bates 1982) and photon emission computed tomography (Garden 1984).

In real world situations, all objects are three-dimensional. However, in most cases, a technique devised for solving a two-dimensional problem can be generalised for three-dimensional uses. Furthermore, in

cases like computed tomography, two-dimensional images can be stacked together to form a three-dimensional reconstruction. It is, therefore, appropriate to start by considering the two-dimensional version of a problem since, besides offering physical insight, it involves less algebraic and computational complexity.

1.2 RAYS

1.2.1 Rays and Caustics

Consider a wave propagating in the direction AA' (Fig. 1.1). Let dA_1 be an element of area on the wave front Γ_1. Since the wave front is in general curved, dA_1 possesses two principal radii of curvature ρ_1, ρ_2. The ray along AA' is called the axial ray while the rays emanating from each point (along the outward normals at the point) on dA_1 form a tube of rays about the axial ray which intersects, as shown in Fig. 1.1, a second wavefront Γ_2 for which the element is of area dA_2. Note that Γ_1 and Γ_2 can be said to be parallel in the 'curvilinear' sense that all the rays impinge upon them perpendicularly. The ray bundle surrounding the axial ray is appropriately called a pencil of rays. Since the direction of power flow is entirely along the rays, and since the propagation is assumed lossless, energy must be conserved. This implies that

$$|E_1|^2 \, dA_1 = |E_2|^2 \, dA_2 \tag{1.2}$$

where E_1 and E_2 are the complex amplitudes of the wave on dA_1 and dA_2 respectively. The ratio of the two elemental areas is given by

$$\frac{dA_1}{dA_2} = \frac{\rho_1 \, \rho_2}{(\rho_1+r)(\rho_2+r)} \tag{1.3}$$

where r is the distance along the axial ray between dA_1 and dA_2. Furthermore, a phase increment of $-\nu \, k \, d\ell$ results when an electromagnetic wave transverses a distance $d\ell$ in a lossless dielectric medium of refractive index ν. Therefore one can express the field E_2 at Γ_2 in terms of the field E_1 at Γ_1 as

$$E_2 = E_1 \left[\frac{\rho_1 \, \rho_2}{(\rho_1+r)(\rho_2+r)}\right]^{\frac{1}{2}} \exp(-j\nu kr) \tag{1.4}$$

where $k = 2\pi/\lambda$ is the wave number. If the radii of curvature are finite but not equal to each other, the field is said to be astigamatic. When

$\rho_1 = \rho_2$, the field is propagated as a spherical wave. If one of the principal radii of curvature is infinite then the field propagates as a cylindrical wave, but if both radii of curvature are infinite, the wave is plane.

When r is $(-\rho_1)$ or $(-\rho_2)$, E_2 is infinite and there is said to be a caustic. In general these are caustic surfaces over which (1.4) gives an infinite value for the field. In some special cases these surfaces are coincident. These can in turn degenerate to a single curve (a caustic locus) or a single point (a point caustic). As a caustic surface is crossed, an additional phase shift of $\pi/2$ must be added to the quantity on the RHS of (1.4).

1.2.2 Reflection and Refraction

If the field given by (1.4) is incidental upon a curved boundary as in Fig. 1.2, then, in general, it will split up into reflected and refracted fields and generates a surface field and a diffracted field. For a plane wave impinging on a planar interface of materials having identical magnetic permeabilities, Snell's laws (cf. Jones 1964, Section 6.5) states that (Fig. 1.3)

(i) The angle of incidence is equal to the angle of reflection, i.e. $\theta = \theta_1$.

(ii) $\nu_1 \sin\theta = \nu_2 \sin\theta_2$

where ν_1 and ν_2 are the refractive indices of the two media.

(iii) For E-polarisation (i.e. electric vector perpendicular to the plane of incidence), the reflection coefficient is

$$R_E = \frac{\nu_1\cos\theta - (\nu_2^2-\nu_1^2 \sin^2\theta)^{\frac{1}{2}}}{\nu_1\cos\theta + (\nu_2^2-\nu_1^2 \sin^2\theta)^{\frac{1}{2}}} \tag{1.5}$$

and the refraction coefficient is

$$T_E = \frac{2\,\nu_1\cos\theta}{\nu_1\cos\theta + (\nu_2^2-\nu_1^2 \sin^2\theta)^{\frac{1}{2}}} \tag{1.6}$$

(iv) For H-polarisation (magnetic vector perpendicular to the plane of incident), the reflection coefficient is

$$R_H = \frac{\nu_2^2 \cos\theta - \nu_1(\nu_2^2-\nu_1^2 \sin^2\theta)^{\frac{1}{2}}}{\nu_2^2 \cos\theta + \nu_1(\nu_2^2-\nu_1^2 \sin^2\theta)^{\frac{1}{2}}} \tag{1.7}$$

and the refraction coefficient is

$$T_H = \frac{2\,\nu_2^2 \cos\theta}{\nu_2^2 \cos\theta + \nu_1(\nu_2^2-\nu_1^2 \sin^2\theta)^{\frac{1}{2}}} \tag{1.8}$$

There are two particularly interesting observations:

(i) If $\nu_2 < \nu_1$ and the incident angle θ is such that $\tan\theta = \nu_2/\nu_1$, then $R_H = 0$. This value of θ is called the Brewster angle.

(ii) If $\nu_2 < \nu_1$ and $\nu_1 \sin\theta > \nu_2$, total reflection occurs and there is no average flow of energy into the second medium. However, a surface wave is generated such that energy enters the second medium along one edge of the primary beam, travels along the interface and then leaves at the other edge, the reflected wave being displaced (Fig. 1.4). This phenomenon was discovered by Göss and Hanchen (1947) and it needs to be taken into account when designing optical fibres and surface waveguides (cf. Felsen and Marcuvitz 1973, Section 1.7).

In general (Fig. 1.2), the reflected and refracted fields are not only dependent on the reflection and refraction coefficients of the local environment about the point of incidence, but are also dependent on the local curvature of the interface, which modifies the curvatures of the reflected and refracted wave fronts, i.e.

$$E_{refl.} = R\,E_{inc.}\left[\frac{\rho_1\,\rho_2}{(\rho_1+r_1)(\rho_2+r_1)}\right]^{\frac{1}{2}} \exp(-j\nu_1 k r_1) \tag{1.9}$$

$$E_{refr.} = T\,E_{inc.}\left[\frac{\rho_1\,\rho_2}{(\rho_1+r_2)(\rho_2+r_2)}\right]^{\frac{1}{2}} \exp(-j\nu_2 k r_2) \tag{1.10}$$

where ρ_1, ρ_2 are the radii of curvature at P, and r_1 and r_2 are measured along the reflected and refracted rays respectively. R and T are the (matrix) reflection and transmission coefficients respectively.

1.3 WAVE EQUATION

The Maxwell's (James Clark Maxwell 1831-1879, cf. Jones 1964, Section 1.1) electromagnetic field equations are:

$$\nabla \times E + \partial B/\partial t = 0 \tag{1.11a}$$

$$\nabla \times H - \partial D/\partial t = J \tag{1.11b}$$

$$\nabla \cdot J + \partial s/\partial t = 0 \tag{1.11c}$$

$$\nabla \cdot B = 0 \tag{1.11d}$$

$$\nabla \cdot D = s \tag{1.11e}$$

where E is the electric field vector,
H is the magnetic field vector,
D is the electric flux density vector,
B is the magnetic flux density vector,
J is the electric current density vector,
s is the electric charge density

and

$$J = \sigma E \tag{1.12a}$$

$$B = \mu H \tag{1.12b}$$

$$D = \varepsilon E \tag{1.12c}$$

$$\mu = \mu_o \mu_r, \quad \varepsilon = \varepsilon_o \varepsilon_r, \quad \varepsilon_r = \nu^2 \tag{1.12d}$$

with

σ = conductivity,
μ = permeability,
μ_r = relative permeability,
ε = permittivity,
ε_r = relative permittivity
ν = refractive index

and μ_o = permeability of free space = $4\pi \times 10^{-7}$ H/m
ε_o = permittivity of free space = $1/36\pi \times 10^{-9}$ F/m
c = speed of light in free space = $(\mu_o \varepsilon_o)^{-\frac{1}{2}} = 3 \times 10^8$ m/s

When considering a time-harmonic field it is convenient to rewrite each of the field vectors (taking V to represent any one of them) as $V \exp(j \omega t)$, where V is now understood to be a function of the spatial coordinates only. The time dependence of V is entirely expressed by $\exp(j\omega t)$, where $j = \sqrt{-1}$ and $\omega = 2\pi f$ is the angular frequency of the field.

The time-harmonic field equations are:

$$\nabla \times E + j\omega B = 0 \tag{1.13a}$$

$$\nabla \times H - j\omega D = J \tag{1.13b}$$

$$\nabla \cdot J + j\omega s = 0 \tag{1.13c}$$

$$\nabla \cdot B = 0 \tag{1.13d}$$

$$\nabla \cdot D = s \tag{1.13e}$$

Manipulating (1.13a) gives (cf. Appendix to Chapter 1 of Morse and Feshbach 1953),

$$\begin{aligned}\nabla \times (\nabla \times E + j\omega B) &= \nabla \times \nabla \times E + j\omega \nabla \times B \\ &= \nabla(\nabla \cdot E) - \nabla^2 E + j\omega\mu(J + j\omega D) \\ &= \nabla(\nabla \cdot D)/\varepsilon - \nabla^2 E + j\omega\mu J - \omega^2 \mu\varepsilon E \\ &= \nabla s/\varepsilon - \nabla^2 E + j\omega\mu J - \omega^2 \mu\varepsilon E = 0\end{aligned} \tag{1.14}$$

i.e.

$$\begin{aligned}\nabla^2 E + \omega^2 \mu\varepsilon E &= j\omega\mu J + \nabla s/\varepsilon \\ &= -S_p\end{aligned} \tag{1.15}$$

where

$$-S_p = j\omega\mu J + \nabla s/\varepsilon \tag{1.16}$$

represents the overall density of the sources of the electromagnetic field. A similar equation can be derived for the magnetic field vector H. As a consequence, each Cartesian component of E and H must satisfy the scalar Helmhotz wave equation:

$$\nabla^2 \Psi + \nu^2 k^2 \Psi = -s_p \tag{1.17}$$

where $k = \frac{2\pi}{\lambda} = 2\pi f/c = \omega(\mu_o \varepsilon_o)^{\frac{1}{2}}$ (1.18)

and Ψ is a Cartesian component of E or H.
Furthermore, Ψ can be divided into two parts, namely the incident wave Ψ_{inc} and the scattered wave Ψ_{sc}, i.e.

$$\Psi = \Psi_{inc} + \Psi_{sc} \tag{1.19}$$

As mentioned in Section 1.1, this thesis is concerned mainly with two-dimensional scattering problems. A two-dimensional scatterer is a cylinder with its axis of generation parallel to the z-axis of a Cartesian coordinate (x,y,z). Furthermore, in a two-dimensional scattering problem,

it is assumed that there is no variation of field components in the z-direction. Let Ω be such a two-dimensional space coinciding with the plane z = 0. So Ω is in the x,y-plane. Partition (Fig. 1.5) Ω into Ω_- and Ω_+, where Ω_- consists of all points inside a scattering boundary C and Ω_+ consists of all points outside the boundary C. Ω_- is further partitioned into Ω_{--} and Ω_{-+}, where Ω_{--} consists of all points inside a circle C_- inscribing C and Ω_{-+} consists of all points in Ω_- not included in Ω_{--}. Similarly, Ω_+ is partitioned into Ω_{++} and Ω_{+-}, where Ω_+ consists of all points outside a circle C_+ circumscribing C and Ω_{+-} consists of all points in Ω_+ not included in Ω_{++}. Let $(\rho;\phi)$ denote the cylindrical polar coordinate of an arbitrary point P in Ω, $(r;\theta)$ denote the cylindrical polar coordinate of an arbitrary point Q on C, and $\hat{n}$ denote the outward normal to C at Q.

Furthermore, any two-dimensional electromagnetic field can be broken down into two parts, one without a z-electric component and one without a z-magnetic component. The part of the field which has only the z-magnetic component is called the H-polarised field while the part of the field which has only the z-electric component is called the E-polarised field.

Since the E and H polarised fields are each scalar, from now on, therefore, the Helmhotz equation (1.17) is used rather than the vector wave equation (1.15). Furthermore, unless otherwise stated, all subsequent quantities representing fields and sources are functions of two space dimensions only.

In general, there is an infinite number of solutions which satisfy the wave equation (1.17). However, in order that Ψ can be a physically viable solution to an electromagnetic field problem, it must also satisfy the Boundary Conditions, the Radiation Condition and the Edge Conditions, all of which are discussed below.

1.3.1 Boundary Conditions

Several commonly encountered boundary conditions in scattering problems are;

(i) Dirichlet boundary condition:

This condition applies to the acoustic velocity potential at a soft boundary or the tangential electric field (and the normal magnetic field) at a perfectly conducting boundary. Referring to Fig. 1.5, the Dirichlet boundary condition requires that $\Psi(Q) = 0$.

(ii) Neumann boundary condition:

This condition applies to the normal derivative of the acoustic velocity potential at a hard boundary or the tangential magnetic field (or normal electric field) at a perfectly conducting boundary. Referring to Fig. 1.5, the Neumann boundary condition requires that $\partial\Psi(Q)/\partial\hat{n} = 0$.

(iii) Impedance boundary condition:

The impedance boundary condition requires that $\Psi(Q) + f(Q)\ \partial\Psi(Q)/\partial\hat{n} = 0$, where $f(Q)$ is called the impedance function of the boundary.

(iv) Penetrable boundary condition:

The penetrable boundary condition requires

$$\Psi_+(Q_+) = g(Q)\ \Psi_-(Q_-) \text{ and } \partial\Psi_+(Q_+)/\partial\hat{n} = h(Q)\ \partial\Psi_-(Q_-)/\partial\hat{n}$$

where $\Psi_+(Q_+) = \lim_{\substack{P\to Q \\ P\in\Omega_+}} \Psi_+(P)$ and $\Psi_-(Q_-) = \lim_{\substack{P\to Q \\ P\in\Omega_-}} \Psi_-(P)$

and $g(Q)$, $h(Q)$ describe the boundary condition at Q. When $g = h \equiv 1$, the penetrable boundary condition reduces to what is here called the uniform boundary condition.

1.3.2 Radiation Condition

Jones (1964, Section 1.27) points out that, in order to ensure that the solution to the wave equation is unique, Ψ_{sc} must have the character of an outgoing wave far away from the scatterer. This is known as the Sommerfeld Radiation Condition. It is formalised by requiring

$$\left.\begin{aligned} &\left|\rho^{\frac{1}{2}}\ \Psi_{sc}(P)\right| << \text{a constant} \\ &\rho^{\frac{1}{2}}\ (\partial\Psi(P)/\partial\rho + j\,k\,\Psi(P)) \to 0 \end{aligned}\right\} \text{ as } \rho \to \infty$$

1.3.3 Edge Conditions

The boundary condition specified in Section 1.3.1 applies only at points where the boundary curve is analytic. At any point Q where C ceases to be analytic, the field Ψ itself becomes singular in the sense that not all of its derivatives exist in the neighbourhood of Q. In order to ensure that Ψ is physically meaningful, it must then be explicitly required that power must be conserved in the neighbourhood of Q. This is formally expressed by

$$\text{Real}\left[\lim_{a\to 0} \int_0^{2\pi}\int_0^a E \times H\, d\,\hat{\Omega}\right] \to 0 \qquad (1.20)$$

where a is the radius of the circle $\hat{C}$ enclosing the edge (Fig. 1.6).

1.4 EXACT SOLUTIONS TO SCATTERING PROBLEMS

Exact solutions to scattering problems are possible only for a few simple shapes whose boundaries coincide with the coordinates of one of the eleven separable coordinate systems (cf. Morse and Feshbach 1953, Section 5.1). Many of those results can be found in the collection of articles edited by Bowman, Senior and Uslenghi (1969). Unfortunately, not all simple objects which satisfy the above criterion can be successfully handled by the method of separation of variables. As mentioned earlier, the problem of diffraction by a dielectric wedge falls into this category.

The eleven separable coordinate systems are:
(i) rectangular, (ii) circular-cylindrical, (iii) elliptic-cylindrical, (iv) parabolic-cylindrical, (v) spherical, (vi) prolate spheroidal, (vii) oblate spheroidal, (viii) parabolic, (ix) conical, (x) ellipsoidal, and (xi) paraboloidal coordinates.

Further discussion of these coordinate systems can be found in the handbook compiled by Moon and Spencer (1971).

1.4.1 General Eigenfunctions

For the case of cylindrical polar coordinates $(\rho;\phi)$, the Helmholtz wave equation (or the monochromatic, or time independent, or reduced wave equation)

$$\nabla^2\Psi + \nu^2 k^2 \Psi = 0 \tag{1.21}$$

for Ψ becomes

$$\left(\frac{\partial^2}{\partial\rho^2} + \frac{1}{\rho}\frac{\partial}{\partial\rho} + \frac{1}{\rho^2}\frac{\partial^2}{\partial\phi^2}\right)\Psi + \nu^2 k^2 \Psi = 0 \tag{1.22}$$

where k is the wave number and ν is the refractive index of the medium. A special solution Ψ_α for Ψ can be constructed by writing

$$\Psi_\alpha = \Psi_\alpha(\rho;\phi) = R\ \Theta \tag{1.23}$$

where

$$R = R(\rho) \text{ and } \Theta = \Theta(\phi) \tag{1.24}$$

Since the functional dependencies upon ρ and ϕ of Ψ_α are separately characterised by the two distinct functions R and Θ, respectively, Ψ_α is said to be

a solution obtained by separation of variables (Morse and Feshbach 1953, Section 5.1). When Ψ_α is substituted for Ψ in (1.22), the latter becomes

$$\frac{\rho^2}{R}\frac{d^2R}{d\rho^2} + \frac{\rho}{R}\frac{dR}{d\rho} + \nu^2 k^2\rho^2 = -\frac{1}{\Theta}\frac{d^2\Theta}{d\phi^2} \tag{1.25}$$

Since the LHS (1.25) is a function of ρ only and the RHS (1.25) is a function of ϕ only, they must both equal a constant in order for (1.25) to be consistent. If this constant is α^2, (1.25) gives rise to the two separate equations

$$\frac{d^2R}{d\rho^2} + \frac{1}{\rho}\frac{dR}{d\rho} + \left(\nu^2k^2 - \frac{\alpha^2}{\rho^2}\right) R = 0$$

and

$$\frac{d^2\Theta}{d\phi^2} + \alpha^2\ \Theta\ = 0 \tag{1.26}$$

whose solutions are (cf. Morse and Feshbach 1953, Section 5.1)

$$R = a_\alpha C_\alpha(k\rho) + b_\alpha C_{-\alpha}(k\rho)$$

and

$$\Theta = c_\alpha \sin(\alpha\phi) + d_\alpha \cos(\alpha\phi) \tag{1.27}$$

and a particular solution to the wave equation (1.21) is then

$$\Psi = R\ \Theta$$

$$= \left[a_\alpha C_\alpha(k\rho) + b_\alpha C_{-\alpha}(k\rho)\right]\left[c_\alpha\sin(\alpha\phi) + d_\alpha(\cos\alpha\phi)\right] \tag{1.28}$$

where $C_\alpha(k\rho)$ is a cylindrical function of (complex) order α (Moon and Spencer 1971, Section 7.09), a_α, b_α, c_α and d_α are expansion coefficients. (1.27) is referred to from now on as the general eigenfunctions for the two-dimensional Helmhotz equation.

1.4.1.1 Properties of Cylindrical Functions

The cylindrical functions $C_\alpha(z)$ include (i) Bessel functions of the first kind $J_\alpha(z)$, (ii) Bessel functions of the second kind $Y_\alpha(z)$, (iii) Hankel functions of the first kind $H_\alpha^{(1)}(z)$, (iv) Hankel functions of the second kind $H_\alpha^{(2)}(z)$. Some properties of the cylindrical functions are (cf. Chapter 9, 10 of Abramowitz and Stegun 1965):

(i)
$$H_\alpha^{(1)}(z) = J_\alpha(z) + j\,Y_\alpha(z) = \frac{j\left[\exp(-j\alpha\pi)\,J_\alpha(z) - J_{-\alpha}(z)\right]}{\sin(\alpha\pi)}$$

$$H_\alpha^{(2)}(z) = J_\alpha(z) - j\,Y_\alpha(z) = \frac{j\left[J_{-\alpha}(z) - \exp(j\alpha\pi)J_\alpha(z)\right]}{\sin(\alpha\pi)} \tag{1.29}$$

(ii) $J_{-n}(z) = (-1)^{(n)} J_n(z)$, $Y_{-n}(z) = (-1)^{(n)} Y_n(z)$

$H_{-\alpha}^{(1)}(z) = \exp(j\alpha\pi) H_{\alpha}^{(1)}(z)$, $H_{-\alpha}^{(2)}(z) = \exp(-j\alpha\pi) H_{\alpha}^{(2)}(z)$ (1.30)

(iii) when $|z|/|\alpha| \to 0$,

$J_\alpha(z) = (z/2)^{\alpha}/\Gamma(1+\alpha)$, $\alpha \notin I_-$

$Y_\alpha(z) = -\Gamma(\alpha)(z/2)^{-\alpha}/\pi$, Real $(\alpha) > 0$

$Y_o(z) \to 2 \ln(z)/\pi$

$H_\alpha^{(1)}(z) \to j Y_\alpha(z)$

$H_\alpha^{(2)}(z) \to -j Y_\alpha(z)$ (1.31)

(iv) when $|z|/|\alpha| \to \infty$,

$J_\alpha(z) \to (2/\pi z)^{\frac{1}{2}} \cos(z-\alpha\pi/2 - \pi/4)$, $|\arg(z)| < \pi$

$Y_\alpha(z) \to (2/\pi z)^{\frac{1}{2}} \sin(z-\alpha\pi/2 - \pi/4)$, $|\arg(z)| < \pi$

$H_\alpha^{(1)}(z) \to (2/\pi z)^{\frac{1}{2}} \exp(j[z-\alpha\pi/2 - \pi/4])$, $-\pi < \arg(z) < 2\pi$

$H_\alpha^{(2)}(z) \to (2/\pi z)^{\frac{1}{2}} \exp(-j[z-\alpha\pi/2 - \pi/4])$, $-2\pi < \arg(z) < \pi$ (1.32)

(v) when $|\alpha| \to \infty$,

$J_\alpha(z) \to (ez/2\alpha)^{\alpha} (2\pi\alpha)^{-\frac{1}{2}}$

$Y_\alpha(z) \to -(e\,z/2\alpha)^{-\alpha} (2/\pi\alpha)^{\frac{1}{2}}$ (1.33)

(vi) generating function:

$$\exp(z(t-1/t)/2) = \sum_{n=-\infty}^{\infty} t^n J_n(z) \qquad (1.34)$$

(vii) additional theorem (Fig. 1.7):

$$C_\alpha(\omega) \begin{matrix}\cos\\ \sin\end{matrix} \alpha\gamma = \sum_{n=-\infty}^{\infty} C_{\alpha+n}(u) J_n(v) \begin{matrix}\cos\\ \sin\end{matrix} n\beta, \quad |v \cdot \exp(\pm j\beta)| < |u| \qquad (1.35)$$

The restriction $|v \exp(\pm j\beta)| < |u|$ is unnecessary when $C = J$ and α is an integer or zero.

(viii) multiplication theorem (Watson 1966, Section 5.21)

$$J_\alpha(\nu z) = \sum_{n=0}^{\infty} F_n(\alpha,\nu) J_{\alpha+2n}(z) \quad , \alpha \notin I_-$$

where $F_n(\alpha,\nu) = (\alpha+2n)\ \nu^{\alpha} \sum_{\ell=0}^{\infty} (-1)^{\ell}\ T_{\ell}(\alpha,\nu,n)$

and $T_{\ell}(\alpha,\nu,n) = \nu^{2\ell}\ \Gamma(\alpha+n+\ell)/(\ell!\ (n-\ell)!\ \Gamma(\alpha+\ell+1))$ (1.36)

1.4.2 General Solution to Wave Equation

1.4.2.1 General Solution

A general solution to the wave equation can be obtained by summing, or integrating Ψ_{α} over a range of α, i.e.

$$\Psi_{\alpha} = \underset{\alpha}{S}\ u(\alpha)\ C_{\alpha}(k\rho)\ \begin{matrix}\cos\\ \sin\end{matrix}\ \alpha\phi \tag{1.37}$$

where $\underset{\alpha}{S}$, which is the Schiff's (1949) symbol, represents a summation over the part of the range of α wherein the latter assumes discrete values and represents an integral over the part of the range where α varies continuously.

1.4.2.2 Choice of Eigenfunctions

In each individual problem, specific eigenfunctions must be chosen in order to suit particular requirements. Several considerations must be taken into account when choosing particular eigenfunctions.

(i) Radiation condition:

Since a wave function must be outgoing far away from the scatterer, the appropriate choice of eigenfunctions in Ω_{++} (Fig. 1.5), must be $H_{\alpha}^{(2)}(k\rho)\ \begin{matrix}\cos\\ \sin\end{matrix}\ \alpha\phi$, in view of the properties listed in (1.32).

(ii) Finiteness:

To ensure that the field remains finite, only Bessel functions of the first kind, of order α, (where $\alpha \in$ {integer}, or Real $(\alpha) > 0$) can be used in a region enclosing the origin O, since (1.31) indicates that the other cylindrical functions are singular at the origin.

(iii) Edge conditions and singularities:

The eigenvalues α must be chosen such that the edge conditions (1.20) and whatever specific singularity requirements are satisfied.

(iv) Orthogonality:

For the eigenfunctions Ψ_{α} to be complete within a region $\tilde{\Omega}$, it must satisfy the orthogonality rule (cf. Morse and Feshbach 1953, Section 6.3):

$$\int\int_{\tilde{\Omega}} \Psi_\alpha \, \Psi_\beta \, d\,\tilde{\Omega} = \begin{cases} \text{a constant}, & \alpha = \beta \\ 0 \quad , & \alpha \neq \beta \end{cases} \tag{1.38}$$

(1.38) immediately implies that the eigenvalues α must be integers if the region $\tilde{\Omega}$ is (a) closed and (b) analytic (Fig. 1.8). Since

$$\int_0^{2\pi} \begin{matrix}\cos\\ \sin\end{matrix} n\phi \begin{matrix}\cos\\ \sin\end{matrix} m\phi \, d\phi = \begin{cases} \varepsilon_m \pi, & m = n \\ 0 \ , & m \neq n \end{cases} \tag{1.39}$$

1.4.3 Analytic Continuation

Consider the regions $\tilde{\tilde{\Omega}}$ and $\ddot{\Omega}$, such that $\tilde{\tilde{\Omega}} \in \tilde{\Omega}$, where $\tilde{\Omega}$ is contained within the part of space where a particular field exists. If a series representation of the field is known to be valid within the region $\tilde{\tilde{\Omega}}$, and is subsequently found to converge within the wider region $\tilde{\Omega}$, then the uniqueness of analytic continuation (cf. Jones 1964, Section 9.5) ensures that the series is a valid representation of the field throughout $\tilde{\Omega}$.

Consider the infinite series representations of Ψ, such that

$$\Psi_P = \Psi(\rho;\phi) = \sum_{n=-\infty}^{\infty} a_n \, \Psi_n \, (\rho;\phi) \tag{1.40}$$

$$\Psi_P = \Psi_i \, (\rho_i;\phi_i) = \sum_{n=-\infty}^{\infty} a_{n,i} \, \Psi_n \, (\rho_i;\phi_i) \tag{1.41}$$

where $(\rho_i;\phi_i)$ are the coordinates of a point $P(\rho;\phi)$ when referred to origin O_i (Fig. 1.9) and $a_{n,i}$ are the expansion coefficients. Furthermore, assuming that there exists $r_{min,i}$ such that Ψ diverges when $\rho_i < r_{min,i}$, the circles C_i must trace out a hull $\tilde{C}$ such that Ψ diverges within $\tilde{\tilde{\Omega}}$ enclosed by $\tilde{C}$. In other words, singularities of the series in (1.40) must reside on $\tilde{C}$ and analytic continuation is possible only in $\tilde{\Omega}$ outside $\tilde{C}$.

1.4.4 Rayleigh Hypotheses

In the nineteenth century Lord Rayleigh (1897) realised that theoretical descriptions of diffraction phenomena would be much simplified if any reradiated field could be represented by a single expansion everywhere outside the object scattering the incident field. For example,

$$\Psi_{sc}\,(P) = \sum_{n=-\infty}^{\infty} b_n \, H_n^{(2)} \, (k\rho) \, \exp(jn\phi), \quad P \in \Omega_+ \tag{1.42}$$

This is called the External Rayleigh hypotheses (cf. Bates 1975a) Similarly, the Internal Rayleigh hypotheses (cf. Bates 1975a) allows a single expansion for the reradiated field everywhere inside the scatterer, e.g.

$$\Psi_{sc}(P) = \sum_{n=-\infty}^{\infty} a_n J_n(k\rho) \exp(jn\phi), \quad P \in \Omega_- \tag{1.43}$$

Since Hankel functions are singular at the origin (cf. (1.31)), there must be a minimum radius of convergence r_{min} such that the series in (1.42) diverges when $\rho < r_{min}$. It is therefore obvious that the external Rayleigh hypotheses is valid if and only if $r_{min} \leq r_-$ (where r_- is the radius of the inscribing circle C_-, (see Fig. 1.5). Similarly, there must be a maximum radius of convergence r_{max} such that the series in (1.43) diverges when $P > r_{max}$. And the internal Rayleigh hypotheses holds only when $r_{max} \geq r_+$ (where r_+ is the radius of the circumscribing circle, see Fig. 1.5).

It has been shown (cf. Bates 1975a) that the series in (1.42) and (1.43) converge in Ω_{++} and Ω_{--} respectively. Bates (1975a) also suggests using the method of conformal transformation to compute the maximum and minimum radii of convergence for (1.42) and (1.43).

Ikuno and Yasuura (1973) have modified the Rayleigh hypotheses such that the scattered far field can be computed with useful accuracy in many situations where the conventional Rayleigh hypotheses fail. Since a finite series must always possess a unique value, they (Ikuno and Yasuura 1973) invoke finite summations for (1.42) and (1.43), i.e.

$$\Psi_{sc}(P) = \sum_{n=-N}^{N} b_n H_n^{(2)}(k\rho) \exp(jn\phi), \quad P \in \Omega_+ \tag{1.44}$$

$$\Psi_{sc}(P) = \sum_{n=-N}^{N} a_n J_n(k\rho) \exp(jn\phi), \quad P \in \Omega_- \tag{1.45}$$

This procedure enables them to rearrange terms within Ω_{+-} and Ω_{-+} even when the conventional Rayleigh hypotheses fail. However, this procedure is not allowable in the limit $N \to \infty$. Consequently, the larger N becomes, the less confidence the procedure inspires, which is unfortunate as N must necessarily increase with the ratio to the wavelength of the linear dimension of a scatterer (see Section 1.5.4 below).

1.5 ANALYTICAL - NUMERICO METHODS

The methods discussed in this section, the so-called analytical - numerico methods can generate solutions of any desired accuracy at least in principle. This is because all these methods are derived analytically (i.e. exactly) without making any prior approximation. However, since a numerical scheme must be invoked to obtain an actual solution, the attainable accuracy of each of these methods is limited by the power of the available computing facility and the efficiency of the algorithm with which the method is implemented.

1.5.1 Matrix Equations

The aim of any analytical - numerico method is to transform the wave equation, together with necessary constraints (i.e. boundary, radiation and edge conditions) into an infinite set of linear algebraic equations, e.g.

$$\sum_{n=0}^{\infty} A_n K_{nm} = B_m , \qquad m = 0,1,2, \ldots \infty \tag{1.46}$$

It is necessary to truncate this system of equations in order to attain a numerical solution. The integers m and n are restricted to the ranges (0,M) and (0,N) respectively, where M and N are particular positive integers. The system can then be re-expressed as the matrix equation

$$\underline{\underline{K}} \; \underline{A} = \underline{B} \tag{1.47}$$

where $\underline{A}$ is a N X 1 vector containing the unknowns A_n, $\underline{B}$ is a M X 1 vector containing the known constants B_m and $\underline{\underline{K}}$ is the known M X N matrix whose elements are the K_{nm}.

1.5.1.1. Constructing Matrix Equations

Physically, the A_n are the expansion coefficients of a certain quantity, $f(\underline{x})$ say, which is required to be determined, e.g.

$$f(\underline{x}) = \sum_{n=0}^{\infty} A_n \Psi_n (\underline{x}) \tag{1.48}$$

where the Ψ_n are the basis functions. This quantity f can either be the unknown field Ψ, the surface current, or any other quantity from which Ψ can be calculated. The B_m are usually the measured data or some known values associated with the incident probing wave function. The K_{nm} describe the

physical processes that relate the A_n to the B_m.

The truncation of the infinite system (1.46) to the finite system (1.47) unavoidably introduces error. The magnitude of this error necessarily depends on M and N. In any real world situation $|A_n|$ must decrease rapidly with increasing n, for $n > \tilde{N}$, where $\tilde{N}$ is some (large but) finite integer. For instance, the scattering pattern of a finite body cannot possess lobes whose effective angular widths are significantly less than the wavelength divided by the body's largest linear dimension, implying that the pattern is effectively characterised by a finite number of Fourier coefficients. It is reasonable to claim, therefore, that

$$|A_n| < \varepsilon, \quad \text{for } n > \tilde{N} \tag{1.49}$$

for any physically meaningful scattering problem, where ε is real, positive and appropriately small. Consequently, once the first $\tilde{N}$ of the A_n have been calculated, the value of f is changed negligibly by adding to it further terms in the summation on LHS (1.48), i.e.

$$\left| \sum_{n=0}^{\tilde{N}+1} A_n \psi_n - \sum_{n=0}^{\tilde{N}} A_n \psi_n \right| < \varepsilon \tag{1.50}$$

Finally, a solution can be said to have been achieved if

$$|A'_n - A''_n| < \varepsilon \tag{1.51}$$

where the A'_n and A''_n are solutions of

$$\sum_{n=0}^{\tilde{N}} A'_n K_{nm} = B_m \tag{1.52a}$$

for $m = 1,2, \ldots, \tilde{N}$

and

$$\sum_{n=0}^{\tilde{N}+1} A''_n K_{nm} = B_m \tag{1.52b}$$

for $m = 1,2, \ldots, \tilde{N},\tilde{N}+1$

1.5.1.2 Relative Convergence

The term 'relative convergence', first introduced by Mittra (1963), describes a special class of problems whose solutions 'converge' in a manner different from those defined in Section 1.5.1.1 Cases of relative convergence occur in bifurcated waveguides (Mittra 1963), mode matching at waveguide discontinuities (Mittra and Lee 1971), moment methods in integral equations (Mittra et al. 1972a) and many others (cf. Wexler 1969, and Mittra and Lee 1971).

The occurrence of relative convergence in such a wide variety of problems may seem surprising at first. However, careful examination of these problems reveals that they inevitably involve the truncation of (more than one) infinite series. In the case of the bifurcated waveguide (cf. Mittra 1963) or the general mode matching problems (cf. Wexler 1969), for instance, the matching of two or more (infinite) series expansions at a common boundary is invoked (see Section 1.5.2 below). These infinite series must then be truncated to facilitate numerical computation. When integral equations (see Section 1.5.4 below) are used, one series expansion only is needed to represent the unknown field, but it is always necessary to expand the kernel (see Section 1.5.4 below) of integration in series form in order to obtain a set of algebraic equations. Therefore, one still has to truncate two infinite series when using the method of moments to solve an integral equation.

For example, if

$$f_1 = \sum_{m=0}^{\infty} A_m \Psi_m (\underline{x})$$

$$f_2 = \sum_{n=0}^{\infty} B_n \Psi_n (\underline{x}) \qquad (1.53)$$

and if the first summation is truncated to $m \in (0,M)$ and the second summation is truncated to $n \in (0,N)$ then the solution is said to converge relatively if $f_1(M) \rightarrow f_1$, $f_2(N) \rightarrow f_2$ only when $M/N = C$, a constant. Mittra et al (1972a) show that this constant C is necessarily determined by physical constraints (e.g. edge conditions and physical dimensions etc.).

1.5.1.3 Solving Matrix Equations

When M in (1.47) is set equal to N, an 'inverse matrix' $\underline{\underline{K}}^{-1}$ (Jacobs et al. 1977) defined by

$$\underline{\underline{K}}^{-1}\ \underline{\underline{K}} = \underline{\underline{I}} \tag{1.54}$$

can always be constructed, unless $\underline{\underline{k}}$ is singular, where

$$I = \begin{bmatrix} 1 & 0 & 0 & . & . & . & 0 \\ 0 & 1 & 0 & . & . & . & 0 \\ . & . & & & & & \\ . & . & & & & & \\ . & . & & & & & \\ 0 & 0 & . & . & . & . & 1 \end{bmatrix} \tag{1.55}$$

is called the identity matrix, and the solution $\underline{A}$ is given by

$$\underline{\underline{K}}^{-1}\ (\underline{\underline{K}}\ \underline{A}) = \underline{\underline{I}}\ \underline{A} = \underline{A} = \underline{\underline{K}}^{-1}\ \underline{B} \tag{1.56}$$

However, this simple-minded approach is often inadequate for the following reasons.

(i) In many actual problems, $||\underline{\underline{K}}|| = \sum_{n,m} |K_{nm}|^2$ is very small. In such circumstances, $||\underline{\underline{K}}^{-1}||$ is large and a small percentage error in the calculation of $\underline{\underline{K}}^{-1}$ tends to result in a large error in $\underline{A}$. (It is worth emphasising that small errors such as the truncation error in numerical computation cannot be avoided in practice).

(ii) In some cases, $\underline{\underline{K}}$ is not square (i.e. $M \neq N$, see Section 1.5.1.2) and therefore $\underline{\underline{K}}^{-1}$ is not defined.

In recent years, the method of Singular Value Decomposition (SVD) (cf. Jacobs ed. 1977) has been used extensively in solving general matrix equations. Any M X N complex matrix $\underline{\underline{K}}$ of rank (i.e. the number of independent rows or columns) r may be factorised in the form (cf. Jacobs ed. 1977)

$$\underline{\underline{K}} = \underline{\underline{U}}\ \underline{\underline{\Sigma}}\ \underline{\underline{V}}^{H} \tag{1.57}$$

where $\underline{\underline{U}}$ and $\underline{\underline{V}}$ are M X M and N X N unitary matrices respectively, the superscript H denotes the Hermitian transpose and $\underline{\underline{\Sigma}}$ is an M X N matrix of the form

$$\underline{\underline{\Sigma}} = \begin{pmatrix} D & 0 \\ 0 & 0 \end{pmatrix} \tag{1.58}$$

with

$$D = \begin{pmatrix} s_1 & 0 & . & . & . & 0 \\ 0 & s_2 & . & . & . & . \\ . & . & . & . & . & . \\ . & . & . & . & . & . \\ 0 & 0 & . & . & . & s_r \end{pmatrix} \tag{1.59}$$

The s_i are the 'singular values' of $\underline{\underline{K}}$, and can be computed accurately

Solving (1.47) is then equivalent to the problem of finding $\underline{A}$ such that $||\underline{\underline{A}}|| = \sum_{n=0}^{\infty} |A_n|^2$ and $\varepsilon^* = ||\underline{\underline{K}}\ \underline{A} - \underline{B}||$ are minimised. Using (1.57), the latter becomes

$$\begin{aligned} \varepsilon^* &= ||\underline{\underline{K}}\ \underline{A} - \underline{B}|| = ||\underline{\underline{U}}\ \underline{\underline{\Sigma}}\ \underline{\underline{V}}^H\ \underline{A} - \underline{B}|| \\ &= ||\underline{\underline{U}}\ (\underline{\underline{\Sigma}}\ \underline{\underline{V}}^H\ \underline{A} - \underline{\underline{U}}^H\ \underline{B})|| = ||\ \underline{\underline{\Sigma}}\ \underline{\underline{C}} - \underline{\underline{E}}\ || \\ &= (s_1c_1 - e_1)^2 + (s_2c_2 - e_2)^2 \\ &\qquad + \ . \ . \ . \ + (s_rc_r - e_r)^2 + e_{r+1}^2 + \ . \ . \ . \ + e_m^2 \end{aligned} \tag{1.60}$$

where $\underline{\underline{C}} = \underline{\underline{V}}^H\ \underline{A}$ and $\underline{\underline{E}} = \underline{\underline{U}}^H\ \underline{B}$. (1.61)

It is seen from (1.60) that the smallest value of ε^* is achieved if $c_i = e_i/s_i$, or

$$\underline{\underline{C}} = \underline{\underline{\Sigma}}^+\ \underline{\underline{E}} \tag{1.62}$$

where

$$\underline{\underline{\Sigma}}^+ = \begin{pmatrix} D^+ & 0 \\ 0 & 0 \end{pmatrix} \tag{1.63}$$

and

$$D^+ = \begin{pmatrix} s_1^{-1} & 0 & . & . & 0 \\ 0 & s_2^{-1} & . & . & 0 \\ . & . & . & . & . \\ . & . & . & . & . \\ 0 & 0 & . & . & s_r^{-1} \end{pmatrix} \tag{1.64}$$

Therefore, from the first equation of (1.61)

$$\underline{\underline{V}}\,\underline{\underline{V}}^H\,\underline{A} = \underline{\underline{I}}\,\underline{A} = \underline{A} = \underline{\underline{V}}\,\underline{C} = \underline{\underline{V}}\,\underline{\underline{\Sigma}}^+\,\underline{E}$$

$$= \underline{\underline{V}}\,\underline{\underline{\Sigma}}^+\,\underline{\underline{U}}^H\,\underline{B} = \underline{\underline{K}}^+\,\underline{B} \tag{1.65}$$

where

$$\underline{\underline{K}}^+ = \underline{\underline{V}}\,\underline{\underline{\Sigma}}^+\,\underline{\underline{U}}^H \tag{1.66}$$

is called the (Moore-Penrose) pseudo-inverse of $\underline{\underline{K}}$.

1.5.1.4 Stability of Matrix Equations

The condition number η of a matrix $\underline{\underline{K}}$ is defined by

$$\eta = ||\underline{\underline{K}}||\;\;||\underline{\underline{K}}^{-1}|| \tag{1.67}$$

In computational practice, the condition number determines the stability of matrix inversion. The relative error in the numerical solution for $\underline{A}$ with respect to small errors in $\underline{\underline{K}}$ and $\underline{B}$, is

$$||\Delta\underline{A}||\,/||\underline{A}|| = \eta(||\Delta\underline{\underline{K}}||/||\underline{\underline{K}}|| + ||\Delta\underline{B}||/||\underline{B}||)$$

$$/(1-\eta\;||\Delta\underline{\underline{K}}||/||\underline{\underline{K}}||) \tag{1.68}$$

1.5.1.5 Filtering

When $\underline{\underline{K}}$ is ill-conditioned (i.e. the condition number η is large or $||\underline{\underline{K}}||$ is small or $||\underline{\underline{K}}^{-1}||$ is large), several of the singular values (normalised by the largest singular value) may become smaller than or close to the relative arithmetic precision (denoted by ε) of the digital computers. If the criterion used for decision on the rank (r) of $\underline{\underline{K}}$ is that all normalised singular values smaller than ε are zero, then $r < N$. However, the remaining normalised singular values that are much smaller than ε to which the elements of $\underline{\underline{K}}$ and $\underline{B}$ have been evaluated, may produce oscillatory components in $\underline{A}$. This numerical instability can be overcome by the use of a filtering matrix (Wall 1980).

The Moore-Penrose inverse is redefined as

$$\underline{\underline{K}}^{++} = \underline{\underline{V}}\,\underline{\underline{F}}\,\underline{\underline{\Sigma}}^+\,\underline{\underline{U}}^H \tag{1.69}$$

where $\underline{\underline{F}}$, the filter matrix, is of block diagonal form with the only non-zero

terms $f_i = s_i^\alpha/(s_i^\alpha + \beta^\alpha)$, i.e.

$$\underline{\underline{F}} = \begin{pmatrix} D^{++} & 0 \\ 0 & 0 \end{pmatrix} \tag{1.70}$$

and

$$D^{++} = \begin{pmatrix} \frac{s_1^\alpha}{s_1^\alpha + \beta^\alpha} & 0 & \cdots & 0 \\ 0 & \frac{s_2^\alpha}{s_2^\alpha + \beta^\alpha} & \cdots & 0 \\ \vdots & \vdots & \ddots & \vdots \\ 0 & 0 & \cdots & \frac{s_r^\alpha}{s_r^\alpha + \beta^\alpha} \end{pmatrix} \tag{1.71}$$

Appropriate choices of α and β can produce a stable regularised solution of $\underline{A}$. Unfortunately, there appears to be no simple rule for choosing α and β optimally in any given problem.

1.5.2 Point Matching (Collocation)

1.5.2.1 Simple Point Matching (SPM)

Point matching is the general term for the numerical technique in which a number of points are selected on a common boundary between two regions and expressions for the fields on each side are equated at these points. In Fig. 1.10, the fields Ψ_1 and Ψ_2 exist in Ω_1 and Ω_2 respectively, i.e.

$$\begin{aligned} \Psi_1(P) &= \sum_{n=0}^{\infty} A_n \Psi_n(P) \quad , \quad P \in \Omega_1 \text{ and} \\ \Psi_2(P) &= \sum_{n=0}^{\infty} B_n \psi_n(P) \quad , \quad P \in \Omega_2. \end{aligned} \tag{1.72a}$$

where the Ψ_n and ψ_n are basis functions and the A_n and B_n are expansion coefficients. It is assumed that the problem is to determine the B_n from the known values of the A_n. It is further assumed that Ω_1 and Ω_2 share a common region $\tilde{\Omega}$, i.e. $\tilde{\Omega} = \Omega_1 \cap \Omega_2$ (Fig. 1.10).

A set of points $P_i \in \tilde{\Omega}$, $i \in (0,N)$ is then chosen in $\tilde{\Omega}$. On equating Ψ_1 and Ψ_2 it is seen that

$$\sum_{n=0}^{\infty} A_n \Psi_n (P_i) = \sum_{n=0}^{\infty} B_n \psi_n (P_i)$$

$$P_i \in \tilde{\Omega} \qquad (1.72b)$$

$$i \in (0,N)$$

and the resultant matrix equation (cf. Section 1.5.1) is solved by an appropriate numerical scheme. Combined with modern computational methods this point-matching technique (or collocation as it is sometimes called) can yield useful numerical results in such problems as radar scattering (James and Gallett 1972), waveguide reflection (Wexler, 1969) etc., particularly as more complicated (or realistic) shapes are encountered (e.g. triangular optical waveguide, James and Gallett, 1973). Of course, the results are not exact, but if sufficient points are used, the numerical solution can converge appropriately to an adequate engineering solution. This can be tested by choosing a larger number of matching points and comparing the new solution numerically with the previous one. If the results are sufficiently close, the solution is taken as satisfactory.

1.5.2.2 Extended Point Matching (EPM)

Very often, Ω_1 and Ω_2 (Fig. 1.10) are chosen (conveniently) to correspond to (existing) physical boundaries. For instance, one would tend to partition a sectorial horn into a section of cylindrical waveguide (Ω_1) and a conical sector (Ω_2) as in Fig. 1.11. The matching is then done on C*. However, this simple-minded approach (hence the name simple point matching) is incorrect in general. As pointed out by Lewin (1970a,b), it is doubtful whether the field expansion in Ω_2 can satisfy the radiation condition and be convergent in $\tilde{\Omega}$ at the same time. The result is correct only if the minimum radius of convergence (see Section 1.4) r_- of $\Psi_2(P)$, $P \in \Omega_2$ is smaller than r_o (of Fig. 1.11).

Another example is given by considering the interior region shown in Fig. 1.12. Note that this region corresponds to the cross-section of a ridge waveguide (Marcuvitz 1951, Section 9.9). The electric field in this region must clearly be symmetrical with respect to the y-axis and satisfy the Dirichlet boundary condition on the boundary C. The expansion

$$\Psi_R = \sum_{n=0}^{\infty} A_n J_{n\alpha} (k\rho_R) \sin n\alpha (\phi_R - \pi) \sin (n \alpha \phi_R) \tag{1.73a}$$

where $\alpha = 2/3$, is valid in the neighbourhood of A and satisfies the appropriate edge condition (see Section 1.3). However, by image theory (Wait 1985, Section 1.7), a singularity for (1.73a) must exist at A*. Therefore, the expansion Ψ_R is valid only for $\rho_R < 2a$. Similarly, the expansion

$$\Psi_L = \sum_{n=0}^{\infty} B_n J_{n\alpha} (k\rho_L) \sin (n \alpha \phi_L) \tag{1.73b}$$

has a singularity at B* and is valid in the neighbourhood of B for $\rho_L < 2a$.

In the method of simple point matching, one simply equates Ψ_R and Ψ_L on $\tilde{C}$ without any further consideration. However, this simple-minded approach is correct only if the circles C_R and C_L, with radius 2a and centres at A and B respectively, enclose $\tilde{C}$ (i.e. $d < \sqrt{3}\, a$) (Fig. 1.12b). On the other hand, if $d \geq \sqrt{3}\, a$, or the circles C_R and C_L do not enclose $\tilde{C}$ (Fig. 1.12c), the expansions Ψ_R and Ψ_L must diverge on $\tilde{C}$. Even though there is still a possibility that equating Ψ_R and Ψ_L may yield a satisfactory result, it is in general incorrect however, and the method of simple point matching fails.

Bates (1967b, 1969a,b, 1973a,b, 1975a) have developed the method of extended point matching (EPM). Instead of matching on $\tilde{C}$ of Fig. 1.12c, an additional expansion,

$$\Psi = \sum_{n=0}^{\infty} D_n \sin (n \pi y/a) \sin((k^2 - (n \pi/a)^2)^{\frac{1}{2}} x) \tag{1.73c}$$

which is valid for $0 \leq y \leq a$ and $-d \leq x \leq d$ is used. The matchings are then carried out on $\tilde{C}_R$ and $\tilde{C}_L$ respectively, i.e.

$$\begin{aligned} \Psi_R (P) &= \Psi(P) , \quad P \in \tilde{C}_R \\ \Psi_L (P) &= \Psi(P) , \quad P \in \tilde{C}_L \end{aligned} \tag{1.74}$$

and the two equations in (1.73) are solved simultaneously to obtain the desired cutoff wavenumber k.

1.5.2.3 Validity of Point Matching

Essentially, there are two ways to determine whether a result obtained by point matching modal expansion across a boundary is valid. One is to resort to the Rayleigh hypotheses as Bates (1967b, 1969b, 1975a), Bates et al. (1973a) do to take into consideration any singularities (Millar 1970 , 1973) characterising the series of two-dimensional harmonic functions used to expand the interior and exterior fields. On the other hand, Lewin (1970a, b) looks at the problem from the point of view of convergence of the field representation in the region where matching is done (i.e. $\tilde{\Omega}$ see Fig. 1.10). He concludes that, if it is convergent there, that is all that needs to be said (however, whether or not this is, in fact, the end of the matter is perhaps not completely clear as yet!).

Although the method of point matching is not always theoretically defensible, nevertheless it provides a computationally and conceptually simple tool for solving a wide variety of electromagnetic problems. Furthermore, the use of an incomplete mode basis and the violation of the Rayleigh hypotheses (in many cases), does not necessarily mean that the results are seriously in error (Burrows 1969a,b, Bates 1975a, Lewin 1970a,b), at least from the point of view of an engineer. Finally, if one resorts to the more rigorous method of extended point matching, satisfactory results can be obtained in more cases (cf. Bates 1967b, 1969a,b, 1973b, 1975a).

1.5.3 Finite Differences/Finite Elements

In a finite-difference scheme a space-time mesh is introduced and Maxwell's equations are replaced by a system of finite-difference equations on the mesh (Yee 1966). An appropriate numerical approach is then invoked to solve for the field at each point of the mesh. Due to the availability of large computers, the method of finite differences has become increasingly popular for solving scattering problems. Davies and Muilwyk (1966) have written a computer program to calculate dominant cutoff frequency, field distribution and characteristic impedance of uniform hollow waveguides of arbitrary shape. Silvester (1969) presents a more general program for waveguide analysis of higher order modes. Johns et al. (1982) investigate the solution of inhomogeneous waveguide problems and the application of the TLM (transmission line modelling) method in imaging wave scattering phenomena. Kunz and Lee (1978) analyse the external response of an aircraft in a transient environment.

A difficulty encountered when trying to solve field problems in this way arises from scattering problems being usually 'open', i.e. the domain in which the field has to be computed is unbounded. Since no computer can store an unlimited amount of data, means must be found for limiting the domain in which the field is computed. This is done by using a mesh of limited size, but one large enough to fully contain the scatterer (Fig. 1.13), and by bounding the outer surface of the mesh far enough from the scatterer that the outgoing nature of the scatterer field can be readily and accurately incorporated into the model of the scattering process (Mur 1981b).

1.5.4 Integral Equations

In general, when the differential form of the wave equation is invoked to describe the propagation of a field Ψ, boundary conditions have to be imposed explicitly, because the differential equation describes only the local behaviour of Ψ. Except where the scattering surfaces coincide with coordinates surfaces (as when the method of separation of variables is applicable).

It can be useful, however, to formulate the determining equation for Ψ in such a manner as to include the boundary conditions implicitly. Such a formulation must relate Ψ not only to its value at neighbouring points but to its values at all points including the boundary points. Integral equations have this property. Since an integral equation contains the boundary conditions, it represents the entire physics of the problem in a very compact form. There are many excellent references on integral equations (cf. Albert and Synge, 1948; Synge, 1948; Morse and Feshbach, 1953 Chapter 8 and Jones, 1964 Chapter 1). The books by Pogorzelski (1966) and Zabreyko (1975) are especially useful for further reading on this subject. More recent references include Bates and Ng (1972), Morita (1978), Morrison (1979) and Jones (1979, Chapter 6).

1.5.4.1 Fredholm, Volterra and Singular Integral Equations

An integral equation is one in which an unknown function appears under single or multiple integral signs. The unknown function may be real or complex. It may also be a function of one or several variables. An integral equation is called linear if it only performs linear operations on the unknown function.

(i) The Fredholm integral equation of the first kind for Ψ can be written generally as

$$\Psi_o(\underline{x}) = \int\int_{\Omega} \Psi(\underline{x}') \; K(\underline{x}, \underline{x}') \; d\underline{x}' \qquad (1.75)$$

where $\Psi_o(\underline{x})$ is a known function, and $\underline{x} \in \Omega_+$, $\underline{x}' \in \Omega_-$ (Fig. 1.5). The quantity $K(\underline{x},\underline{x}')$ is called the kernel of the integral equation.

(ii) The general form of the Fredholm integral equation of the second kind for Ψ is

$$\Psi(\underline{x}) = \Psi_o(x) + \eta \iint_{\Omega-} \Psi(\underline{x}') K(\underline{x}, \underline{x}') d\underline{x}' \qquad (1.76)$$

Unlike the Fredholm integral equation of the first kind, which is in general ill-posed, the Fredholm integral equation of the second kind always possesses a solution which can be expressed as a power series in the parameter η and is uniformly convergent for $|\eta|$ sufficiently small (cf. Pogorzelski 1966).

(iii) Volterra Integral Equation of the first and second kind.

Volterra integral equations are defined in the same way as Fredholm equations except that their upper limits of integration are variable.

(iv) Singular Integral Equation.

When one or both limits of integration are infinite, or when the kernel becomes infinite at one or more pointswithin the range of integration, an integral equation is said to be singular.

1.5.4.2 Volume and Surface Integral Equations

Two basic forms of integral equation which are often encountered in scattering problems are:

(i) Volume Integral Equation

The volume-source method (cf. Stratton 1941, Section 8.2; Morse and Feshbach 1953, Chapter 8 and Jones 1964, Chapter 1), called the polarisation-source approach by Bates and Ng (1972), is an example of how to formulate a scattering problem as an integral equation. The integral equation is of the form

$$\Psi(P) = (\nu^2-1)\, k^2 \iint_{\Omega-} \Psi(P)\, g(P, P')\, d\Omega_{..}, \quad P \in \Omega_+ \qquad (1.77)$$

where g is the free space Green's function.

(ii) Surface Integral Equation.

By appealing to Green's theorem, the scattered wave can be expressed in terms of radiation from sources existing only on the boundary (cf. Stratton 1941, Section 8.1; Morse and Feshbach 1953, Chapter 8 and Jones 1964, Chapter 1

Morita (1978) has listed a collection of the surface integral repres-

entations for electromagnetic scattering from dielectric cylinders. One example is

$$\Psi(P) = \int_C \left[\Psi(Q)\ \nabla g\ (P,Q) - g(P,Q)\ \nabla\Psi\ (Q)\right] \cdot \hat{n} dC \tag{1.78}$$

where $\hat{n}$ is the outward normal to the boundary C.

1.5.4.3 Solution of Integral Equations

Analytical solutions for Ψ can be obtained from integral equations for only a few special cases (cf. Morse and Feshbach 1953, Chapter 8), where analytical tools like, for instance, the Fourier transform (cf. Berntsen 1983), Kontorowich and Lebedev transform (cf. Jones 1964, Section 9.13) or the Factorization technique (Wiener-Hopf method) (cf. Noble 1958) can be applied. However, integral equations can always be solved numerically (arbitrarily accurately, in principle) by the method of moments (cf. Harrington 1968). Many authors (cf. Hashimoto and Fujisawa, 1970; van den Berg, 1981; Cohoon, 1980; Sarkar, Siarkiewicz and Startton, 1981; Harrington, 1968) have made detailed studies of matrix solutions to the integral equations which arise in scattering problems.

Subdividing the region Ω_- of Fig. 1.5 into subregions, i.e.

$$\Omega_- = \Omega_1 \cup \Omega_2 \ldots \cup \Omega_i \cup \ldots \cup \Omega_m \tag{1.79}$$

The basis functions Ψ_n^i are then chosen such that they are independent and complete (cf. Section 1.4.2) within the subregion Ω_i. The unknown wave function Ψ can then be expanded as

$$\Psi = \sum_{n=-\infty}^{\infty} A_n^i \Psi_n^i (\underline{x}_i) , \quad \underline{x}_i \in \Omega_i \tag{1.80}$$

(1.80) forms the basis of the method of moments and is substituted into the integral equations to evaluate the A_n^i.

For the sake of simplicity, take M = 1 (i.e. $\Omega_- = \Omega_1$), and if (1.80) is substituted into (1.75), the latter becomes

$$\Psi_o (\underline{x}) = \int\int_{\Omega_-} \sum_{n=-\infty}^{\infty} A_n \Psi_n (\underline{x}') K (\underline{x}, \underline{x}')\, d\underline{x}' \tag{1.81}$$

The kernel $K(\underline{x},x')$, which is a (function of the) Green's function can often be expanded in the form

$$K(\underline{x},\underline{x}') = \sum_{m=-\infty}^{\infty} B_m \Psi_m(\underline{x}) \Psi_m(\underline{x}') \tag{1.82}$$

where the B_m are of fixed (known) values. Furthermore, $\Psi_o(\underline{x})$ can always be expressed as a sum of the basis (eigen) functions

$$\Psi_o(\underline{x}) = \sum_{\ell=-\infty}^{\infty} D_\ell \Psi_\ell(\underline{x}) \tag{1.83}$$

where the D_ℓ are known. Assuming that (1.80), (1.82) and (1.83) are absolutely convergent, the sequence of summations and integration can be interchanged. (1.81) then becomes

$$\sum_{m=-\infty}^{\infty} \Psi_m(\underline{x}) \sum_{n=-\infty}^{\infty} A_n \left[B_m \int\int_{\Omega_-} \Psi_m(\underline{x}') \Psi_n(\underline{x}') \, d\underline{x}'\right]$$

$$= \sum_{\ell=-\infty}^{\infty} D_\ell \Psi_\ell(\underline{x}) \tag{1.84}$$

Since the Ψ_m form a complete set, the orthorgonality rule,

$$\int_{\Omega} \Psi_m(\underline{x}) \Psi_n(\underline{x}) \, d\underline{x} = \begin{cases} \text{a constant}, & m = n \\ 0, & m \neq n \end{cases} \tag{1.85}$$

applies. Therefore, (1.81) finally becomes

$$\sum_{n=-\infty}^{\infty} A_n K_{\ell n} = D_\ell \tag{1.86}$$

for $\ell = -\infty, \ldots 1, 0, 1, \ldots \infty$, with

$$K_{\ell n} = B_\ell \int\int_{\Omega_-} \Psi_\ell(\underline{x}') \Psi_n(\underline{x}') \, d\underline{x}' \tag{1.87}$$

In practice, the summation limits in (1.86) must be truncated to (-N,N), i.e.

$$\sum_{n=-N}^{N} A_n K_{\ell n} = D_\ell \tag{1.88}$$

in order that the computation can be carried out in a computer. Then (1.88) can be written as a matrix equation

$$\underline{\underline{K}} \, \underline{A} = \underline{D} \tag{1.89}$$

where $\underline{A}$, $\underline{D}$ are (2N+1) x 1 vectors, and $\underline{\underline{K}}$ is a (2N+1) x (2N+1) matrix. The A_n can then be evaluated using an appropriate matrix inversion scheme, such that

$$\underline{A} = \underline{\underline{K}}^{-1} \underline{C} \tag{1.90}$$

can be calculated efficiently (cf. Section 1.5.1).

In order to describe fully the field behaviour in the vicinity of a scatterer, the number of basis functions used must be such that (cf. Cabayan et al. 1973 and Seagar et al. 1984)

$$N \alpha (r_+/\lambda)^{\ell} \tag{1.91}$$

where λ is the wavelength and r_+ is the largest dimension of the scatterer, and $\ell = 1$ for two-dimensional scattering problems and $\ell = 2$ for three-dimensional problems. The advantage of surface integral equations over volume integral equations is apparent since the amount of computer time and storage required for performing the matrix inversion are proportional to N^2 and N^3 respectively.

1.5.5 The Null Field Method

1.5.5.1 Underlying Principle

In most of the literature on formulating scattering problems as integral equations, the latter describe the actual physical behaviour of fields outside, on the surface, and in the interior, of a scatterer. The integral equations discussed in Section 1.5.4 are of this type. This section is concerned with an integral equation which constrains the behaviour of the fields in physical space by invoking conditions in regions where they cannot actually propagate. Despite the somewhat unphysical motivation, the formulation, which is based on Waterman's (1965) matrix method, is computationally useful. The particular manifestation of Waterman's approach which is of interest here is the null-field method (cf. Bates 1980b).

In essence, the null-field method requires that equivalent sources, set up on the surface of the scatterer, radiate in such a way as to extinguish the incident field within the scatterer. Theoretically (or mathematically), the null-field method is based on the Huygens principle, the Ewald-Oseen's extinction theorem and Love's equivalence principle, all of which describe the same fundamental concept in different ways.

(i) Huygens principle (cf. Baker and Copson 1953, Born and Wolf 1970, Sections 3.3, 8.2 and 8.3):

(a) Huygens construction:

This states that each element of a wave-front may be regarded as the centre of a secondary disturbance which gives rise to spherical wavelets, and moreover that the position of the wave-front at any later time is the envelope of all such wavelets.

(b) Huygens-Fresnel theory:

The basic idea of the Huygens-Fresnel theory is that the disturbance existing at any point arises from the superposition of secondary waves that proceed from a surface situated between the point and the sources.

(c) Huygens-Kirchhoff theory:

This states that the solution of the homogeneous wave equation, at an arbitrary point in the field, can be expressed in terms of the values of the field and its normal derivative at all points on an arbitrary closed surface surrounding the point.

(ii) Ewald-Oseen's extinction theorem (cf. Born and Wolf 1970, Section 2.4):

This states that an external electromagnetic disturbance travelling at the speed of light in vacuum is exactly cancelled out and replaced in the scatterer by the secondary disturbance travelling at some other appropriate speed.

(iii) Love's equivalence principle (cf. Jones 1964).

This states that the sum of the average rates at which energy is scattered and absorbed by a scatterer is equal to the average rate at which energy is supplied by the sources of the incident field.

1.5.5.2 Historical Background

(i) Waterman's extended boundary condition method:

Waterman (1965) develops a set of matrix equations for his so-called extended boundary equation. Using a procedure similar to the method of moments (Harrington 1968), Waterman (1965) expands the 'induced' surface sources in series of 'regular wave functions', which are complete and orthorgonal and are the basic set of eigenfunctions of the wave functions. He further constructs (Waterman 1968, 1971) a T matrix and a Q matrix from this eigenfunction expansion to relate the incident and scattered fields and incident and surface sources respectively.

Pattanayak and Wolf (1972) derive (independently, though not in as much detail as Waterman does), a set of integral equations from the Ewald-Oseen extinction theorem for solving general scattering problems. Bolomey and Wirgin (1974) compare the numerical results of scattering solutions based on Waterman's approach with other previously established results. Agarwal (1976) formally relates Waterman's extended boundary condition to the generalised extinction theorem and the Huygen's principle.

(ii) Bates and Wall's Null field method:

Bates (1967b,1968, 1969a,b) applies the concept of the extinction theorem to derive a method of 'complete point matching'. Bates and Wall (1977) take the idea further and construct a noble procedure which enables one to solve a scalar diffraction problem (direct or inverse, exact or approximate) for a body of arbitrary shape for both Dirichlet and Neumann boundary conditions. Since then, many authors, including Varadan and Varadan (1980), Kristensson and Strom (1981) and Bostrom (1984), have contributed to this topic.

1.5.5.3 Mathematical Derivation

Define $g(P,P'|\mu)$ to be the Green's function at the point P in a homogeneous space of refractive index μ due to a point source of unit amplitude at P'. Let the total wave function be Ψ. The space Ω is partitioned into Ω_- and Ω_+, where Ω_- consists of all points inside a scatterer and Ω_+ consists of all points outside the scatterer (Fig. 1.14, also Fig. 1.5). Let $\tilde{\Omega}$ denote either Ω_+ or Ω_- and let $\tilde{C}$ be the closed curve(s) bounding $\tilde{\Omega}$. Consider the expression

$$\int_{\tilde{C}} \left[\Psi(Q)\ \nabla g\ (P,Q|\mu) - g(P,Q|\mu)\ \nabla\Psi(Q)\right].\ \hat{n}\ d\tilde{C}(Q) \qquad (1.92)$$

where Q is a point on $\tilde{C}$ and $\hat{n}$ is the outward unit normal to $\tilde{C}$ at Q. Applying the divergence theorem (Stratton 1941, Section 1.3), (1.92) becomes

$$\iint_{\tilde{\Omega}} \nabla \left[\Psi\ \nabla g - g\ \nabla\Psi\right]\ d\tilde{\Omega}$$

$$= \iint_{\tilde{\Omega}} \left[\Psi\ \nabla^2 g - g\ \nabla^2\Psi\right]\ d\tilde{\Omega} \qquad (1.93)$$

Now since the wave function Ψ and Green's function g must satisfy their appropriate wave equations, i.e.

$$\nabla^2 g + k^2 g = - S_P \tag{1.94a}$$

$$\nabla^2 \Psi_{SC} + \nu^2 k^2 \Psi_{SC} = 0 \tag{1.94b}$$

$$\nabla^2 \Psi_{inc} + k^2 \Psi_{inc} = - S_{P_o} \tag{1.94c}$$

Where Ψ_{inc} is the incident wave function due to the source S_{P_o}, Ψ_{SC} is the scattered wave function, ν is the refractive index of Ω_- and S_P is the source which generates g. On substituting (1.94) into (1.93), gives

$$\int_{\tilde{C}} \left[\Psi(Q)\ \nabla g\ (P,Q|\mu) - g\ (P,Q|\mu)\ \nabla\Psi\ (Q)\right] .\ \hat{n}\ dC\ (Q)$$

$$= \int\int_{\tilde{\Omega}} \left[\Psi\ \nabla^2 g - g\ \nabla^2\ \Psi\right]\ d\tilde{\Omega}$$

$$= - \Psi_{inc}\ (P)\ ,\quad \mu = 1,\quad P \in \Omega_- \tag{1.95a}$$

$$= \Psi_{SC}\ (P)\ ,\quad \mu = 1,\quad P \in \Omega_+ \tag{1.95b}$$

$$= 0\ ,\quad \mu = \nu,\quad P \in \Omega_+ \tag{1.95c}$$

$$= \Psi_{SC}\ (P)\ ,\quad \mu = \nu,\quad P \in \Omega_- \tag{1.95d}$$

Although Ψ_{inc}, the incident wave, is known, the resultant integral equation cannot be solved analytically in general. So the method of moments (Harrington 1968) is invoked to transform it into a set of matrix equations, which are solved by an appropriate numerical scheme, in the same manner as discussed in Section 1.5.1.

1.5.5.4 The Circular Null-Field Method

The wave function $\Psi \in \Omega_-$ can always be expanded in terms of series of basis wave functions Ψ_n, i.e.

$$\Psi = \sum_{n=o}^{\infty} A_n\ \Psi_n \tag{1.96a}$$

where each Ψ_n is the solution to the two-dimensional wave equation obtained by the method of separation of variables (see Section 1.4). For cylindrical polar coordinates,

$$\Psi_n = J_n (k\rho) \begin{matrix}\cos \\ \sin\end{matrix} (n\phi) \qquad (1.96b)$$

Furthermore, the Green's function $g = -j/4\ H_o^{(2)} (kR)$ can be expanded using the Addition Theorem for Bessel Functions (Watson 1966, Section 11.3) to give

$$g = -j\ H_o^{(2)} (kR)/4$$

$$= \begin{cases} -j/4 \sum_{m=1}^{\infty} \varepsilon_m H_m^{(2)} (k\rho)\ J_m (k\rho')\ \cos m(\phi-\phi'), & \rho > \rho' \\ -j/4 \sum_{m=1}^{\infty} \varepsilon_m H_m^{(2)} (k\rho')\ J_m (k\rho)\ \cos m(\phi-\phi'), & \rho < \rho' \end{cases} \qquad (1.97)$$

where $R = (\rho^2 + \rho'^2 - 2\rho\rho' \cos(\phi-\phi'))^{\frac{1}{2}}$. (See Fig. 1.15).

For the sake of simplicity, the incident wave Ψ_{inc} is taken to be a plane wave. This involves no loss of generality since any physically realisable incident wave can be expressed as a combination of plane waves (cf. Clemmow 1966). Therefore

$$\Psi_{inc} = \exp(j\,k\,\rho \cos(\phi - \theta)) = \sum_{m=o}^{\infty} \varepsilon_m j^m \cos m(\phi - \theta)\ J_m (k\rho) \qquad (1.98)$$

where θ is the incident angle of the plane wave.

Refer to Fig. 1.16. With the help of (1.96), (1.97) and (1.98), (1.95a) can be rewritten as

$$\int_C \{ \Big[\sum_{n=o}^{\infty} A_n J_n (kr) \begin{matrix}\cos \\ \sin\end{matrix} (n\theta) \Big]$$

$$\partial \Big[-j/4 \sum_{m=o}^{\infty} \varepsilon_m H_m^{(2)} (kr)\ J_m (k\rho) \cos m(\phi-\theta) \Big] / \partial n$$

$$- \partial \Big[\sum_{n=o}^{\infty} A_n J_n (kr) \begin{matrix}\cos \\ \sin\end{matrix} (n\theta) \Big] / \partial \hat{n}$$

$$\Big[-j/4 \sum_{m=o}^{\infty} \varepsilon_m H_m^{(2)} (kr)\ J_m (k\rho) \cos m(\phi-\theta) \Big] \} dC$$

$$= -\sum_{m=o}^{\infty} \varepsilon_m j^m \cos m(\phi - \theta)\ J_m (k\rho) \qquad (1.99)$$

where the locus of $P(\rho; \phi)$ describes a circle C_- inscribing C, so that r is always greater than ρ.

Both the LHS and RHS of (1.99) are Fourier-Bessel series (Watson 1966, Section 18.1). Re-arranging the sequence of summations, integrations and differentiations, and separating the odd and even terms of the Fourier series, gives

$$\sum_{m=o}^{\infty} \begin{matrix}\cos\\ \sin\end{matrix} (m\phi)\ J_m(k\rho) \sum_{n=o}^{\infty} A_n \int_C \{\left[J_n(kr) \begin{matrix}\cos\\ \sin\end{matrix} (n\theta)\right]$$

$$\partial\left[-j/4\ \varepsilon_m H_m^{(2)}(kr) \begin{matrix}\cos\\ \sin\end{matrix} (m\theta)\right]/\partial n$$

$$- \partial\left[J_n(kr) \begin{matrix}\cos\\ \sin\end{matrix} (n\theta)\right]/\partial\hat{n} \quad \left[-j/4\ \varepsilon_m H_m^{(2)}(kr) \begin{matrix}\cos\\ \sin\end{matrix} (m\theta)\right]\} dC$$

$$= \sum_{m=o}^{\infty} \begin{matrix}\cos\\ \sin\end{matrix} (m\phi)\ J_m(k\rho) \left[-\varepsilon_m j^m \begin{matrix}\cos\\ \sin\end{matrix} (m\theta)\right] \qquad (1.100)$$

Finally, on comparing the coefficients of the Fourier-Bessel series on both sides of (1.100), it is seen that

$$\sum_{n=o}^{\infty} A_n \int_C \{\left[J_n(kr) \begin{matrix}\cos\\ \sin\end{matrix} (n\theta)\right] \partial\left[-j/4\ \varepsilon_m H_m^{(2)}(kr) \begin{matrix}\cos\\ \sin\end{matrix} (m\theta)\right]/\partial\hat{n} -$$

$$\partial\left[J_n(kr) \begin{matrix}\cos\\ \sin\end{matrix} (n\theta)\right]/\partial\hat{n}$$

$$\left[-j/4\ \varepsilon_m H_m^{(2)}(kr) \begin{matrix}\cos\\ \sin\end{matrix} (m\theta)\right]\} dC$$

$$= -\varepsilon_m j^m \begin{matrix}\cos\\ \sin\end{matrix} (m\theta) \qquad (1.101)$$

1.5.5.5 Beyond the Original Derivation

In principle, the circular null-field method introduced in the previous section can be applied to scattering problems for bodies of arbitrary shape (Fig. 1.18). Furthermore, one can invoke the null-field condition in any area $\tilde{\Omega}$ within Ω_-(Fig. 1.18). The method of analytic continuation would then ensure that the field vanishes everywhere within Ω_-. It should be noted that since the normal derivative of the LHS (1.95) does not exist, one cannot 'continue' (1.95) into Ω_+.

However, computational experience (cf. Bates and Wall 1977) shows that the rate of convergence to a stable solution depends very much on the factor ζ, which is defined by

$$\zeta = \text{area of } \tilde{\Omega}/\text{area of } \Omega_{-} \tag{1.102}$$

where $\tilde{\Omega} \equiv \Omega_{--}$, which is a circle as in Fig. 1.5, in the case of the circular null-field method (Fig. 1.16).

It is therefore obvious that the circular null-field method becomes less efficient for the scatterers typified by Figs 1.17b,d and Fig. 1.17a when the aspect ratio (i.e. b/a) is large. To overcome the difficulty of large aspect ratio (Fig. 1.17a), Bates and Wall (1977) propose that the null-field condition should be imposed on ellipses inscribing elongated scatterers, and the basis wave function introduced in (1.96) be replaced by Mathiew functions (Moon and Spencer 1971, Section 7.11). Marked improvement (Bates and Wall 1977) of up to 10 orders of magnitude in stability (Section 1.5.1) has been achieved.

When a scatterer is of infinite or semi-infinite size (e.g. Fig. 1.17b,d), the ratio ζ defined in (1.102) is always small irrespective of the (finite) size of the inscribing circle or ellipse. The modifications discussed in the previous paragraph cannot then be applied. In particular instances, for example, scattering by periodic structures (gratings) and rough surfaces (Fig. 1.17b), the null-field condition can be satisfied on planes behind the scattering surfaces (Waterman 1975 and Bates 1974 respectively). In Chapter 3 and Chapter 8 of this thesis, a 'radial null-field method' is introduced, and is invoked to solve scattering problems for another class of infinte bodies, notably, the infinite wedges.

Other extensions which have been made to the full-field method include:

(i) When solving (1.95), in general, one expands Ψ in its basis functions (1.96) and obtains $\partial\Psi/\partial\hat{n}$ by performing analytic differentiation, i.e. if

$$\Psi = \sum_{n=-\infty}^{\infty} A_n J_n (k\rho) \exp (jn\phi) \tag{1.103a}$$

and if $\partial\Psi/\partial\hat{n} = 1/\rho \; \partial\Psi/\partial\phi$, then

$$\partial\Psi/\partial\hat{n} = 1/\rho \sum_{n=-\infty}^{\infty} A_n (jn) J_n (k\rho) \exp (jn\phi) \tag{1.103b}$$

However, sometimes it may be more convenient (Wong 1972, Morita 1979 and Bates 1980b) to express Ψ and $\partial\Psi/\partial\hat{n}$ in separate series, i.e.

$$\Psi = \sum_{n=-\infty}^{\infty} A_n J_n (k\rho) \exp (jn\phi) \qquad (1.104a)$$

and

$$\partial\Psi/\partial\hat{n} = \sum_{n=-\infty}^{\infty} B_n J_n (k\rho) \exp (jn\phi) \qquad (1.104b)$$

Two sets of equations are thus required for the two sets of variables A_n and B_n. The equations can be obtained by invoking the null-field condition in both the interior and exterior of the scatterer, i.e. (1.95c) is used in conjunction with (1.95a).

(ii) Iskander et al (1982) set up an iterative procedure to speed up the rate of convergence (i.e. to reduce the number of basis functions required to achieve a stable solution) when calculating the A_n (cf. (1.101)).

(iii) To speed up numerical computation using asymptotic expansions, Boström (1983a) modifies Waterman's original approach to give a Taylor-like series for the Q matrix. Waterman (1983) proposes an (approximate) diffusion model facilitating numerical computation of the T matrix.

1.5.5.6 Uniqueness and Solvability

In the T-matrix (extended boundary condition) approach, Waterman (1965) relates the scattered field to the incident wave via a T-matrix. This approach therefore relies primarily on the assumption of the validity of the external Rayleigh hypotheses. On the other hand, Bates (1975a) points out that in the case of null-field method, only the surface field and its normal derivative are calculated. The null-field method is then still correct even when the Rayleigh hypotheses fails. When the Rayleigh hypotheses is valid, the surface field calculated is the true surface field, i.e.

$$\lim_{\substack{P\to Q \\ P\in\Omega_-}} \Psi_- (P) \equiv \Psi_{surface} \equiv \lim_{\substack{P\to Q \\ P\in\Omega_+}} \Psi_+ (P) \qquad (1.104c)$$

On the other hand, when the Rayleigh hypotheses is not valid, (1.104c) does not hold and the surface field calculated is not necessarily the 'true' surface field, but one can still evaluate the exact scattered field (Bates 1975a). Ramm (1982a,b) proposes a formal proof for a scattering body with Dirichlet boundary conditions. He (Ramm 1982a,b) shows that the A_n of (1.96), evaluated from the (truncated) null-field equations converge even though the Rayleigh

hypotheses is not valid in general. Kristenson, Ramm and Ström (1982) extend the proof of Ramm (1982a,b) to include the Neumann boundary conditions. They (Ramm 1982a,b and Kristenson et al 1982) find that when the A_n are to be evaluated from the set of null-field equations (e.g. (1.101)), where m, n are truncated to (0,M) and (0,N) respectively,

(i) the resultant matrix equation is solvable for sufficiently large M,

(ii) the A_n and Ψ_n of (1.96) converge when M and N are sufficiently large,

(iii) the rate of convergence of A_n depends on the choice of the eigenfunctions Ψ_n, which must be complete and independent,

(iv) the null-field equations are stable with respect to small perturbations of data (i.e. matrix coefficients in (1.101)).

On the other hand, Kristenson et al (1982) point out that although the scattered far field calculated is exact and independent of the surface field expansion if the former is calculated from an infinite set of equations (1.101), the same need not be true if the equations are truncated. Furthermore, the questions of uniqueness and convergence for penetrable bodies and infinite scatterers have yet to be answered.

Other contributions on the subject of uniqueness and solvability of the null-field method include:

(i) Colton and Kress (1983) show that acoustic wave scattering for the Dirichlet, Neumann, impedance and transmission boundary-value problems can be solved uniquely by the null-field equation (1.95).

(ii) Martin (1980, 1982) proves that in solving the scattering and radiation problems of acoustics, the infinite system of null-field equations always has precisely one solution (i.e. the A_n in (1.101) are unique).

1.5.5.7 Application

The main advantage of the null-field method is the freedom one has in invoking the null-field conditions (i.e. vanishing field) within whichever part of the (interior) of the scatterer leads to the best numerical stability. The field can then be shown to vanish everywhere in the interior, in view of the analytic continuability.

Many authors have applied, in one form or another, the null-field method, or extended boundary condition, or extinction theorem, in the solution

of acoustic, electromagnetic or elastic scattering problems. Representative of these are Grzesik (1980) in his analytic consideration of field matching through 'volume suppression' and Weaver and Pao (1979) in their solution of scattering by a ribbon-shaped obstacle with the Neumann boundary condition. There are also the comprehensive researches of Strom (1974, 1975), Bostrom (1983b, 1984), Bates (1975a), Varadan and Varadan (1981, 1982) and their colleagues. The book edited by Varadan and Varadan (1980) serves as an important source wherein both applications and many theoretical and numerical considerations are disucced in considerable detail.

1.6 APPROXIMATE SOLUTIONS

As mentioned in Section 1.4, exact analytical solutions to scattering problems are limited to a small class of simple shapes whose surfaces coincide with those of orthogonal curvilinear coordinate systems. Furthermore, most such solutions are developed as infinite series of functions, which often converge slowly. On the other hand, the truncation limit N introduced in (1.88) for matrix solutions of scattering problems must increase with increasing frequency (i.e. shorter wavelength). In the latter circumstance, one must therefore resort to approximate methods in view of the limited capacity of the computer.

1.6.1 Geometrical Optics (GO)

It is seen from (1.4) that the field E,H at any point can be written as

$$E(k,R) = E_o(k,R) \exp(-jk\bar{s}(k,R)) \tag{1.105a}$$

$$H(k,R) = H_o(k,R) \exp(-jk\bar{s}(k,R)) \tag{1.105b}$$

Substituting (105) into the time-harmonic field equations (1.13), the latter become

$$\nabla\bar{s} \times H_o + (\varepsilon_o/\mu_o)^{\frac{1}{2}} E_o = \nabla \times H_o/(jk) \tag{1.106a}$$

$$\nabla\bar{s} \times E_o - (\mu_o/\varepsilon_o)^{\frac{1}{2}} H_o = \nabla \times E_o/(jk) \tag{1.106b}$$

$$E_o \cdot \nabla\bar{s} = \nabla \cdot E_o/(jk) \tag{1.106c}$$

$$H_o \cdot \nabla\bar{s} = \nabla \cdot H_o/(jk) \qquad (1.106d)$$

in a source-free environment (ie S=J=0)
Elimination of H_o from this set of equations yields

$$(1 - \nabla\bar{s}\cdot\nabla\bar{s})\, E_o + 1/(jk)\, (\nabla^2\bar{s} + 2(\nabla\bar{s}\cdot\nabla))\, E_o + (1/jk)^2\, (\nabla \times \nabla \times - \nabla\,\nabla\cdot) E_o = 0 \qquad (1.107)$$

The last term in (1.107) is equivalent to $-(\nabla^2 E_o)/(jk)^2$. Hence, unless E_o changes rapidly over distances comparable to a wavelength (e.g. a shadow-light boundary, focal regions, etc.), as $k\to\infty$ the last term in (1.107) may be neglected. Consequently, (1.107) is satisfied if

$$\nabla\bar{s} \cdot \nabla\bar{s} = 1 \qquad (1.108a)$$

$$\left[\nabla^2\bar{s} + 2\,(\nabla\bar{s}\cdot\nabla)\right] E_o = 0 \qquad (1.108b)$$

(1.108a) is called the eikonal equation of geometrical optics and indicates that in the limit $k\to\infty$ the function $\bar{s}$ is independent of k. (In a medium other than free space, the eikonal equation is $\nabla\bar{s}.\nabla\bar{s} = \mu_r\varepsilon_r$). Similarly, (1.108b), which is called the first transport equation, indicates that E_o is independent of k in the limit $k\to\infty$.

Equation (1.108) represents asymtoptic solutions of the electromagnetic field which are subject to certain geometrical laws. Historically, these laws were first recognised in the field of optics, inasmuch as typical apparatus are at least many thousands of wavelengths in linear dimensions so that the asymtoptic approximations are often valid.

(i) Basic assumption:
If a source is near a non-planar interface between two media, each point on the interface behaves locally as if it were part of an infinite planar interface and that the incident field behaves locally as a plane wave.

(ii) Fermat's principle:
Reflected or refracted rays from a point S to a point P are those rays for which the optical path length between S and P with one point on the interface between two media is stationary with respect to infinitestimal variation in path (cf. Born and Wolf 1970).

(iii) Limitation:

Geometrical optic approximation are no longer valid if the curvature of either the incident wavefront or the interface is too small for $\nabla^2 E_o/(jk)^2$ to be neglected in (1.107). Weiss (1968) presents a useful account of the geometrical optics limit.

1.6.2 Physical Optics (PO)

1.6.2.1 Planar Physical Optics (PPO)

Consider a perfectly conducting body illuminated by a source as indicated in Fig. 1.19. Provided that the body is large and the surface is smoothly varying with large radii of curvature compared to the wavelength, it may be assumed that each point on the surface behaves locally as if it were part of an infinite ground plane. The tangential component of the magnetic field H at the surface of a ground plane is given by twice the incident field H_{inc}. Over the illuminated portion of the surface S the surface current density is approximated by

$$J_s = 2\hat{n} \times H_{inc} \tag{1.109}$$

and the surface current is taken to be zero over the shadow region. The scattered fields are then calculated from the surface current density (cf. Bouwkamp 1954, Jones 1964).

Physical optics has many deficiencies. It is unsuitable for predicting the scattered field near or within the shadow region where the neglected currents are important. It fails when the effects of multiple scattering cannot be neglected. It does not predict any polarisation dependence for fields back-scattered from perfectly conducting bodies. It can violate reciprocity. But with all these, physical optics provides a useful approximate solution to many interesting and important diffraction problems. Especially, it usually predicts the strongest part of the scattering (i.e. speculars) accurately, and often does so even when the radii of curvature are only a few wavelengths. For example, Kildal (1982) finds that the PPO solution for the directivity of a parabolic reflector antenna has an accuracy of $0.22(\lambda/D^2)$ db on axis. Bates (1974) finds that the approximation (1.109) satisfies the optical extinction theorem (or extended boundary condition or null-field condition) with increasing accuracy the further one penetrates into the interior of the scatterer.

1.6.2.2 Extended Physical Optics (EPO)

Bates and Wall (1977) generalise the method of physical optics. In the case of planar physical optics discussed in the last section, the illuminated region (denoted by C_+) is defined as the collection of points Q, such that the line QS, where S is the source point, does not intercept C (Fig. 1.20a). Similarly, the shadow region (denoted by C_-) is defined as the collection of points Q', such that the line Q'S must intercept C between Q' and S. In the extended physical optics (EPO), Bates and Wall (1977) define 'generalised' illuminated and shadowed regions.

The dashed line in Fig. 1.20b represents a curved coordinate line. In a particular coordinate system (u_1,u_2,u_3), the coordinate u_1 increases monotonically with distance from O, along the coordinate line. The coordinates u_2 and u_3 have particular, constant, values. For a particular coordinate line, e.g. QQ' (Fig. 1.20b), the value of u_1 is denoted by $u_1(m)$ at the point(s) where QQ' intercepts C for the mth time. The 'illuminated' region is then defined as the collection of points Q, for each of which the value of u_1 is equal to $u_1(1)$. Similarly, the 'shadowed' region is defined as the collection of points Q' for each of which the value of u_1 is equal to $u_1(m)$, where $m > 1$. In such a coordinate system (u_1,u_2,u_3), the incident monochromatic field can be written as (Moon and Spencer 1971)

$$\Psi_{inc} = \sum_{\ell=0}^{\infty} \sum_{m=-\ell}^{\ell} c_{\ell m}\, a_{\ell m}\, \hat{J}_{\ell m}(k,u_1)\, \hat{Y}_{\ell m}(k,u_2,u_3) \qquad (1.110)$$

where the $c_{\ell m}$ are normalisation constants appropriate for the particular coordinate system for which $\hat{J}_{\ell m}(\cdot)$ and $\hat{Y}_{\ell m}(\cdot)$ are everywhere regular radial and angular eigenfunctions. The $a_{\ell m}$ are constants characterising the form of the incident wave.

Bates and Wall (1977) then go on to define

$$J_s(P) = 0 , \quad P \in C_- \qquad (111a)$$

and derive from the null-field equation (cf. Bates and Wall 1977)

$$J_s(P) = \frac{w(u_2,u_3)}{\Delta(u_2,u_3)} \sum_{\ell=0}^{\infty} \sum_{m=-\ell}^{\ell} \frac{a_{\ell m}\, \hat{Y}_{\ell m}(k,u_2,u_3)}{\hat{I}_{\ell m}\, \hat{h}^{(2)}_{\ell m}(k,u_1)} , \quad p \in C_+ \qquad (111b)$$

where $w(u_2,u_3)$ is a weighting function depending upon the particular coordinate system being used. $\Delta(u_2,u_3)$ is defined by

$$dC = \Delta(u_2,u_3)\, du_2 du_3 \tag{1.111c}$$

The $h^{(2)}_{\ell m}(\cdot)$ are the 'outgoing' radial eigenfunctions, which are singular at $u_1 = 0$, and $\hat{I}_{\ell m}$ are particular normalisation constants.

In the case of cylindrical polar coordinates $(\rho;\phi,z)$, the double summation of (1.110) and (1.111b) reduces to a single summation over $m\varepsilon(-\infty,\infty)$. Furthermore $w(\rho;\phi) = 1$, $\hat{I}_{\ell m} = \varepsilon_m \pi$, where ε_m is the Neumann constant, $\Delta(u_2,u_3) = (dC/d\phi)^{-1}$, $\hat{h}^{(2)}_{\ell m}(k,u_1) = H^{(2)}_m(k\rho)$, $\hat{Y}_{\ell m}(k,u_2,u_3) = \exp(jm\phi)$, and the cylindrical physical optics (CPO) is characterised by (Bates and Wall 1977):

$$J_s(P) = 0, \quad P \in C_- \tag{1.112a}$$

$$J_s(P) = \frac{1}{\pi dC/d\phi} \sum_{m=-\infty}^{\infty} \frac{a_m \exp(jm\phi)}{\varepsilon_m H^{(2)}_m(k\rho)} \quad P \in C_+ \tag{1.112b}$$

1.6.3 Born Approximation

Let Ψ be the total wave function, Ψ_{sc} be the scattered wave function and Ψ_{inc} be the incident wave function respectively. The wave equation

$$\nabla^2\Psi + k^2\Psi = -k^2(\nu^2-1)\,\Psi \tag{1.113}$$

is valid in the whole of space apart from the region where the sources of Ψ_{inc} are situated. The scattered field is given by Jones (1964, Section 1.17);

$$\Psi_{sc}(\underline{x},k) = k^2/4\pi \int\int_{\Omega_-} \left[\nu^2(\underline{x}')-1\right] \Psi(\underline{x}',k)\, \frac{\exp(jk|\underline{x}-\underline{x}'|)}{[\underline{x}-\underline{x}']}\, d\underline{x}'$$

$$\underline{x} \in \Omega_+ \tag{1.114}$$

where the refractive index ν satisfies.

$$\nu = \begin{cases} 1, & \underline{x} \in \Omega_+ \\ \nu(\underline{x}), & \underline{x} \in \Omega_- \end{cases} \tag{1.115}$$

The Born approximation, also known as Rayleigh-Gans approximation (Jones 1964, Section 6.13) states that if $|\nu(\underline{x})-1|$ is sufficiently small, $\Psi(\underline{x}',k)$ can be approximated by $\Psi_{inc}(\underline{x}',k)$ for $\underline{x}' \in \Omega_-$.

(1.114) then becomes

$$\Psi_{sc}(\underline{x},k) = k^2/4\pi \int\int_{\Omega_-} |\nu^2(\underline{x}')-1|\, \Psi_{inc}(\underline{x}',k)\, \frac{\exp(jk[\underline{x}-\underline{x}'])}{[\underline{x}-\underline{x}']}\, d\underline{x}' ,$$

$$\underline{x} \in \Omega_+ \tag{1.116}$$

However, in order for the Born approximation to hold, differences in amplitude and phase between the total wave function and the incident wave function, due to the variable refractive index, must be small. Since differences tend to grow with the distance transversed, the integrated value of the deviation of the refractive index from unity must be small (Wade 1979). This depends on the size of the domain Ω_- as well as on the refractive index.

1.6.4 Rytov Approximation

Basically, the difference between the Born and Rytov approximations is the way in which the scattered field is defined. In Born's approach Ψ_{sc} is defined by $\Psi = \Psi_{inc} + \Psi_{sc}$ whereas Rytov defines

$$\Psi = \Psi_{inc} \exp(\Psi^*/\Psi_{inc}) \simeq \Psi_{inc}(1 + \Psi^*/\Psi_{inc} + \ldots) \tag{1.117}$$

In the limit as Ψ^*/Ψ_{inc} becomes small, $\Psi^* \to \Psi_{sc}$, and the two approximate procedures become identical. However, Rytov approximation eliminates the dependence on the size of the scattering domain by requiring only that $(\nu-1)\lambda$ be small, where ν is the refractive index and λ is the wavelength.

1.6.4.1 Original Rytov Approximation

The total, incident and scattered waves are defined by

$$\Psi = \exp(\gamma) \tag{1.118}$$

$$\Psi_{inc} = \exp(\gamma_o) \tag{1.119}$$

$$\Psi^* = \gamma^* \Psi_{inc} \tag{1.120}$$

and

$$\gamma = \gamma_o + \gamma^* \tag{1.121}$$

Since Ψ_{inc} and Ψ^* must satisfy the respective wave equations, substituting (1.118) through (1.121) into the scalar wave equation (1.113) gives

$$\nabla\gamma_o \cdot \nabla\gamma_o + \nabla^2\gamma_o + k^2 = 0 \tag{1.122}$$

and

$$\nabla^2\gamma^* + 2\nabla\gamma_o \cdot \nabla\gamma^* + \nabla\gamma^* \cdot \nabla\gamma^* = -k^2(\nu^2-1) \tag{1.123}$$

or

$$\nabla^2\Psi^* + k^2\Psi^* = -\left[k^2(\nu^2-1) + \nabla\gamma^* \cdot \nabla\gamma^*\right] \Psi_{inc} \tag{1.124}$$

The Rytov approximation requires $\nabla\gamma^* << \nabla\gamma_o$ which is equivalent to neglecting the term $\nabla\gamma^*\cdot\nabla\gamma^*$ in (1.124). Then Ψ^* is given by

$$\Psi^*(\underline{x}) = \gamma^*(\underline{x})\ \Psi_{inc}(\underline{x}) = \Psi_{inc}(\underline{x})\ \ell n\left[\frac{\Psi_{sc}(\underline{x}) + \Psi_{inc}(\underline{x})}{\Psi_{inc}(\underline{x})}\right]$$

$$= k^2/4\pi \int\int_{\Omega_-} \left[\nu^2(\underline{x}')-1\right]\ \Psi_{inc}(\underline{x}', k)$$

$$\frac{\exp(jk[\underline{x}-\underline{x}'])}{[\underline{x}-\underline{x}']}\ d\underline{x}', \quad \underline{x} \in \Omega_+ \tag{1.125}$$

1.6.4.2 Extended Rytov Approximation

Recently, Bates et al. (1976) and Dunlop et al. (1976) have developed a method which takes partial account of the $\nabla\gamma^*\cdot\nabla\gamma^*$ term neglected in Rytov's approach. When the medium is such that refraction predominates over reflection, the wave motion can be approximated closely by tubes of rays (Felsen and Marcuvitz 1973, Section 1.7).

Denoting P as the starting point of a ray, $\hat{s}$ as the unit tangential vector at a point Q on the (curved) ray path and $\hat{\tau}$ as the unit vector at Q on the (straight) ray of Ψ_{inc}. Then Ψ can be approximated by

$$\Psi = \exp(\gamma_o + \gamma^*) \simeq \nu^{-\frac{1}{2}} \exp\left(\int_P^Q \nu\, ds\right) \tag{1.126}$$

i.e.

$$\gamma_o + \gamma^* = jk \int_P^Q \nu\, ds - 1/2\ \ell n\ (\nu) \tag{1.127}$$

Since $\nabla\gamma_o = jk\hat{\tau}$, (1.127) gives

$$\nabla\gamma^* = jk\ (\nu\hat{s}-\hat{\tau}) - 1/2\ \nabla\ \ell n\ (\nu) \tag{1.128}$$

On assuming that $\hat{S}\cdot\hat{\tau} \simeq 1$ (1.124) becomes

$$\nabla^2\Psi^* + k^2\Psi^* = -\left[2\ k^2(\nu -1) - j\ k(\nu-1)\ \partial\ \ell n\ \nu/\partial\tau\right.$$

$$\left. + 1/4\ (\nabla \ell n\nu)\cdot(\nabla\ \ell n\nu)\right]\ \Psi_{inc} \tag{1.129}$$

and Ψ^* is given by

$$\Psi^*(\underline{x}) = \gamma^*(\underline{x})\ \Psi_{inc}(\underline{x}) = \Psi_{inc}(\underline{x})\ \ell n\ \frac{\Psi_{sc}(\underline{x}) + \Psi_{inc}(\underline{x})}{\Psi_{inc}(\underline{x})}$$

$$= k/4\pi \int\int_{\Omega_-} \{(\nu-1)\ (2k - j\partial \ell n\ \nu/\partial\tau) + 1/4\ [(\nabla \ell n\nu)\cdot(\nabla \ell n\nu)]\}$$

$$\Psi_{inc}(\underline{x}')\ \frac{\exp(jk[\underline{x}-\underline{x}'])}{[\underline{x}-\underline{x}']}\ d\underline{x}'\ ,\qquad \underline{x}\ \varepsilon\ \Omega_+ \tag{1.130}$$

The advantage of this modified method is that it takes partial account of ray curvature while the main disadvantage is that the term in the bracket of {. . . .} in (1.130) is now a function of both position and wave number. Therefore, more numerical computation is needed. Furthermore, when solving an inverse problem, scattering measurements must be made over several different frequencies.

1.6.5 Geometrical Theory of Dirrfaction (GTD)

The inadequacies of the classical techniques of physical optics and geometrical optics are most apparent at points on the scattering body where the radius of curvature is small (such as at edges, corners or vertices), or when the contribution from the geometrical shadow region becomes important. To correct for these defects, Keller (1962) extends geometrical optics by introducing additional rays called diffracted rays. These are rays produced by scattering from sharp edges or points, or discontinuities in curvature of the surfaces of bodies, or by incident rays which graze reflecting surfaces. Keller expresses the complex amplitude of each of his diffracted rays in terms of a diffraction coefficient, which is here denoted by D. Because the electromagnetic field is a vector quantity, D is in general a matrix operator. The diffracted ray E_{diff} can be written (cf. James 1976; Section 4.1 also Section 1.2 of this thesis):

(a) for a vertex ($\rho_1 = \rho_2 = 0$):

$$E_{diff} = D\ E_{inc}\ r^{-1}\ \exp(-j\nu kr) \tag{1.131}$$

where ν is the refractive index of the medium and ρ_1, ρ_2 are the radii of curvature at the diffracting point, r is the distance measured from the point of incidence, and E_{inc} is the incident ray.

(b) for a curved-edge ($\rho_1 = 0$):

$$E_{diff} = D\, E_{inc}\, r^{-\frac{1}{2}} \left[\frac{\rho_2}{\rho_2 + r}\right]^{\frac{1}{2}} \exp(-jvkr) \qquad (1.132)$$

(c) for a straight-edge ($\rho_1 = 0$, $\rho_2 = \infty$):

$$E_{diff} = D\, E_{inc}\, r^{-\frac{1}{2}} \exp(-jvkr) \qquad (1.133)$$

(d) for a surface grazed by the incident ray:

$$E_{diff} = D\, E_{inc} \left[\frac{\rho_1\ \rho_2}{(\rho_1+r)\ (\rho_2+r)}\right] \exp(-jvkr) \qquad (1.134)$$

Each diffracted ray has many of the properties of a direct or reflected ray:

(i) It travels in a straight line (in a homogeneous medium).

(ii) Its magnitude is inversely proportional to the square root of the cross-sectional area of a tube of rays.

(iii) Its phase is proportional to the length of the ray (relative to some arbitrary reference).

(iv) Its polarisation is constant along a ray for a linearly polarised incident ray.

However, a number of pertinent characteristics of a typical diffracted ray deserve special mention:

(v) The rays resembles a cylindrical wave emerging radially from edges or points (Fig. 1.21). At its place of origin the intensity and polarisation of the ray are linearly related to the incident wave by the matrix diffraction coefficient D.

(vi) At places where the cross-section of a tube of rays converges to a point or line (caustic), a correction factor must be introduced to prevent the intensity from becoming infinite.

For simple shapes for which rigorous solutions exist (these are the so-called canonical problems), the diffraction coefficients and caustic correction factors can be obtained by comparing the geometrical-optics solutions with the exact solutions. In the case of a real-world scatterer of complicated shape, the total scattered field can be approximated (often to an impressive accuracy) by vectorially summing the rays emerging from each of the individual diffracting points on the scatterer. Other properties of diffracted rays can be summerised by the three Fermat principles.

(i) Fermat's principle of edge diffraction:

An edge-diffracted ray from a point P to a point Q is a curve which has stationary optical length among all curves from P to Q with one point on the edge. i.e. A diffracted ray and the corresponding incident ray make equal angles with the edge at the point of diffraction, provided they are both in the same medium. They lie on opposite sides of the plane normal to the edge at the point of diffraction. When the two rays lie in different media, the ratio of the sine of the angles between the incident and diffracted rays and the normal plane is the reciprocal of the ratio of the indices of refraction of the two media (i.e. they obey Snell's law).

(ii) Fermat's principle of tip diffraction:

A vertex-diffracted ray from a point P to a point Q is a curve which has stationary optical length among all curves from P to Q passing through the vertex. i.e. A diffracted ray and the corresponding incident ray may meet at a vertex of a boundary surface.

(iii) Fermat's principle of surface diffraction:

A surface-diffracted ray from a point P to a point Q is a curve which makes stationary the optical length among all curves from P to Q having an arc on the boundary surface. i.e. An incident ray and the resulting surface diffracted ray in the same medium are parallel to each other at the point of diffraction and lie on the opposite sides of the plane normal to the ray at this point. When the two rays lie in different media, they obey the law of refraction. The surface ray travels along the surface in a manner determined by the usual differential equations for rays on a surface. Therefore in a homogeneous medium it is an arc of a geodesic or shortest path on the surface.

The geometrical theory of diffraction is one of the many analytical developments in the last two decades that have transformed the design of radiating structures (in radio engineering). One of the earliest examples was given by Kinber (1962) in calculating radiation from a sectoral horn. Although GTD was initially devised on the basis that the diffracting body is large compared with the wavelength, inclusion of higher order diffraction effects can extend this technique, in some cases, to structures having dimensions of less than a wavelength. Examples are given by Yu and Ruddick (1967) on diffraction by a strip and Ruddick and Wu (1969) on parallel plate waveguide radiation. A particularly useful application for GTD is in reflector antenna analysis. The applications discussed by Kinber (1962), James and Kermedelidis (1973), James (1976) are just a few of the many which can be found in the literature.

Important recent developments of the GTD include an accuracy test for high-frequency asymptotic solutions (Mittra 1979), a technique to combine GTD and the moment method (Thiele and Newhouse 1975, BURNSIDE et al. 1975). The book on GTD by James (1976) deserves special mention. The large and rapidly growing literature on GTD is quoted in the aforementioned references and in the references of Tiberio and Kouyoumjian (1979), Pathak et al. (1981) and Luebbers (1984).

Throughout the last quarter century the geometrical theory of diffraction (GTD) has proved very useful for approximately (but nevertheless remarkably accurately) in solving a wide variety of electromagnetic problems

However, virtually all the successful solutions are for perfectly conducting bodies whose corresponding canonical problems can be solved rigorously. Therefore, if the horizons of GTD are to be significantly expanded in the future, it is apparent that additional solutions for penetrable bodies need to be developed. In later chapters, one of the most important cannonical problems, that for the penetrable wedge, is studied in detail.

1.6.6 Physical Theory of Diffraction (PTD)

Just as the geometrical theory of diffraction is an extension of geometrical optics, the physical theory of diffraction is a generalisation of physical optics. Originally, it was Fock (1945) who suggested this method for diffraction around a smooth convex surface, and Ufimtsev (1971) extends the concept to include any shape which deviates from an infinite planar metallic surface.

In the case of planar physical optics, the current existing on the illuminated portion of a perfectly conducting surface is calculated from the incident ray using (1.109). This means that on each element of the body's irradiated surface, the same current is excited as on an ideally conducting surface of infinite dimension tangent to this element. It is obvious that in reality the current induced on the scatterer's surface must differ (as a consequence of the surface curvature) from the value given by (1.109). Bates and Wall (1977) generalise the concept of physical optics (cf. Section 1.6.2.2). Their method becomes exact when the totally reflecting scattering body coincides with a particular coordinate surface.

On the other hand, Ufimtsev (1971) extends physical optics by adding on to the current density J_s (calculated from (1.109)), a current density J_d, which results from the curvature of the scatterer. The total current density is thus

$$J_t = J_s + J_d \tag{1.135}$$

This additional current J_d radiates an edge wave which propagates along the scatterer's surface. Secondary diffraction is also taken into account by J_d.

It is quite clear from (1.135) that Ufimtsev's (1971) approach is similar to Keller's (1962) method of additional 'diffracted' rays. Unfortunately, it is often necessary to evaluate complicated integrals. Furthermore, PTD does not give physical insight into the interaction between the incident wave and the scattering surface. On the other hand, the physical theory of diffraction, being a more sophisticated approach compared to the geometrical theory of diffraction, finds application in the region of caustics and ray boundaries where GTD fails. A comprehensive comparison between the geometrical theory of diffraction and the physical theory of diffraction can be found in Knott and Senior (1974).

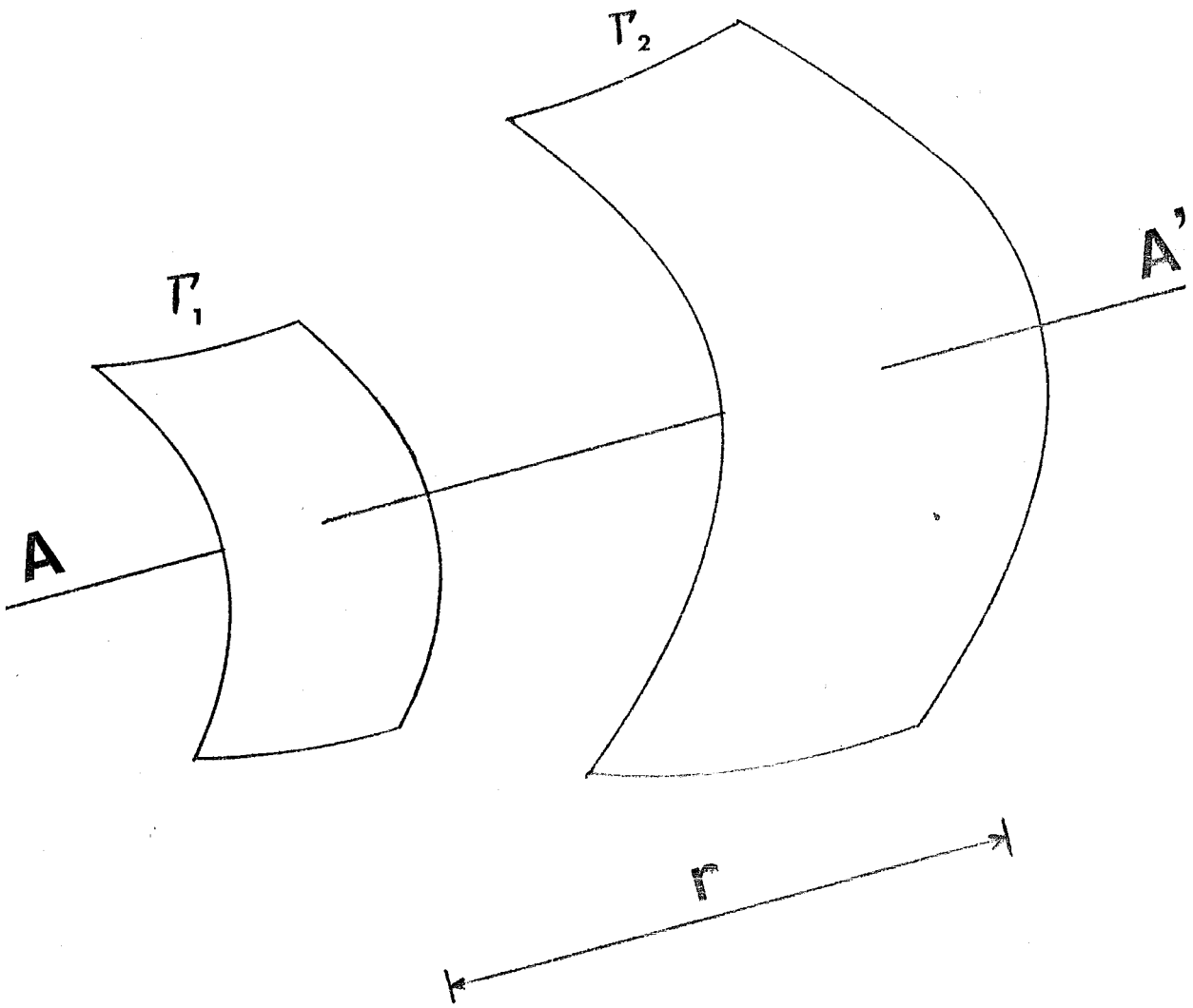

FIGURE 1.1 A pencil of rays. Γ_1 and Γ_2 are successive wavefronts associated with the ray AA.

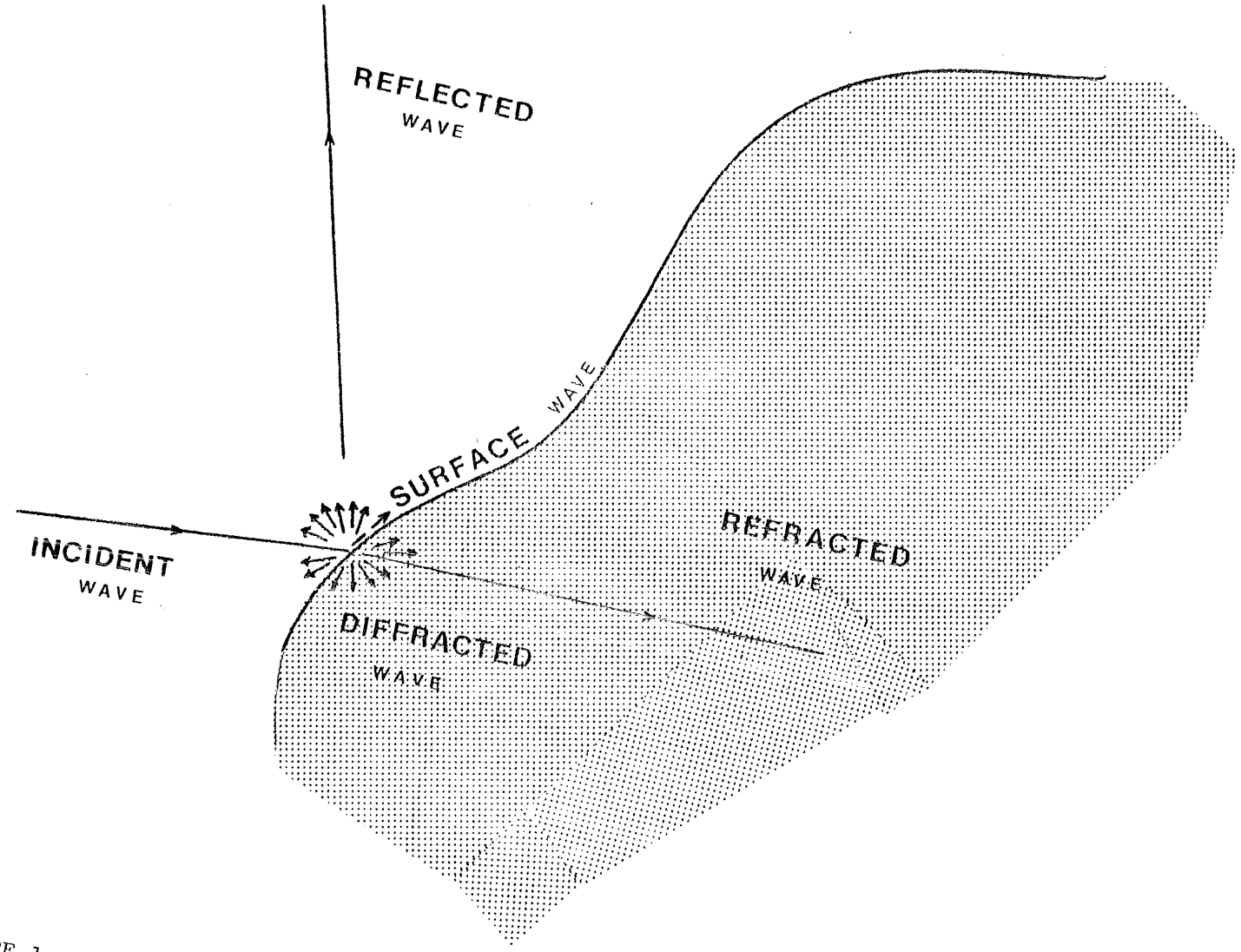

FIGURE 1.2 Reflection and refraction at a general surface. Diffracted waves and surface waves are also generated.

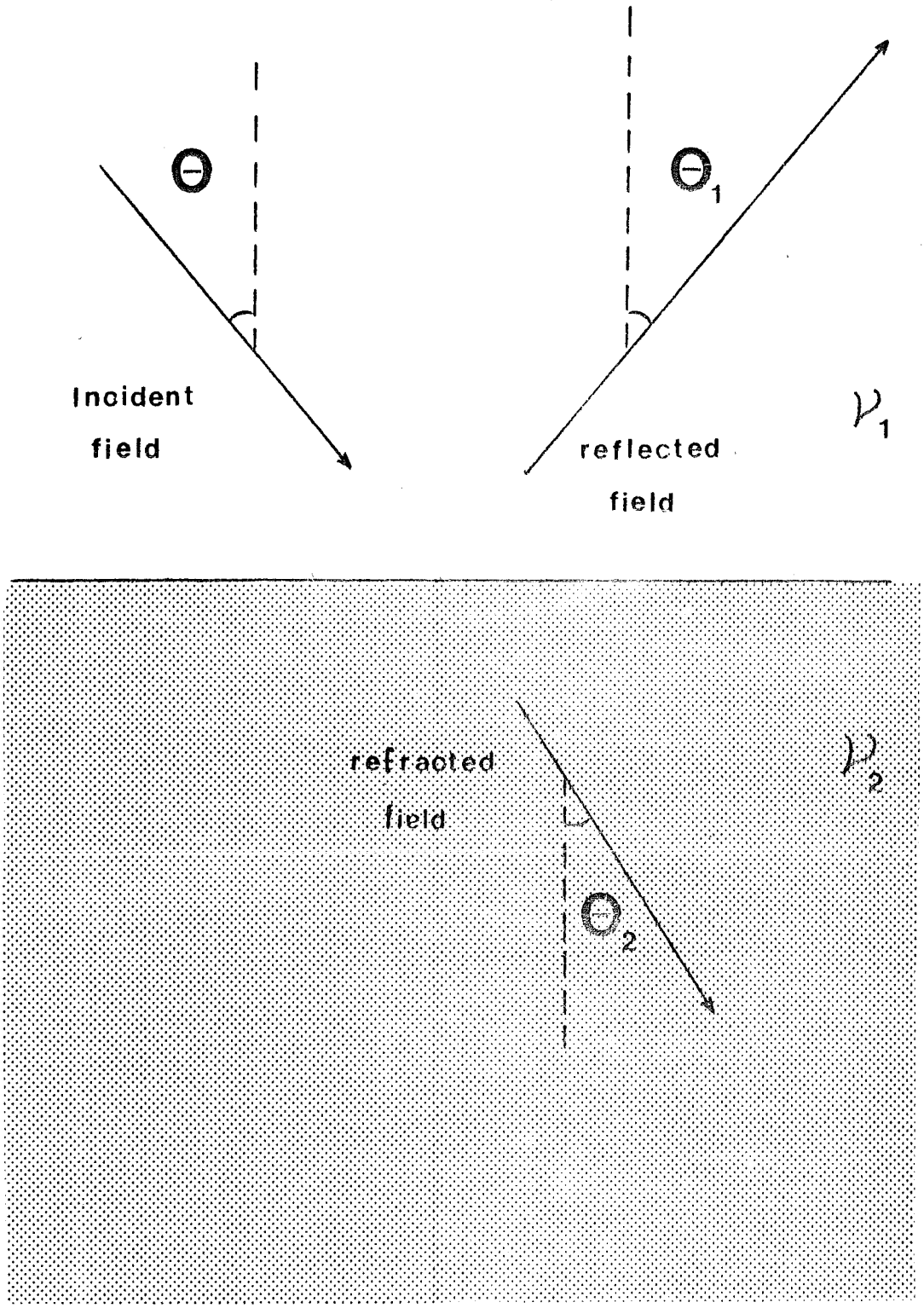

FIGURE 1.3 Refraction at a plane surface. ν_1 and ν_2 are the refractive indexes of the two regions. Snell's law must be satisfied at the interface.

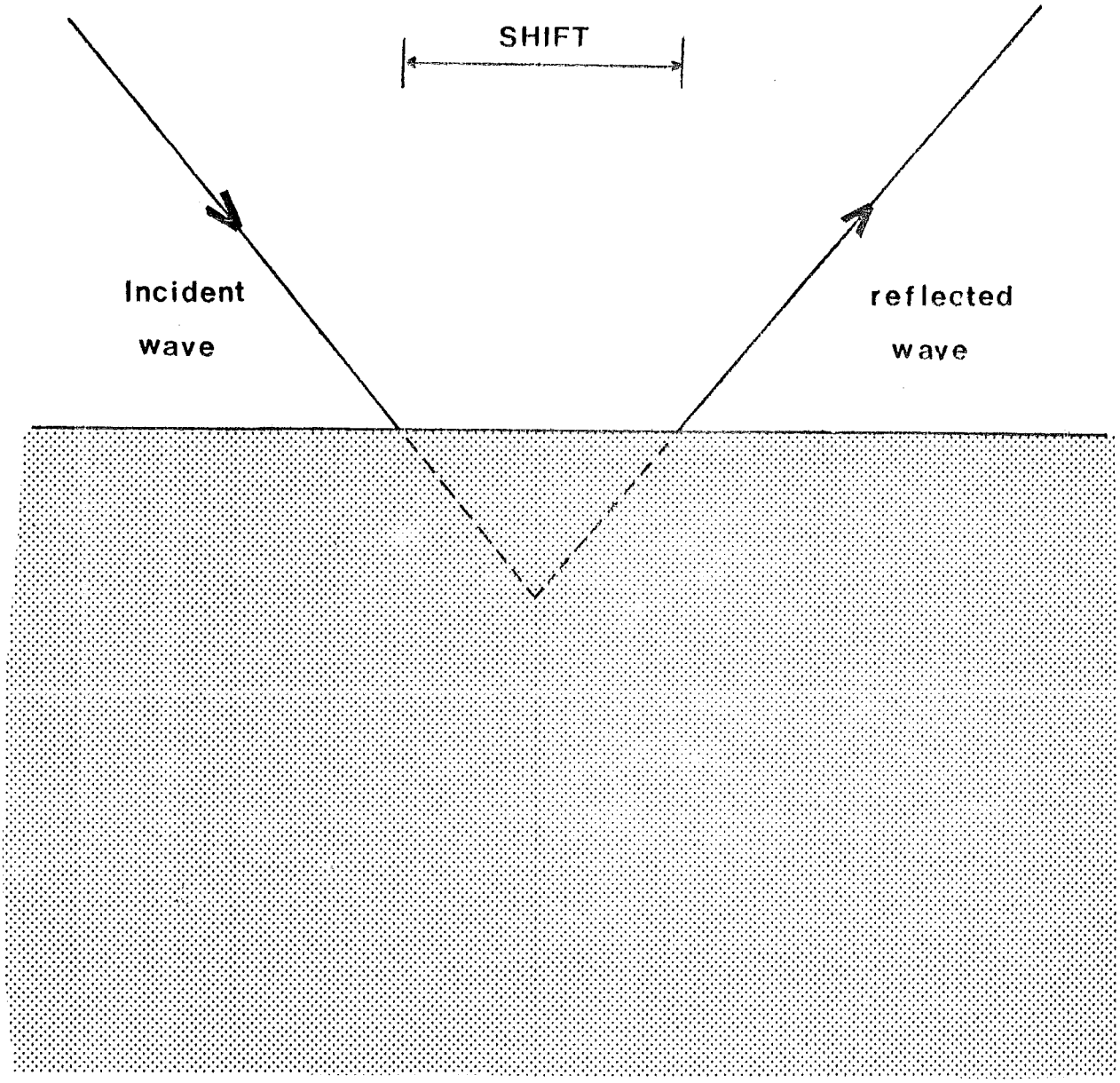

FIGURE 1.4 Goss-Hanchen shift. Energy is transmitted into the less dense (shaded) medium as an evanescent wave. There is a shift in the reflected wave from the incident wave (in the denser medium).

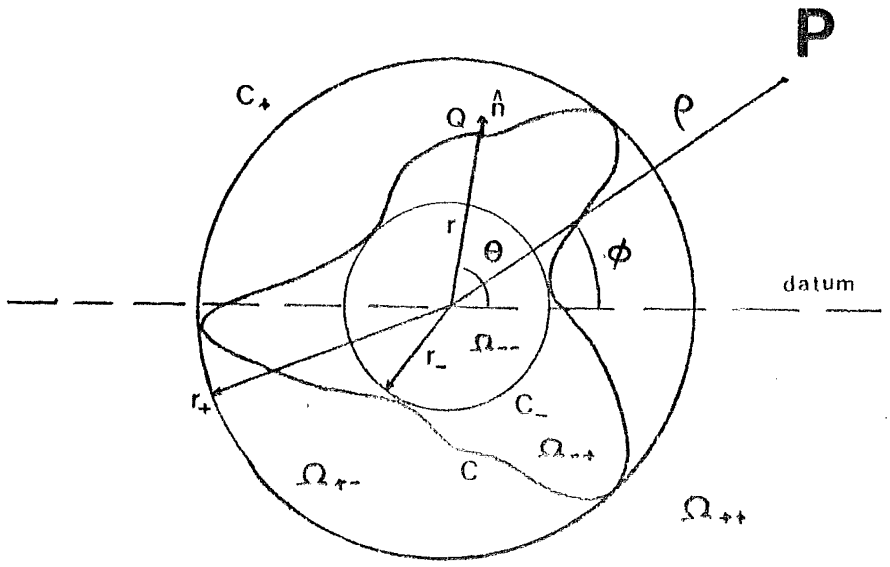

FIGURE 1.5 Partitioning of two-dimensional surface Ω. The region outside the scatterer C is denoted Ω_+. The region inside C is denoted Ω_-. The region inside C_-, a circle inscribing C, is Ω_{--}, while Ω_{-+} is the region within Ω_- but not in Ω_{--}. The region outside C_+, a circle circumscribing C, is Ω_{++}, while Ω_{+-} is the region within Ω_+ but not in Ω_{++}.

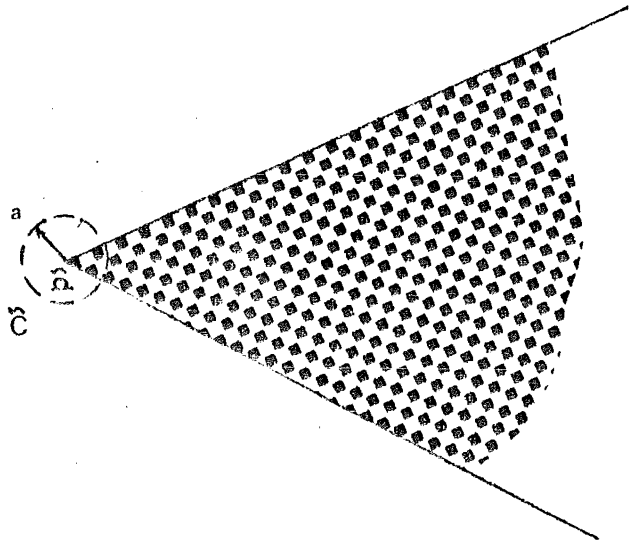

FIGURE 1.6 The neighbourhood of an edge. Power must be conserved in the region $\tilde{\Omega}$ enclosed by a circle $\tilde{C}$ of radius a about the apex.

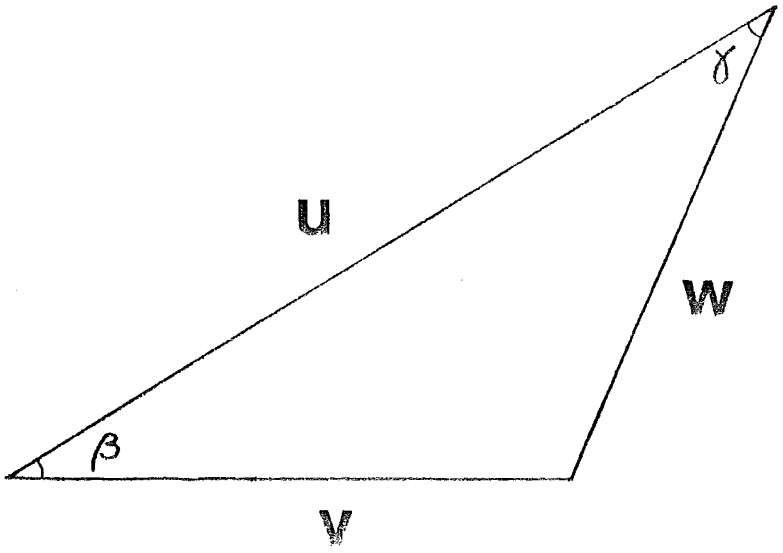

FIGURE 1.7 Geometry used in addition theorem for Bessel functions.

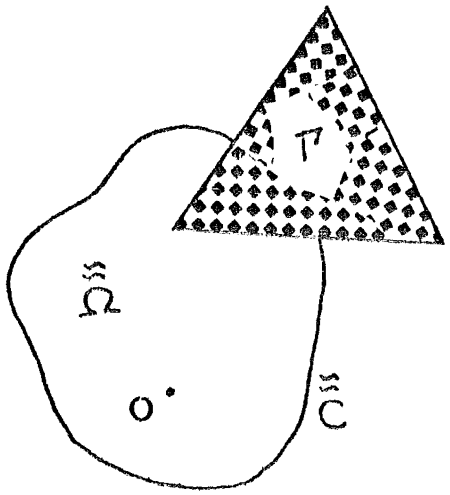

(a)

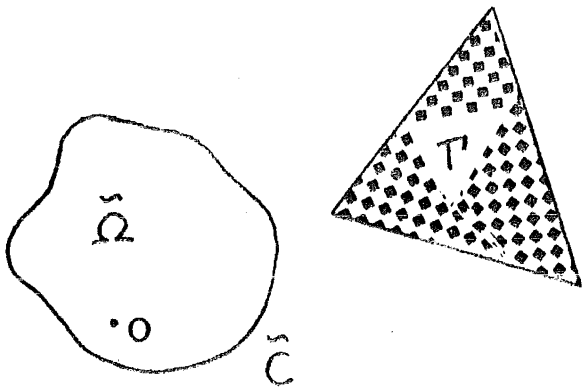

(b)

FIGURE 1.8 Definition of (a) open region $\tilde{\Omega}$, whose boundary $\tilde{C}$ intersects a non-analytic region Γ, (b) closed region $\tilde{\Omega}$, whose boundary $\tilde{C}$ does not intersect Γ.

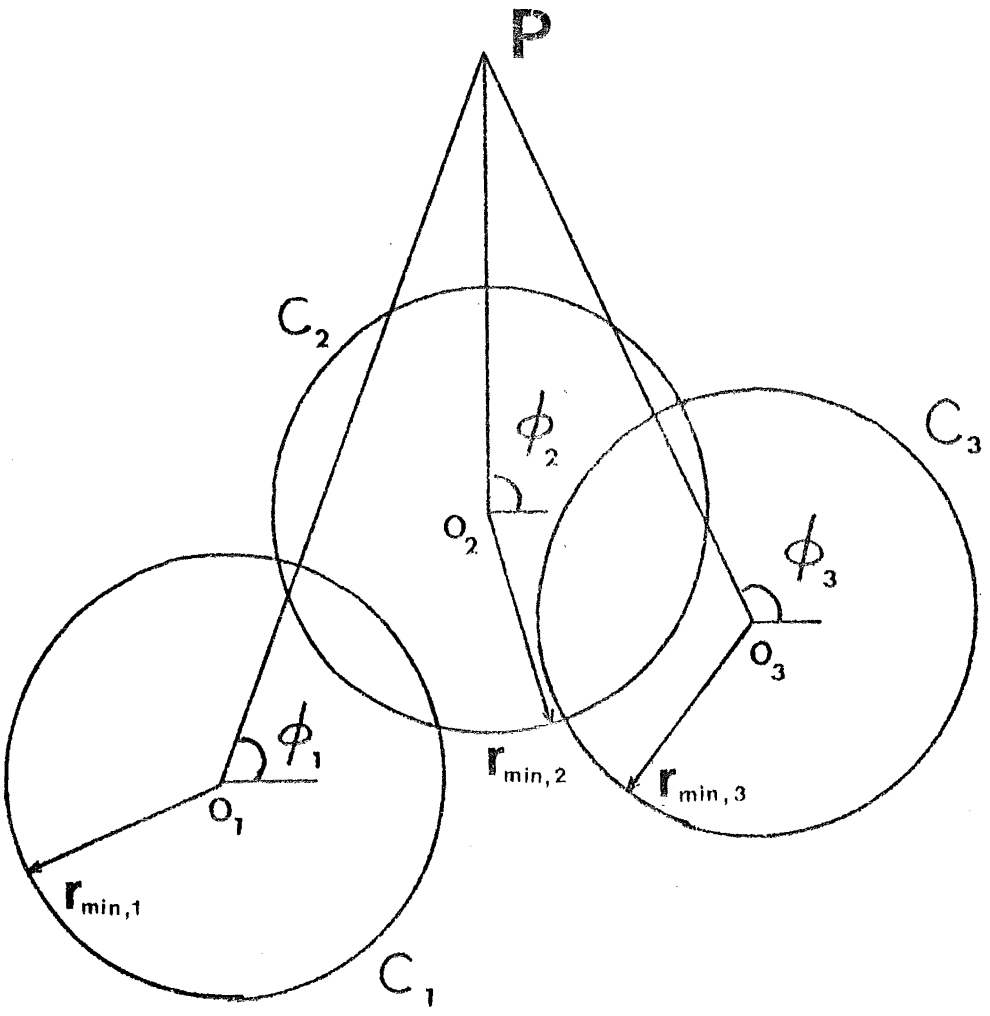

FIGURE 1.9 Coordinates of a point P when referred to origins O_1, O_2, and O_3. The $r_{min,i}$ are the minimum radii of convergence when expanding an electromagnetic field at P with respect to the origins O_i.

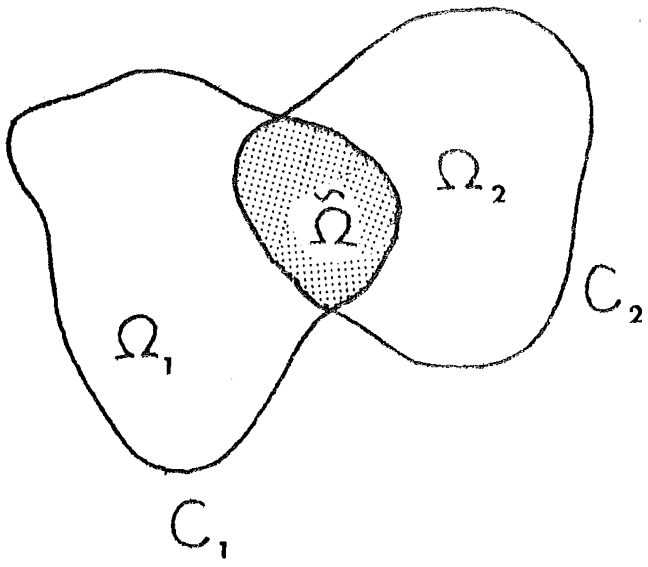

FIGURE 1.10 The common region $\tilde{\Omega}$ of Ω_1 and Ω_2, i.e. $\tilde{\Omega} = \Omega_1 \cap \Omega_2$.

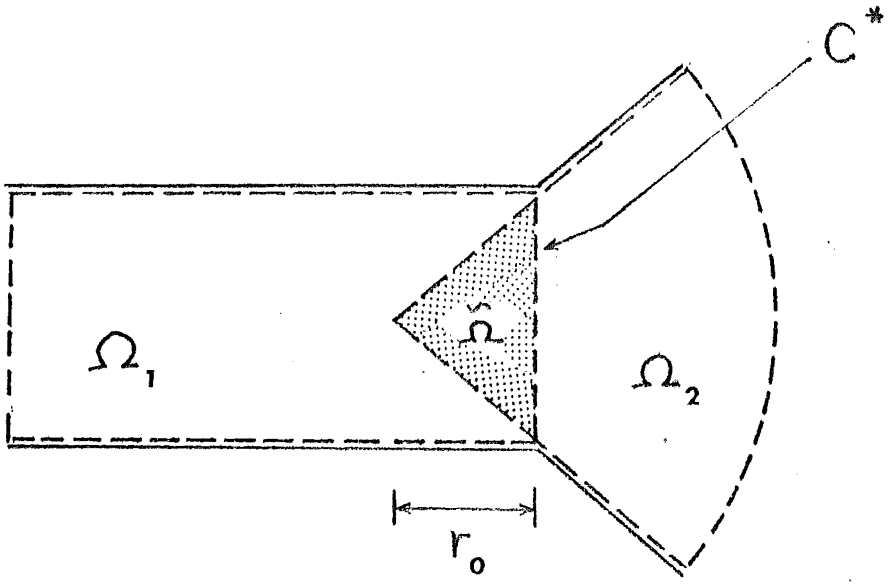

FIGURE 1.11 The sectoral horn can be partitioned into two regions, Ω_1 being the circular cylindrical part and Ω_2 the conical part. The intersecting region is $\tilde{\Omega}$.

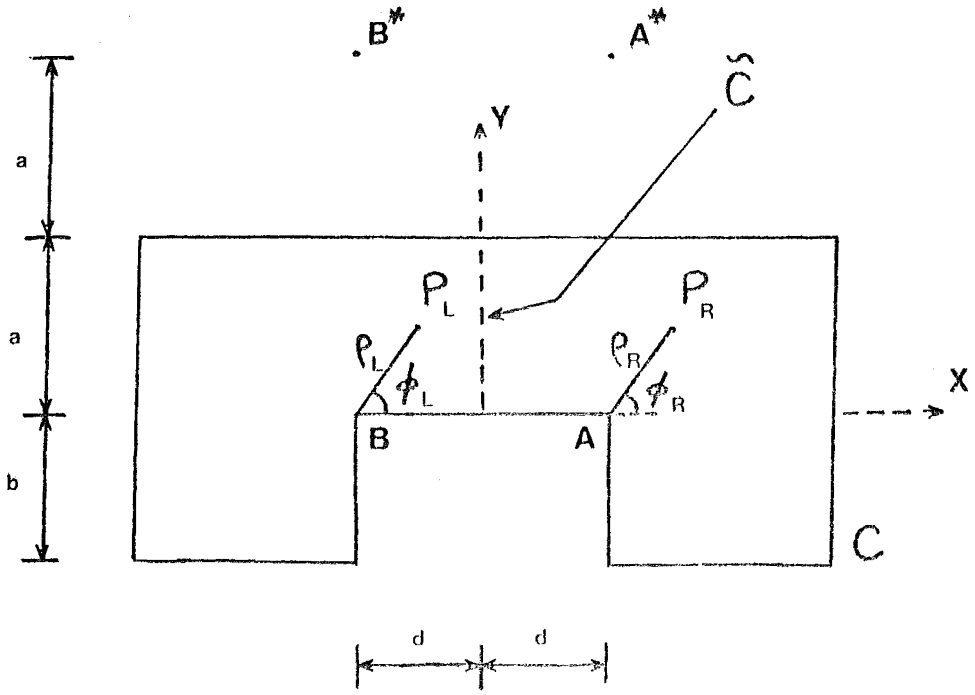

FIGURE 1.12a (a) Geometry of a ridge waveguide. A point in space is denoted by P_R and P_L, and given the coordinates $(\rho_R;\phi_R)$ and $(\rho_L;\phi_L)$, when referred to the points A and B respectively. (b) Point matching of fields on $\tilde{C}$ is possible when $d < \sqrt{3}\ a$. (c) Fields can only be matched on $\tilde{C}_L$ and $\tilde{C}_R$ when $d > \sqrt{3}\ a$.

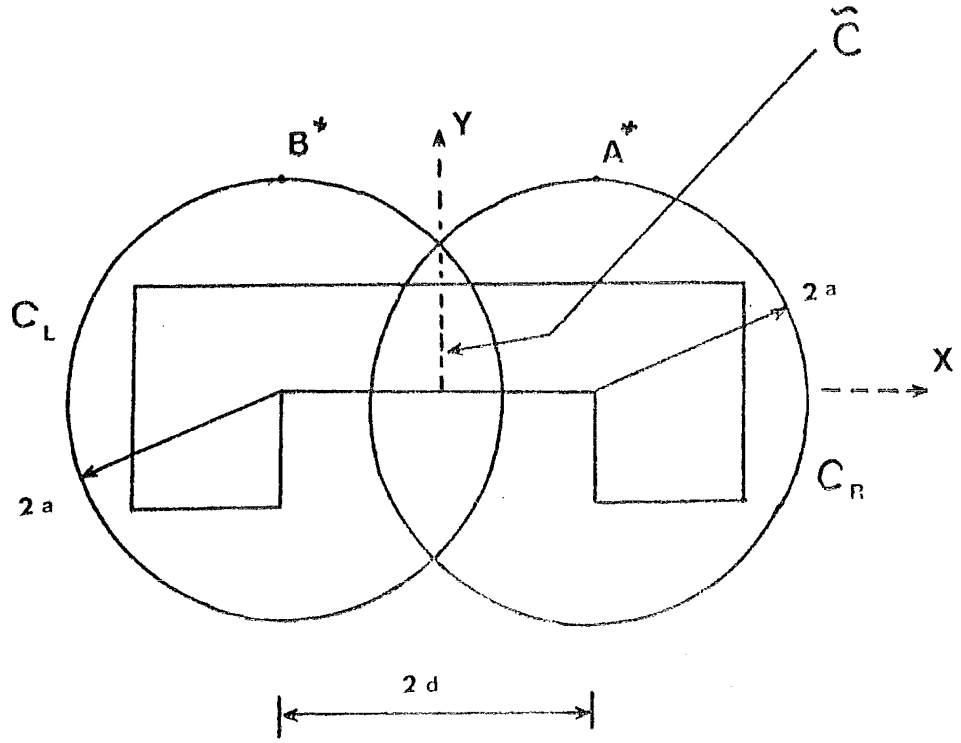

FIGURE 1.12b (a) Geometry of a ridge waveguide. A point in space is denoted by P_R and P_L, and given the coordinates $(\rho_R; \phi_R)$ and $(\rho_L; \phi_L)$, when referred to the points A and B respectively. (b) Point matching of fields on $\tilde{C}$ is possible when $d < \sqrt{3}\ a$. (c) Fields can only be matched on $\tilde{C}_R$ and $\tilde{C}_L$ when $d > \sqrt{3}\ a$.

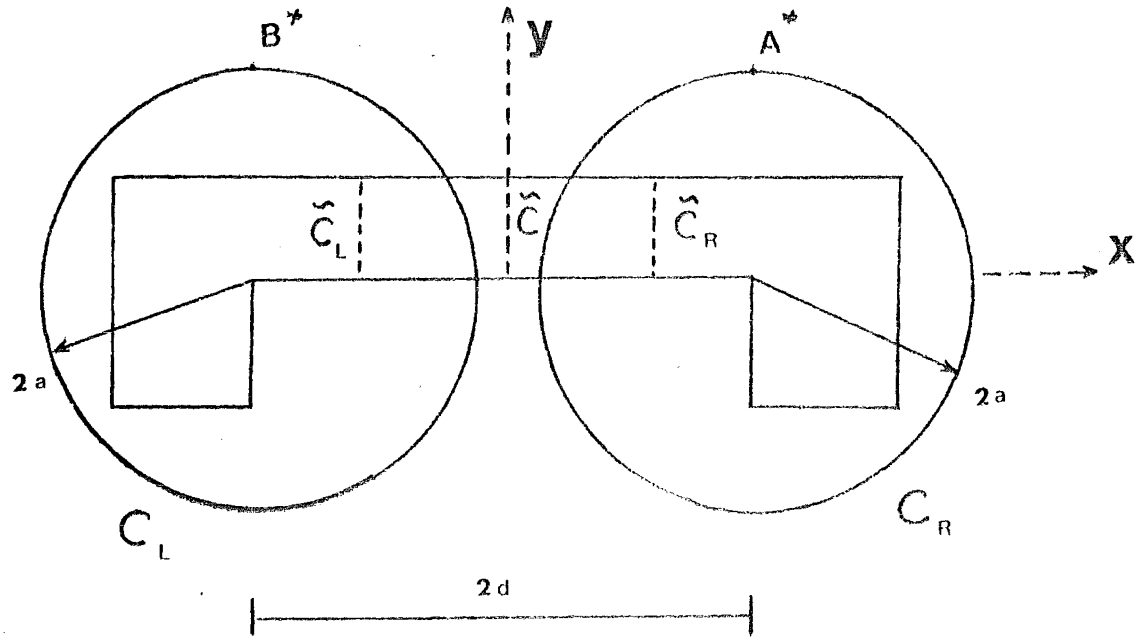

FIGURE 1.12c (a) Geometry of a ridge waveguide. A point in space is denoted by P_R and P_L, and given the coordinates $(\rho_R; \phi_R)$ and $(\rho_L; \phi_L)$, when referred to the points A and B respectively. (b) Point matching of fields on $\tilde{C}$ is possible when $d < \sqrt{3}\ a$. (c) Fields can only be matched on $\tilde{C}_R$ and $\tilde{C}_L$ when $d > \sqrt{3}\ a$.

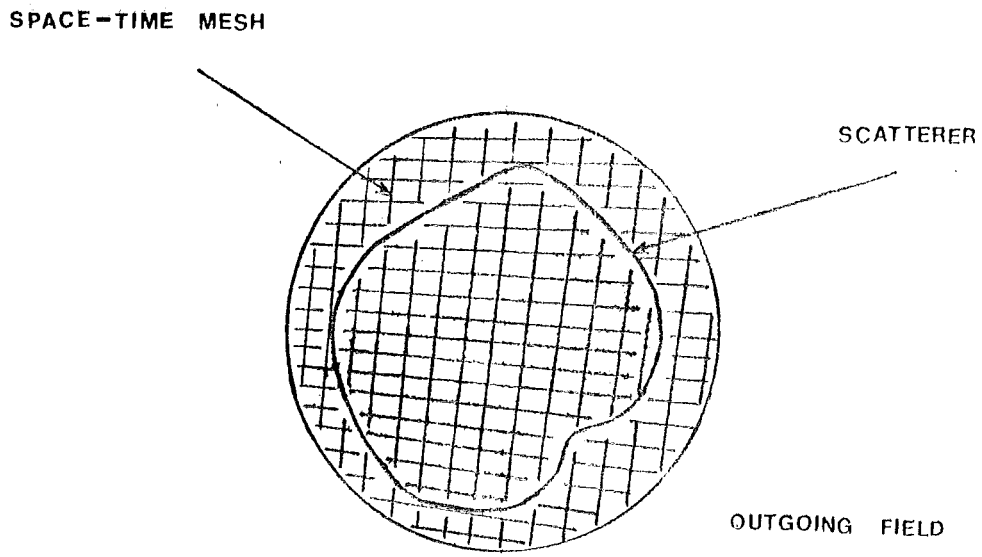

FIGURE 1.13 In the finite difference/finite element technique, the space close to the scatterer is divided into space-time mesh. The field outside this region is modelled as an outgoing field.

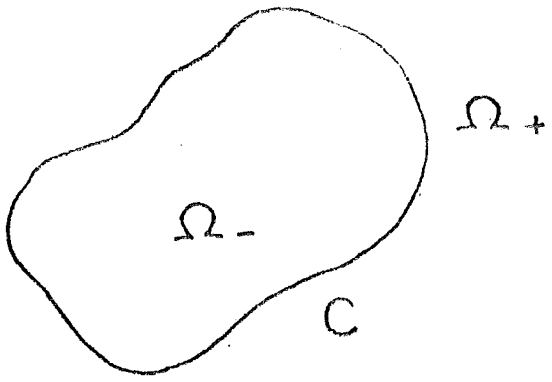

FIGURE 1.14 Two-dimensional space is denoted by Ω. The region within the scatterer is Ω_- and the region outside the scatterer is Ω_+. i.e. $\Omega = \Omega_- \cup \Omega_+$.

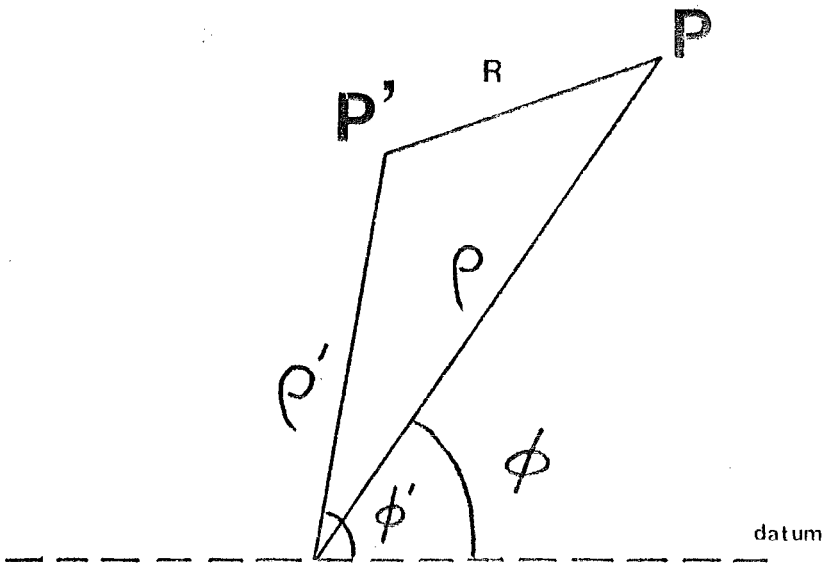

FIGURE 1.15 Coordinates of field point $P(\rho;\phi)$ and source point $P'(\rho';\phi')$.

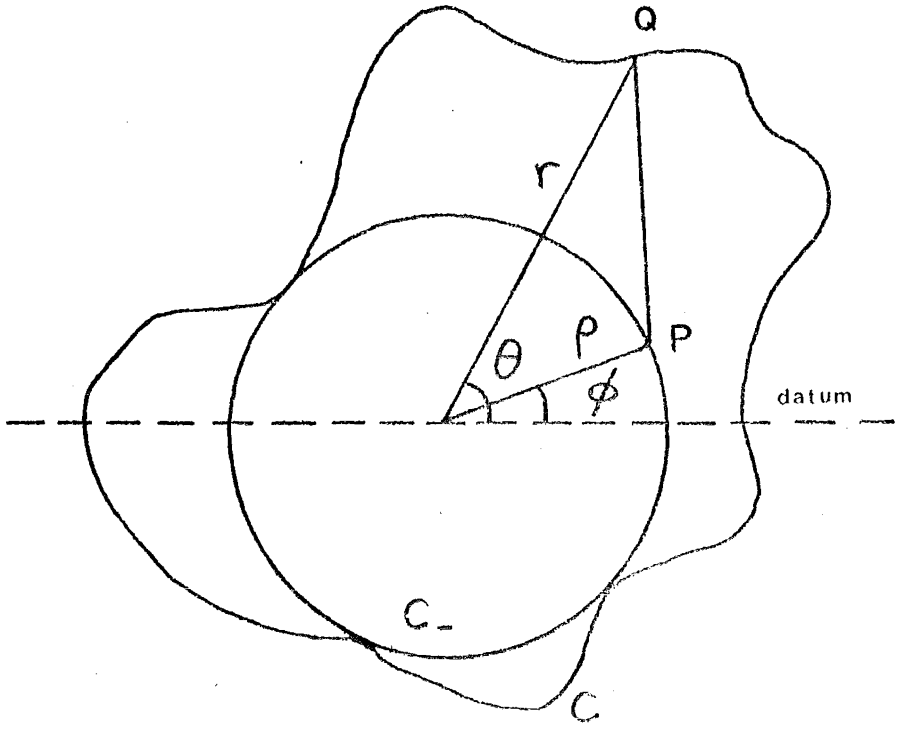

FIGURE 1.16 Coordinate system for scattering problems. A point Q on the boundary C of the scatterer has coordinates $(r;\theta)$. A point P on a circle C inscribing C has the coordinates $(\rho;\phi)$.

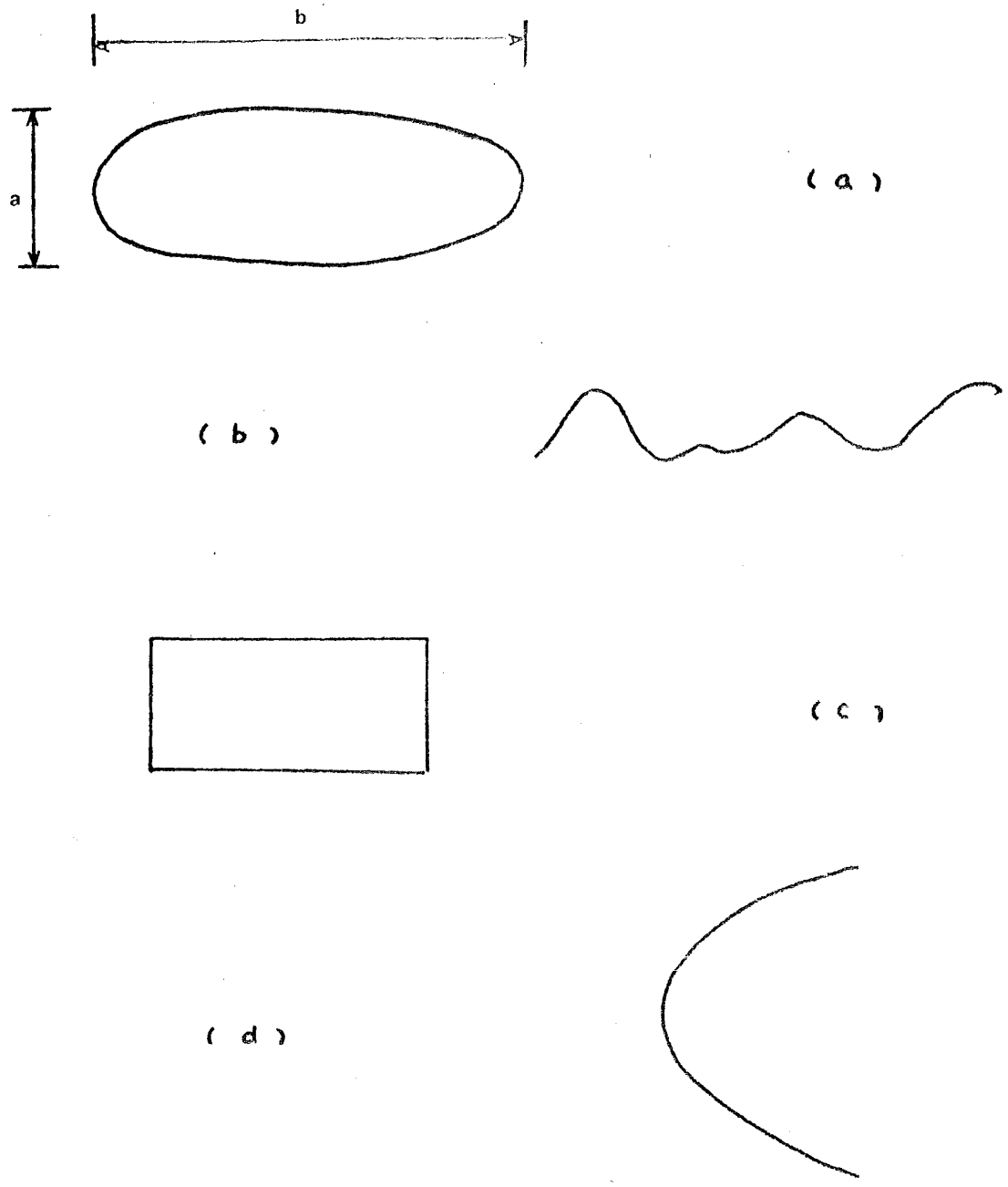

FIGURE 1.17 Four two-dimension canonical scatterers.

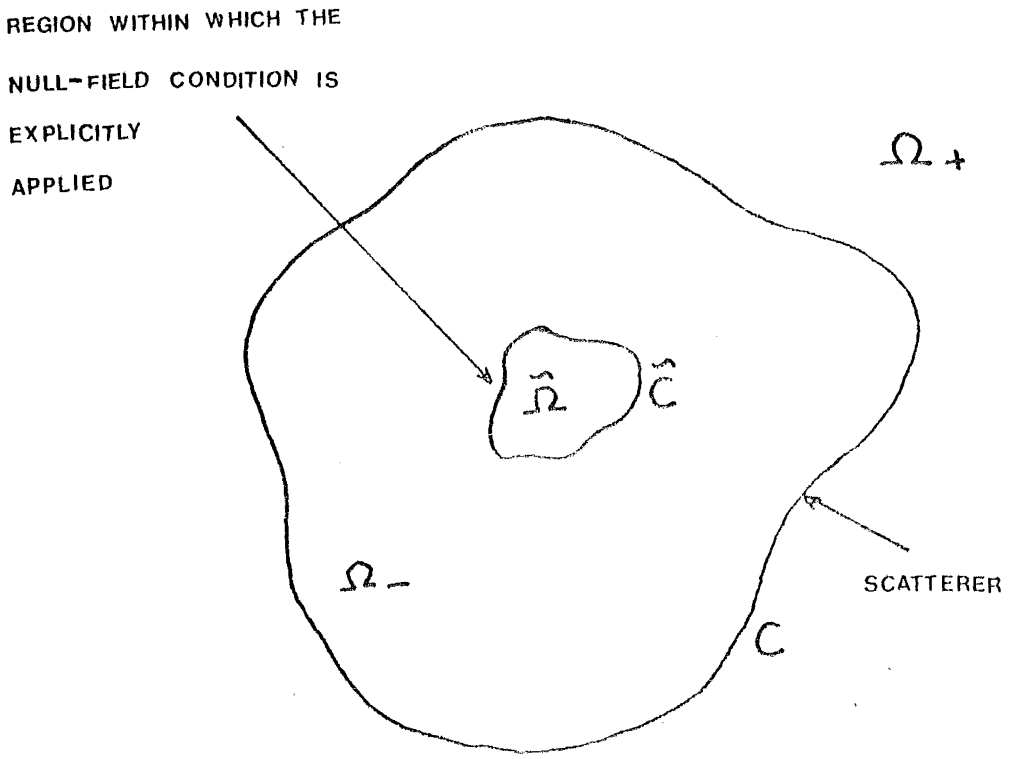

FIGURE 1.18 In theory, the null-field condition can be applied to any region (e.g. $\tilde{\Omega}$) within the scatterer Ω_- for scattering calculation.

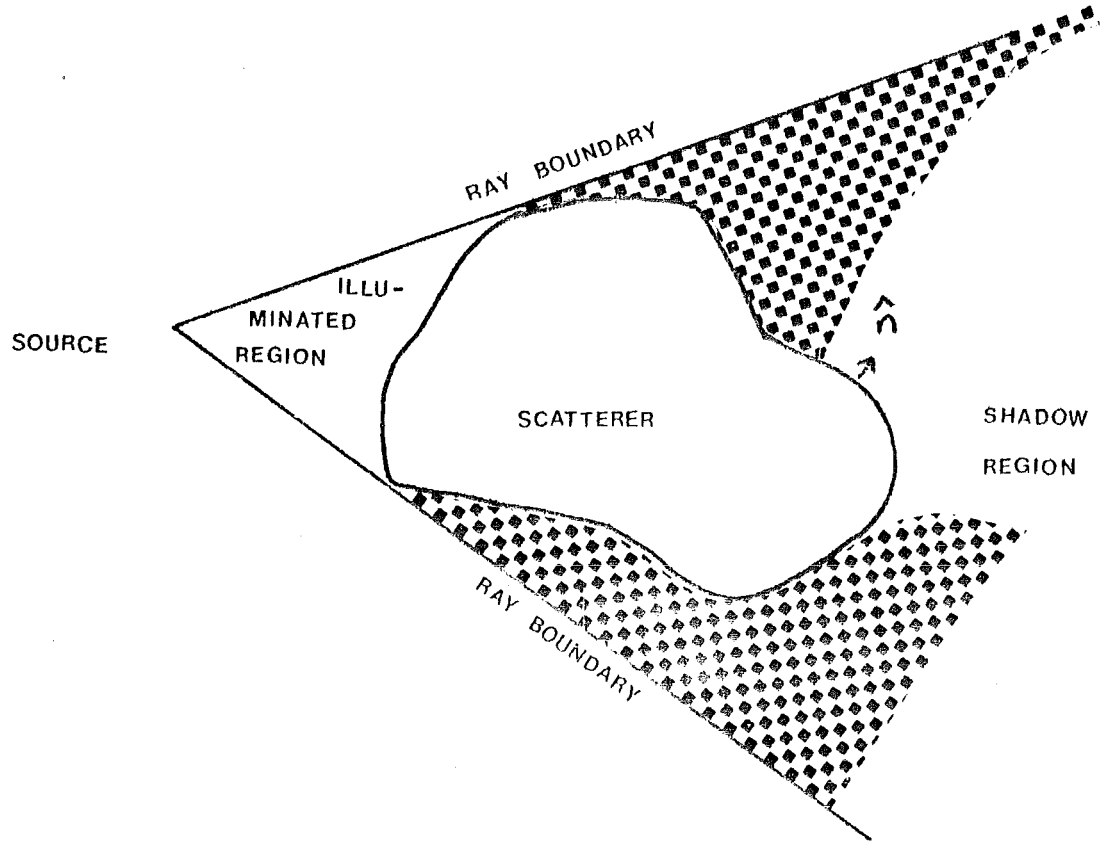

FIGURE 1.19 Illuminated and shadowed (shaded) regions of a scatterer.

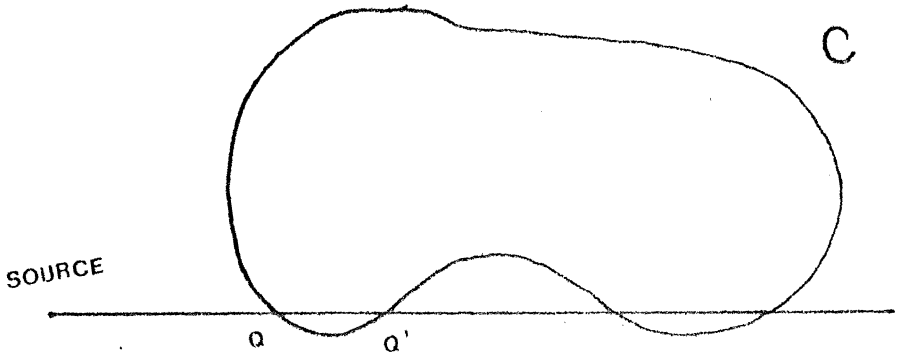

(a)

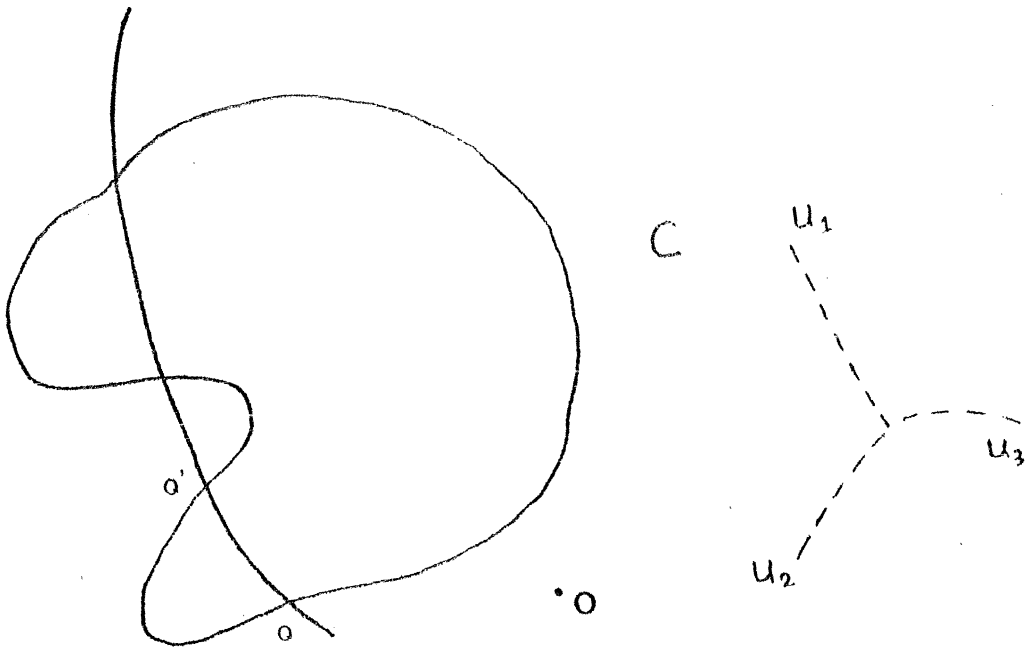

(b)

FIGURE 1.20 (a) Straight ray in planar physical optics. (b) Curved ray in extended physical optics.

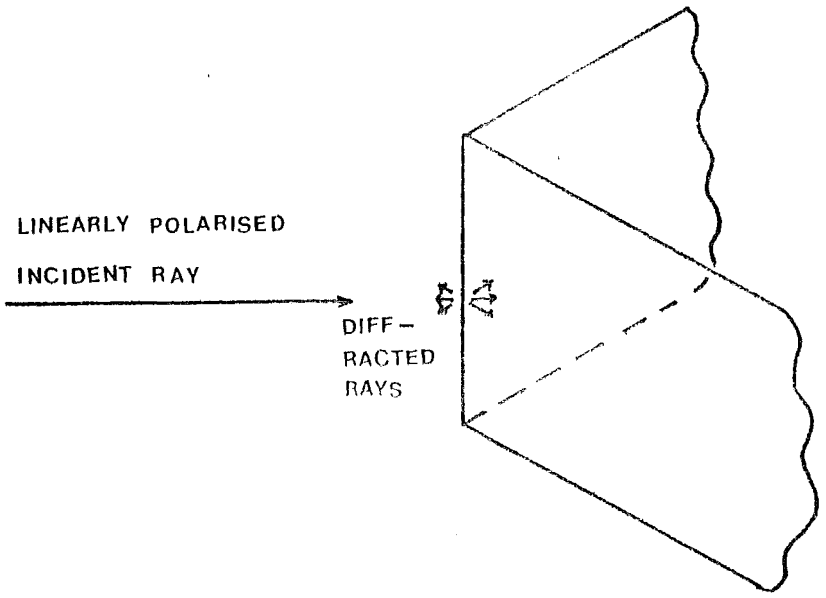

FIGURE 1.21 Edge diffracted rays in the geometrical theory of diffraction They must behave as outgoing waves at a distance far away from the edge.

CHAPTER TWO

ASPECTS OF INVERSE SCATTERING

2.1 INTRODUCTION

The general direct and inverse problems are defined in Section 1.1. While Chapter 1 is devoted to the direct problem, the inverse problem is discussed in this chapter.

An every-day example of an inverse problem is the inference by a human brain of the size, shape, surface texture and material composition of an object from the light, which it emits and scatters, detected by a pair of eyes. Another more sophisticated example is provided by medical radiography, in which properties of tissues are deduced from the attenuation of X-ray beams passing through human bodies. The concern in this chapter is with the theory of techniques which permit inverse scattering problems to be solved either accurately or approximately by operating in computers on measured data.

Let the field incident upon a scatterer be defined by the set

$$D = \{d_1, d_2, \ldots . d_\ell\} \tag{2.1}$$

of space-time functions d_i (here called probing functions). When an incident field impinges on the scatterer it induces re-radiating sources in it. Let the set

$$G = \{g_1, g_2, \ldots . g_m\} \tag{2.2}$$

of space-time functions g_i (here called distribution functions) represent these induced sources. The set

$$F = \{f_1, f_2, \ldots . f_k\} \tag{2.3}$$

of space-time functions f_i represent the measured fields re-radiated by the induced sources.

The sets D and F constitute the data for the inverse scattering problem, the goal of which is to quantitatively infer as much as possible concerning the set P of the parameters characterising the physical properties of the scatterer, where

$$P = \{p_1, p_2, \ldots p_j\} \tag{2.4}$$

Note that the sets D and P constitute the data for the direct

scattering problem, which leads to a unique F through the set

$$E = \{e_1, e_2 \ . \ . \ . \ . \ e_n\} \tag{2.5}$$

of operators, each generates a scattered field, i.e. $e_i(D,P|G) \rightarrow f_i$, where the vertical line between P and G reminds the reader that the set G must be constructed, whether implicitly or explicitly, before F can be generated. All this is conveniently summarised by the mapping

$$E : D, G \rightarrow F \tag{2.6}$$

2.2 COHERENCE, INCOHERENCE AND PARTIAL COHERENCE

The concept of coherence, or equivalently incoherence, can be thought of as the measure of correlation between two sources (or electromagnetic waves). As mentioned in Section 1.2, the variation of intensity in an electromagnetic beam can be described in terms of changes in the cross-sectional area of a tube of rays. However, when two beams are superimposed, the distribution of intensity then depends on the degree of coherence of the beams. If the two beams originate from the same source, their fluctuations are in general correlated, and the intensity in the region of superposition varies from point to point between maxima which exceed the sum of the intensities in the individual beams, and minima which may be zero. This phenomenon is called interference. When the beams come from different sources, the fluctuations are in general only partially correlated when averaged over times long compared to the reciprocal of the bandwidths of the beams. For time short compared to these, full interference is manifest. However, for the longer times, if the two sources are statistically independent (or incoherent as is usually said), the interference disappears, so that the total intensity at any point is the sum of the intensities of the two beams. When many beams (a typical one represented by the wave function ψ_i) are present their averaged (over times long compared to their reciprocal bandwidths) intensities are given by

$$I_{incoh} = \sum_i |\psi_i|^2 \tag{2.7}$$

when the sources are completely incoherent, and

$$I_{coh} = \left|\sum_i \psi_i\right|^2 \tag{2.8}$$

when the sources are fully coherent (cf. Beran and Parrent 1974).

Virtually all naturally occurring sources of electromagnetic radiation are incoherent, in the sense that the effective widths of the autocorrelation functions of the densities of the sources are a few wavelengths at most. The great majority of optical imaging theory, for instance, relates only to incoherent radiation (cf. Born and Wolf 1970, Chapter 10), two important characteristics of which are its linearity and statistical stationarity.

(1) Linearity

A system is linear if the addition of inputs produces simply an addition of corresponding outputs. Thus, if $g_1(x)$ is an input that produces an output $f_1(x)$ denoted by

$$g_1(x) \longrightarrow f_1(x) \tag{2.9a}$$

and if

$$g_2(x) \longrightarrow f_2(x) \tag{2.9b}$$

then

$$ag_1(x) + bg_2(x) \longrightarrow af_1(x) + bf_2(x) \tag{2.9c}$$

(2) Stationarity

Stationarity implies that if the location of the input is changed, i.e. $g_1(x)$ is replaced by $g_1(x-x_o)$, the only effect on the output is to correspondingly change its location; i.e.

$$g_1(x-x_o) \longrightarrow f_1(x-x_o) \tag{2.10}$$

More importantly, the possibility of obtaining unique solutions to inverse source problems depends very much on knowledge of the coherence properties of the radiated field. When the sources exhibit any degree of mutual coherence, it is possible to solve the inverse problem uniquely (see Section 2.3 for further discussion on uniqueness) if and only if the sources are situated on a closed surface. However, for incoherent sources in free space, it is always possible to obtain unique solutions to inverse source problems.

For virtually all inverse scattering problems, the fields exhibit finite degrees of mutual coherence, and there does not seem to be any advantage in taking the coherence properties of these fields into account. Traditional approaches to inverse scattering are introduced in Sections 2.3 and 2.4.

General fields are neither fully coherent nor strictly incoherent. Two points worth noting are:

(i) Strictly incoherent and strictly coherent fields are physically unobtainable and are only mathematical idealizations.

(ii) One cannot ignore the possibility of intermediate states of coherence, i.e. what happens conceptually if some strictly coherent light and some strictly incoherent light are mixed?

Consideration of the above two points leads naturally to the concept of the complex degree of coherence (cf. Beran and Parrent 1974).

(a) Spatial Coherence:

Let $\psi_n(t) = \psi(x_n,t)$ and $\psi_{P_1}(t)$, $\psi_{P_2}(t)$ be two wavefronts at points P_1 and P_2 (Fig. 2.1) respectively. Let P be the point where the two wavefronts meet and r_1 and r_2 be the distances P_1P and P_2P respectively. Then, at P

$$\psi_P(t) = \psi_{P_1}(t-t_1) + \psi_{P_2}(t-t_2) \tag{2.11}$$

where $t_1 = r_1/c$ and $t_2 = r_2/c$ and c is the speed of light in the medium. The resultant intensity at P is an observable quantity and is the time averaged measure given by

$$I_P = \langle \psi_P(t)\ \psi_P^*(t) \rangle \tag{2.12}$$

where the angular brackets denote a time average, i.e.

$$\langle f(t) \rangle = \lim_{T\to\infty} 1/2T \int_{-T}^{T} f(t)\ dt \tag{2.13}$$

Hence

$$\begin{aligned} I_P = {} & \langle \psi_{P_1}(t-t_1)\ \psi_{P_1}^*(t-t_1) \rangle \\ & + \langle \psi_{P_2}(t-t_2)\ \psi_{P_2}^*(t-t_2) \rangle \\ & + \langle \psi_{P_1}(t-t_1)\ \psi_{P_2}^*(t-t_2) \rangle \\ & + \langle \psi_{P_2}(t-t_2)\ \psi_{P_2}^*(t-t_1) \rangle \end{aligned} \tag{2.14}$$

Writing

$$\tau = t_2 - t_1 \tag{2.15}$$

(2.14) then becomes

$$I_P = I_{P_1} + I_{P_2} + 2 \text{ Real } (\Gamma_{12}(\tau)) \tag{2.16}$$

where

$$I_{P_1} = \langle \psi_{P_1}(t)\ \psi^*_{P_1}(t) \rangle \tag{2.17a}$$

$$I_{P_2} = \langle \psi_{P_2}(t)\ \psi^*_{P_2}(t) \rangle \tag{2.17b}$$

$$\Gamma_{12}(\tau) = \langle \psi_{P_1}(t+\tau)\ \psi^*_{P_2}(t) \rangle \tag{2.17c}$$

The term $\Gamma_{12}(\tau)$ is a cross correlation function and is called the mutual coherence function while I_{P_1} and I_{P_2} are autocorrelation functions which are appropriately rewritten as $\Gamma_{11}(0)$ and $\Gamma_{22}(0)$, respectively. They are conventionally called self-coherence functions.

The complex degree of coherence $\gamma_{12}(\tau)$ is defined by

$$\gamma_{12}(\tau) = \Gamma_{12}(\tau) / \left[\Gamma_{11}(0)\Gamma_{22}(0)\right]^{\frac{1}{2}} \tag{2.18}$$

(b) Temporal coherence:

Temporal coherence effects arise from the finite spectral width of the source radiation. Strictly monochromatic radiation is, of course, perpetually coherent. However, if the sources have a narrow but finite spectral width, and if

$$\Delta f << \bar{f} \tag{2.19}$$

where $\bar{f}$ is the mean frequency and Δf the width of the spectrum, then one can define the mutual intensity function μ_{12} by

$$\mu_{12} = \Gamma_{12}(0) = \langle \psi_{P_1}(t) \psi^*_{P_2}(t) \rangle \tag{2.20}$$

now the source is assumed to be at P while P_1 and P_2 are the observation points.

If the source is small but of finite size, one may also write

$$\mu_{12} = \exp(j\left[(|\underline{x}_{P_1}|^2 - |\underline{x}_{P_2}|^2)/(r_1+r_2)\right]) \iint_{\Omega} |\psi(\underline{x}',t)|^2 \exp(2jk\left[\underline{x}_{P_1} - \underline{x}_{P_2}\right]/ \left[r_1+r_2\right])\ d\underline{x}' \Big/ \iint_{\Omega} |\psi(\underline{x}',t)|^2\ d\underline{x}' \tag{2.21}$$

for $|\underline{x}_{P_1} - \underline{x}_{P_2}| << r_1, r_2$, where $\underline{x}_{P_1}$ and $\underline{x}_{P_2}$ are the position vectors of P_1 and P_2 respectively and Ω is the volume enclosing the source. It is seen

from (2.21) that one can say that $|\mu_{12}|$ is equal to the absolute value of the normalized Fourier transform of the intensity function of the source. Detailed treatments of partially coherent fields and their applications can be found in the books by Born and Wolf (1970) and Beran and Parrent (1974).

2.3 DIMENSIONALITY DIFFICULTY, UNIQUENESS AND STABILITY

2.3.1 Dimensionality Difficulty

Consider Fig. 2.2 which applies to a situation where a perturbed field is measured on the circle C with radius b outside a scattering domain Γ with radius a. Within the scattering domain is embedded a medium characterised by a generalised constitutive parameter $\Lambda(\rho;\phi)$. Denoting the total field and scattered field by ψ and ψ_{sc} respectively, the polarisation source formulation (cf. Bates and Ng 1972) gives

$$\psi_{sc}(b;\theta,k) = -jk^2/4 \int_0^a \int_0^{2\pi} [\Lambda(\rho;\phi,k)-1]\ \psi(\rho;\phi,k)\ H_o^{(2)}(kR)\rho d\phi d\rho \tag{2.22}$$

where

$$R = (b^2 + \rho^2 - 2b\rho\cos(\theta-\phi))^{\frac{1}{2}}$$

ψ_{sc} can be expanded in the following trigonmetric Fourier series (see Section 1.4)

$$\psi_{sc}(b;\theta,k) = -jk^2/4 \sum_{m=-\infty}^{\infty} A_m(b,k)\ H_m^{(2)}(kb)\ \exp(jm\theta) \tag{2.23}$$

and the Hankel function in the integral of (2.22) is given by (using the Addition Theorem for Bessel functions (Watson 1966, Section 11.3):

$$H_o^{(2)}(kr) = \sum_{m=-\infty}^{\infty} H_m^{(2)}(kb)\ J_m(k\rho)\ \exp(jm(\theta-\phi)) \tag{2.24}$$

Substituting (2.23) and (2.24) into (2.22) and equating the Fourier coefficient then gives

$$A_m(b,k) = A_m(k) = \int_0^a \int_0^{2\pi} [\Lambda(\rho;\phi)-1]\ \psi(\rho;\phi,k)\ J_m(k\rho)\ \exp(-jm\phi)\ \rho d\phi d\rho \tag{2.25}$$

for all integers m.

Inspection of (2.22) and (2.25) reveals that the measured data are two-dimensional in the sense that they are characterised by sets of two variable parameters (θ,k) or (m,k), and it is clear from (2.25) that no more information

is gained by making measurements on more than one circle, since (2.25) is not a function of b.

In any particular physical situation, the generalised constitutive parameter $\Lambda(\rho;\phi,k)$ can be expressed as a sum of terms each having a simple k-dependence, and is therefore regarded as a two-dimensional, rather than a three-dimensional, unknown. However, $\psi(\rho;\phi,k)$ is essentially a three-dimensional unknown. It is therefore impossible to invert either (2.22) or (2.25) straightforwardly to obtain a solution for $\Lambda(\rho;\phi)$, unless means can be found to eliminate or approximate $\psi(\rho;\phi,k)$. This is what Bates (1984) calls the dimensionality difficulty. What one does is, first measure the perturbed fields for a general set of (θ,k) or (m,k) and then attempt to formulate algorithm for reconstructing $\Lambda(\rho;\phi)$. Note that the perturbed field must always be measured for more than one frequency in order to evaluate $\Lambda(\rho;\phi)$ to a specific accuracy.

Bates (1984) decomposes the incident wave (probing function) into its ℓth partial wave; i.e.

$$\Psi_{inc} = \sum_{\ell=-\infty}^{\infty} \Psi_{\ell} \exp(j\ell\phi) \tag{2.26}$$

and defines $Z_{\ell m}$ as the mth component of the impedance (measured on the measurement circle in Fig. 2.2) with respect to the ℓth partial wave as

$$Z_{\ell} = \Psi_{\ell}/\partial\Psi_{\ell}/\partial\rho = \sum_{m=-\infty}^{\infty} Z_{\ell m} \exp(jm\theta) \tag{2.27}$$

Bates (1984) then proceeds to derive a system of homogeneous equations. After setting its determinant to zero for non-trivial solutions, he obtains an expression of the form

$$D_{\ell}(k,\Lambda(\rho;\phi),\ Z_{\ell m}) = 0 \tag{2.28}$$

which must be solved for all l and k. Note that LHS (2.28) exhibits no explicit dependence upon b.

2.3.2 Uniqueness and Stability

In the far field - near field reconstruction problem (cf. Deschamps and Cabayan 1972, Cabayan et al. 1973) often encountered in antenna aperture pattern analysis, the field up to the antenna aperture is to be reconstructed from knowledge of the measured far field. It has been shown (Baltes 1978) that uniqueness can be ensured in this case.

Unfortunately, in general at least, knowledge of a field outside a scattering region is not necessarily sufficient to enable one to reconstruct the object (or source distribution) uniquely. It is quite possible to construct a physically realizable potential (or equivalently a scalar index of refraction) such that any member of a finite set of incoming monochromatic plane waves with different wave vector leads to a vanishing scattered field outside the object (c.f. Devaney and Sherman 1982). Moreover, many charge-current distributions can be non-radiating, and therefore necessarily lead to at most a static field outside the distribution. A classic example of the non-unique nature of inverse (source) problems is illustrated in Fig. 2.3, where uniform source distributions (of appropriate amplitudes) on C_3, C_2, C_1 or 0 produce identical fields at all points P outside C_3.

However, a unique solution may be obtained if additional information is available. For example, to be aware that the radiation emitted by a source distribution is spatially incoherent is to be presented with a highly significant piece of prior information. Similarly, the source density can be constructed (regardless of the degree of coherence), if it only has value on a known surface.

Hadamard (1923) introduced the concept of ill-posedness in the field of partial differential equations. The inverse problem is ill-posed in the sense that the measured scattered field must be continued back inside the scatterer in order to be able to solve the problem. Consider the following Fredholm integral equation of the first kind:

$$\int_a^b f(x')\ K(x,x')\ dx' = g(x)\ , \quad c \leq x \leq d \tag{2.30}$$

where the kernel K(x,x') is continuous in both x and x'. Assuming that there exists a unique solution f corresponding to g, one might add to that solution a function $f_n(x) = C_n \sin(nx)$ where C is an arbitrary constant. But the Riemann-Lebesgue theorem (Pogorzeski 1966) states that

$$\lim_{n\to\infty} \int_a^b K(x,x')\ \sin(nx')dx' = 0 \tag{2.31}$$

Hence, taking the constant C_n and the integer n sufficiently large, many widely different functions $\bar{f} = f + f_n$ can give approximately the same g. Therefore, the equation is ill-posed in the sense that a small variation in g may lead to a large difference in f.

In order to be able to handle ill-posed problems adequately, one must develop stable computational methods relying on prior knowledge of properties of the admissible solutions, global bounds, smoothness conditions, positivity constraints, statistical properties, etc. The problem is first to incorporate the supplementary constraints in the computational algorithm, which leads to regularisation theory where one imposes prescribed bounds on the class of admissible solutions. One can then apply the method of linear mean square estimation (optimum filtering, cf. Section 1.5.1.5) to restrain the solutions according to the given prior knowledge and data accuracy.

However, one must bear in mind that the solution (if it exists at all) is only as good as the accuracy of the data measured and the mathematical model proposed. Due to the nature of the problem, it is necessary to continue the measured data into a region removed from where the measurements are made, so that the question of existence may still be in doubt. Furthermore, the same conditions that lead to the stability problem (for instance, the above example involving (2.31)) also pose questions concerning uniqueness of the solution. Therefore, the solution obtained at best corresponds to the measured data, but not necessarily to the actual scattering process.

Useful discussions of uniqueness and computational stability for inverse problems are given by Devaney and Sherman (1982), Cabayan et al. (1973), Deschamps and Cabayan (1972), Bamberger et al. (1979). The books edited by Baltes (Inverse Source Problems 1978, Inverse Scattering Problems 1980) in Topics in Current Physics series are also valuable in this area.

2.4 TOWARDS A GLOBAL SOLUTION

Many specific inverse scattering problems have been solved, to date. They fall into the following two categories:

(i) Perfectly conducting bodies

The inverse reconstruction of perfectly conducting bodies has been attempted (successfully), either exactly or approximately, by many authors. Examples are Bates (1969c), Weston and Boerner (1969), Bates (1970), Boerner et al. (1971), Vandenberghe and Boerner (1972a,b), Tabbara (1973), Das and Boerner (1978), Meckelburg (1982).

(ii) General inverse scattering problems

Apart from the one-dimensional situation where the method of Gel'fand and Levitan can be applied, approximations to the wave equation must be

invoked. These approximations include geometrical optics, Kirchoff's approach to diffraction theory and the Born approximation, a comprehensive review of these can be found in Collin (1972).

However in order to obtain a solution (hopefully) to the general inverse scattering problem, one must inevitably return to the wave equation. Generally, one can either attempt to invert the 'direct' operator (2.6) or simply fit a model to the measured data.

There are two possible ways one can approach each of these problems - via the time domain or the frequency domain. The former is usually easier conceptually because one can build up a picture of sequential interactions between the wave and the body. This can be readily appreciated in the idealised situation for which the interior of the scattering domain is empty, apart from isolated regions whose linear dimensions are smaller, and whose separations are greater, than the inherent resolution of the imaging system. The interaction of the waves and their consequent evolution, can then be simply evaluated at a sequence of distinct instants within each region. Unfortunately, it is not as simple as this in general. Also, numerical instability in the time domain approach has limited its application. Nevertheless, pertinent references are scattered throughout the literature, e.g. Bates and Millane (1981), Lesselier (1982) and the many papers in the March 1981 issue of the IEEE Transaction on Antennas and Propagation.

2.4.1 State of the Art Techniques

2.4.1.1 Inversion of the Scattering Operator

The technique of inversion of the scattering operator seeks to relate directly the measured data to the scatterer (or source distribution) without evaluating any intermediate values, or making any first approximation to the solution. Bates (1975b)has proposed an approach to overcome the dimensionality difficulty and has subsequently developed the method into a global technique in his other publication (1984).

As already discussed in Section 2.3, each $Z_{\ell m}$, which is the mth component of the impedance on the measuring circle with respect to the ℓth incident partial wave, must be measured. The wave equation is then manipulated to eliminate the unknown, high-dimensional, total wave function within the scattering region to obtain

$$D_{\ell}\ (k, A(\rho;\phi),\ Z_{\ell m}) = 0 \qquad (2.32)$$

for all l,k, where D_{ℓ} is the determinant of a set of homogeneous equations

generated by the ℓth partial wave (see Bates 1984 for detail).

It might appear to be a straightforward matter to solve for $\Lambda(\rho;\phi)$ through (2.32). Unfortunately, it is not so. As (2.32) is a multiple eigenvalue problem characterising a set of nonlinear equations, factors such as solvability, uniqueness, computer storage and execution time can pose tremendous problems for a realistic situation. Therefore, the technique has to remain beyond the state-of-the-art until numerical methods are formulated for rapid solution of (2.32). Nevertheless, this global approach provides an insight into the resolution limits to the inverse problem, as is shown in Section 2.4.2.

2.4.1.2 Model Fitting

The technique of model fitting is to assume a certain model for the scatterer, solve the direct scattering problem, either by the method of Frechet derivative (cf. Roger 1981) or calculation of the total internal field (Johnson and Tracy 1983a,b, 1984) or otherwise (e.g. the null-field method, see Section 2.7), and modify the model accordingly after comparing the calculated and measured scattering data. The advantage of this approach is that, in principle, at least, it is applicable to all classes of scatterers, with any amount of available information. More information simply leads to better numerical stability, faster convergence, larger tolerance on the initial guess and probably, uniqueness. Although the last property may be difficult to achieve in a complicated situation with insufficient data, this technique nevertheless presents a conceptually simple approach to a global solution.

2.4.2 Resolution Limits

In any real life situation, noise and other uncertainties associated with a measuring process are always inevitable. However, there are few authors who have concerned themselves with the resolution limit imposed by these uncertainties. One explanation may be that approximation of one sort or another must be made in all the inverse methods used. Hence the resolution limits are actually governed by the degree of approximation rather than the measurement uncertainties. Cabayan et al. (1973) and Bates et al. (1980) have discussed briefly the question of resolution limits. Seagar et al. (1984) have produced simple comprehensive formulas using an idea from Bates (1984). The following discussion summarises the contribution by the author of this thesis to the paper by Seagar et al. (1984).

To determine the constitutive parameters, a researcher starts by measuring the reflection coefficients R_ℓ and calculates the impedance Z_ℓ on the measurement circle (Fig. 2.2) for the ℓth partial incident wave. However, it must be noted that experimental measurement error is always inevitable, therefore the calculated impedance Z_ℓ must contain an error ∂Z_ℓ (due to the measurement error ∂R_ℓ), and is characterised by the quantity ε_ℓ, defined by (Seagar et al. 1984)

$$\varepsilon_\ell = \left| \partial Z_\ell / Z_\ell \, / \partial R_\ell \right| \tag{2.33}$$

which can be approximated by (Seagar et al. 1984)

$$\varepsilon_\ell \simeq 2 \, / \left| \cos(2kb) + 2 \, R_\ell \exp(-2jkb) \right| \tag{2.34}$$

for $|\ell| << kb$ and $|R_\ell| << 1$. The expected value of ε_ℓ, which indicates the percentage error in Z_ℓ for a small perturbation in R_ℓ, spans a wide range because $|\cos(2kb)|$ can assume any value between zero and unity. Consequently, when R_ℓ is small, the maximum and minimum values of ε_ℓ are given by

$$\varepsilon_{\ell(\text{maximum})} \simeq 1/|R_\ell| \tag{2.35a}$$

$$\varepsilon_{\ell(\text{minimum})} \simeq 2 \tag{2.35b}$$

Fig. 2.4 is a plot of $|R_1 \varepsilon_1|$ verses kb for a range of R_1 calculated from the exact expression for ε_ℓ (equation (18) of Seagar et al. 1984) and is found that (2.34) provides a reasonably good estimate for $R_1 << 0.1$. The calculated value is also within a factor of two of its correct value for R_1 as large as 0.6. Fig. 2.5 illustrates the fact that the behaviour of ε_ℓ is similar for all values of ℓ, provided $kb/|\ell|$ is large enough.

Since the size of the measuring circle kb is under the control of the experimenter, and since there is no additional information to be gained by measuring the impedances on more than one circle, it is only reasonable to choose a value of kb such that

(i) it is convenient to the experimenter, and

(ii) the value

$$z_\ell = \left| \partial Z_\ell / \partial(kb) / Z_\ell \right| \tag{2.36}$$

is small.

Fig. 2.6 shows that z_ℓ has a local maximum at kb = $|\ell|$ and decreases with increasing kb. This ensures that for small R_ℓ, z_ℓ is reasonably small for most values of $|\ell| < kb$.

And finally, the percentage error in evaluating the constitutive parameter (defined in Section 2.3) is given by

$$|\partial\Lambda(\rho)/\Lambda| = |\partial R_\ell \cos(2\ell) \sum_{n=1}^{\infty} \alpha_{\ell,n}^2 B_n J'_\ell(\alpha_{\ell,n}\rho/b)/[\cos(2kb) + 2R_\ell \exp(-2jkb)]| \quad (2.37)$$

where the $B_\ell = B_{\ell,n}$ and are the expansion coefficients of the total wave function (with respect to the ℓth incident wave):

$$\text{i.e.} \quad \psi_\ell(\rho;\phi,k) = \sum_{m=-\infty}^{\infty} \sum_{n=1}^{\infty} B_{\ell,n}(k) J_m(\alpha_{\ell,n}\rho/b) \exp(jm\phi) \quad (2.38)$$

The $\alpha_{\ell,n}$ in (2.37) and (2.38) are defined by

$$\alpha_{\ell,n} = \alpha_n = bZ_\ell J_\ell(\alpha_{\ell,n})/J'_\ell(\alpha_{\ell,n}) \quad (2.39)$$

It is found that (Seagar et al. 1984) the percentage change in $\alpha_{\ell,n}$ with respect to percentage error in Z_ℓ decreases as α_n increases:

$$\eta_\ell = |\partial\alpha_{\ell,n}/\alpha_{\ell,n}/\partial Z_\ell/Z_\ell| = |\cos(2\alpha_n)/2\alpha_n| \quad (2.40)$$

Furthermore, when n is large, $\alpha_{\ell,n}$ can be approximated (from 2.39) by

$$\alpha_{\ell,n} \simeq |\ell| + 2n\pi \quad (2.41)$$

Fig. 2.7 shows the behaviour of η_ℓ with respect to α_n for various values of ℓ.

(2.37) indicates that the resolution of a measurement scheme depends upon the number of independent parameters B_n that are abstracted from the data. However, to resolve detail of finite size (Δ say) in $\Lambda(\rho;\phi)$ one need only account for a finite number of Fourier coefficients in (2.38). The first summation thus runs from - M to M, where the integer M is large enough for the summation to be capable of reproducing detail of the required size at the circumference of the cross-section, i.e. (cf. Cabayan et al. 1973)

$$M = \pi b/\Delta \quad (2.42)$$

Similarly, only a finite number of terms (N_m say) need be considered in the second summation in (2.38). Each basis function can usually be thought of

as a two-dimensional spatial frequency component. The spatial wavelength in the ρ direction is $2\pi b/\alpha_{\ell,n}$. Using (2.41), N_m is thus given by

$$N_m = b/2\Delta - |\ell|/2\pi \tag{2.43}$$

Finally, it is clear from (2.38), (2.42) and (2.43) that an order of magnitude estimate of the total number of spatial frequency components, to whose complex amplitudes the measurement scheme must be sensitive, is

$$N_o + 2 \sum_{m=1}^{M} N_m = \pi b^2/2\Delta^2 \tag{2.44}$$

2.4.3 Experimental Measurement of Scattering Data

Section 2.4.2 above summarises the theoretical limitation in the resolution of general imaging procedure with respect to the experimental measurement error. However, one other aspect of experimental measurement of scattering data is so important that it warrants a special mention.

In most practical situations, such as radar (cf. Bates 1969C, 1970) or optics (cf. Bates 1982), one can often only measure accurately the scattering pattern, or radar cross-section or the magnitude of the Fourier transform of the image. Meaningful phase measurement tends to be difficult (and sometimes impossible) to contrive (Bates 1982). Therefore, when devising inverse scattering procedures, it is worth keeping constantly in mind that such limitations exist.

2.5 A SIMPLE ALGORITHM FOR THE SOLUTION OF THE INVERSE SOURCE PROBLEM

As already discussed in Section 2.2, it is possible to reconstruct a source distribution exactly only if the sources are mutually incoherent, or, if the sources are coherent, they lie on a closed surface. In this section, an algorithm is proposed to reconstruct an arbitrary distribution of discrete, isolated coherent sources. Although the method cannot claim uniqueness (and there is no attempt to do so), it nevertheless provides a simple and efficient way of estimating the number and position of radiating sources within an enclosed region. It is also worth noting that this method is similar to the back-propagation method recently introduced for ultrasonic computed tomography (cf. Garden 1984).

The field radiated by the sources, which are enclosed in the domain Γ of radius a, is measured on the measuring circle C (Fig. 2.8) and is given by

$$\psi_Q = \psi(b;\theta,k) = \sum_{n=1}^{N} a_n H_o^{(2)} (k\tau_{n,Q}) \tag{2.45}$$

where the a_n are the complex amplitude of the N radiating sources and the $\tau_{n,Q}$ are the distances from the nth source position $P_n(\rho;\phi)$ to the measuring point $Q(b;\theta)$. According to Huygen's principle, the field on the measuring circle can be regarded as secondary wavefronts which re-radiate everywhere into space. Therefore, if we construct the back propagation at any point P within the measuring circle such that it is completely characterised by the quantity

$$I_P(\rho;\phi) = \left| S_Q \psi_Q(b;\theta,k) H_o^{(1)} (k\tilde{\tau}_{P,Q}) \right| \tag{2.46}$$

where $\tilde{\tau}_{P,Q}$ is the distance from a point Q on the measuring circle to the point P within the radiating domain and S is the Sebiffi symbol introduced in Section 1.4. $_Q$

Consider an example where one source is situated at $(\rho_o;\phi_o)$. $\psi(b;\theta,k)$ is then equal to $-jH_o^{(2)}(k\tau)/4$ and the quantity $I_P(\rho;\phi)$ defined in (2.46) is then

$$I_P(\rho;\phi) = \left| 1/4 \int_o^{2\pi} H_o^{(1)} (k\tilde{\tau}) H_o^{(2)} (k\tau) \, d\theta \right| \tag{2.47}$$

Using the Addition theorem for Bessel functions (Watson 1966, Section 11.3), I_P is expanded as

$$I_P(\rho;\phi) = \left| 1/4 \int_o^{2\pi} \sum_{m=-\infty}^{\infty} H_m^{(1)} (kb) J_m(k\rho) \right.$$

$$\exp(jm(\theta-\phi)) \sum_{n=-\infty}^{\infty} H_n^{(2)} (kb) J_n (k\rho_o)$$

$$\left. \exp(j_n(\theta-\phi_o)) \, d\theta \right| \tag{2.48}$$

which reduces, on evaluating the integral, to

$$I_P(\rho;\phi) = \pi/2 \left| \sum_{m=-\infty}^{\infty} H_n^{(1)} (kb) H_{-n}^{(2)} (kb) J_{-n}(k\rho) \right.$$

$$\left. J_n(k\rho_o) \exp(jn(\phi-\phi_o)) \right| \tag{2.49}$$

Since $J_n(x) = (-1)^n J_n(x)$ and $H^{(2)}_{-n}(x) = (-1)^n H^{(2)}_n(x)$ (Abramowitz and Stegun 1965, equations 9.1.5 and 9.1.6) then

$$I_P(\rho;\phi) = \pi/2 \left| \sum_{n=-\infty}^{\infty} H^{(1)}_n(kb)\, H^{(2)}_n(kb)\, J_n(k\rho)\, J_n(k\rho_o)\, \exp(jn(\phi-\phi_o)) \right| \tag{2.50}$$

Furthermore, if the series is truncated to (-N,N), then

$$I_P(\rho;\phi) \simeq \pi/2 \left| \sum_{n=-N}^{N} H^{(1)}_n(kb)\, H^{(2)}_n(kb)\, J_n(k\rho)\, J_n(k\rho_o)\, \exp(jn(\phi-\phi_o)) \right| \tag{2.51}$$

However, when $kb \gg N$, $H^{(1)}_n(kb)\, H^{(2)}_n(kb) \simeq 2/\pi kb$, (Abramowitz and Stegun 1965, equations 9.2.3 and 9.2.4), it is seen that

$$I_P(\rho;\phi) \simeq 1/kb \left| \sum_{n=-N}^{N} J_n(k\rho)\, J_n(k\rho_o)\, \exp(jn(\phi-\phi_o)) \right| \tag{2.52}$$

which can be approximated by the infinite series,

$$I_P(\rho;\phi) \simeq 1/kb \left| \sum_{n=-\infty}^{\infty} J_n(k\rho)\, J_n(k\rho_o)\, \exp(j_n(\phi-\phi_o)) \right| \tag{2.53}$$

Finally, again using the Addition Theorem for Bessel functions (Watson 1966, Section 11.3)

$$I_P(\rho;\phi) \simeq 1/kb\, J_o(k|\underline{\rho}-\underline{\rho}_o|) \tag{2.54}$$

It is clear that $I_P(\rho;\phi)$ has a maximum at $\underline{\rho}(\rho;\phi) = \underline{\rho}_o(\rho_o;\phi_o)$, the source position.

In practice, the field can only be observed at a discrete set of points, defined by the set $\{\theta_m;\ m = 1,2, \ldots M\}$ of angles, on the measurement circle. Set $\{\Psi_m;\ m = 1,2, \ldots M\}$ of measured fields is defined by

$$\Psi_m = \Psi(b;\ \theta_m) \tag{2.55}$$

The quantity I_P is then given by

$$I_P(\rho;\phi) = \left| \sum_{m=1}^{M} \Psi_m\, H^{(1)}_o(k\tilde{\tau}_{P,m}) \right| \tag{2.56}$$

where M is the number of measurement points and $\tilde{\tau}_{P,m} = |\underline{r}_m - \underline{\rho}_P|$ with $\underline{r}_m = \underline{r}_m(b;\theta_m)$ and $\underline{\rho}_P = \underline{\rho}_P(\rho_P,\phi_P)$. It is clear from (2.56) that although I_P is susceptible to measurement errors in ψ_m (in both phase and magnitude), it cannot be corrupted by an arbitrary choice of phase reference, i.e. if

$$\tilde{\psi}_m = \exp(j\theta)\psi_m \tag{2.57}$$

then

$$\tilde{I}_P(\rho;\phi) = \left| \sum_{m=1}^{M} \tilde{\psi}_m H_o^{(1)}(k\tilde{\tau}_{P,m}) \right| = \left| \exp(j\theta) \sum_{m=1}^{M} \psi_m H_o^{(1)}(k\tilde{\tau}_{P,m}) \right|$$

$$= I_P(\rho;\phi) \tag{2.58}$$

Since a, the radius within which the sources are situated, is fixed, and one can arrange b such that $k\tilde{\tau}_{P,m} >> 1$, one can use the uniform asymptotic form of Hankel function (Watson 1966, Section 7.2) to reduce (2.56) to

$$I_P(\rho;\phi) = \left| \sum_{m=1}^{M} \psi_m (2/\pi k\tilde{\tau}_{P,m})^{\frac{1}{2}} \exp(jk\tilde{\tau}_{P,m} - j\pi/4) \right.$$

$$\left. \left[1 + \sum_{\ell=1}^{\infty} (0,\ell)\ (j/2k\tilde{\tau}_{P,m})^{\ell} \right] \right| \tag{2.59}$$

where $$(0,\ell) = (-1)^{\ell}\ (1^2)\ (3^2)\ \ldots\ (2\ell-1)^2/2^{2\ell}\ \ell! \tag{2.60}$$

Figs. 2.9 to 2.14 depict some of the results of computer experiments. Two isolated sources, situated at $(\rho;0)$ and $(\rho;\pi/2)$ are imaged with different ρ and using various number of measurement points.
The sources are assumed to have unit amplitude (i.e $a_1 = a_2 = 1$)
Fig. 2.9 indicates that when 20 measurement points are used with the separation between the sources $k\zeta = 1.42$ ($k\rho = 1.0$) the resolution of the system is inadequate to isolate the two sources. However, the algorithm does provide a strong indication of from where the radiation originates. In Fig. 2.10, the sources are at $k\rho = 5.0$, with the separation $k\zeta = 7.07$. It can be seen that the reconstruction is much more faithful, with the highest side-lobe having only one-third of the actual source intensity. In Fig. 2.11, the sources are at $k\rho = 10.0$ with the separation $k\zeta = 14.14$. In this case, the main-lobe is sharpened considerably, which gives a clear indication of the sources' positions. Unfortunately, the peaks of the side-lobes have been increased to slightly more than half of that of the main-lobe. As a consequence, the image appears cloudy. The number of measurement points is increased to 30 in Fig. 2.12 while the source separation remains unchanged.

The image is seen to be 'cleaned' considerably in this case and a satisfactory image results, as shown in Fig. 2.13 where the number of measurement points is increased to 50. In Fig. 2.14, the value of a_1 is (1,0) and the value of a_2 is (0,1), i.e. there is a phase quadrature between the two sources. With the rest of the parameters identical to those of Fig. 2.13, the clarity of the image in Fig. 2.14 suggests that the reconstruction procedure is insensitive with respect to the relative phase of the sources.

From the evidence of Figs. 2.9 to 2.14, it can be concluded that this simple procedure shows considerable promise. It is also worthwhile emphasising that the reconstructions produced by this algorithm may neither be unique, nor as good as indicated in Figs. 2.13 and 2.14, when a more complicated situation is encountered. On the other hand, (2.59) can be computed rapidly, but with computing time of course increasing with larger ka and finer resolution. This method might be very useful for producing the first estimate to be used in a more sophisticated procedure.

2.6 INVERSE SOURCE AND INVERSE SCATTERING - THE SEQUEL

Remote sensing, (i.e. the inverse source or the inverse radiation problem) has always been treated as a special branch of the general inverse problem. El-Behery and MacPhie (1978) write about maximum likelihood estimation of the positions of point radio sources. Bressan and Conciaro (1982) have produced an optimum inversion method for the remote probing of defective phase shifters in phased arrays. Porter and Devaney (1982) obtain a unique solution to the inverse source problem by minimizing the source energy. However, the possibility of using a solution of the inverse source problem as the first step to the estimation of the shape of scatterer in the more general inverse scattering problem, seems to have been overlooked so far.

There are two ways in which a solution to the inverse source problem can be used as a first estimate in a solution to the inverse scattering problem.

(i) Speckle points

Points within the scatterer where $\nabla\Lambda$ (Λ is the general constitutive parameter defined in Section 2.3) is large, or there is an abrupt change in boundary, or corners, which scattered more readily than points where $\nabla\Lambda$ is small. Therefore, by assuming that the scatterer consists of a finite number of simple (coherent) sources at these singular points, one can determine the position of the scattering points, and by joining them, make a rough drawing of the shape of the scatterer.

(ii) Polarisation source

By resorting to the method of polarisation sources, and assuming a finite number of discrete polarisation sources (cf. Johnson and Trac y 1983, Trac y and Johnson 1983, Johnson et. al. 1984), one can form a first order estimate of the strength of each source (at pre-determined positions) and this estimate can be used for subsequent iterations.

2.7 APPLICATION OF NULL-FIELD METHOD TO INVERSE SCATTERING

Although the null-field method (cf. Section 1.5.5) has mainly been invoked in the context of direct problems, it has been shown to have at least limited application to inverse problems (Bates 1970, Bates and Wall 1977). In this section, a new approach in the sense of model fitting (or direct - inverse iteration, see Section 2.4.1) is introduced to extend the horizon of the application of null-field method to the solution of the general inverse scattering problem. Let

$$r(\theta) = \sum_{\ell=-L}^{L} g_\ell \exp(j\ell\theta) \tag{2.61}$$

describe the shape of a scatterer with known refractive index ν, and let

$$f(r(\theta),\theta,\nu) = \sum_{n=o}^{N} d_n f_n (r(\theta),\theta,\nu) \tag{2.62}$$

represent the field on the surface of the scatterer, where the g_ℓ and d_n are expansion coefficients and the f_n are basis functions. Note that since the d_n are functions of g_ℓ , then

$$\partial f(r(\theta),\theta,\nu)/\partial g_\ell \neq \sum_{n=o}^{N} d_n \partial f_n(r(\theta),\theta,\nu)/\partial g_\ell \tag{2.63}$$

Define

$$\partial f(r(\theta),\theta,\nu)/\partial g_\ell = \sum_{n=o}^{\infty} C_{n,\ell} f_n(r(\theta),\theta,\nu) \tag{2.64}$$

where the $C_{n,\ell}$ are expansion coefficients. The incident wave is (see Section 1.4)

$$\psi_{inc} = \sum_{n=-\infty}^{\infty} a_n \exp(-jn\phi)\ j^n J_n (k\rho) \tag{2.65}$$

while the scattered wave is (see Section 1.4)

$$\psi_{sc} = \sum_{n=-N}^{N} b_n \, j^n \exp(-jn\phi) \, H_n^{(2)} (k\rho) \tag{2.66}$$

and the normalised radar cross-section (Bowman et al. 1969, Section 1.2.5) is

$$\sigma(\phi) = \left| \sum_{n=-N}^{N} j^n \exp(-jn\phi) \, b_n \right|^2 \tag{2.67}$$

As mentioned in Section 2.4.3, one is unable to measure phase information accurately, and the radar cross-section is usually the only data available. The advantage of this extended null-field inversion procedure is therefore apparent since it requires no phase information from the measuring data.

The procedure to reconstruct $r(\theta)$ is as follows:-

Step (i)

Estimate the g_ℓ, the shape factor of the scatterer defined in (2.61), either by prior knowledge or any crude estimation procedure such as the algorithm introduced in Section 2.5. The d_n can then be calculated from the Null-Field Equation as:

$$a_m = -j/4 \sum_{n=o}^{N} d_n \int_o^{2\pi} \Big[\nabla f_n(r(\theta),\theta,\nu) \, H_m^{(2)} (kr(\theta)) \exp(jm\theta) - f_n(r(\theta),\theta,\nu) \nabla H_m^{(2)} (kr(\theta)) \exp(jm\theta) \Big] \cdot \hat{n} d\theta \tag{2.68}$$

where

$$\hat{n} = (\hat{a}_r - (1/r \, dr(\theta)/d\theta) \, \hat{a}_\theta)/(1+|1/r \, dr(\theta)/d\theta|^2)^{\frac{1}{2}} \tag{2.69}$$

and

$$dr(\theta)/d\theta = \sum_{\ell=-L}^{L} g_\ell \, (j\ell) \exp(j\ell\theta) \tag{2.70}$$

by means of matrix inversion (see Section 1.5.1).

Step (ii)

Calculate estimates of b_n, which is equal to RHS (2.68) when $H_m^{(2)}(\cdot)$ is replaced by $J_m(\cdot)$. Then calculate $\sigma(\phi)$ from (2.67). Compare $\sigma(\phi)$ with the measured data, thus obtaining $d\sigma(\phi)$.

Table 2.1

Results of five computer runs ka of a circular is 2.0. The initial estimate of ka is 4.0. The data given is $\vartheta(0)$ with a 10% random error.

run #	# of iteration steps	Final Result	% error
1	6	2.006	0.3
2	5	1.996	0.2
3	6	1.992	0.4
4	6	1.994	0.3
5	5	2.004	0.2

Step (iii)

The original estimate is updated (i.e. $g_{\ell,k+1} = g_{\ell,k} + \Delta g_{\ell,k}$, where $g_{\ell,k}$ is the value of g_ℓ at the kth iteration) and the iterative procedure is continued until the $\Delta g_{\ell,k}$ are less than an arbitrary small constant, ε say.

In order to test the validity and efficiency of this procedure, computer experiments have been carried out to estimate (i) the size of a perfectly conducting circular cylinder, and (ii) the size and refractive index of a dielectric circular cylinder (Fig. 2.15).

Fig. 2.16 shows the numerical convergence of ka(=2.0) with respect to N, and the number of iterations used, starting from different estimates of ka. Fig. 2.16a,b, and c are situations where either $\sigma(0)$ (=1.708), $\sigma(\pi/2)$ (=0.161) or $\sigma(\pi)$ (=8.049) is given. It is quite clear that even when the first estimate of ka is grossly in error, satisfactory results can still be achieved after as few as 5 iterations. It is also quite clear that the convergence is more oscillatory and the range of (possible) estimates (which leads to correct results) is smaller when $\sigma(\phi)$ is small. When $\sigma(0)$ is given with a 10% (maximum) random error and the crude estimate of ka is 4.0, Table 2.1 shows the results of five successive runs. Note that the iterative steps used are equal to or fewer than 6 in each case and the results indicate an error of less than 0.5% in the final value calculated for ka. Furthermore, if $\sigma(0)$, $\sigma(0.1)$ and $\sigma(0.2)$ are given (each with a 10% maximum random error), it is found that the (averaged) result is within 0.05% of the actual value.

When $\sigma(0)$ and $\sigma(\pi)$, each with a 10% maximum random error, are given for a dielectric circular cylinder (of ka = 2.0 and ν = 1.5), and one starts with estimation errors of 5% (i.e. first estimate ka = 1.9, ν = 1.425), the final (averaged) results are obtained within 10 iterations to an accuracy of better than 0.5%.

For the sake of clarity and ease in numerical computation, examples are presented only for circular cylinders. However, the results clearly indicate that one can evaluate the scattering profile from limited information such as the radar cross-section (without phase information). When sufficient measurements are made, it may even be possible to obtain a unique solution provided the initial estimate is close enough to the actual solution. Unfortunately, it seems to be impossible to theoretically characterise the

class of scatterers for which this procedure can be effective, nor to obtain a general expression for the 'closeness' required for the initial estimate.

2.8 FROM DIRECT TO INVERSE PROBLEMS

Ever since the day Adam ate the forbidden fruit, we have been driven by our urge for knowledge to try and discover the secrets of our mysterious Mother Nature. Ways and means have thus been devised by people who attempt to venture into the worlds lying beyond the vision of our naked eyes.

Some of the earliest inverse problems encountered were astronomical. Since the time of Aristotle (384-322 BC) men have been interested in the heavenly bodies and a giant step was made in 1609 when Hariot (1560-1621) and Galileo (1564-1642) discovered the satellites of Jupiter with their refracting telescopes. Three centuries later, Rontgen (1845-1923) discovered X-rays which enabled him to see inside living tissue, so that the 'vision' beyond our naked eyes thus entered a new era. In the following years, the theory of 'imaging' has developed so rapidly that astronomy, medicine, crystallograph, oceanology and geology are just a few of the areas where inverse theory has been found to be useful. Backus and Gilbert (1967, geophysical), Newton (1970, general physics), Weston (1972, mathematical consideration), Weston (1974, general physics), Parker (1972, geophysical), Parker (1977, geophysical), Sabatier (1978, antenna analysis), Jordan and Ahn (1979, antenna analysis), Jannson and Janicki (1980, optical), Sleeman (1982, acoustic), Bates (1982, astronomical), Vogelzang et al. (1983, optical), Sabatier (1983, mathematical considerations), mark progress in various fields throughour the years.

As has been mentioned in Section 2.4.1, one way of solving an inverse problem is to propose a model, calculate the perturbed field, compare the calculated field with measured data and subsequently modify the model. Naturally, when a scattering body has corners, one must be able to model diffraction by these corners. Unfortunately, it is possible only with perfectly conducting bodies. This procedure would be useless in the case of penetrable bodies with corners, since one does not yet know how to calculate the field diffracted by a penetrable edge. Therefore, it is apparent that we should try to understand thoroughly every possible direct situation (including the penetrable wedge problem) before we are able to take another step forward in the direction of solving inverse problems.

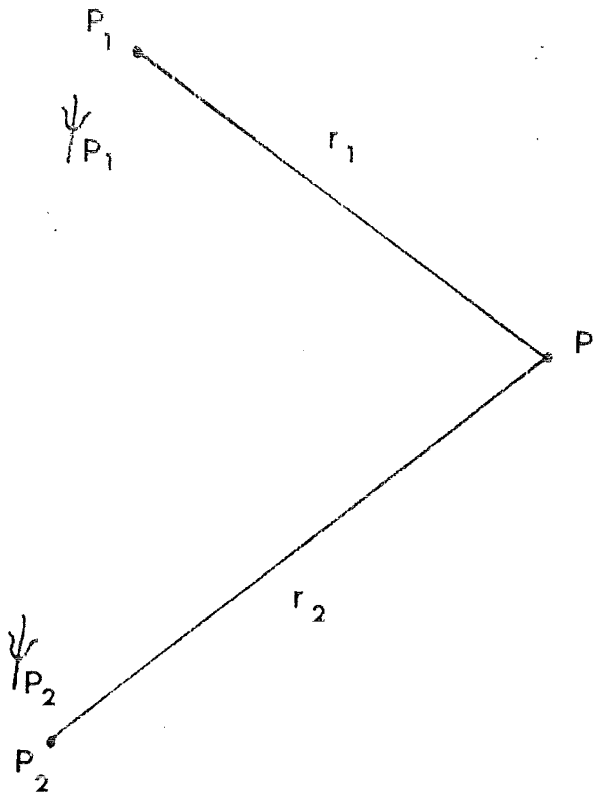

FIGURE 2.1 Source points P_1, P_2 and field point P. The fields at P_1 and P_2 are Ψ_{P_1}, and Ψ_{P_2} respectively.

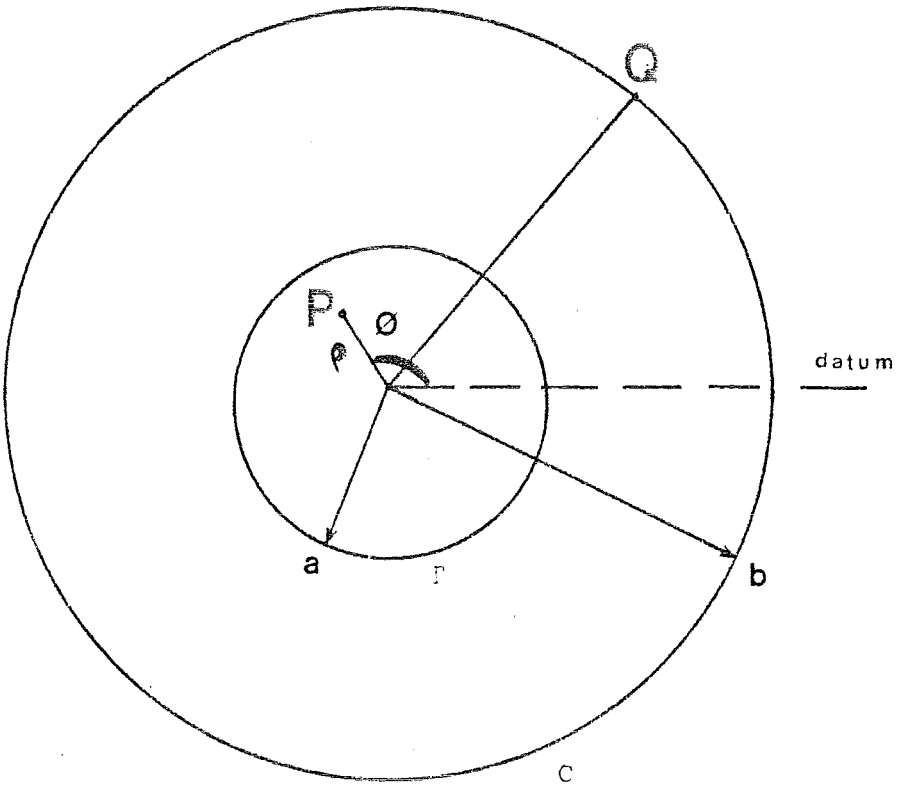

FIGURE 2.2 Geometry for inverse scattering measurement. The scattering region is within the circle Γ of radius a. The fields are measured on the circle C of radius b. A point in Γ has the coordinate $P(\rho;\phi)$ while a point Q on C has the coordinate $(b;\theta)$.

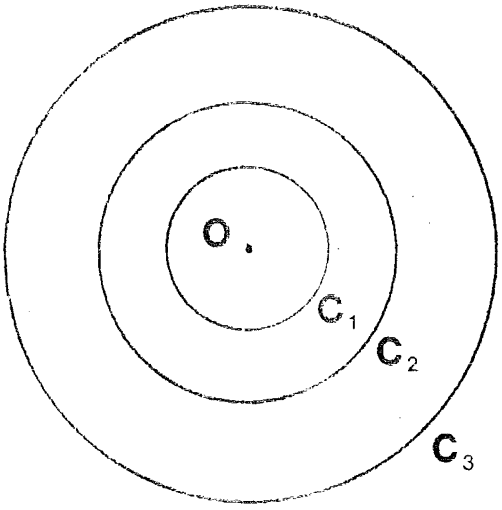

FIGURE 2.3 Cocentric ring sources at O, C_1, C_2 and C_3.

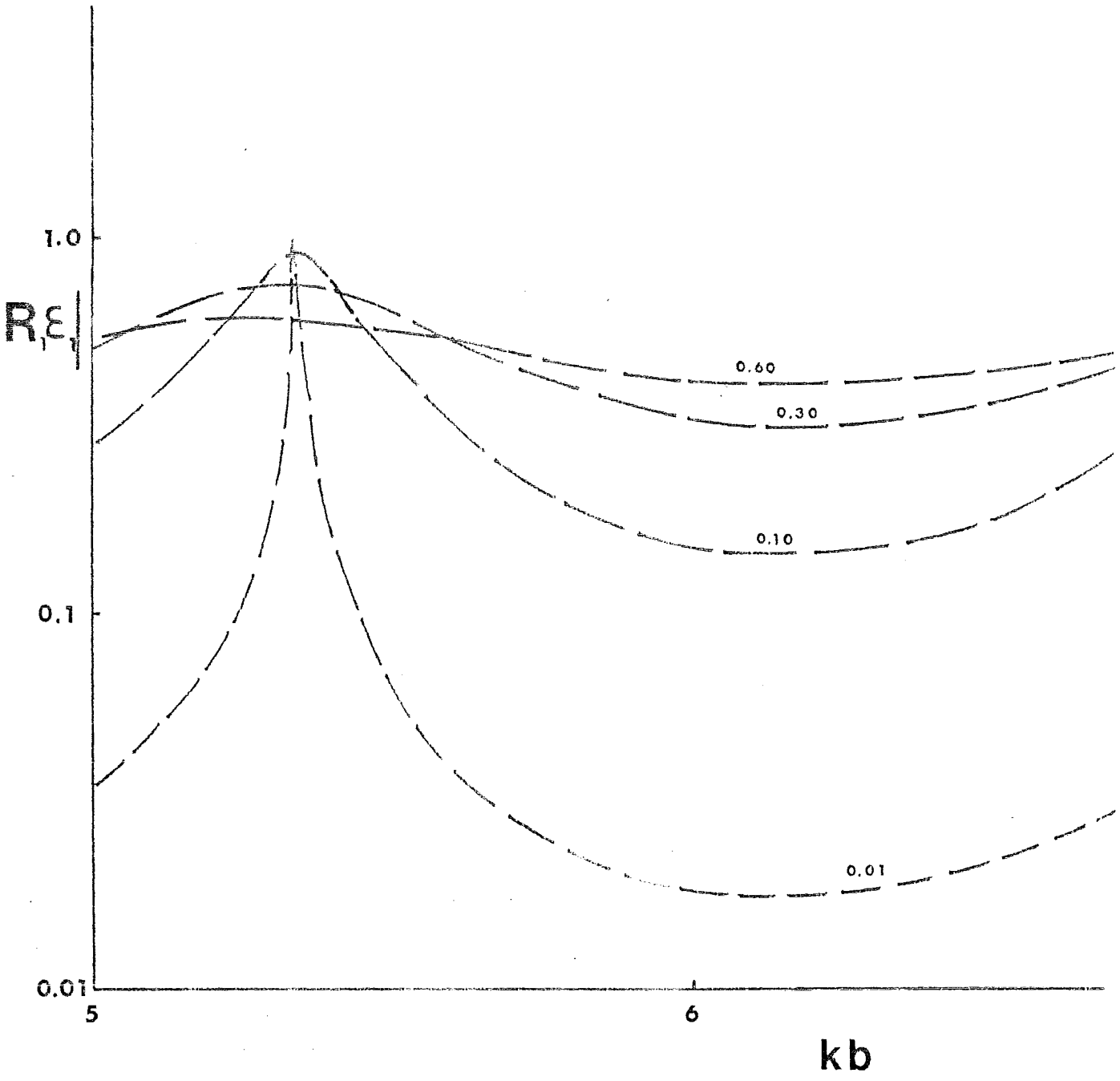

FIGURE 2.4 Plot of $|R_1\varepsilon_1|$ versus kb. This plot displays the effect of measurement error on calculated impedance (see(2.33)). The variable is the value of R_1.

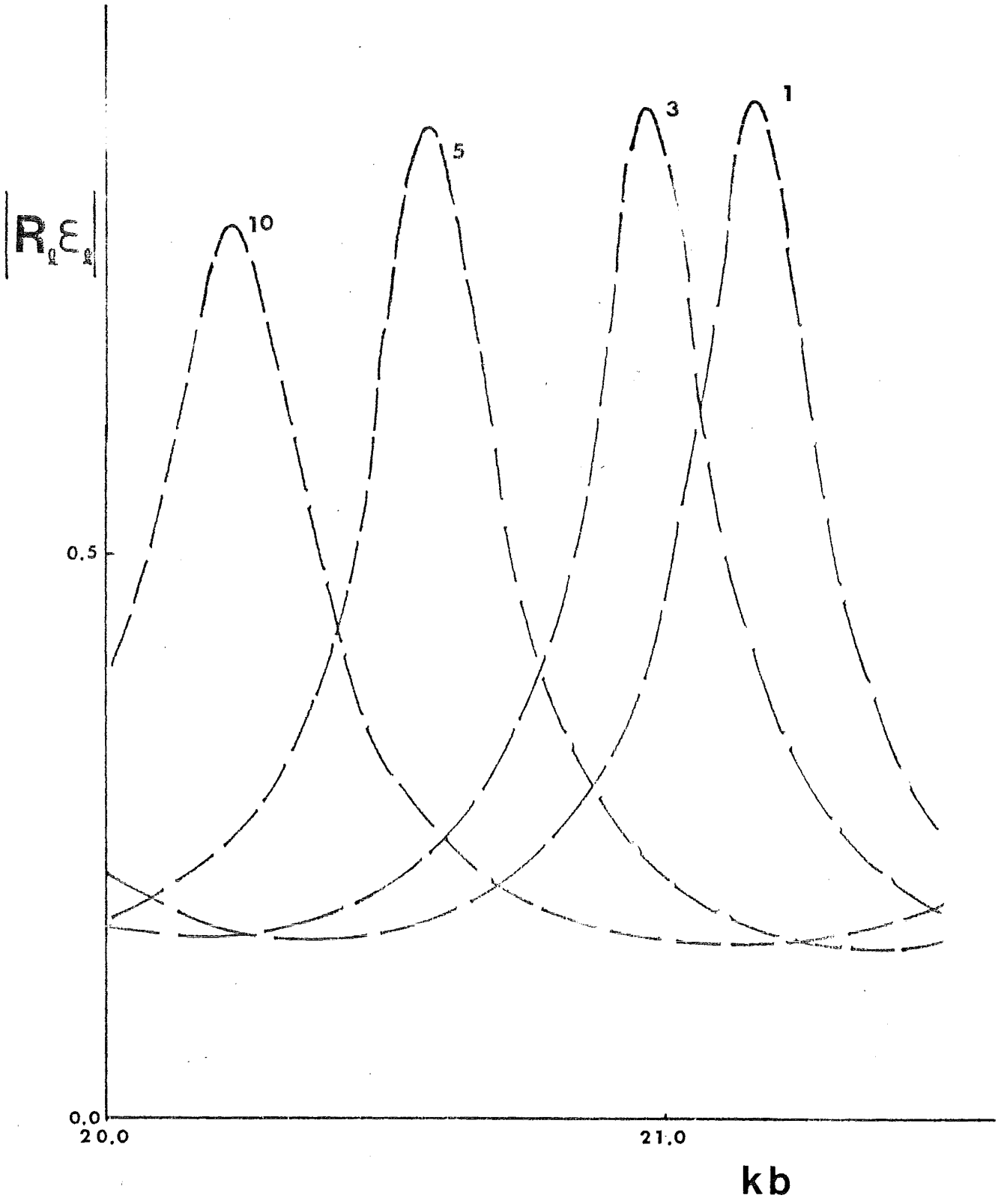

FIGURE 2.5 Plot of $|R_\ell \varepsilon_\ell|$ versus kb. This plot displays the variation of measurement error with respect to the size of measurement circle C. The variable is the value of ℓ.

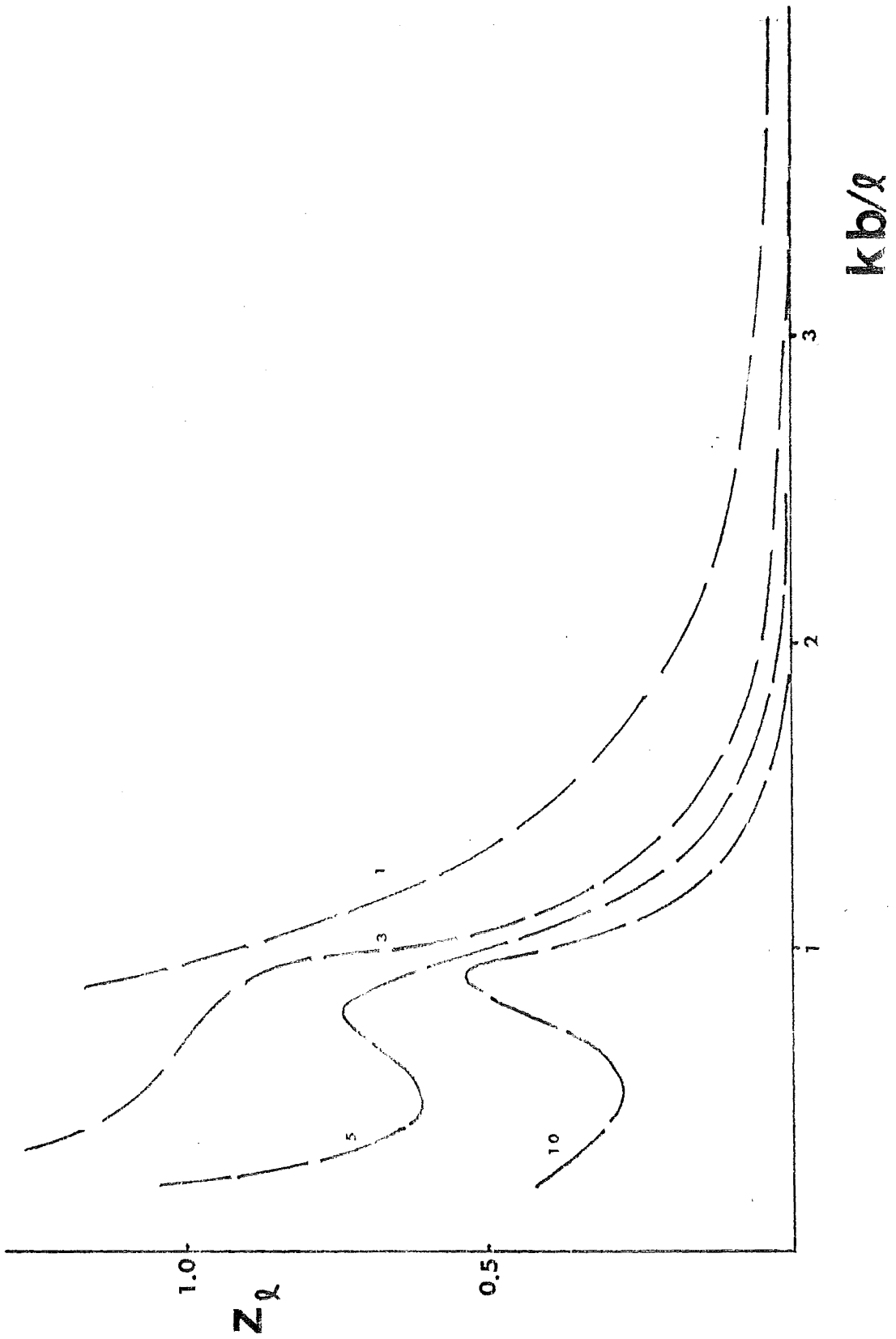

FIGURE 2.6 Plot of z_ℓ versus kb. This plot displays the variation of error in calculated impedance with respect to the size of measurement circle C. The variable is the value of ℓ.

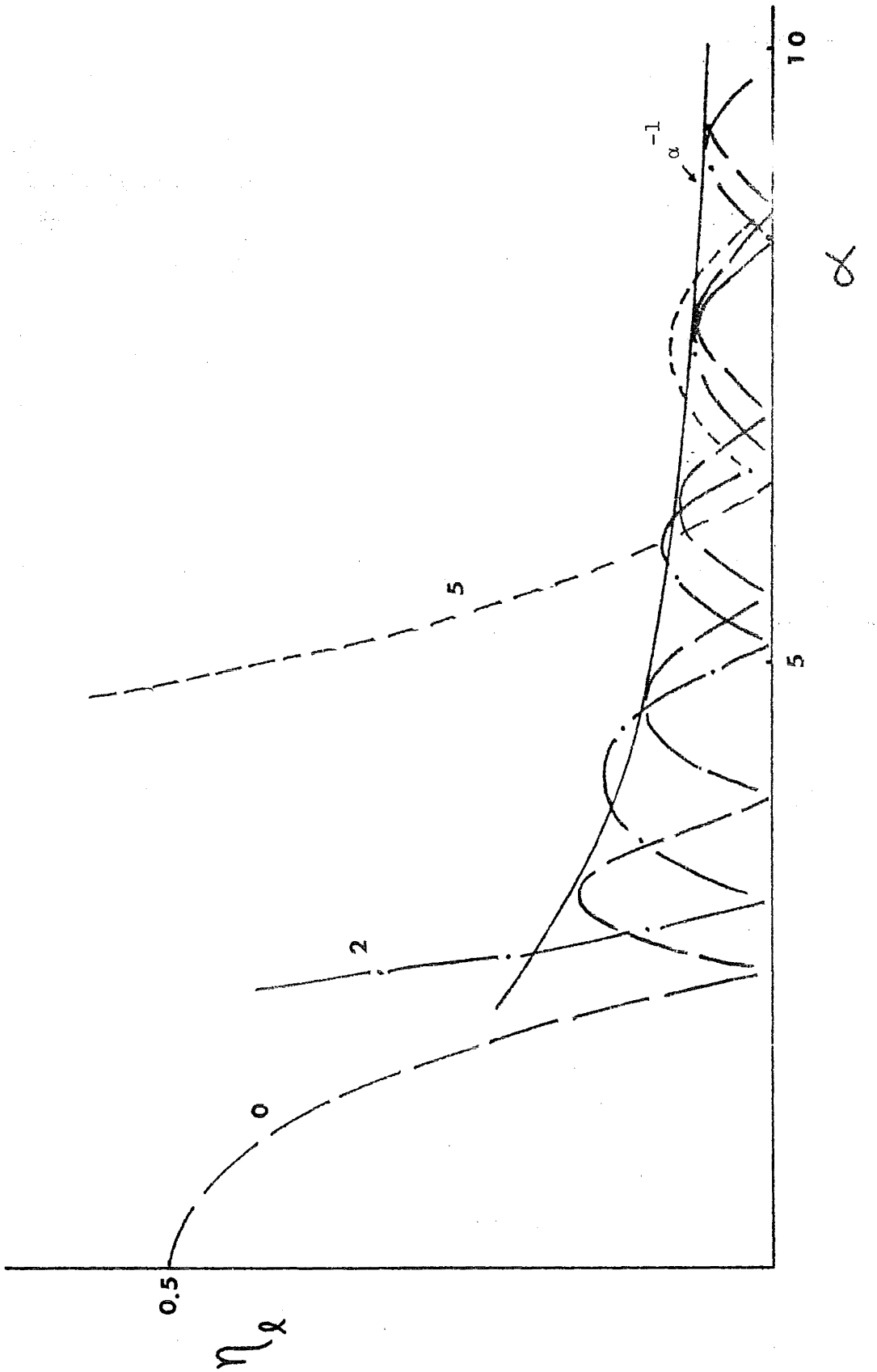

FIGURE 2.7 Plot of η_ℓ versus α. This plot displays the percentage error in calculated eigenvalues with respect to percentage error in impedance. The variable is the value of ℓ.

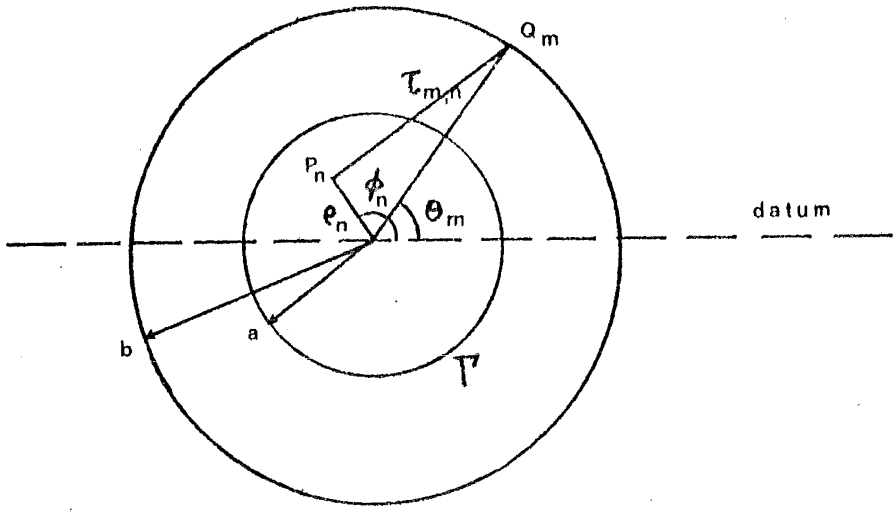

FIGURE 2.8 Geometry of inverse source problem. The (isolated) sources are situated within the circle Γ of radius a. The nth source, at point P_n has the coordinate $(\rho_n; \phi_n)$. A measurement point Q_m has the coordinate $(b; \theta_m)$.

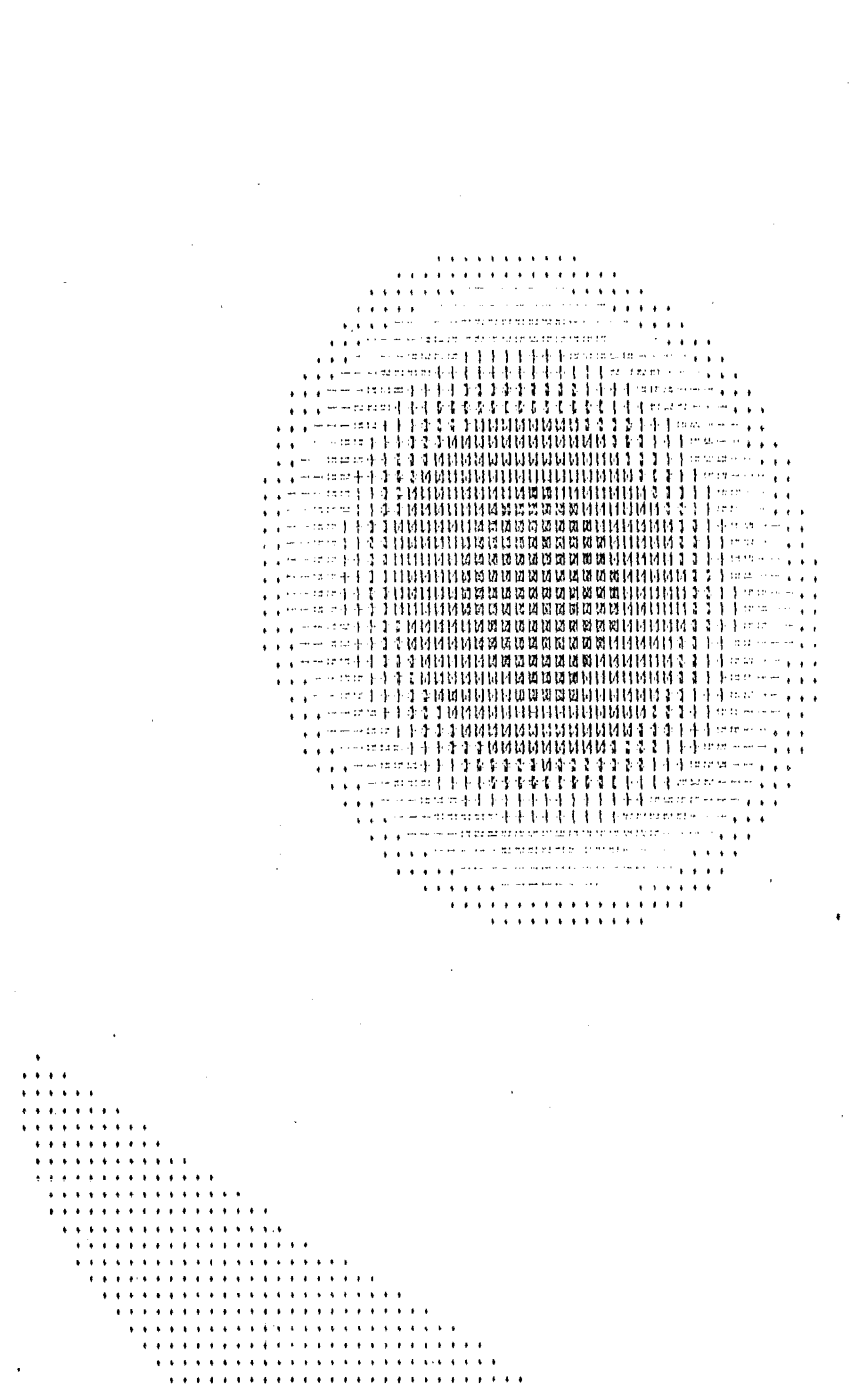

FIGURE 2.9 Reconstruction of two point sources of unit amplitude and situated at (ρ = 1.0; ϕ = 0.0) and (ρ = 1.0; ϕ = $\pi/2$) respectively. The number (M) of measurement points is 20 and they are distributed evenly on a circle with radius $kb = 10\pi$, where k = 1.0.

FIGURE 2.10 Reconstruction of the same point sources described in Fig. 2.9. Only that now k = 5.0.

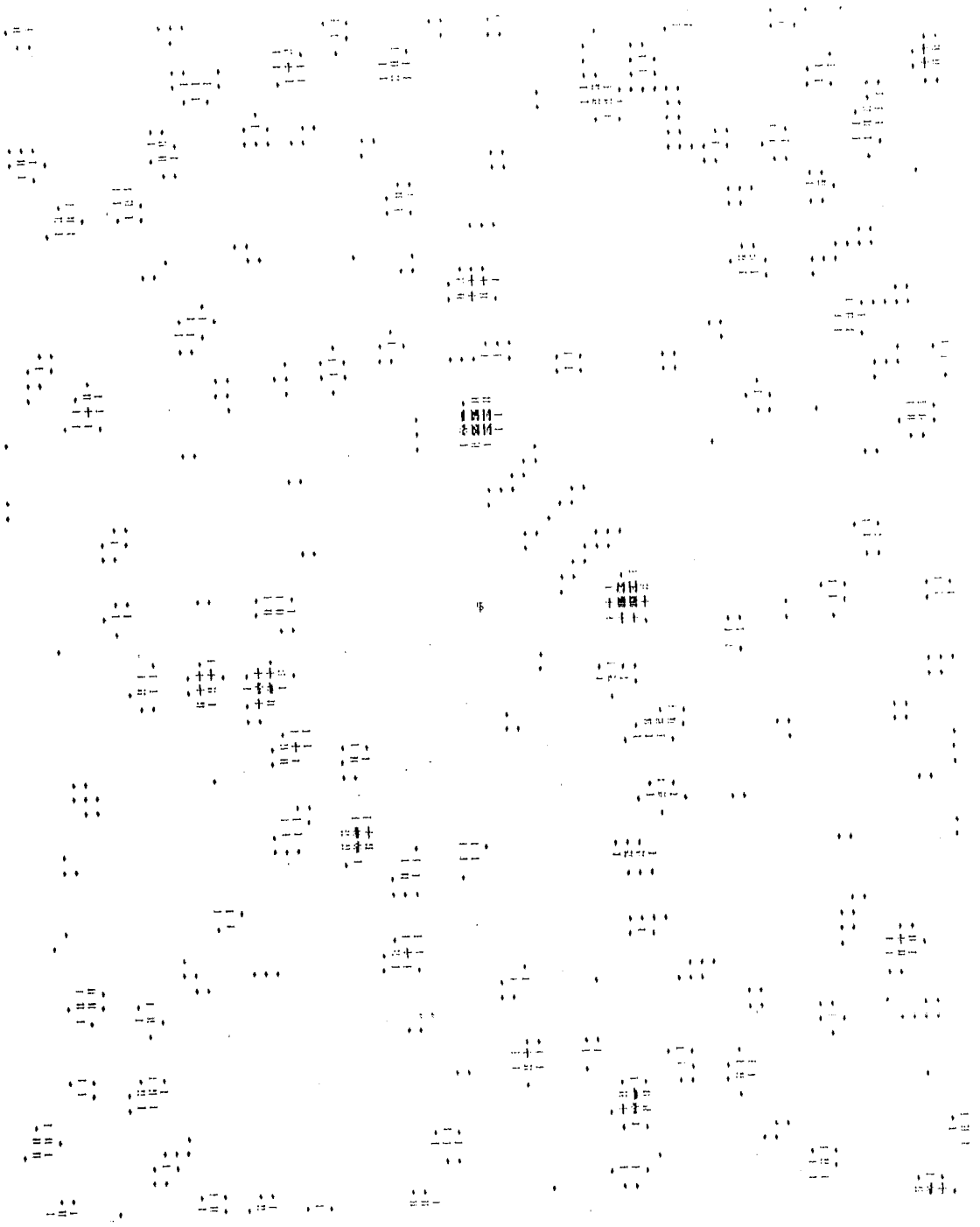

FIGURE 2.11 Reconstruction of the same point sources described in Fig. 2.9. Only that now k = 10.0.

FIGURE 2.12 Reconstruction of two point sources of unit amplitude and situated at (ρ = 1.0; ϕ = 0.0) and (ρ = 1.0; ϕ = $\pi/2$) respectively. The number (M) of measurement points is 30 and they are distributed evenly on a circle with radius kb = **100**π, where k = 10.0.

FIGURE 2.13 Reconstruction of the same point sources as described in Fig. 2.12. Only that now M = 50.

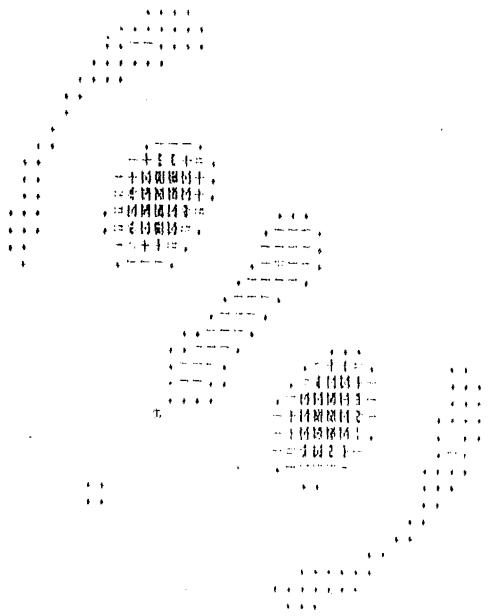

FIGURE 2.14 Reconstruction of two point sources of amplitudes (1.0,0.0) and (0.0,1.0) and situated at ($\rho = 1.0$; $\phi = 0.0$) and ($\rho = 1.0$; $\phi = \pi/2$) respectively. The number (M) of measurement points is 50 and they are distributed evenly on a circle with radius $kb = 100\pi$, where $k = 10.0$.

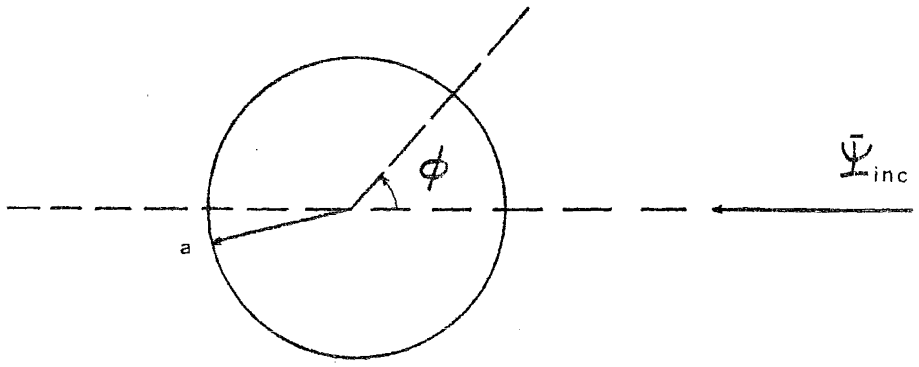

FIGURE 2.15 Circular cylinder (conducting or dielectric) of radius a used for testing of reconstruction procedure described in Section 2.7.

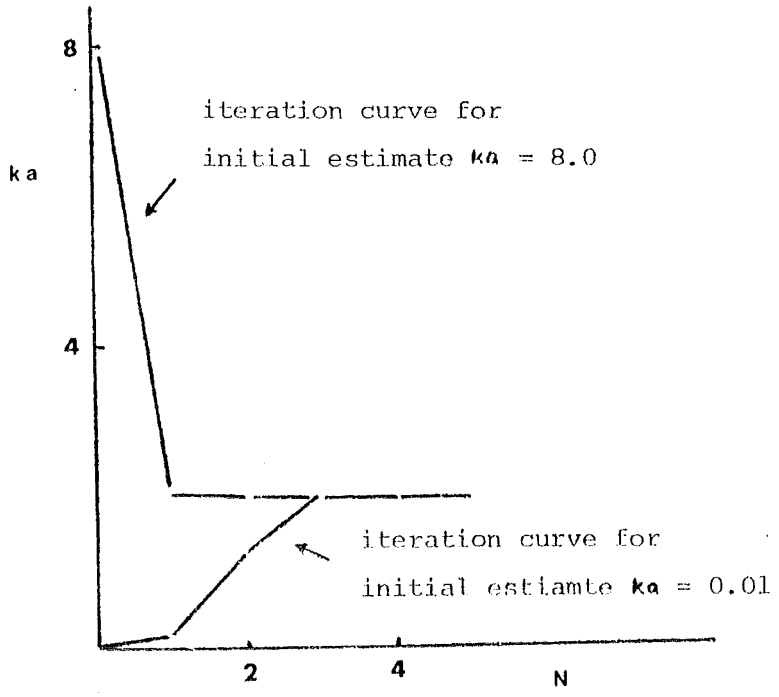

FIGURE 2.16a Reconstruction of the circular cylinder shown in Fig. 2.15. The value of ka is 2.0. The figures show convergence of ka versus N, the number of iterations required to arrive at the final results, starting from various initial guess of ka. The data given is the scattering cross section $\sigma(\phi)$. (a) $\sigma(\phi) = \sigma(0) = 1.708$, (b) $\sigma(\phi) = \sigma(\pi/2) = 0.161$ and (c) $\sigma(\phi) = \sigma(\pi) = 8.049$.

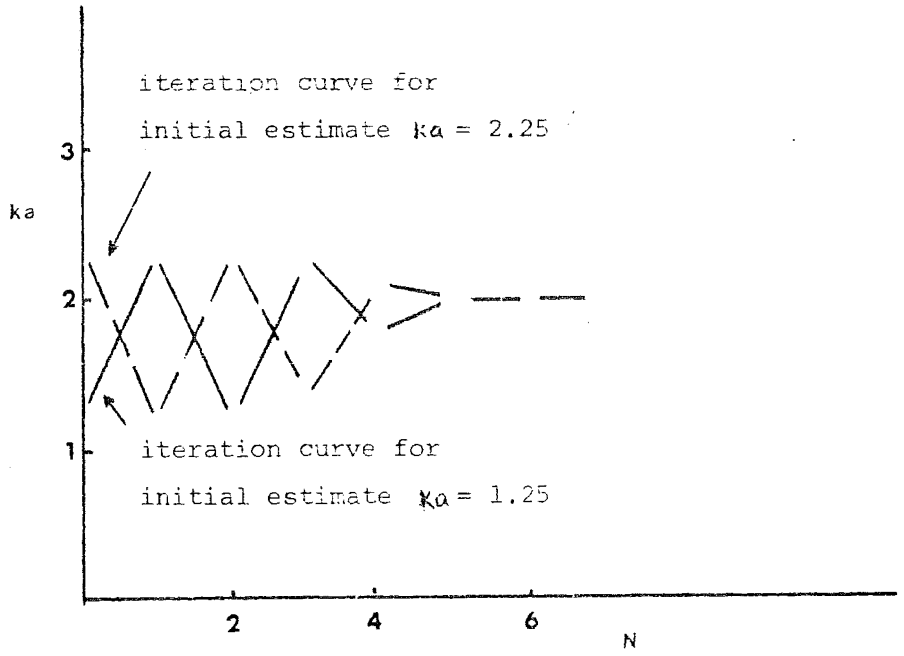

FIGURE 2.16b Reconstruction of the circular cylinder shown in Fig. 2.15. The value of ka is 2.0. The figures show convergence of ka versus N, the number of iterations required to arrive at the final results, starting from various initial guess of ka. The data given is the scattering cross section $\sigma(\phi)$. (a) $\sigma(\phi) = \sigma(0) = 1.708$, (b) $\sigma(\phi) = \sigma(\pi/2) = 0.161$ and (c) $\sigma(\phi) = \sigma(\pi) = 8.049$.

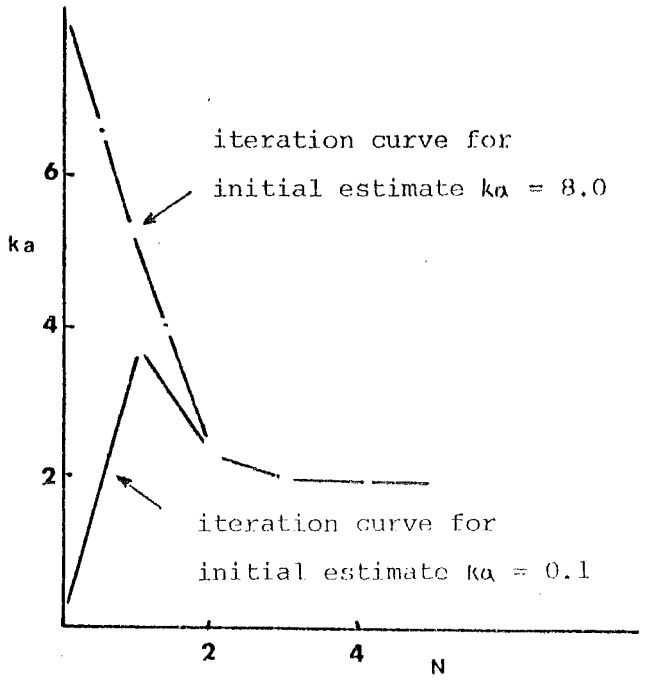

FIGURE 2.16c Reconstruction of the circular cylinder shown in Fig. 2.15. The value of ka is 2.0. The figures show convergence of ka versus N, the number of iterations required to arrive at the final results, starting from various initial guess of ka. The data given is the scattering cross section $\sigma(\phi)$. (a) $\sigma(\phi) = \sigma(0) = 1.708$, (b) $\sigma(\phi) = \sigma(\pi/2) = 0.161$ and (c) $\sigma(\phi) = \sigma(\pi) = 8.049$.

P A R T II

THE INFINITE WEDGES

CHAPTER THREE

THE PERFECTLY CONDUCTING WEDGE

3.1 INTRODUCTION

Many authors have written on the subject of diffraction by perfectly conducting wedges. Some early discussions are by Poincare (1892, 1897), Macdonald (1895), Sommerfeld (1896), Bromwich (1915), Carslaw (1920), Jones and Pidduck (1950) and Keller and Blank (1951). Bouwkamp (1946) describes in detail the singularities occurring at sharp edges while Kontorowich and Lebedev (1939) introduce the transform method now known by their names. Oberhettinger (1954) reviews the pertinent literature comprehensively.

Many other aspects of conducting wedge diffraction have also been studied by Bates (1967a, computational), King (1971, experimental), Lang (1973, wedges in the presence of resistive sheet), Hurd (1976, wedges covered with dielectric) and Thiel (1982, computational). Chu and Kouyoumjian (1965) consider the surface wave diffraction by a wedge. Bates and Hunter (1969), Mohsen and Hamid (1971) and Lewin (1971) have discussed diffracted by conducting wedges in the near incident field. Chan and Felsen (1977) and Tiberio and Kouyoumjian (1982) study the scattering of pulses by conducting wedges.

Other useful papers include those by: for three-dimensional scattering, Filippov (1964); on wedges with round corners, Ross and Hahmid (1971) and Eguiluz (1976); on elastic wave scattering, Kostrov (1966), Kraut (1968), Zemell (1975), Kapustianskii (1976), Poruchikov (1976), Larsen (1980), Gautesen (1983) and Papadopoulous (1983); on absorbing wedge, Karal and Karp (1958), Felsen (1959), Karp and Karal (1959), Karal, Karp, Chu and Kouyoumjian (1961) and Chu, Kouyoumjian, Karal and Karp (1962); on calculation of (asymptotic) diffraction coefficients, Lewis and Boersama (1969), Kouyoumjian (1965), Latz (1973) and James (1977) on new approaches ,

Cautesen (1982, integral representation), Ciarkowshi, Boersma and Mittra (1984, spectral domain method) and Kim and Thiele (1982, hybrid technique). Finally, on engineering applications, Lewin (1969), James and Kerdemelidis (1973), Chadha and Gupta (1981), Petit and Cadhilac (1983), Wirgin and Petit (1982) and Sugimoto and Kozaki (1983) use the perfectly conducting wedge solution in the formulation of engineering problems.

3.2 THE KONTOROWICH-LEBEDEV TRANSFORMATION

The transform invented by Kontorowich and Lebedev (1939) is useful for constructing radial solutions to boundary value problems involving two-dimensional wave equations.

The usual form of the transform and its inverse are (Jones 1964, Section 9.13):

$$F(\alpha) = \int_0^\infty f(x)\, H_\alpha^{(2)}(x)\, dx, \quad |\text{Real } (\alpha)| < 1 \tag{3.1}$$

$$xf(x) = -1/2 \int_{-j\infty}^{j\infty} \alpha\, J_\alpha(x)\, F(\alpha)\, d\alpha \tag{3.2}$$

However, Jones (1980) points out that while most of the solutions which have so far been derived with the aid of the transform pair stated above are correct, the formulation is incorrect in general. The integral in (3.2) converges if and only if $F(\alpha)$ decays sufficiently rapidly at infinity, a requisite not satisfied in many practical situations. Jones (1980) shows further that the transform pair does not exist for the particularly elementary function $f(x) = \exp(-ax)$, $R(a) > 0$. Jones (1980) suggests the alternate form:

$$xf(x) = \lim_{\varepsilon \to 0^+} -1/2 \int_{-j\infty}^{j\infty} \exp(\varepsilon\alpha^2)\, \alpha\, J_\alpha(x)\, F(\alpha)\, d\alpha \tag{3.3}$$

which yields the same result as (3.2) and can be rigorously justified.

3.2.1 Kontorowich-Lebedev Transform and Perfectly Conducting Wedges

As an illustration of the use of the transform, the problem of a perfectly conducting wedge irradiated by harmonic electromagnetic waves from a line source parallel to the wedge, as considered by Jones (1964 Section 9.14, pp 510) is now presented.

Let the faces of a perfectly conducting wedge coincide with the semi-infinite planes $\phi = \chi$ and $2\pi - \chi$, where the wedge angle equals 2χ (Fig. 3.1). A line source is situated at $(\rho_o ; \phi_o)$.

The problem thus reduces to finding the solution to the inhomogeneous wave equation

$$\nabla^2 \Psi + k^2 \Psi = - 1/\rho_o \; \delta(\rho - \rho_o) \; \delta(\phi - \phi_o) \tag{3.4}$$

with the required boundary conditions that $\Psi(\rho;\phi)$ vanishes on the faces of the wedge.

Multiply (3.4) by $\rho \, H_\alpha^{(2)}(k\rho)$, where $R(\alpha) = 0$, and integrate, with respect to ρ, from 0 to ∞. RHS(3.4) straightforwardly reduces to $- H_\alpha^{(2)}(k\rho_o) \; \delta(\phi - \phi_o)$, while the LHS becomes

$$\begin{aligned}
&\int_o^\infty (\nabla^2 \Psi + k^2 \Psi) \; \rho H_\alpha^{(2)}(k\rho) \; d\rho = \int_o^\infty \left[1/\rho \; \partial(\rho \partial\Psi/\partial\rho)/\partial\rho \right. \\
&\quad \left. + 1/\rho^2 \; \partial^2\Psi/\partial\phi^2 + k^2 \Psi \right] \; \rho H_\alpha^{(2)}(k\rho) \; d\rho \\
&\quad = \int_o^\infty \left[\partial(\rho \partial\Psi/\partial\rho)/\partial\rho \; H_\alpha^{(2)}(k\rho) + 1/\rho \; \partial^2\Psi/\partial\phi^2 \; H_\alpha^{(2)}(k\rho) \right. \\
&\quad \left. + k^2 \rho \; \Psi \; H_\alpha^{(2)}(k\rho) \right] d\rho = \left[\rho \partial\Psi/\partial\rho \; H_\alpha^{(2)}(k\rho) \right]_o^\infty \\
&\quad + \int_o^\infty \left[-k\rho \; \partial\Psi/\partial\rho \; H_\alpha^{(2)'}(k\rho) + k^2 \rho \Psi \; H_\alpha^{(2)}(k\rho) \right] d\rho \\
&\quad + \partial^2 \left(\int_o^\infty \Psi \; H_\alpha^{(2)}(k\rho) \; d\rho/\rho \right)/\partial\phi^2 = \left[\rho \partial\Psi/\partial\rho \; H_\alpha^{(2)}(k\rho) \right]_o^\infty \\
&\quad - \left[\Psi \; k\rho \; H_\alpha^{(2)'}(k\rho) \right]_o^\infty + \int_o^\infty \Psi \left[k^2 \rho^2 \; H_\alpha^{(2)''}(k\rho) + k\rho \; H_\alpha^{(2)'}(k\rho) \right] d\rho/\rho \\
&\quad + \int_o^\infty k^2 \rho \Psi \; H_\alpha^{(2)}(k\rho) \; d\rho + \partial^2 \left(\int_o^\infty \Psi \; H_\alpha^{(2)}(k\rho) \; d\rho/\rho \right)/\partial\phi^2
\end{aligned} \tag{3.5}$$

Invoking Bessel's equation (Watson 1966, Chapter 1), (3.5) can be reduced further to

$$\left[\rho\partial\Psi/\partial\rho\ H_\alpha^{(2)}(k\rho) - \Psi\, k\rho\ H_\alpha^{(2)\prime}(k\rho)\right]_0^\infty$$

$$+ \int_0^\infty \Psi(\alpha^2-k^2\rho^2)\ H_\alpha^{(2)}(k\rho)\ d\rho/\rho + \int_0^\infty k^2\ \rho^2\Psi H_\alpha^{(2)}(k\rho)\ d\rho/\rho$$

$$+ \partial^2\left(\int_0^\infty \Psi H_\alpha^{(2)}(k\rho)\,d\rho/\rho\right)/\partial\phi^2 = \left[\rho\ \partial\Psi/\partial\rho\ H_\alpha^{(2)}(k\rho) - \Psi\, k\rho\ H_\alpha^{(2)\prime}(k\rho)\right]_0^\infty$$

$$+ \int_0^\infty \alpha^2\ \Psi\ H_\alpha^{(2)}(k\rho)\ d\rho/\rho + \partial^2\left(\int_0^\infty \Psi\ H_\alpha^{(2)}(k\rho)\ d\rho/\rho\right)/\partial\phi^2 \qquad (3.6)$$

The upper limit in the first term of (3.6) goes to zero since

$$\lim_{\rho\to\infty}\left[\rho\partial\Psi/\partial\rho\ H_\alpha^{(2)}(k\rho) - \Psi\, k\rho\ H_\alpha^{(2)\prime}(k\rho)\right]$$

$$= \lim_{\rho\to\infty}\left[\rho\ \partial\Psi/\partial\rho\ H_\alpha^{(2)}(k\rho) - \Psi\ \rho\ \partial\ H_\alpha^{(2)}(k\rho)/\partial\rho\ \right]$$

$$= \lim_{\rho\to\infty}\left[\rho\ \partial\Psi/\partial\rho\ H_\alpha^{(2)}(k\rho) - \Psi\rho\partial\ H_\alpha^{(2)}(k\rho)/\partial\rho\right.$$

$$\left. + j\ k\rho\Psi\ H_\alpha^{(2)}(k\rho) - j\ k\rho\Psi\ H_\alpha^{(2)}(k\rho)\ \right]$$

$$= \lim_{\rho\to\infty}\rho^{\frac{1}{2}}\ H_\alpha^{(2)}(k\rho)\ \left[\rho^{\frac{1}{2}}\ \partial\Psi/\partial\rho + j\ k\rho^{\frac{1}{2}}\ \Psi\ \right]$$

$$- \lim_{\rho\to\infty}\rho^{\frac{1}{2}}\ \Psi\ \left[\rho^{\frac{1}{2}}\partial H_\alpha^{(2)}(k\rho)/\partial\phi + j\ k\rho^{\frac{1}{2}}\ H_\alpha^{(2)}(k\rho)\right] = 0 \qquad (3.7)$$

where

$$\lim_{\rho\to\infty}\ \rho^{\frac{1}{2}}\ H_\alpha^{(2)}(k\rho) \longrightarrow \text{a constant}$$

$$\lim_{\rho\to\infty}\ \rho^{\frac{1}{2}}\ \left[\partial\ H_\alpha^{(2)}(k\rho)/\partial\rho + j\ k\ H_\alpha^{(2)}(k\rho)\right] \longrightarrow 0 \qquad (3.8)$$

and

$$\lim_{\rho\to\infty}\rho^{\frac{1}{2}}\ \Psi \longrightarrow \text{a constant}$$

$$\lim_{\rho\to\infty}\rho^{\frac{1}{2}}\ \left[\partial\Psi/\partial\rho + j\ k\ \Psi\right] \longrightarrow 0 \qquad (3.9)$$

are the Sommerfeld radiation conditions (Jones 1964, Section 1.27).

The lower limit in the first term of (3.6) goes to zero since the edge conditions (Jones 1964, Section 9.2) for E-polarised fields on perfectly conducting wedge require $\lim_{\rho\to o} \Psi\rho^t$ $0 \leq t \leq 1$.

Finally, one gets

$$\left[\partial^2/\partial\phi^2 + \alpha^2\right] \int_o^\infty \Psi\, H_\alpha^{(2)}(k\rho)\, d\rho/\rho = - H_\alpha^{(2)}(k\rho_o)\ \delta(\phi-\phi_o) \tag{3.10}$$

Denoting $\Theta = \int_o^\infty \Psi\, H_\alpha^{(2)}(k\rho)\, d\rho/\rho$, the problem thus reduces to solving the partial differential equation

$$\partial^2\Theta/\partial\phi^2 + \alpha^2\Theta = - H_\alpha^{(2)}(k\rho_o)\ \delta(\phi-\phi_o) \tag{3.11}$$

subject to the boundary conditions previously imposed on Ψ.

A general solution for Θ is

$$\begin{aligned}\Theta &= a_\alpha \sin(\alpha\phi) + b_\alpha \cos(\alpha\phi), \qquad \phi < \phi_o \\ &= e_\alpha \sin(\alpha\phi) + f_\alpha \cos(\alpha\phi), \qquad \phi > \phi_o\end{aligned} \tag{3.12}$$

where a_α, b_α, e_α, f_α are expansion coefficients. The Dirichlet boundary conditions require that

(i) $\Psi(\rho;\chi) = 0$

i.e. $a_\alpha \sin(\alpha\chi) + b_\alpha \cos(\alpha\chi) = 0$ (3.13)

(ii) $\Psi(\rho;2\pi-\chi) = 0$

i.e. $e_\alpha \sin\alpha(2\pi-\chi) + f_\alpha \cos\alpha\ (2\pi-\chi) = 0$ (3.14)

Also, at $\phi = \phi_o$, field continuation requires $\Psi(\rho_o;\phi_{o+}) = \Psi(\rho_o;\phi_{o-})$ i.e.

$$a_\alpha \sin(\alpha\phi_o) + b_\alpha \cos(\alpha\phi_o) = e_\alpha \sin(\alpha\phi_o) + f_\alpha \cos(\alpha\phi_o) \tag{3.15}$$

Integrating (3.11) with respect to ϕ from ϕ_{o-} to ϕ_{o+} gives

$$(\partial\Theta/\partial\phi)_{\phi_{o+}} - (\partial\Theta/\partial\phi)_{\phi_{o-}} + \alpha^2 \int_{\phi_{o-}}^{\phi_{o+}} \Theta\, d\phi = - H_\alpha^{(2)}(k\rho_o) \tag{3.16}$$

However, $\int_{\phi_o}^{\phi_{o+}} 0 \, d\phi = 0$ from (3.15). Therefore, substituting (3.12) into (3.16) gives

$$(\partial\theta/\partial\phi)_{\phi_{o+}} - (\partial\theta/\partial\phi)_{\phi_{o-}}$$

$$= -a_\alpha \alpha \cos(\alpha\phi_o) + b_\alpha \alpha \sin(\alpha\phi_o) + e_\alpha \alpha \cos(\alpha\phi_o) - f_\alpha \alpha \sin(\alpha\phi_o)$$

$$= -H_\alpha^{(2)}(k\rho_o) \tag{3.17}$$

Solving (3.13), (3.14), (3.15) and (3.17) simultaneously for a_α, b_α, e_α and f_α leads to

$$a_\alpha = H_\alpha^{(2)}(k\rho_o) \cos(\alpha\chi) \sin\alpha(\phi_o - 2\pi + \chi)/\alpha \sin 2\alpha(\pi-\chi)$$

$$b_\alpha = -H_\alpha^{(2)}(k\rho_o) \sin(\alpha\chi) \sin\alpha(\phi_o - 2\pi + \chi)/\alpha \sin 2\alpha(\pi-\chi)$$

$$e_\alpha = -H_\alpha^{(2)}(k\rho_o) \sin\alpha(\phi_o - \chi) \cos\alpha(2\pi-\chi)/\alpha \sin 2\alpha(\pi-\chi)$$

$$f_\alpha = H_\alpha^{(2)}(k\rho_o) \sin\alpha(\phi_o - \chi) \sin\alpha(2\pi-\chi)/\alpha \sin 2\alpha(\pi-\chi) \tag{3.18}$$

Finally,

$$\theta = \int_o^\infty \Psi H_\alpha^{(2)}(k\rho) \, d\rho/\rho = H_\alpha^{(2)}(k\rho_o) \sin\alpha(\phi-\chi)$$

$$\sin\alpha(\phi_o - 2\pi + \chi)/\alpha \sin 2\alpha(\pi-\chi), \quad \phi < \phi_o \tag{3.19}$$

$$\theta = H_\alpha^{(2)}(k\rho_o) \sin\alpha(\phi_o - \chi) \sin\alpha(\phi - 2\pi + \chi)/\alpha \sin 2\alpha(\pi-\chi), \quad \phi > \phi_o \tag{3.20}$$

Note that (3.19) and (3.20) are the Kontorowich - Levedev transform of Ψ/ρ for $\phi < \phi_o$ and $\Phi > \phi_o$ respectively. Therefore, applying the inverse transform,

$$\Psi = \lim_{\varepsilon\to 0+} 1/2 \int_{-j\infty}^{j\infty} \exp(\varepsilon\alpha^2)\alpha J_\alpha(k\rho) H_\alpha^{(2)}(k\rho_o) \sin\alpha(\phi-\chi) \sin\alpha(\phi_o - 2\pi + \chi)$$

$$d\alpha/\alpha \sin 2\alpha(\pi-\chi), \quad \phi < \phi_o$$

$$= \lim_{\varepsilon\to 0+} 1/2 \int_{-j\infty}^{j\infty} \exp(\varepsilon\alpha^2)\alpha J_\alpha(k\rho) H_\alpha^{(2)}(k\rho_o) \sin\alpha(\phi_o - \chi) \sin\alpha(\phi - 2\pi + \chi)$$

$$d\alpha/\alpha \sin 2\alpha(\pi-\chi), \quad \phi > \phi_o \tag{3.21}$$

For $\rho_o > \rho$, the integrands in (3.21) vanish at infinity in the right half plane (Fig. 3.2). Therefore, on closing the contour of integration at infinity in the right half plane, Cauchy's residue theorem (cf. Kreyszig 1972, Section 16.3) gives

$$\Psi = -\frac{1}{2(2\pi j)} \sum_{n=1}^{\infty} (-1)^n J_{n\alpha}(k\rho)\, H^{(2)}_{n\alpha}(k\rho_o) \sin n\alpha(\phi-\chi)$$

$$\sin n\alpha(\phi_o - 2\pi + \chi)/2(\pi-\chi), \qquad \phi < \phi_o$$

$$= -\frac{1}{2(2\pi j)} \sum_{n=1}^{\infty} (-1)^n J_{n\alpha}(k\rho)\, H^{(2)}_{n\alpha}(k\rho_o) \sin n\alpha(\phi_o-\chi)$$

$$\sin n\alpha(\phi - 2\pi + \chi)/2(\pi-\chi), \qquad \phi > \phi_o \tag{3.22}$$

where $\alpha = \pi/2(\pi-\chi)$.

i.e. $$\Psi = -\frac{\pi j}{2(\pi-\chi)} \sum_{n=1}^{\infty} J_{n\alpha}(k\rho)\, H^{(2)}_{n\alpha}(k\rho_o)$$

$$\sin n\alpha(\phi-\chi) \sin n\alpha(\phi_o-\chi), \qquad \chi<\phi<2\pi-\chi, \qquad \rho > \rho_o$$

$$= -\frac{\pi j}{2(\pi-\chi)} \sum_{n=1}^{\infty} J_{n\alpha}(k\rho)\, H^{(2)}_{n\alpha}(k\rho_o)$$

$$\sin n\alpha(\phi-\chi) \sin n\alpha(\phi_o-\chi), \qquad \chi<\phi<2\pi-\chi, \qquad \rho < \rho_o \tag{3.23}$$

by reciprocity.

3.2.2 Kontorowich - Lebedev Transform and Penetrable Wedges

Although it seems at first sight plausible that the Kontorowich-Lebedev transform should be applicable to the penetrable wedge, it unfortunately turns out not to be so, for the following reasons.

The penetrable wedge problem involves solving

$$\nabla^2\Psi_+ + k^2\Psi_+ = -\frac{1}{\rho_o}\,\delta(\rho-\rho_o)\,\delta(\phi-\phi_o)$$

and

$$\nabla^2\Psi_- + \nu^2 k^2 \Psi_- = 0 \tag{3.24}$$

simultaneously, where Ψ_+ and Ψ_- respectively are the wave functions outside and inside the penetrable wedge and ν is the refractive index of the wedge. Furthermore, appropriate boundary conditions must be satisfied on the faces of the wedge.

Multiplying the above two equations by $\rho H_\alpha^{(2)}(k\rho)$, and manipulating these in the same way as described in Section 3.2.1, gives

$$(\partial^2/\partial\phi^2 + \alpha^2) \int_0^\infty \Psi_+ H_\alpha^{(2)}(k\rho)\, d\rho/\rho = - H_\alpha^{(2)}(k\rho_o)\, \delta(\phi-\phi_o)$$

and

$$(\partial^2/\partial\phi^2 + \alpha^2) \int_0^\infty \Psi_- H_\alpha^{(2)}(k\rho)\, d\rho/\rho + (\nu^2-1) \int_0^\infty k^2 \rho^2 \Psi_\mp H_\alpha^{(2)}(k\rho)\, d\rho/\rho = 0 \qquad (3.25)$$

Comparing (3.25) with (3.10), it is clear that, one cannot reduce (3.25) into a simple partial differential equation involving only angular variables by defining

$$\Theta_+ = \int_0^\infty \Psi_+ H_\alpha^{(2)}(k\rho)\, d\rho/\rho$$

$$\Theta_- = \int_0^\infty \Psi_- H_\alpha^{(2)}(k\rho)\, d\rho/\rho \qquad (3.26a)$$

The point is that a single transform for fields both inside and outside the wedge is inadequate.

On the other hand, if two transforms are used, i.e.

$$\Theta_+ = \int_0^\infty \Psi_+ H_\alpha^{(2)}(k\rho)\, d\rho/\rho$$

and

$$\Theta_- = \int_0^\infty \Psi_- H_\alpha^{(2)}(\nu k\rho)\, d\rho/\rho \qquad (3.26b)$$

it transpires that Θ_+ and Θ_- satisfy the two equations

$$\partial^2\Theta_+/\partial\phi^2 + \alpha^2\, \Theta_+ = - H_\alpha^{(2)}(k\rho_o)\, \delta(\phi-\phi_o)$$

and

$$\partial^2\Theta_-/\partial\phi^2 + \alpha^2\, \Theta_- = 0 \qquad (3.26c)$$

Unfortunately, there is no simple way of matching Θ_+ and Θ_- across the faces of the wedge.

3.3 APPLYING THE NULL-FIELD METHOD TO PERFECTLY CONDUCTING WEDGE PROBLEMS

3.3.1 The Integral $I_{m,\alpha}$, $\alpha \neq I$

The integral $I_{m,\alpha}$ which is needed subsequently, is defined by

$$I_{m,\alpha} = H_m^{(2)}(k\rho) \int_0^{\rho} J_m(kr)\, J_\alpha(kr)\, r^{-1}\, dr + J_m(k\rho) \int_\rho^{\infty} H_m^{(2)}(kr)\, J_\alpha(kr) r^{-1}\, dr \qquad (3.27)$$

Using equation (13) of Watson (1966), Section 5.11, (3.27) can be re-written as

$$I_{m,\alpha} = H_m^{(2)}(k\rho) \left[- kr\, J_{m+1}(kr)\, J_\alpha(kr)/(m^2-\alpha^2) + J_m(kr)\, J_{\alpha+1}(kr)\, kr/(m^2-\alpha^2) + J_m(kr)\, J_\alpha(kr)/(m+\alpha)\right]_0^{\rho}$$
$$+ J_m(k\rho) \left[-kr\, H_{m+1}^{(2)}(kr)\, J_\alpha(kr)/(m^2-\alpha^2) + kr\, H_m^{(2)}(kr)\, J_{\alpha+1}(kr)/(m^2-\alpha^2) + H_m^{(2)}(kr)\, J_\alpha(kr)/(m+\alpha)\right]_\rho^{\infty}, \quad \alpha \neq m \qquad (3.28)$$

When $\alpha = m \neq 0$, equation (6) of Watson (1966), Section 5.12, shows that

$$I_{m,m} = -1/2m\, H_m^{(2)}(k\rho) \left[J_0^{\,2}(kr) + 2\sum_{n=1}^{m-1} J_n^{\,2}(kr) + J_m^{\,2}(kr)\right]_0^{\rho}$$
$$- 1/2m\, J_m(k\rho) \left[H_0^{(2)}(kr)\, J_0(kr) + 2\sum_{n=1}^{m-1} H_n^{(2)}(kr)\, J_n(kr) + H_m^{(2)}(kr)\, J_m(kr)\right]_\rho^{\infty} \qquad (3.29)$$

However, there is no simple formula for $I_{0,0}$. Fortunately, $I_{0,0}$ is not required for the work described in this thesis, and there is therefore no need to consider the case when $\alpha = m = 0$.

(i) when $\alpha = m$, $\alpha \notin I$

$$I_{m,\alpha} = H_m^{(2)}(k\rho) \left[-k\rho\, J_{m+1}(k\rho)\, J_\alpha(k\rho)/(m^2-\alpha^2) + k\rho\, J_m(k\rho)\, J_{\alpha+1}(k\rho)/(m^2-\alpha^2) + J_m(k\rho)\, J_\alpha(k\rho)/(m+\alpha)\right]$$
$$- J_m(k\rho) \left[-k\rho\, H_{m+1}^{(2)}(k\rho)\, J_\alpha(k\rho)/(m^2-\alpha^2) + k\rho\, H_m^{(2)}(k\rho)\, J_{\alpha+1}(k\rho)/(m^2-\alpha^2) + H_m^{(2)}(k\rho)\, J_\alpha(k\rho)/(m+\alpha)\right]$$

$$- H_m^{(2)}(k\rho) \lim_{r\to 0} \left[-kr\, J_{m+1}(kr)\, J_\alpha(kr)/(m^2-\alpha^2) + kr\, J_m(kr)\, J_{\alpha+1}(kr)/(m^2-\alpha^2) + J_m(kr)\, J_\alpha(kr)/(m+\alpha)\right]$$

$$+ J_m(k\rho) \lim_{r\to\infty} \left[-kr\, H_{m+1}^{(2)}(kr)\, J_\alpha(kr)/(m^2-\alpha^2) + kr\, H_m^{(2)}(kr)\, J_{\alpha+1}(kr)/(m^2-\alpha^2) + H_m^{(2)}(kr)\, J_\alpha(kr)/(m+\alpha)\right] \tag{3.30}$$

On substituting the asymptotic expansions for the Bessel and Hankel functions, as defined by (1.31) and (1.32), into (3.30), the latter becomes

$$I_{m,\alpha} = - k\rho\, J_\alpha(k\rho) \left[H_m^{(2)}(k\rho)\, J_{m+1}(k\rho) - H_{m+1}^{(2)}(k\rho)\, J_m(k\rho)\right]/(m^2-\alpha^2)$$

$$- H_m^{(2)}(k\rho) \lim_{r\to 0} \left[-\frac{kr}{m^2-\alpha^2}\left\{\frac{(kr)^{m+1}}{\Gamma(m+2)}\,\frac{(kr)^\alpha}{\Gamma(\alpha+1)} - \frac{(kr)^m}{\Gamma(m+1)}\,\frac{(kr)^{\alpha+1}}{\Gamma(\alpha+2)}\right\}\right.$$

$$\left. + \frac{1}{m+\alpha}\,\frac{(kr)^m}{\Gamma(m+1)}\,\frac{(kr)^\alpha}{\Gamma(\alpha+1)}\right] + J_m(k\rho) \lim_{r\to\infty} \left[-\frac{kr}{m^2-\alpha^2}\left\{(2/\pi k\rho)^{\frac{1}{2}}\right.\right.$$

$$\exp(-j\left[kr-m\pi/2-\pi/2-\pi/4\right])\,(2/\pi kr)^{\frac{1}{2}}\cos(kr-\alpha\pi/2-\pi/4)$$

$$\left.\left. - (2/\pi kr)^{\frac{1}{2}}\exp(-j\left[kr-m\pi/2-\pi/4\right])(2/\pi kr)^{\frac{1}{2}}\cos(kr-\alpha\pi/2-\pi/2-\pi/4)\right\}\right.$$

$$\left. + \frac{1}{m+\alpha}\,(2/\pi kr)^{\frac{1}{2}}\exp(-j\left[kr-m\pi/2-\pi/4\right])(2/\pi kr)^{\frac{1}{2}}\cos(kr-\alpha\pi/2-\pi/4)\right] \tag{3.31}$$

Note that the bracketed quantity in the first term of (3.31) is a Wronskian (cf. Abramowitz and Stegun, equation 9.1.16, 1965) and is equal to

$$H_m^{(2)}(k\rho)\, J_{m+1}(k\rho) - H_{m+1}^{(2)}(k\rho)\, J_m(k\rho) = -2j/\pi k\rho \tag{3.32}$$

(3.31) then becomes

$$I_{m,\alpha} = - k\rho\, J_\alpha(k\rho)(-2j/\pi k\rho)/(m^2-\alpha^2) + \frac{H_m^{(2)}(k\rho)}{m^2-\alpha^2}\left[\frac{1}{\Gamma(\alpha+1)\,\Gamma(m+2)} - \frac{1}{\Gamma(\alpha+2)\,\Gamma(m+1)}\right] \lim_{r\to 0} (kr)^{m+\alpha+2}$$

$$- \frac{H_m^{(2)}(k\rho)}{m+\alpha}\,\frac{1}{\Gamma(\alpha+1)\,\Gamma(m+1)} \lim_{r\to 0} (kr)^{m+\alpha}$$

$$+ \frac{2J_m(k\rho)}{\pi(m+\alpha)} \lim_{r\to\infty} \frac{1}{kr} \exp(-j[kr-m\pi/2-\pi/4])$$

$$\cos(kr-\alpha\pi/2-\pi/4) - \frac{J_m(k\rho)}{\pi(m^2-\alpha^2)} \lim_{r\to\infty} \Big[\exp(-j[kr-m\pi/2-\pi/2-\pi/4])$$

$$\exp(j[kr-\alpha\pi/2-\pi/4]) + \exp(-j[kr-m\pi/2-\pi/2-\pi/4])$$

$$\exp(-j[kr-\alpha\pi/2-\pi/4]) - \exp(-j[kr-m\pi/2-\pi/2-\pi/4])$$

$$\exp(j[kr-\alpha\pi/2-\pi/2-\pi/4]) - \exp(-j[kr-m\pi/2-\pi/4])$$

$$\exp(-j[kr-\alpha\pi/2-\pi/2-\pi/4])\Big] \qquad (3.33)$$

Since $\alpha \neq I_-$ and $\alpha \neq m$, the second and third terms of (3.33) must tend to zero when $r\to 0$. Furthermore, the fourth term of (3.33) must tend to zero when $r\to\infty$. Therefore, (3.33) becomes

$$I_{m,\alpha} = 2j\, J_\alpha(k\rho)/\pi(m^2-\alpha^2) - J_m(k\rho)/\pi(m^2-\alpha^2) \lim_{r\to\infty} \Big[\exp(j\,\pi/2)$$

$$\exp(j[m\pi/2-\alpha\pi/2]) + \exp(j\pi)\exp(-j2kr)\exp(j[m\pi/2+\alpha\pi/2])$$

$$- \exp(-j\pi/2)\exp(j[m\pi/2-\alpha\pi/2])$$

$$- \exp(j\pi)\exp(-2jkr)\exp(j[m\pi/2+\alpha\pi/2])\Big]$$

$$= 2j\exp(-j\alpha\pi/2)\left[\exp(j\alpha\pi/2)\, J_\alpha(k\rho) - \exp(jm\pi/2)\, J_m(k\rho)\right]/\pi(m^2-\alpha^2) \qquad (3.34)$$

(ii) when $\alpha = m \neq 0$,

$$I_{m,m} = -H_m^{(2)}(k\rho)\left[J_o^2(k\rho) + 2\sum_{n=1}^{m-1} J_n^2(k\rho) + J_m^2(k\rho)\right]/2m$$

$$+ J_m(k\rho)\left[H_o^{(2)}(k\rho)\, J_o(k\rho) + 2\sum_{n=1}^{m-1} H_n^{(2)}(k\rho)\right.$$

$$\left. J_n(k\rho) + H_m^{(2)}(k\rho)\, J_m(k\rho)\right]/2m$$

$$+ H_m^{(2)}(k\rho)/2m \lim_{r\to 0}\left[J_o^2(kr) + 2\sum_{n=1}^{m-1} J_n^2(kr) + J_m^2(kr)\right]$$

$$- J_m(k\rho)/2m \lim_{r\to\infty}\left[H_o^{(2)}(kr)\, J_o(kr) + 2\sum_{n=1}^{m-1} H_n^{(2)}(kr)\, J_n(kr)\right.$$

$$\left. + H_m^{(2)}(kr)\, J_m(kr)\right] \qquad (3.35)$$

Again using the asymptotic expansions for Bessel and Hankel functions, as defined by (1.31) and (1.32), (3.35) becomes

$$I_{m,m} = 1/2m \sum_{n=o}^{m-1} \varepsilon_n J_n(k\rho) \left[H_n^{(2)}(k\rho)\, J_m(k\rho) - H_m^{(2)}(k\rho)\, J_n(k\rho)\right]$$

$$+ 1/2m\, H_m^{(2)}(k\rho) \lim_{r\to o} \left[\left(\frac{(kr)^o}{\Gamma(1)}\right)^2 + 2\sum_{n=1}^{m-1}\left(\frac{(kr)^n}{\Gamma(n+1)}\right)^2 + \left(\frac{(kr)^m}{\Gamma(m+1)}\right)^2\right]$$

$$- 1/2m\, J_m(k\rho) \lim_{r\to\infty} \Big[(2/\pi kr)^{\frac{1}{2}} \exp(-j[kr-\pi/4])(2/\pi kr)^{\frac{1}{2}} \cos(kr-\pi/4)$$

$$+ 2\sum_{n=1}^{m-1} (2/\pi kr)^{\frac{1}{2}} \exp(-j[kr-n\pi/2-\pi/4])(2/\pi kr)^{\frac{1}{2}} \cos(kr-n\pi/2-\pi/4)$$

$$+ (2/\pi kr)^{\frac{1}{2}} \exp(-j[kr-m\pi/2-\pi/4])(2/\pi kr)^{\frac{1}{2}} \cos(kr-m\pi/2-\pi/4)\Big]$$

$$= 1/2m \sum_{n=o}^{m-1} \varepsilon_n J_n(k\rho)\left[H_n^{(2)}(k\rho)\, J_m(k\rho)\right.$$

$$\left. - H_m^{(2)}(k\rho)\, J_n(k\rho)\right] + H_m^{(2)}(k\rho)/2m \qquad (3.36)$$

3.3.2 E-Polarisation

When the incident field is a plane wave electrically-polarised parallel to the axis of an infinite perfectly conducting wedge (Fig. 3.3), the total field is given by (Bates 1965)

$$\Psi = \alpha \sum_{n=o}^{\infty}{}' \varepsilon_n j^{n\alpha} J_{n\alpha}(k\rho) \left[\cos n\alpha\,(\theta-\phi) - \cos n\,\alpha(\theta+\phi-2\chi)\right] \qquad (3.37)$$

where $\chi<\theta<2\pi-\chi$ is the angle of incidence of the plane wave, $\alpha = \pi/(2\pi-2\chi)$ and the faces of the wedge coincide with the planes $\phi=\chi$ and $2\pi-\chi$ (Fig. 3.3). It is obvious from (3.37) that Ψ satisfies the Dirichelet boundary condition ($\Psi(\rho;\,{}^{\chi}_{2\pi-\chi}) = 0$). Furthermore

$$\partial\Psi/\partial\phi = \alpha^2 \sum_{n=o}^{\infty}{}' \varepsilon_n\, n\, j^{n\alpha} J_{n\alpha}(k\rho) \left[\sin n\alpha(\theta-\phi) + \sin n\alpha(\theta+\phi-2\chi)\right] \qquad (3.38)$$

The null-field equation (1.95a) is

$$\int_C \left[\Psi\, \nabla g - g\, \nabla\Psi\right] dC = -\Psi_{inc} \qquad (1.95a)$$

Since RHS(1.95a) has the form - i.e. (1.34) - of the generating function for Bessel functions, it can be written as

$$-\Psi_{inc} = -\exp(jk\rho\cos(\theta-\phi)) = -\sum_{n=o}^{\infty} \varepsilon_n j^n \cos n(\theta-\phi)\, J_n(k\rho) \qquad (3.39)$$

With $\Psi(\rho; \frac{\chi}{2\pi-\chi}) = 0$, LHS(1.95a) can be manipulated as follows:

$$\int_C [-g\nabla\Psi]dC = -\int_{\infty}^{o} [-g(1/r)\,\partial\Psi/\partial\theta]_{\theta=\chi}\, dr$$

$$+\int_o^{\infty} [-g(-1/r)\,\partial\Psi/\partial\theta]_{\theta=2\pi-\chi}\, dr = \int_{\infty}^{o} (g)(1/r)\,\partial\Psi/\partial\theta\, dr$$

$$+\int_o^{\infty} g(1/r)\,\partial\Psi/\partial\theta\, dr = \int_o^{\infty} (-)(-j/4)\, H_o^{(2)}(kR)(1/r)\,\partial\Psi/\partial\theta\, dr$$

$$+\int_o^{\infty} (-j/4)\, H_o^{(2)}(kR)(1/r)\,\partial\Psi/\partial\theta\, dr \qquad (3.40)$$

Expanding the Hankel function by the addition theorem (cf. Section 1.4.1.1) gives

$$\text{RHS}(3.40) = -j/4\Big[-\int_o^{\rho}\sum_{m=o}^{\infty} \varepsilon_m H_m^{(2)}(k\rho)\, J_m(kr)\cos m(\chi-\phi)\,\alpha^2 \sum_{n=o}^{\infty} \varepsilon_n\, n\, j^{n\alpha}$$

$$J_{n\alpha}(kr)\left[\sin n\alpha(\theta-\chi) + \sin n\alpha(\theta+\chi-2\chi)\right] r^{-1}\, dr$$

$$-\int_{\rho}^{\infty}\sum_{m=o}^{\infty} \varepsilon_m H_m^{(2)}(kr)\, J_m(k\rho)\cos m(\chi-\phi)$$

$$\alpha^2 \sum_{n=o}^{\infty} \varepsilon_n\, n\, j^{n\alpha} J_{n\alpha}(kr)\left[\sin n\alpha(\theta-\chi) + \sin n\alpha(\theta+\chi-2\chi)\right] r^{-1}\, dr$$

$$+\int_o^{\rho}\sum_{m=o}^{\infty} \varepsilon_m H_m^{(2)}(k\rho)\, J_m(kr)\cos m(2\pi-\chi-\phi)$$

$$\alpha^2 \sum_{n=o}^{\infty} \varepsilon_n\, n\, j^{n\alpha} J_{n\alpha}(kr)\left[\sin n\alpha(\theta-2\pi+\chi)\right.$$

$$\left.+ \sin n\alpha(\theta+2\pi-\chi-2\chi)\right] r^{-1}\, dr$$

$$+\int_{\rho}^{\infty}\sum_{m=o}^{\infty} \varepsilon_m H_m^{(2)}(kr)\, J_m(k\rho)\cos m(2\pi-\chi-\phi)$$

$$\alpha^2 \sum_{n=o}^{\infty} \varepsilon_n\, n\, j^{n\alpha} J_{n\alpha}(kr)\left[\sin n\alpha(\theta-2\pi+\chi) + \sin n\alpha(\theta+2\pi-\chi-2\chi)\right]$$

$$r^{-1}\, dr$$

$$= - j/4(-2)\alpha^2 \sum_{n=o}^{\infty} \varepsilon_n n j^{n\alpha} \sin n\alpha(\theta-\chi) \sum_{m=o}^{\infty} \varepsilon_m \cos m(\chi-\phi) I_{m,n\alpha}$$

$$- j/4(2)\alpha^2 \sum_{n=o}^{\infty} \varepsilon_n n j^{n\alpha} \sin n\alpha(\theta-\chi)(-1)^n \sum_{m=o}^{\infty} \varepsilon_m \cos m(\chi+\phi) I_{m,n\alpha} \qquad (3.41)$$

Substituting from (3.34) into (3.41), the latter gives

$$\text{RHS}(3.40) = j\,\alpha^2/2 \sum_{n=o}^{\infty} \varepsilon_n n j^{n\alpha} \sin n\alpha(\theta-\chi) \sum_{m=o}^{\infty} \varepsilon_m \left[\cos m(\chi-\phi) - (-1)^n \cos m(\chi+\phi)\right]$$

$$(-2j) \exp(-jn\alpha\pi/2) \left[\exp(jm\pi/2) J_m(k\rho) - \exp(jn\alpha\pi/2)\, J_{n\alpha}(k\rho)\right]$$

$$/\pi(m^2 - (n\alpha)^2) \qquad (3.42)$$

On comparing (3.39) with (3.42), it is clear that if RHS(3.39) is to equal RHS(3.42), the coefficient of $J_{n\alpha}(k\rho)$ in (3.42) must equal zero for all n. From (3.42), the coefficients of $J_{n\alpha}(k\rho)$ are

$$c_{n,\alpha} = -\alpha^2 \varepsilon_n n j^{n\alpha} \sin n\alpha(\theta-\chi) \quad \frac{1}{\pi} \sum_{m=o}^{\infty} \varepsilon_m \left[\cos m(\chi-\phi) \mp \cos m(\chi+\phi)\right]/(m^2 - (n\alpha)^2) \qquad (3.43)$$

where the upper sign is taken when n is even and the lower sign is taken when n is odd.

Re-arranging, (3.42) can be written as

$$c_{n\alpha} = -\alpha^2 \varepsilon_n n j^{n\alpha}/\pi \sin n\alpha(\theta-\chi) \left[-1/(n\alpha)^2 + 2 \sum_{m=1}^{\infty} \cos m(\chi-\phi)/(m^2-(n\alpha)^2) \pm 1/(n\alpha)^2 \mp 2 \sum_{m=1}^{\infty} \cos m(\chi+\phi)/(m^2-(n\alpha)^2)\right] \qquad (3.44)$$

Using equation (1.445.6) of Gradshteyn and Ryzhik (1965), the coefficients $c_{n\alpha}$ are found to be

$$c_{n\alpha} = -\alpha^2 \varepsilon_n n j^{n\alpha}/\pi \sin n\alpha(\theta-\chi) \left[-1/(n\alpha)^2 + 1/(n\alpha)^2 - \pi \cos n\alpha(\pi-\chi+\phi)/2n\alpha\sin(n\alpha\pi) \pm 1/(n\alpha)^2 \mp 1/(n\alpha)^2 \pm \pi \cos n\alpha(\pi-\chi-\phi)/2n\alpha\sin(n\alpha\pi)\right]$$

$$= \alpha^2 \varepsilon_n n j^{n\alpha} \sin n\alpha(\theta-\chi) \left[\cos n\alpha(\pi-\chi+\phi) \mp \cos n\alpha(\pi-\chi-\phi)\right]/2n\alpha\sin(n\alpha\pi)$$

$$= \mp \varepsilon_n j^{n\alpha} \sin n\alpha(\theta-\chi) \begin{matrix}\sin\\ \cos\end{matrix} (n\alpha(\pi-\chi)) \begin{matrix}\sin\\ \cos\end{matrix} (n\alpha\phi)/ \sin(n\alpha\pi)$$

$$= \mp \varepsilon_n j^{n\alpha} \sin n\alpha(\theta-\chi) \begin{matrix}\sin\\ \cos\end{matrix} (n\alpha\phi) \begin{matrix}\sin\\ \cos\end{matrix} (n\pi/2)/ \sin(n\alpha\pi) = 0 \qquad (3.45)$$

since $\sin(n\pi/2) = 0$ when n = even, and $\cos(n\pi/2) = 0$ when n = odd.
Because of (3.45), (3.42) becomes

$$\text{RHS(3.40)} = \sum_{m=o}^{\infty} \varepsilon_m J_m(k\rho) \left[\alpha^2/\pi \sum_{n=o}^{\infty} \varepsilon_n n j^{n\alpha} \sin n\alpha(\theta-\chi) \exp(j \left[m-n\alpha\right]\pi/2)\right.$$

$$\left. \{\cos m(\chi-\phi) - (-1)^n \cos m(\chi+\phi)\} /(m^2-(n\alpha)^2)\right]$$

$$= \sum_{m=o}^{\infty} J_m(k\rho) \, 2\alpha^2 \varepsilon_m j^m/\pi \left[\cos m(\chi-\phi) \sum_{n=o}^{\infty} n \sin n\alpha(\theta-\chi)\right.$$

$$/(m^2-(n\alpha)^2) - \cos m(\chi+\phi) \sum_{n=o}^{\infty} n(-1)^n \sin n\alpha(\theta-\chi)$$

$$\left. / (m^2-(n\alpha)^2)\right]$$

$$= \sum_{m=o}^{\infty} J_m(k\rho) \, (-2/\pi) \, \varepsilon_m j^m \left[\cos m(\chi-\phi)\right.$$

$$\sum_{n=o}^{\infty} n(-1)^n \sin(n\alpha(\theta-\chi)+n\pi)/(n^2-(m/\alpha)^2)$$

$$\left. - \cos m(\chi+\phi) \sum_{n=o}^{\infty} n(-1)^n \sin n\alpha(\theta-\chi)/(n^2-(m/\alpha)^2)\right] \qquad (3.46)$$

Using equation (1.445.5) of Gradshteyn and Rzyhik (1965), (3.46) becomes

$$\text{RHS(3.40)} = - \sum_{m=o}^{\infty} J_m(k\rho)(2/\pi) \, \varepsilon_m j^m \left[(\pi/2)\right.$$

$$\cos m(\chi-\phi) \sin(m\left[2\pi-\alpha(\theta-\chi)-\pi\right]/\alpha)$$

$$/\sin(m\pi/\alpha) - (\pi/2) \cos m(\chi+\phi)$$

$$\left. \sin(m\left[-\alpha(\theta-\chi)\right]/\alpha)/\sin(m\pi/\alpha)\right]$$

$$= - \sum_{m=0}^{\infty} J_m(k\rho)\ \varepsilon_m\ j^m \left[\cos m(\chi-\phi)\ \sin\left[2m(\pi-\chi) - m(\theta-\chi)\right]\right.$$

$$/\sin(2m\left[\pi-\chi\right])$$

$$\left. - \cos m(\chi+\phi)\ \sin\left[-m(\theta-\chi)\right]/\sin(2m\left[\pi-\chi\right])\right]$$

$$= - \sum_{m=0}^{\infty} J_m(k\rho)\ \varepsilon_m\ j^m \left[\cos m(\chi-\phi)\ \sin m(\theta+\chi)\right.$$

$$\left. - \cos m(\chi+\phi)\ \sin m(\theta-\chi)\right]/\sin(2m\chi)$$

$$= - \sum_{m=0}^{\infty} J_m(k\rho)\ \varepsilon_m\ j^m \left[\sin m(\theta+\phi) + \sin m(\theta-\phi+2\chi) - \sin m(\theta-2\chi+\phi)\right.$$

$$\left. - \sin m(\theta+\phi)\right]/2\sin(2m\chi)$$

$$= - \sum_{m=0}^{\infty} J_m(k\rho)\ \varepsilon_m\ j^m \left[2\cos m(\theta-\phi)\ \sin(2m\chi)\right]/2\sin(2m\chi)$$

$$= - \sum_{m=0}^{\infty} \varepsilon_m\ j^m \cos m(\theta-\phi)\ J_m(k\rho) \qquad (3.47)$$

Comparing (3.47) with (3.39) shows that the null-field condition is satisfied.

3.3.3 H - Polarisation

When the incident plane wave is magnetically-polarised parallel to the axis of an infinite perfectly conducting wedge (Fig. 3.3), the total field is given by (Bates 1965)

$$\Psi = \alpha \sum_{n=0}^{\infty} \varepsilon_n\ j^{n\alpha}\ J_{n\alpha}(k\rho)\left[\cos n\alpha(\theta-\phi) + \cos n\alpha(\theta+\phi-2\chi)\right] \qquad (3.48)$$

where θ is the incident angle, $\chi<\theta<2\pi-\chi$ and $\alpha = \pi/2(\pi-\chi)$. In the H-polarisation $\partial\Psi(\rho;\ {}_{2\pi-\chi}^{\ \chi})/\partial n = \pm 1/\rho\ \partial\Psi(\rho;\ {}_{2\pi}^{\ \chi})/\partial\phi=0$ and hence the LHS of the null-field equation (1.95a) is

$$\int_C \Psi\ \nabla g\ dC = \int_0^{\infty} \Psi\ \partial g/\partial\theta\ r^{-1}\ dr \Big|_{\theta=\chi} - \int_0^{\infty} \Psi\ \partial g/\partial\theta\ r^{-1}\ dr \Big|_{\theta=2\pi-\chi}$$

$$= -j/4 \int_0^{\infty} \Psi\left[\partial H_0^{(2)}(kR)/\partial\theta\right]\ r^{-1}\ dr \Big|_{\theta=\chi}$$

$$+j/4 \int_0^{\infty} \Psi\left[\partial H_0^{(2)}(kR)/\partial\theta\right]\ r^{-1}\ dr \Big|_{\theta=2\pi-\chi} \qquad (3.49)$$

Expanding the Hankel function by the addition theorem (1.35) gives

$$\text{RHS}(3.49) = -j/4 \int_0^{\rho} \alpha \sum_{n=o}^{\infty} \varepsilon_n j^{n\alpha} J_{n\alpha}(kr) \left[\cos n\alpha(\theta-\theta) + \cos n\alpha(\theta+\theta-2\chi)\right]$$

$$\partial\left[\sum_{m=o}^{\infty} \varepsilon_m H_m^{(2)}(k\rho)\, J_m(kr) \cos m(\theta-\phi)\right]/\partial\theta \; r^{-1} \, dr \Big|_{\theta=\chi}$$

$$- j/4 \int_{\rho}^{\infty} \alpha \sum_{n=o}^{\infty} \varepsilon_n j^{n\alpha} J_{n\alpha}(kr) \left[\cos n\alpha(\theta-\theta)\right.$$

$$\left. + \cos n\alpha(\theta+\theta-2\chi)\right] \partial\left[\sum_{m=o}^{\infty} \varepsilon_m H_m^{(2)}(kr)\, J_m(k\rho) \cos m(\theta-\phi)\right]/\partial\theta \; r^{-1} \, dr \Big|_{\theta=\chi}$$

$$+ j/4 \int_0^{\rho} \alpha \sum_{n=o}^{\infty} \varepsilon_n j^{n\alpha} J_{n\alpha}(kr) \left[\cos n\alpha(\theta-\theta) + \cos n\alpha(\theta+\theta-2\chi)\right]$$

$$\partial\left[\sum_{m=o}^{\infty} \varepsilon_m H_m^{(2)}(k\rho)\, J_m(kr) \cos m(\theta-\phi)\right]/\partial\theta \; r^{-1} \, dr \Big|_{\theta=2\pi-\chi}$$

$$+ j/4 \int_{\rho}^{\infty} \alpha \sum_{n=o}^{\infty} \varepsilon_n j^{n\alpha} J_{n\alpha}(kr) \left[\cos n\alpha(\theta-\theta)\right.$$

$$\left. + \cos n\alpha(\theta+\theta-2\chi)\right] \partial\left[\sum_{m=o}^{\infty} \varepsilon_m H_m^{(2)}(kr)\, J_m(k\rho) \cos m(\theta-\phi)\right]$$

$$/\partial\theta \; r^{-1} \, dr \Big|_{\theta=2\pi-\chi}$$

$$= -j/4 \left[-2\alpha \sum_{n=o}^{\infty} \varepsilon_n j^{n\alpha} \cos n\alpha(\theta-\chi) \sum_{m=o}^{\infty} m\, \varepsilon_m \sin m(\chi-\phi)\, I_{m,n\alpha}\right.$$

$$\left. -2\alpha \sum_{n=o}^{\infty} \varepsilon_n j^{n\alpha} \cos n\alpha(\theta-\chi)(-1)^n \sum_{m=o}^{\infty} m\, \varepsilon_m \sin m(\chi+\phi)\, I_{m,n\alpha}\right] \tag{3.50}$$

where $I_{m,n\alpha}$ is defined by (3.34). Substituting the value of $I_{m,n\alpha}$ into (3.50), the latter becomes

$$\text{RHS}(3.49) = j\alpha/2 \sum_{n=o}^{\infty} \varepsilon_n j^{n\alpha} \cos n\alpha(\theta-\chi) \sum_{m=o}^{\infty} \varepsilon_m m \{\sin m(\chi-\phi) + (-1)^n$$

$$\sin m(\chi+\phi)\} \; (-2j/\pi) \exp(-jn\alpha\pi/2) \{\exp(jm\pi/2)\, J_m(k\rho)$$

$$- \exp(jn\alpha\pi/2)\, J_{n\alpha}(k\rho)\}/(m^2-(n\alpha)^2) \tag{3.51}$$

Again, it is clear that the coefficients of $J_{n\alpha}(k\rho)$ in (3.51) must equal zero for all n if the null-field condition is to be satisfied. From (3.51), the coefficients of $J_{n\alpha}(k\rho)$ are

$$d_{n\alpha} = -\alpha\,\varepsilon_n\, j^{n\alpha} \cos n\alpha(\theta-\chi)$$

$$\frac{1}{\pi}\left[\sum_{m=o}^{\infty} \frac{m\,\varepsilon_m \sin m(\chi-\phi)}{m^2-(n\alpha)^2}\right.$$

$$\left.\pm \sum_{m=o}^{\infty} \frac{m\,\varepsilon_m \sin m(\chi+\phi)}{m^2-(n\alpha)^2}\right] \qquad (3.52)$$

where the upper sign is taken when n is even and the lower sign is taken when n is odd. Using equation (1.445.5) of Gradshteyn and Ryzhik (1965),

$$d_{n\alpha} = -\alpha\varepsilon_n\, j^{n\alpha}/\pi \cos n\alpha(\theta-\chi)\left[\frac{\pi}{2}\,\frac{\sin n\alpha(\pi-\chi+\phi)}{\sin(n\alpha\pi)}\right.$$

$$\left.\pm\,\frac{\pi}{2}\,\frac{\sin n\alpha(\pi-\chi-\phi)}{\sin(n\alpha\pi)}\right]$$

$$= -\alpha\,\varepsilon_n\, j^{n\alpha} \cos n\alpha(\theta-\chi)\,\left[\sin n\alpha(\pi-\chi+\phi) \pm \sin n\alpha(\pi-\chi-\phi)\right]/2\sin(n\alpha\pi)$$

$$= -\alpha\,\varepsilon_n\, j^{n\alpha} \cos n\alpha(\theta-\chi)\,\begin{matrix}\cos\\ \sin\end{matrix}(n\alpha\phi)\,\begin{matrix}\sin\\ \cos\end{matrix} n\alpha(\pi-\chi)/\sin(n\alpha\pi)=0 \qquad (3.53)$$

since $\sin n\alpha(\pi-\chi) = \sin(n\pi/2) = 0$ when n = even, and $\cos n\alpha(\pi-\chi) = \cos(n\pi/2) = 0$ when n = odd. As a consequence of (3.53), (3.51) becomes

$$\text{RHS(3.49)} = \sum_{m=o}^{\infty} J_m(k\rho)\,(\alpha/\pi)\,\varepsilon_m\, m \sum_{m=o}^{\infty} \varepsilon_n\, j^{n\alpha} \cos n\alpha(\theta-\chi)$$

$$\exp(j[m-n\alpha]\pi/2)\,\left[\sin m(\chi-\phi) + (-1)^n \sin m(\chi+\phi)\right]/(m^2-(n\alpha)^2)$$

$$= \sum_{m=o}^{\infty} J_m(k\rho)\,(\alpha/\pi)\,\varepsilon_m\, m\, j^m \left[\sin m(\chi-\phi) \sum_{n=o}^{\infty} \varepsilon_n \cos n\alpha(\theta-\chi)/(m^2-(n\alpha)^2)\right.$$

$$\left.+ \sin m(\chi+\phi) \sum_{n=o}^{\infty} \varepsilon_n\,(-1)^n \cos n\alpha(\theta-\chi)/(m^2-(n\alpha)^2)\right]$$

$$= -\sum_{m=o}^{\infty} J_m(k\rho)\; m\,\varepsilon_m\, j^m/\alpha\pi \left[\sin m(\chi-\phi) \sum_{n=o}^{\infty} \varepsilon_n(-1)^n \cos(n\alpha(\theta-\chi) + n\pi)/\right.$$

$$(n^2-(m/\alpha)^2) + \sin m(\chi+\phi) \sum_{n=o}^{\infty} \varepsilon_n (-1)^n \cos n\alpha(\theta-\chi)/(n^2-(m/\alpha)^2) \Big] \qquad (3.54)$$

Using equations (1.445.6) of Gradshteyn and Rzyhik (1965), (3.54) becomes

$$\text{RHS}(3.49) = -\sum_{m=o}^{\infty} J_m(k\rho)\, m\, \varepsilon_m\, j^m/\alpha\pi \Big[\sin m(\chi-\phi) \{-(\alpha/m)^2 + (\alpha/m)^2$$

$$- \alpha\pi \cos(m(2\pi-\alpha(\theta-\chi)-\pi)/\alpha)/m \sin(m\pi/\alpha)\}$$

$$+ \sin m(\chi+\phi) \{-(\alpha/m)^2 + (\alpha/m)^2 - \alpha\pi \cos(m(-\alpha(\theta-\chi))/\alpha)/m \sin(m\pi/\alpha)\}\Big]$$

$$= \sum_{m=o}^{\infty} J_m(k\rho)\, \varepsilon_m\, j^m \Big[\sin m(\chi-\phi) \cos m(\theta+\chi) + \sin m(\chi+\phi)$$

$$\cos m(\theta-\chi)\Big]/\sin(2m(\pi-\chi))$$

$$= -\sum_{m=o}^{\infty} J_m(k\rho)\, \varepsilon_m\, j^m \Big[-\sin m(\theta+\phi) + \sin m(\theta+2\chi-\phi) + \sin(2\chi+\phi-\theta)$$

$$+ \sin m(\theta+\phi)\Big]/2 \sin(2m\chi)$$

$$= -\sum_{m=o}^{\infty} J_m(k\rho)\, \varepsilon_m\, j^m \frac{2 \sin(2m\chi) \cos m(\theta-\phi)}{2 \sin(2m\chi)}$$

$$= -\sum_{m=o}^{\infty} \varepsilon_m\, j^m \cos m(\theta-\phi)\, J_m(k\rho) \qquad (3.55)$$

Comparing (3.55) with (3.39) shows that the null-field condition is satisfied.

3.4 DISCUSSION

Perfectly conducting wedges (or metal wedges) can be considered special cases of penetrable wedges when the (complex) refractive indices of the latter approach infinity or zero. However, this does not mean that one can generalise the established methods for solving conducting wedge problems to the general penetrable wedge situation. For example, it is shown in Section 3.2.2 that one cannot use the Kontorowich-Levedev transform to solve the penetrable wedge problem in a simple way.

Basically, the difficulties arise from the more general boundary conditions required for the penetrable wedge. For the conducting wedge, the required boundary condition (that the tangential electric field vanishes on the faces of the wedge) can be satisfied easily by expanding the wave function in basis functions whose angular dependence is characterised by $\sin(n\pi/2(\pi-\chi)\phi)$, where the integer n runs from 1 to ∞.

For the penetrable wedge, however, one has to match the fields (and their normal derivatives) inside and outside (the wedge) across the faces of the wedge. One may expand the field outside the penetrable wedge as

$$\Psi_+ = \sum_{n=0}^{\infty}{}' A_n J_n(k\rho) \begin{matrix}\cos\\ \sin\end{matrix} (n\phi) \tag{3.56}$$

and the field inside the penetrable wedge as

$$\Psi_- = \sum_{n=0}^{\infty}{}' B_n J_n(\nu k\rho) \begin{matrix}\cos\\ \sin\end{matrix} (n\phi) \tag{3.57}$$

and set $\Psi_+ = \Psi_-$ and $\partial\Psi_+/\partial\phi = \partial\Psi_-/\partial\phi$ at $\phi = \pm\chi$. In (3.56) and (3.57), the arguments of the Bessel functions differ by the factor ν, which is the refractive index of the wedge. Unfortunately, there is no easy way of comparing Bessel functions of different arguments. Although it is possible to resort to the multiplication theorem of Watson (1966, Section 5.21), the procedure tends to become hopelessly unstable numerically as soon as the value of ν differs significantly from unity.

Section 4.1 presents a detailed discussion of several of the difficulties encountered in attempting to solve the penetrable wedge diffraction problem, while Chapters 5 through 8 describe various possible approaches to tackling this long standing problem.

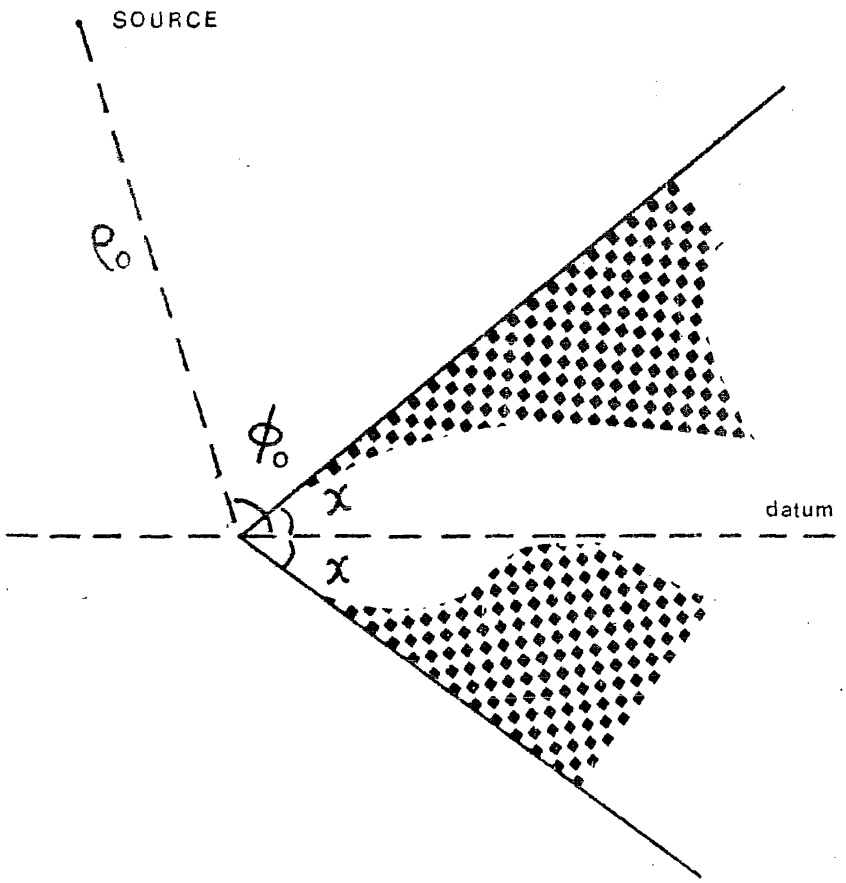

FIGURE 3.1 The infinite perfectly conducting wedge illuminated by a line source at $(\rho_o ; \phi_o)$. The wedge surfaces coincide with the plane $\phi = \pm\chi$.

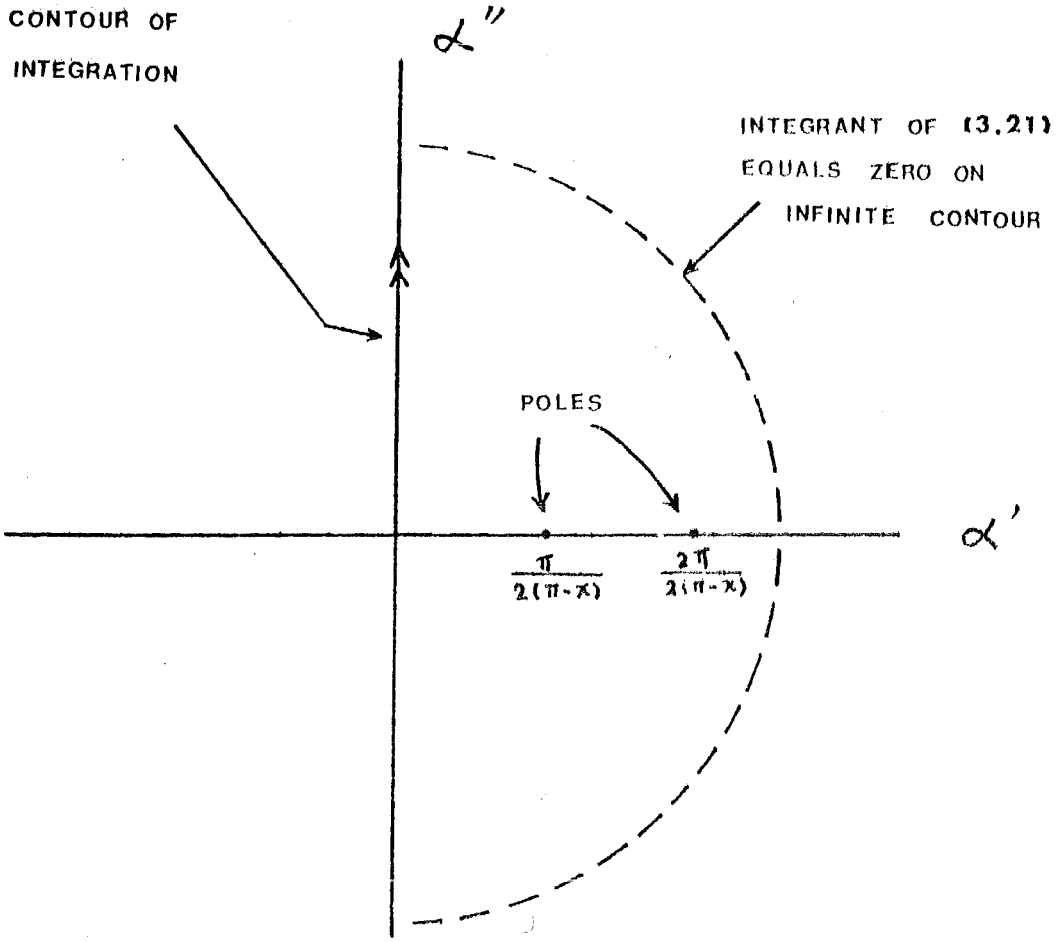

FIGURE 3.2 The complex plane.

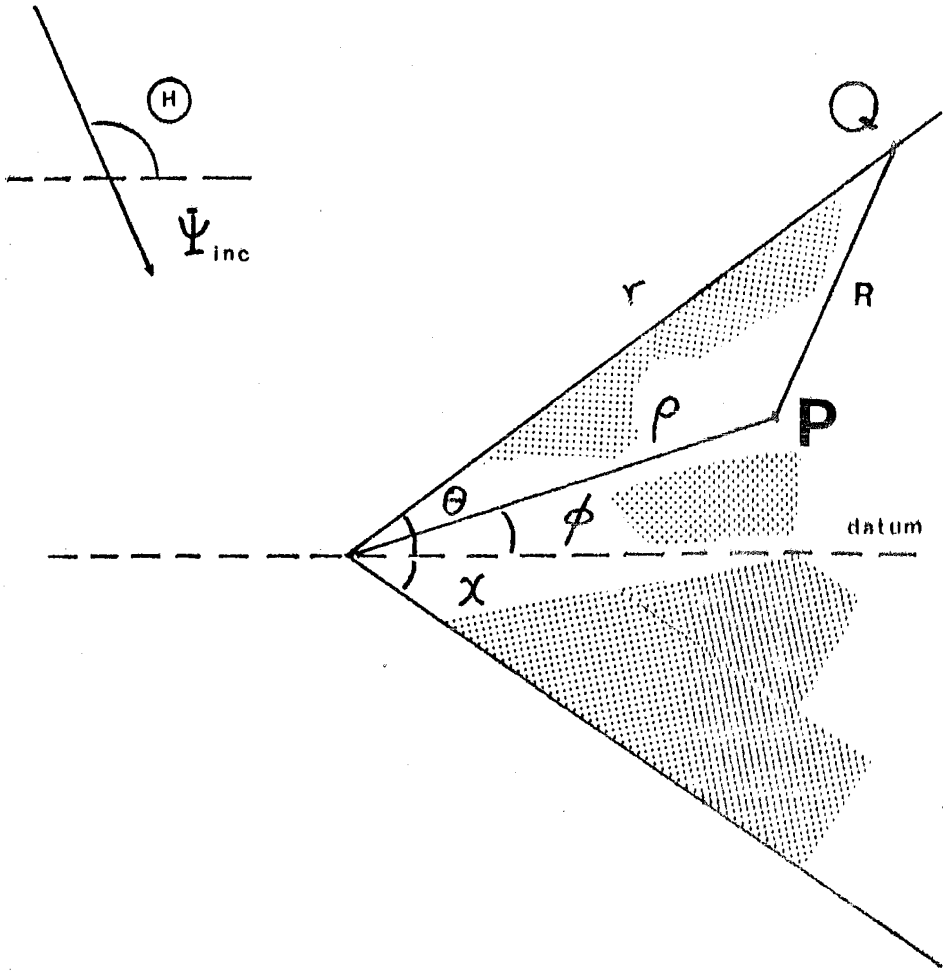

FIGURE 3.3 Plane wave scattering by a perfectly conducting wedge. The incoming wave Ψ_{inc} is incident at an angle θ. The wedge surfaces coincide with $\phi = \pm\chi$. A point P in space has the coordinates $(\rho;\phi)$. A point Q on the wedge surface has the coordinates $(r;\ \theta = \chi)$.

CHAPTER FOUR

THE INFINITE PENETRABLE WEDGE DIFFRACTION PROBLEM - INTRODUCTION AND REVIEW OF LITERATURE

Unlike the perfectly conducting wedge diffraction problem, which was solved successfully before the end of the last century (cf. Macdonald 1895 and Sommerfeld 1896), the penetrable wedge diffraction problem still excites controversy today.

Whereas new approaches are introduced and their merits are assessed in the next chapters, this chapter is essentially an introduction to the penetrable wedge diffraction problem. In Section 4.1, several difficulties which one may encounter when attempting the problem of penetrable wedge diffraction are discussed. Commonly used notations and terms are also defined in this section. Finally, Sections 4.3 and 4.4 give brief reviews of the literature on right-angled and arbitrarily-angled dielectric wedges respectively.

4.1 GENERAL DIFFICULTIES IN SOLVING THE PENETRABLE WEDGE PROBLEM

The penetrable wedge is the major topic of this thesis. Its geometry is shown in Fig. 4.1

The wedge is infinitely long in the z-direction. The semi-infinite wedge surfaces coincide with the planes $\phi=\chi$ and $2\pi-\chi$. Arbitrary points in space and on the wedge surfaces are denoted by P, with coordinates $(\rho;\phi)$, and Q with coordinates $(r;\pm\chi)$, respectively. The refractive index of the wedge is ν while the refractive index of the remaining space is 1, i.e. $\nu = 1$ for $\chi < \phi < 2\pi-\chi$ while ν has some other constant value for $-\chi < \phi < \chi$.

The penetrable wedge problem is difficult because the wave function has to satisfy the edge, boundary and radiation conditions simultaneously. Furthermore, the lack of any scaling factor, since the wedge is of infinite extent and the radius of curvature of the apex is zero, creates additional difficulties when one attempts to obtain a numerical solution.

(i) Edge conditions:

Just what are the correct edge conditions for a penetrable wedge is still a much researched topic, as indicated by Meixner (1972), Hurd (1977, 1976), Bobrovnikov and Zamaraeva (1973), Davies (1976), Dobrzyuski and Maradudin (1972), Andersen and Solodoukhov (1978) and Bates (1973, 1980a) The conditions suggested by these authors are examined in detail in Sections 4.2 and 5.7.

(ii) Boundary conditions:

As pointed out in Section 3.4, the arguments for the cylindrical eigenfunctions used in field expansions are $k\rho$ and $\nu k\rho$, outside and inside the wedge respectively. There is no easy way to match cylindrical functions of different arguments. In the case where the cylindrical functions are Bessel functions of the first kind, one may resort to the multiplication theorem of Watson (1966, Section 5.21), which takes the form

$$J_\alpha(\nu x) = \sum_{n=o}^{\infty} F_n(\alpha,\nu)\, J_{\alpha+2n}(x) \tag{4.1}$$

The asymptotic form of $J_{\alpha+2n}(x)$ is

$$\lim_{n\to\infty} J_{\alpha+2n}(x) \rightarrow (ex/(\alpha+2n))^{\alpha+2n} \tag{4.2}$$

while the asymptotic form of $F_n(\alpha,\nu)$ is

$$\lim_{n\to\infty} F_n(\alpha,\nu) \rightarrow n^n \tag{4.3}$$

It is clear from (4.2) and (4.3) that (4.1) is an absolutely converging series. However, consider the following simple situation, in which the problem is to evaluate the variables B_m from the equation

$$\sum_{m=o}^{\infty} B_m J_m(\nu k\rho) \cos m\chi = \sum_{m=o}^{\infty} A_m J_m(k\rho) \cos m\chi \tag{4.4}$$

where the A_m are known. Although this is a simplified situation and does not correspond to any particular physical problem, it helps to highlight the difficulties associated with the use of the multiplication theorem. (4.4) can be expanded as

$$\sum_{m=o}^{\infty} B_m \cos m\chi \sum_{n=o}^{\infty} J_{m+2n}(k\rho)\, F_n(m,\nu) = \sum_{m=o}^{\infty} A_m \cos m\chi\, J_m(k\rho). \tag{4.5}$$

Since the $J_\ell(\kappa\rho)$ are independent functions, equating their coefficients in (4.5) gives

$$\sum_{\ell=0}^{m} B_\ell \cos \ell\chi \; F_{(m-\ell)/2}^{(\ell,\nu)} = A_m \cos m\chi, \text{ for } m = 0,1,2, \ldots \text{ and } (m-\ell)/2 \; \varepsilon I_{0,+} \qquad (4.6)$$

It has already been indicated in (4.3) that the $F_{(m-\ell)/2}^{(\ell,\nu)}$ are rather large quantities, especially when m is large. On the other hand, the A_m and B_m are comparatively small. A small percentage error in calculation of $F_{(m-\ell)/2}^{(\ell,\nu)}$ can therefore cause large percentage errors in the B_m calculated from (4.6).

(iii) Radiation condition:

In order to ensure that power flow be finite, it is necessary to use Bessel functions of the first kind as eigenfunctions when writing down expansions for the wave function close to the apex (cf. Section 1.4.2.2). However, the expansion coefficients must then be such that the wave function is an outgoing wave as $\rho \to \infty$.

On the other hand, one may utilise Hankel functions of the second kind as the eigenfunctions for ρ greater than a certain value, ρ_o say (where ρ_o is the minimum radius of convergence, (cf. Section 1.4.3), and keep the Bessel functions expansion for ρ smaller than ρ_o. Unfortunately, this method of solution leads to 'relative convergence' difficulties (see Section 1.5.1.2 and 7.5).

(iv) Dielectric wedge mode:

Consider a rectangular waveguide with a cross section as shown in Fig. 4.2. It is well known (cf. Marcuvitz 1951) that the z-component of the electric field in such a waveguide (for any electromagnetic field polarised in the z-direction) is of the form

$$\Psi = A \sin(m\pi x/2a) \sin(n\pi y/2b) \exp(j[k^2 - (m\pi/2a)^2 - (n\pi/2b)^2]^{\frac{1}{2}} z) \qquad (4.7)$$

where m and n are integers and A is an arbitrary constant. The spatial variations of Ψ are depicted in Fig. 4.2 for some values of m and n. These variations are called standing wave patterns because they are stationary with respect to time. A field like (4.7) which can exist in a structure all by itself (or in other words produce a standing wave pattern) is called a mode. Each field pattern (or standing wave pattern) is completely characterised by its corresponding values of m and n.

In the case of a perfectly conducting wedge (Fig. 4.3), a field of the form

$$\Psi = B\, J_{n\alpha}\,(k\rho)\, \sin n\alpha(\phi-\chi),\ \alpha = \pi/2(\pi-\chi) \qquad (4.8)$$

represents standing waves in the angular direction (between the walls of the wedge - see Fig. 4.3).

Bates (1973, 1980a) argues, however, that no such 'free-modes' exists for penetrable wedges of arbitrary angles and (complex) refractive indexes. On the other hand, Maurer and Felsen (1967) indicate that a form of 'travelling mode' can still exist in the case of a penetrable wedge. These different viewpoints of the concept of 'physical mode' are discussed further in Section 5.3.

4.1.1 Some Notation and Terminology

It is appropriate here to introduce certain notation and terminology which is referred to frequently in what follows. The field diffracted by a (penetrable) wedge is taken to be either E-polarised (electric field parallel to, and magnetic field perpendicular to, the z-direction - see Fig. 4.1) or H-polarised (magnetic field parallel to, and electric field perpendicular to, the z-direction). The total field, which is denoted $\Psi = \Psi(\rho;\phi)$, does not vary in the z-direction, i.e. $\partial\Psi/\partial z = 0$.

(i) Apex (edge):

The apex (or edge) of a wedge is where the surface ceases to be analytic, e.g. the point O in Fig. 4.1.

(ii) Wedge angle:

The wedge angle is the angle between the two faces of the wedge, i.e. 2χ in Fig. 4.1.

(iii) Edge field:

An edge field is defined, with reference to Fig. 4.1, by

$$\Psi_{edge} = \lim_{\rho\to 0} \Psi(\rho;\phi) \qquad (4.9)$$

(iv) Reflection and refraction boundaries:

The reflection and refraction boundaries defined herewith are only physical idealisations because Ψ is necessarily an analytic function of ρ and ϕ everywhere except on the faces of the wedge and (in some cases) at the apex. The incident wave and the specular parts of the reflected and refracted waves

can be usefully regarded as being composed of rays (see Section 1.2). Each incident ray, when striking the wedge surface, is assumed to generate a reflected ray and a refracted ray (cf. Section 1.2) as if the incoming ray is incident upon an infinite interface. In Fig. 4.4, an incoming ray is shown incident on a penetrable wedge at an angle Θ. At a point P_1, say, on the upper face L, of the wedge, the incident ray is reflected and refracted. The angles of reflection γ_1 and refraction γ_2 are determined by Snell's law (cf. Section 1.2). Similarly, at a point P_2, say, on the lower face L_2 of the wedge, the incident ray is reflected and refracted. It is seen from Fig. 4.4 that the reflected ray from the upper wedge surface exists only for $\chi \leq \phi \leq \gamma_1$. The radial line $\phi = \gamma_1$, $0 < \rho < \infty$ is then called the reflection boundary (for the ray reflected from the upper wedge surface). Similarly, the ray refracted from the upper wedge surface exists only for $-\gamma_2 \leq \phi \leq \chi$. The radial line $\phi = -\gamma_2$, $0 < \rho < \infty$ is called the refraction boundary (for the ray refracted from the upper wedge surface). Reflection and refraction boundaries from the lower surface are also defined in the same way. In a more complicated situation, where the (upper/lower) refraction boundaries intersect the opposite (i.e. lower/upper) wedge surfaces, secondary refraction/reflection takes place. The secondary reflection/refraction boundaries are similarly defined.

4.2 SINGULARITY AT THE APEX

Bouwkamp (1946) points out that the field diffracted by a sharp perfectly conducting edge must be singular, in that certain spatial derivatives of the field must become infinite at the edge. This fact is, of course, well known (Jones 1964, Section 9.14). Some questions remain, however, for penetrable wedges.

Meixner (1972) suggests that the edge field of a penetrable wedge (Fig. 4.1) should be expandable in the form

$$\Psi = a_{-1}\rho^{\alpha-1} + a_o\rho^{\alpha} + a_1\rho^{\alpha+1} + \ldots + a_n\rho^{\alpha+n} + \ldots \qquad (4.10)$$

which is clearly singular as $\rho \to 0$, unless α is a positive integer. The value of α is determined by

$$(1-\zeta)/(1+\zeta) = \pm \sin \alpha\pi \,/ 2\sin \alpha(2\chi-\pi) \qquad (4.11)$$

where the upper sign is taken when the field Ψ is an even function of ϕ and the lower sign is taken when the field Ψ is an odd function of ϕ. Also $\zeta = 1$ for an E-polarised (H-polarised) electromagnetic wave and a dielectric (magnetically permeable) wedge, and $\zeta = \varepsilon_r$ for an H-polarised electromagnetic wave and a dielectric wedge, and $\zeta = \mu_r$ for an E-polarised electromagnetic wave and a permeable wedge. Hurd (1977) observes that Meixner holds that the behaviour of Ψ, for a dielectric wedge having a wedge angle of 2χ (Fig. 4.1) or $2\pi-\chi$, is governed by (4.11). However, it is well known (Jones 1964, Section 9.14) that the edge field (or its spatial derivative) of a perfectly conducting wedge ($\nu\to\infty$) can be infinite only when $2\chi<\pi$. Hurd (1977) examines Meixner's (1972) proposition that the field near the apex can be expressed by (4.10) and, by means of an example, infers (but does not prove) that the postulate is correct. Hurd (1977) then goes on to suggest that a discontinuity of edge behaviour must exist when $\nu\to\infty$. Hurd (1977) indicates that this singular field behaviour for a metallic corner reflector (of angle $3\pi/2$) exists only within a minute fraction of a wavelength from the corners and is therefore unobserved in the normal experimental situation. Hurd (1977) further indicates that although the eigenvalue α is less than unity (but greater than zero), the expansion coefficient α_{-1} may well tend to zero when $\nu\to\infty$, thus resulting in a finite field strength.

Andersen and Solodoukhov (1978) also comment on the field behaviour for a dielectric wedge, for which $\chi > \pi/2$; when $\nu\to\infty$. They show (from their equations 6 and 8) that field can be infinite for a dielectric (or finite conducting) wedge, for which $\chi > \pi/2$. However, they fail to point out that the 'magnitude' of the field in the dielectric wedge must decrease with increasing ν.

Andersen and Solodoukhov further argue that Meixner's (1972) field expansion (4.10) is inconsistent for wedge angles which are rational multiples of π and is therefore invalid in general. Andersen and Solodoukhov (1978) argue that, while the edge conditions are determined by (4.11), i.e.

$$D(\alpha) = (1-\zeta)/(1+\zeta) \mp \sin\alpha\pi/2\sin\alpha(2\chi-\pi) \qquad (4.12)$$

the boundary conditions require, for higher power of ρ, solution of inhomogeneous equations of the form

$$\underline{\underline{k}}\ \underline{A} = \underline{B} \qquad (4.13)$$

The determinant of $\underline{\underline{k}}$ is of the form $D(\alpha+2n)$, where n indicates the order of coefficients as defined in (4.10). It is clear from (4.12) that for a

certain value of wedge angle 2χ such that $2\chi = M\pi/N$, where M and N are arbitrary integers, $D(\alpha+2n)$ must necessarily be zero. Andersen and Solodoukhov conclude that there is no solution for (4.13) and the boundary condition cannot be satisfied. They find therefore, that Meixner's (1972) expansion (cf. (4.10)) cannot be valid.

It is, of course, well known in elementary linear algebra (cf. Kreyszig 1979, Section 3.5) that (4.13) is inconsistent if the determinant of $\underline{\underline{k}}$ is zero. However, consider a set of n homogeneous equations,

$$\underline{\underline{k}}^{\dagger}\ \underline{x} = 0 \tag{4.14}$$

which has a non-trivial solution when the determinant of $\underline{\underline{k}}^{\dagger}$ equals zero. If one can partition $\underline{x}$ into the form

$$\underline{x} = \begin{bmatrix} \underline{Y} \\ \underline{Z} \end{bmatrix} \tag{4.15}$$

where

$$\underline{Y} = \begin{bmatrix} x_1 \\ x_2 \\ . \\ . \\ . \\ x_m \end{bmatrix}, \qquad \underline{Z} = \begin{bmatrix} x_{m+1} \\ x_{m+2} \\ . \\ . \\ . \\ x_n \end{bmatrix} \tag{4.16}$$

and

$$\underline{\underline{k}}^{\dagger} = \left[\begin{array}{c|c} \underline{\underline{k}}_1 & 0 \\ \hline 0 & \underline{\underline{k}}_2 \end{array}\right] \tag{4.17}$$

where $\underline{\underline{k}}_1$ is a m X m matrix and $\underline{\underline{k}}_2$ is a (n-m) X (n-m) matrix, and if one assumes that the determinant of $\underline{\underline{k}}_1$ equals zero while the determinant of $\underline{\underline{k}}_2$ is arbitrary, then (4.14) can be re-written as

$$\underline{\underline{k}}^{+}\ \underline{x} = \left[\begin{array}{c|c} \underline{\underline{k}}_1 & 0 \\ \hline 0 & \underline{\underline{k}}_2 \end{array}\right] \begin{bmatrix} \underline{Y} \\ \\ \underline{Z} \end{bmatrix}$$

$$= \underline{\underline{k}}_1 \underline{Y} + \underline{\underline{k}}_2\ \underline{Z} = 0 \tag{4.18}$$

or

$$\underline{\underline{k}}_1\ \underline{Y} = -\ \underline{\underline{k}}_2\ \underline{Z} \tag{4.19}$$

It is clear from (4.14) that a solution for $\underline{Y}$, $\underline{Z}$ and $\underline{x}$ exists and therefore there must be a solution to (4.19).

Referring to the derivation of Andersen and Solodoukhov (1978), it is found that their set of so-called 'inhomogeneous' equations (4.13) is in fact equivalent to (4.19). The n-component vector B on RHS (4.13) is actually part of the solution space. The argument (Andersen and Solodoukhov 1978) that Meixner's (1972) expansion (cf. (4.10)) is invalid therefore cannot be rigorously justified. Bates (1980a) employs a Bessel function expansion for the edge field and arrives at results similar to (4.11). However, Bates (1980)'s derivation is more comprehensive and is reviewed in detail in Chapter 5.

Meixner's (1972) expansion has been used by Lang (1973) to determine the edge condition for a perfectly conducting wedge with its exterior region partitioned by a resistive sheet (Fig. 4.5). Lang (1973) shows that the behaviour of an electromagnetic field at the edge is altered as a result of the presence of the resistive sheet but its edge behaviour is independent of the resistance value. In particular, the edge field is now regular. This assures the finiteness of the energy dissipated on the resistive sheet in the vicinity of the edge. Brook and Kharadly (1977) apply Meixner's (1972) expansion to a multi-dielectric wedge (Fig. 4.6) and find that, in the case of a three-dielectric wedge configuration (i.e. n = 3, cf. Fig. 4.6), the edge field and its derivatives are always finite if the angle of the wedge having the highest dielectric constant is greater than $\pi/2$. Hurd (1976), using a similar technique, though limited to the static case, analyses the edge condition for a configuration similar to that depicted in Fig. 4.6, but with $\nu_1 \to \infty$.

Bobrovnikov and Zamaraeva (1973), using a static charge method for the multidielectric wedge (Fig. 4.6), arrive at equations similar to those obtained by Meixner (1972) and Brook and Kharadly (1977).

A completely different approach is adopted by Dobrzynski and Maradudin (1972) to derive comprehensive electrostatic resonance (or 'mode') curves for wedges. They expand the edge field in hyperbolic functions and modified Bessel functions of imaginary orders, i.e.

$$\Psi = \sum_{n=o}^{\infty} A_n J_{j\mu_n}(k\rho) \begin{matrix}\cosh \\ \sinh\end{matrix} \mu_n \phi \qquad (4.20)$$

The edge field so constructed is decaying away from the surface of the wedge. However, Davies (1976) points out that this method of constructing the edge field leads to infinite field energy in the neighbourhood of the edge. It is therefore not clear how this method can be extended from semiconductor, superconductor and/or plasma physics, to which negative resistances apply, to the conventional dielectric wedge situation. Davies (1976) rounds the wedge to a hyperbola and Eguiluz and Maradudin (1976) study the parabolic wedge. However, there must be some doubt about their results since they (Davies 1976 and Eguiluz and Maradudin 1976) employ the technique of Dobrzynski and Maradudin (1972).

4.3 THE RIGHT-ANGLED DIELECTRIC WEDGE

The problem of diffraction by a right-angled dielectric wedge has been attacked by several people (cf. Radlow 1964, Kuo and Plonus 1967, Kraut and Lehman 1969, Rawlins 1977a, Wu and Tsai 1977, Sinha, Guha and Gupta 1980, Hudson 1982, Hoenders 1982 and Joo, Ra and Shin 1980, 1984). Unfortunately, it has not been possible to extend the methods described in these papers to the general case of a dielectric wedge of arbitrary angle. Therefore, it seems that there is no need to give a lengthy review of these papers. A statement of the techniques used would suffice. Specific features which may be of interest to the reader are listed. Results and equations which can be used for comparison with those obtained in this thesis have also been included. Some conclusions are offered in Section 4.3.1.

(i) Radlow (1964):

Using a two-dimensional Laplace transformation, Radlow (1964) shows that the right-angled dielectric wedge problem is equivalent to a generalised Wiener-Hopf factorisation problem involving two complex variables.

(ii) Kuo and Plonus (1967):

Kuo and Plonus (1967) present a systematic way of obtaining the diffracted field of a right-angled dielectric wedge, in an integral form, by approximating the inverse Laplace transform of Radlow (1964).

(iii) Kraut and Lehman (1969):

Kraut and Lehman (1969) obtain a singular integral equation by Fourier-transforming the polarisation source formulation (cf. Bates and Ng 1972) of the right-angled dielectric wedge diffraction problem. A solution of the singular integral equation is then constructed as a power series in the index of refraction. This series converges when the index of refraction

is near unity. The first order approximation to the edge field is given by Kraut and Lehman (1969) as

$$\Psi_{edge} = \Psi_{inc} \left[1-(\nu^2-1)/8\right] \tag{4.21}$$

when the (E-polarised) plane wave is incident parallel to one face of the right-angled wedge (i.e. grazing incidence).

Kraut and Lehman (1969) also criticise the method of Radlow (1964). Kraut and Lehman (1969) indicate that the edge field evaluated by Radlow (1964) is

$$\Psi_{edge} = \left[2/(1+\nu)\right]^{\frac{1}{2}} \tag{4.22}$$

Note that RHS (4.22) is the square root of the refraction coefficient for a plane wave normally incident on a dielectric half plane. It therefore cannot be correct. Kraut and Lehman (1969) also indicate that no rigorous justification has been given for the approximation scheme used by Kuo and Planus (1967).

(iv) Aleksandrova and Khizhnyak (1975):

The polarisation source formulation (cf. Bates and Ng 1972)

$$E(\underline{r}) = E_{inc}(\underline{r}) + k^2 (\nu^2-1)/4\pi \int\int_{\Omega}\int E(\underline{r}') \frac{\exp(jk|\underline{r}-\underline{r}'|)}{|\underline{r}-\underline{r}'|} d\underline{r}' \tag{4.23}$$

is used by Aleksandrova Khizhnyak (1975) to derive the field diffracted by a right-angled dielectric wedge when the incident field is arbitrarily polarised. The scattered field inside the wedge (Fig. 4.4) is expressed (Aleksandrova and Khizhnyak 1975) as a superposition of plane refracted waves and an unknown wave originating from the vicinity of the edge, i.e.

$$\Psi = \sum_n A_n \exp(j\nu k\rho \cos\phi_n) + \int_{\alpha} \frac{\exp(j\left[tx+(\nu^2k^2-t^2)^{\frac{1}{2}}y\right])}{(\nu^2k^2-t^2)^{\frac{1}{2}}} f(t)\, dt \tag{4.24}$$

where the contour α is to be defined. The subscript n determines the number of waves produced in the wedge because of refraction at its faces. The transformation

$$\int_{-\infty}^{\infty} \frac{\exp(jk|\underline{r}-\underline{r}'|)}{|\underline{r}-\underline{r}'|} d\underline{r}' = \pi j H_o^{(1)}\left(k\left[(x-x')^2+(y-y')^2\right]^{\frac{1}{2}}\right)$$

$$= j\int_{\infty}^{\infty} \frac{\exp(j\left[\omega|y-y'| + (k^2-\omega^2)^{\frac{1}{2}}|x-x'|\right])}{(k^2-\omega^2)^{\frac{1}{2}}} d\omega \tag{4.25}$$

(which can be found in Clemmow 1966, Section 1.11) is used to transform the integral in (4.23) to a singular form. The diffracted wave is sought in the form of a Sommerfeld integral with initially unknown weight function f(t). The extinction theorem (cf. Section 1.5.5) is satisfied for $\underline{r} \in \Omega$, when the first term on RHS (4.23), which is the incident wave, is cancelled by a corresponding term produced from the integral of RHS (4.23). In this way, f(t) is inferred.

(v) Rawlins (1977a):

Starting from the polarisation source formulation (cf. Bates and Ng 1972), and assuming a Neuman series solution for the diffracted field, (i.e. the diffracted field is written as a power series in $(1-\nu^2)$), Rawlins (1977) obtains explicit formulas for the edge and diffracted fields of a right-angled dielectric wedge. However, the solution is limited to wedges having refractive index ν, $1 < \nu < \sqrt{2}$.

Referring to Fig. 4.7, some results obtained by Rawlins (1977) are:

E - polarised incident field

$$\Psi_{inc} = \exp(jk\rho \cos(\phi-\theta)) \tag{4.26}$$

reflected field

$$\Psi_{refl.1} = -(\nu^2-1)\exp(-jk\rho\cos(\phi+\theta))/4\cos^2\theta$$

$$\Psi_{refl.2} = -(\nu^2-1)\exp(jk\rho\cos(\phi+\theta))/4\sin^2\theta \tag{4.27}$$

refracted field

$$\Psi_{refr.1} = (\sin\theta + (\nu^2-\cos^2\theta)^{\frac{1}{2}})\exp(jk\rho[\cos\phi\cos\theta + (\nu^2-\cos^2\theta)^{\frac{1}{2}}\sin\phi])/2(\nu^2-\cos^2\theta)^{\frac{1}{2}}$$

$$\Psi_{refr.2} = (\cos\theta + (\nu^2-\cos^2\theta)^{\frac{1}{2}})\exp(jk\rho[\sin\phi\sin\theta + (\nu^2-\cos^2\theta)^{\frac{1}{2}}\cos\phi])/2(\nu^2-\cos^2\theta)^{\frac{1}{2}} \tag{4.28}$$

far diffracted field

$$\Psi_{diff.1} = j2(\nu^2-1)|Q|F(|Q|)\ \exp(j[k\rho+\pi/4])/2\ (2\pi k\rho)^{\frac{1}{2}}$$

$$(\sin\theta - \sin\phi)(\cos\theta - \cos\phi)$$

$$\Psi_{diff.2} = j(\nu^2-1)\ \exp(j[\nu k\rho + \pi/4])/2\ (2\pi\nu k\rho)^{\frac{1}{2}}\ (\sin\theta - (\nu^2-\cos^2\theta)^{\frac{1}{2}})$$

$$\left[\frac{2|Q''|\ F(|Q''|)}{\cos\phi - \nu\cos\theta} + \frac{2|Q'|\ F(|Q'|)(\nu\sin\phi-(\nu^2-\cos^2\theta)^{\frac{1}{2}})}{(\cos\theta - \nu\cos\phi)(\sin\theta - \nu\sin\phi)} \right] \quad (4.29)$$

edge field

$$\Psi_{edge} = \left[1 - \frac{\nu^2-1}{4\pi}\left(\frac{\theta}{\sin^2\theta} - \frac{\cos\theta}{\sin\theta} + \frac{\pi/2-\theta}{\cos^2\theta} - \frac{\sin\theta}{\cos\theta}\right)\right] \quad (4.30)$$

where

$$Q = -(2k\rho)^{\frac{1}{2}}\cos([\phi+\theta]/2)\ \sin([\phi-\theta]/2)/\sin\phi$$

$$Q' = (k\rho/2\nu)^{\frac{1}{2}}([\nu^2-\cos^2\theta]^{\frac{1}{2}} - \nu\cos\phi)/\sin\phi$$

$$Q'' = (k\rho/2\nu)^{\frac{1}{2}}(\cos\theta - [\nu^2-\cos^2\theta]^{\frac{1}{2}}\cos\phi)/\sin\phi \quad (4.31)$$

and F(z) is the Fresnel integral given by

$$F(z) = \exp(-jz^2)\int_z^{\infty}\exp(jt^2)dt \quad (4.32)$$

(vi) Wu and Tsai (1977):

Writing the unknown surface field as a combination of the geometrical optics field and an extra diffracted field, Wu and Tsai (1977) obtain a numerical solution to the (H-polarised) right-angled dielectric wedge diffraction problem by (c.f. Fig. 4.8)

(a) taking the diffracted field to be effectively zero for $r \geq r_N$ where r_N is chosen arbitrarily

(b) partitioning r_N into n equal segments of length ΔC_n with

$$\Delta C_n \in (r_{n-1}, r_n) \text{ and } \Delta C_1 \in (0, r_1)$$

(c) expanding the diffracted field and its normal derivative as

$$\Psi(r) = \sum_{n=1}^{N} A_n P_n(r)$$

$$\partial\Psi(r)/\partial\hat{n} = \sum_{n=1}^{N} B_n P_n(r) \quad (4.33)$$

where the A_n and B_n are unknown coefficients which have to be found, and

$$P_n(r) = \begin{cases} 1 , & \text{for } r \in \Delta C_n \\ 0 , & \text{otherwise} \end{cases} \qquad (4.34)$$

which is called a pulse-basis function.

(d) approximating the surface integral equations formulation (1.78) by truncating the infinite integral to $r \leq r_M$, where

$$r_M \geq r_N \qquad \text{(Fig. 4.8)}$$

(e) solving the matrix equation arising from the method of moment in steps (a) to (d) to obtain the diffracted field.

Although the geometrical optics field actually extends to infinity, the Greens function (Hankel function in this case) decays as the half-power of distance. Therefore, Wu and Tsai (1977) conclude that the approximation (d) above is justified. Wu and Tsai (1977) show that convergence can be achieved even when r_M is as small as 10λ. The result which Wu and Tsai (1977) obtained for $\varepsilon_r = 1000$ shows good agreement with the perfectly conducting wedge diffraction solution given by Burnside et al. (1975).

(vii) Sinha, Guha and Gupta (1980):

Using techniques similar to those employed by Wu and Tsai (1977), Sinha, Guha and Gupta (1980) obtain a solution for the (E-polarised) right-angled dielectric wedge diffraction problem.

(viii) Hudson (1982):

Several interesting points which are made by Hudson (1982):

(a) The perturbation (i.e. diffraction) arising from the deviation of the value ν from unity is not regular, and the Neumann series approximation used by Rawlins (1977a) is incorrect.

(b) If the wave is at grazing incidence, the scattered wave decays as the inverse half-power of the distance.

(c) If the wave is incident on the wedge at arbitrary angle, the scattered wave decays faster than the inverse power of the distance in the illuminated region while it decays as the inverse power of the distance in the shadow region.

Unfortunately, statement (c) contradicts the well established fact (cf. Keller 1962) that the scattered wave must decay as the half-power of the distance. Therefore, there must be some doubt about the results obtained by Hudson (1982) and his comment on Rawlins's (1977a) analysis.

(ix) Hoenders (1982):

Hoenders (1982) formulates the total field near a right-angled dielectric wedge as the superposition of a suitably chosen unperturbed field. This unperturbed field is the sum of the incident and reflected (or refracted) fields, as if the incoming field is incident on an infinite plane. The extra 'perturbed' field must then restore the boundary conditions. This line of attack is similar to the method adopted in this thesis and is discussed in detail in Chapter 8.

(x) Joo, Ra and Shin (1980, 1984):

Joo, Ra and Shin (1980) obtain a comprehensive solution to the right-angled dielectric wedge problem. As they (Kim, Ra and Shin 1983) have since extended their formulation to include the dielectric wedge of arbitrary angle, it is therefore more appropriate to postpone detailed discussion of their results until section 4.4

4.3.1 Discussion

Unfortunately, it has not been found possible to extend the methods used for right-angled wedges to the general case of arbitrarily-angled dielectric wedges. Some authors have attempted to do so (cf. Aleksandrova and Khizhnyak 1975 and Kim, Ra and Shin 1983), but their results have all been shown to be incorrect (cf. Section 4.4 below). In addition, most authors have not been able to produce explicit formulas, from which diffracted fields can be calculated. Furthermore, few numerical results have been presented. So far, only Rawlins (1977a) has given comprehensive formulas from which verifiable numerical results can be obtained.

4.4 THE DIELECTRIC WEDGE OF ARBITRARY ANGLE

There are about a dozen articles scattered through the literature which attempt to solve, or claim to have solved, the problem of diffraction by a dielectric wedge of arbitrary angle. This section presents a brief review of these articles in chronological order:

(i) Vasil'ev and Solodoukhov (1970, 1971)

Vasil'ev and Solodoukhov (1970) claim to have produced, for the first time, numerical results of the (E-polarised) field diffracted by arbitrarily-angled dielectric wedges. Unfortunately, the original paper, which was presented at a conference in Leningrad, is not available. In a later paper, however, Vasil'ev and Solodoukhov (1971) suggest a numerical scheme for solving the problem of diffraction by an arbitrarily-angled dielectric wedge of an arbitrarily polarised incidence wave.

Beginning with the polarisation source formulation (cf. Bates and Ng 1972) for the induced current, Vasil'ev and Solodoukhov (1971) first represent the total induced current as a sum of the physical optics current (see Section 1.6.2) and an unknown additional current. This additional edge-diffracted current is taken to decay away from the apex and is assumed to be negligible for $\rho \geq \rho_o$, where ρ_o is chosen arbitrarily. The infinite volume integral is then truncated (in a fashion similar to that effected by Wu and Tsai 1977) to $\rho \leq \rho_1$. Again ρ_1 is chosen arbitrarily. The resultant integral equation is then solved by the method of moments. Finally, it must be mentioned that Vasil'ev and Solodoukhov (1971) find it necessary to 'round' the apex of the wedge, in the manner indicated in Fig. 4.9. They further indicate that the results converge when ρ_2 is taken to be less than 0.1λ.

(ii) Kaminetzky and Keller (1972)

Employing the boundary layer method (cf. Jones 1964, Section 11.13), Kaminetzky and Keller (1972) derive the diffraction coefficient for high order edges and vertices.

(iii) Balling (1973a,b)

Balling (1973a,b) obtains a solution for a dielectric wedge excited by a magnetic line source (Fig. 4.10). An approach similar to geometrical

optics is adopted. As shown in Fig. 4.10, a ray emerging from the source, making an angle θ with the datum, is traced out. Whenever this ray encounters a face of the wedge (e.g. point P_2), it is reflected and refracted. A lateral wave (or surface wave, cf. Section 1.2.2, Göss-Hanchen shift) is also generated. The resultant wave solution is constructed by integrating over θ within the range of 0 to 2π. Balling (1973a,b) obtains close agreement between calculated and experimental results.

(iv) Bates (1973)

Published and unpublished, respectively, work by Bates (1973, 1980a) relates to the penetrable wedge for general boundary conditions and arbitrary polarisation. Detailed discussion of this work is postponed until Chapter 5.

(v) Vasil'ev and Solodoukhov (1974)

As a follow-up to their earlier paper, Vasil'ev and Solodoukhov (1974) present further details of their analysis. However, no explicit formulas for scattering patterns (like those of Rawlins 1977a) are given. Furthermore, the surface current plots are all for right-angled wedges having complex refractive index ν values of 2-j0.2 and 1.2-j0.1. Therefore, it is impossible to compare their results with those obtained by other authors, who are concerned solely with real refractive indices.

(vi) Nefedev and Sivov (1974)

This is a purely ray-optical (geometrical optics) treatment of an arbitrary-angled penetrable wedge illuminated by any E-polarised incident wave. The results might form useful initial estimates for a perturbation approach to the penetrable wedge diffraction problem.

(vii) Kaminetzky and Keller (1975)

a complement to their earlier (1972) paper, wherein they derive diffraction coefficient for a dielectric wedge of angle $2\chi \simeq \pi$, Kaminetzky and Keller (1975) derive:

(a) diffraction coefficients for arbitrary-angled dielectric wedge of refractive index $\nu \simeq 1$,

(b) diffraction coefficients for dielectric wedges of small wedge angles.

Kaminetzky and Keller (1975) express the scattered field as a perturbation, which is why the restrictions inherent in (a) and (b) above are necessary. They also formulate this perturbed field as a function of the incident field by using Green's theorem. The resultant integral is then evaluated asymptotically for the diffraction coefficients.

The main results given by Kaminetzky and Keller are (c.f. Fig. 4.11)

(a) For wedges of small refractive indexes and uniform boundary conditions (cf. Section 1.3.1), the diffraction coefficient $D(\phi,\theta)$ is given, for $-\chi<\phi<3\pi/2-\chi$, by

$$D(\phi,\theta) = \frac{2\exp(-j\pi/4)\ \sin\chi}{(8\pi)^{\frac{1}{2}}(\sin\theta + \sin\phi)} \left[\frac{1}{\sin(\chi+\theta) - \sin(\chi-\phi)} \right.$$

$$\left. - \frac{1}{\sin(\chi-\theta) - \sin(\chi+\phi)} \right] \qquad (4.36)$$

(b) For wedges of small angle having uniform boundary conditions, the diffraction coefficient $D(\phi,\theta)$ is given, for $-\chi<\phi<3\pi/2-\chi$, by

$$D(\phi,\theta) = \frac{2\chi\ \exp(-j\pi/4)(1-\nu^2)}{(8\pi)^{\frac{1}{2}}(\sin\theta + \sin\phi)^2} \qquad (4.37)$$

(viii) Aleksandrova and Khizhnyak (1976, 1978)

A procedure similar to that presented in an earlier paper (Aleksandrova and Khizhnyak 1975) is adopted to solve for the problem of diffraction by a dielectric wedge of arbitrary angle. Therefore, comments made in Section 4.3 on this particular method are also applicable here. A further point worth noting is that Lewin and Screenivasiak (1978) say that the solution of Aleksandrova and Khiznyak (1976) is incorrect.

(ix) Berntsen (1978)

As a preliminary to a later paper (Berntsen 1983), Berntsen (1978) indicates that the problem of diffraction by an arbitrarily-angled dielectric wedge can be solved by manipulating the Fourier transform of a polarisation source formulation into a form which is suitable for numerical computation. The important feature of Berntsen's (1978) paper is that is shows the diffracted wave must radiate from the neighbourhood of the edge and must decay as the inverse half-power of the distance.

(x) Kost (1978)

Kost (1978) calculates the characteristic impedance of a dielectric wedge excited by two magnetic line sources (Fig. 4.12). He uses the expansion

$$\Psi_- = \sum_\alpha A_\alpha \sin\alpha(\pi-\chi)\ \sin\alpha|\phi|\,(\rho/\rho_o)^\alpha, \quad \rho < \rho_o$$

$$= \sum_\alpha B_\alpha \sin\alpha(\pi-\chi)\ \sin\alpha|\phi|\,(\rho/\rho_o)^{-\alpha}, \quad \rho > \rho_o \qquad (4.38)$$

$$\Psi_+ = \sum_\alpha A_\alpha \sin\alpha(\pi-|\phi|) \sin\alpha\chi(\rho/\rho_o)^\alpha, \rho > \rho_o$$

$$= \sum_\alpha B_\alpha \sin\alpha(\pi-|\phi|) \sin\alpha\chi(\rho/\rho_o)^{-\alpha}, \rho < \rho_o \qquad (4.39)$$

for fields inside and outside the wedge. The boundary conditions are

$$\Psi_-(\rho;\pm\chi^-) = \Psi_+(\rho;\pm\chi^+) \qquad (4.40)$$

$$\partial\Psi_-(\rho;\pm\chi^-)/\partial\phi = \nu^2\partial\Psi_+(\rho;\pm\chi^+)/\partial\phi \qquad (4.41)$$

It is seen that Ψ_- and Ψ_+ satisfy (4.40) implicitly, while (4.41) determines the eigenvalue α. On substituting (4.38) and (4.39) into (4.41), the eigenvalue α is then given as the solution of

$$\nu^2 \sin\alpha(\pi-\chi) \cos\chi + \cos\alpha(\pi-\chi) \sin\alpha\chi = 0 \qquad (4.42)$$

The expansion coefficients (A_α and B_α) are then determined by equating the (total) fields at $\rho = \rho_o$.

(xi) Berntsen (1983)

As a follow-up to an earlier paper (Berntsen 1978), a solution for an arbitrarily-angled dielectric wedge is derived. Berntsen (1983) obtains a singular integral equation by Fourier-transforming the polarisation source formulation (cf. Bates and Ng 1972). This approach is shown (Berntsen 1983) to degenerate into the equation of Kraut and Lehman (1969) when the wedge angle $2\chi = \pi/2$. A subsequent inverse transform leads to a Fredholm integral equation and a solution is constructed as a Neuman series. The integral equation is then solved numerically. Two important suggestions are made by Berntsen (1983):

(a) The error of the physical optics and geometrical optics approximation increases with increasing value of refractive index ν. This error also increases with increaseing ϕ (Fig. 4.13), i.e. away from the back-scattered region.

(b) In contradiction to a reported result (Kumar 1981), Bernsten shows that the diffraction patterns of dielectric wedges do not always have maximas at reflection boundaries (cf. Section 4.1.1). The results given in Table II of Berntsen (1983) are plotted as scattering patterns in Fig. 4.13.

The paper by Berntsen (1983) contains a lengthy justification for his approach. Unfortunately, few numerical results are given. Furthermore, it is not clear why his calculations are for somewhat bizzare values for the incident angle θ - i.e. 1.043 in (his) Table I and 0.315 in Table II. This makes the task of comparing the given results with those obtained by other authors a very difficult one.

(xii) Kim, Ra and Shin (1983)

Joo, Ra and Shin (1980, 1984) present a solution for the right-angled dielectric wedge. They subsequently extend their original approach to dielectric wedges of arbitrary angle. Their starting point is similar to that of some other authors (cf. Kraut and Lehman 1969, Bernsten 1983), i.e. from the Fourier transform of the polarisation source formulation. The unknown surface field is expressed as a combination of the physical optics field and an unknown edge diffracted field. This unknown edge diffracted (surface) field is further expanded as a two-dimensional multipole series using the pulse-basis type functions of Wu and Tsai 1977 (see also Section 4.3 where the pulse-basis function is defined by (4.34)). After some manipulation in the Fourier domain, the inverse transforms are evaluated using the method of steepest descents (cf. Felsen and Marcuvitz 1973, Section 1.6). This reduces to a system of algebraic equations with the expansion coefficients of the edge field as the unknowns. These equations are then solved numerically. The extension from the right-angled wedge to an arbitrarily-angled wedge involves only the calculation of the multiple refracted and reflected waves at the surfaces of the wedge.

Many numerical results and plots of scattering patterns are given by Kim et al (1983) and Joo et al (1980, 1984). The validity of their results is, quote, 'assured by two limits of relative dielectric constant ε_r of the wedge', unquote. For the case of right-angled wedge, quote, 'for small ε_r, the calculated total asymptotic field approaches Rawlins's (1977a) Neumann series solution, for large ε_r, the edge diffraction pattern is shown to approach that of a perfectly conducting wedge', unquote.

However, the results obtained by Kim, Joo, Ra and Shin cannot be correct for the following reasons:

(a) The far scattered field derived by Kim et al. is always zero at the surfaces of the wedge, irrespective of the refractive index of the wedge, the wedge angle or the angle of incident wave θ. This is obviously wrong.

Furthermore, the diffracted portion of the far scattered field calculated by Rawlins (1977a) for the right-angled wedge, or by Kaminetzky and Keller (1972, 1975) for the arbitrarily-angled wedge, is not zero at the wedge surface.

(b) When $\varepsilon_r \to \infty$, the diffraction pattern of Ra et al. approaches that of a perfectly conducting wedge. However, it must be noted that the (E-polarised) far diffracted field is always zero on a perfectly conducting surface. Therefore this agreement cannot be used as a proof of the validity of Ra et al's method unless they can prove that the generalisation stated in (a) is true.

(c) For small ε_r, the calculated total asymptotic field approaches Rawlins' (1977a) solution. This comparison is again misleading. For small ε_r one would expect the diffracted field to be only a small percentage of the total field. For example, if the diffracted field is, say 1% of the total field, then Ra et al. are comparing 1.01 (total of incident, reflected or refracted and diffracted field of Rawlins 1977a) with 1.00 (of their solution, where diffracted field equals to zero). Comparison of small quantities in such a manner is difficult to justify.

4.4.1 Conclusion

In the above discussion, it seems that the results of research into penetrable wedges of arbitrary angle so far presented in the literature are either (i) incorrect (Vasil'ev and Solodoukhov 1970, 1971, 1974, Aleksandrova and Khizhynak 1976, 1978 and Kim, Joo, Ra and Shin 1980, 1983, 1984), (ii) difficult to verify (Berntsen 1978, 1983), or (iii) of a special nature (Balling 1973a, b, Nefedev and Sivov 1974 and Bates 1973), which cannot be easily extended to a general solution.

Only Kaminetzky and Keller (1972, 1975) have presented comprehensive formulas enabling one to calculate diffracted fields easily. Unfortunately, because they use a perturbation model, their solutions are of somewhat restricted validity. More comprehensive and general solutions are introduced in Chapters 5, 7 and 8. Detailed discussions of the respective merits of these new methods are presented in the relevant chapters.

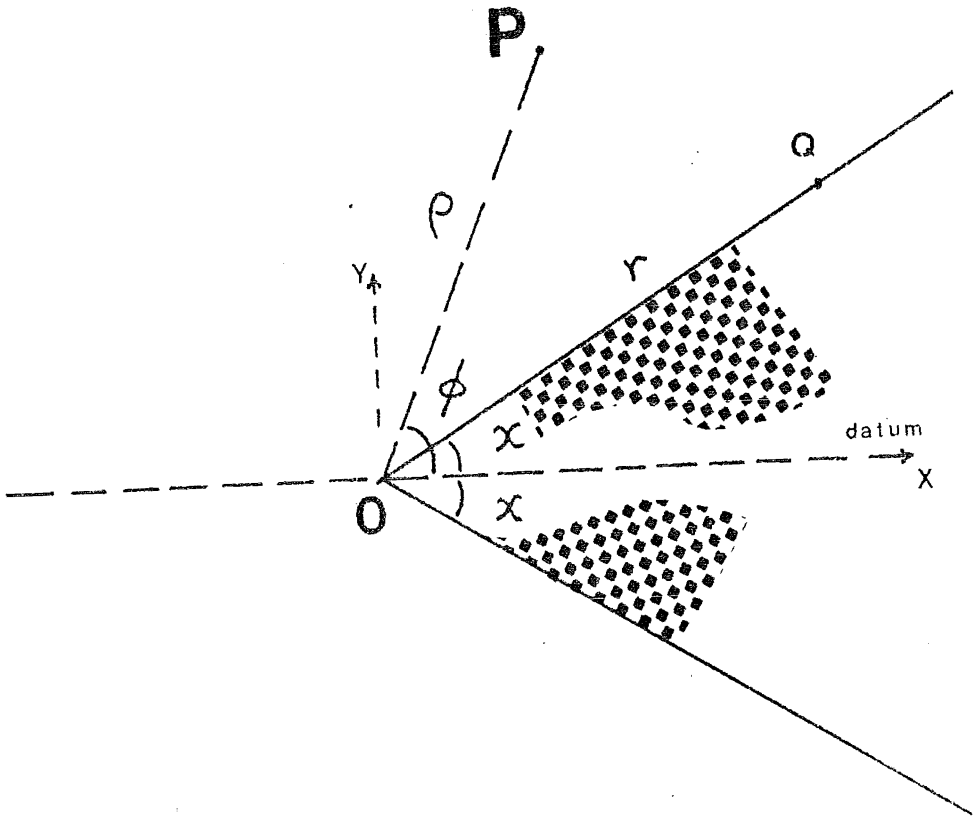

FIGURE 4.1 Configuration of, and coordinates for, the infinite wedge. Note that z-axis is perpendicular to the paper. The wedge angle is 2χ. Arbitrary point in space and on the wedge surface are denoted by P, with coordinates $(\rho;\phi)$, and Q with coordinates $(r;\chi)$, respectively.

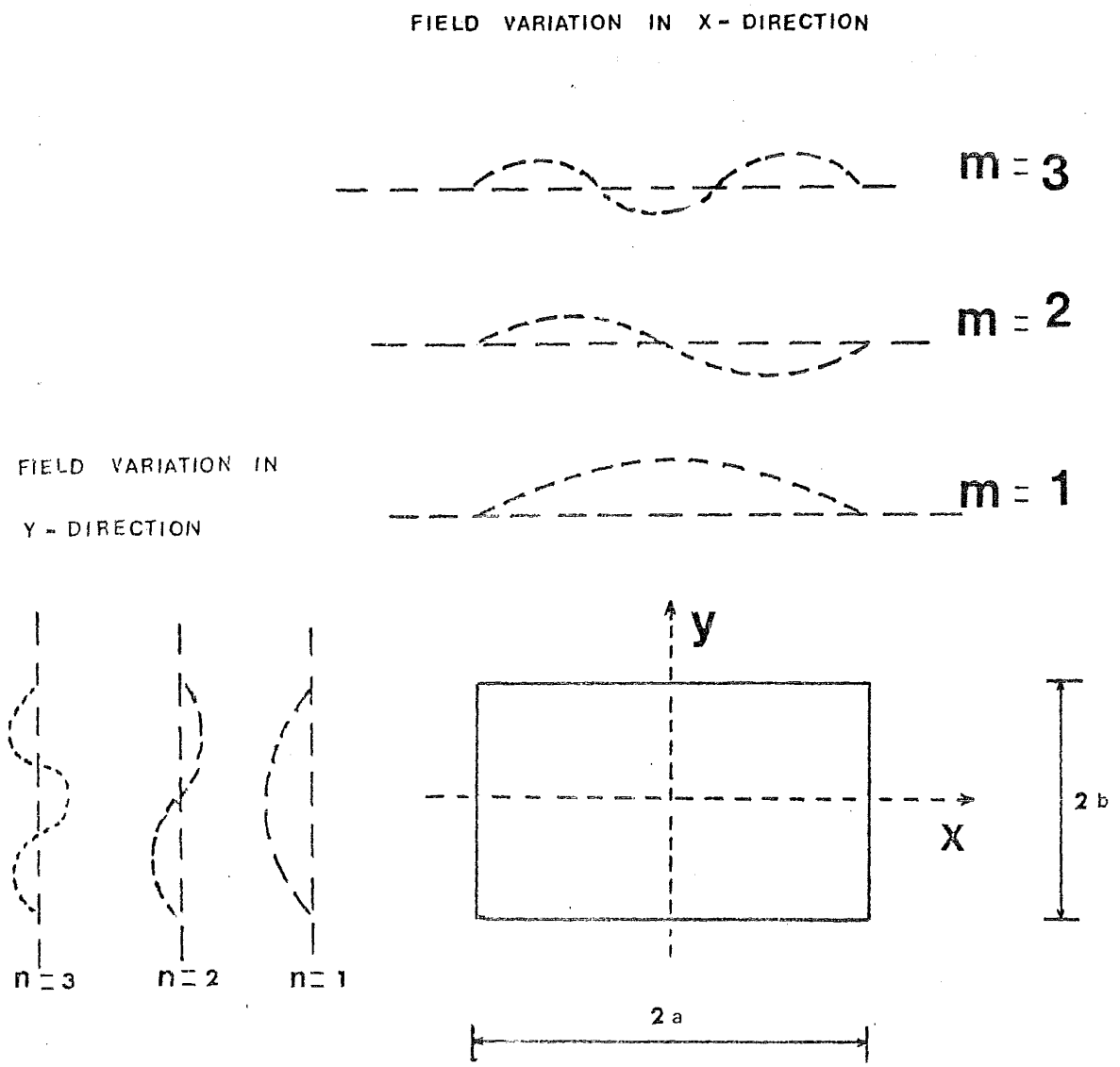

FIGURE 4.2 Free modes in a rectangular waveguide.

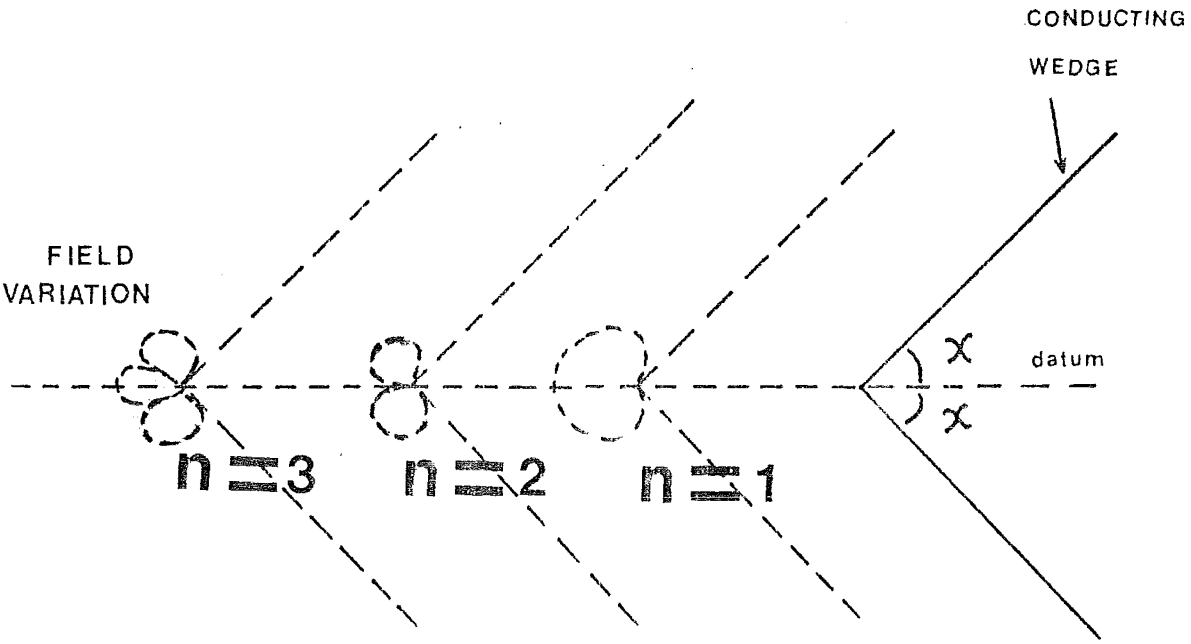

FIGURE 4.3 Free modes of a perfectly conducting wedge.

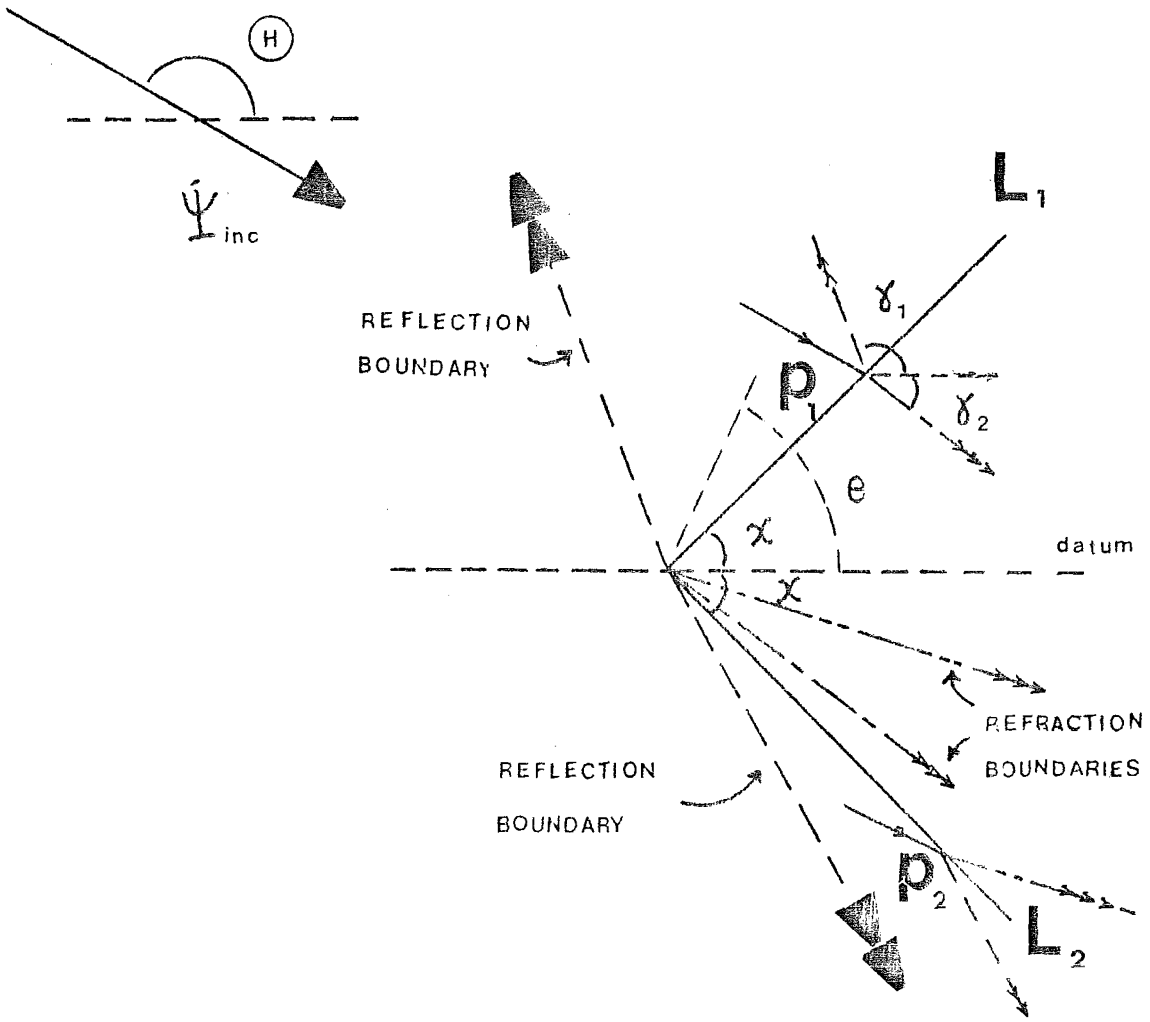

FIGURE 4.4 Reflection and refraction boundaries of an infinite penetrable wedge illuminated by a plane wave at an angle θ. The reflection boundaries are indicated by double arrows while the refraction boundaries are indicated by triple arrows.

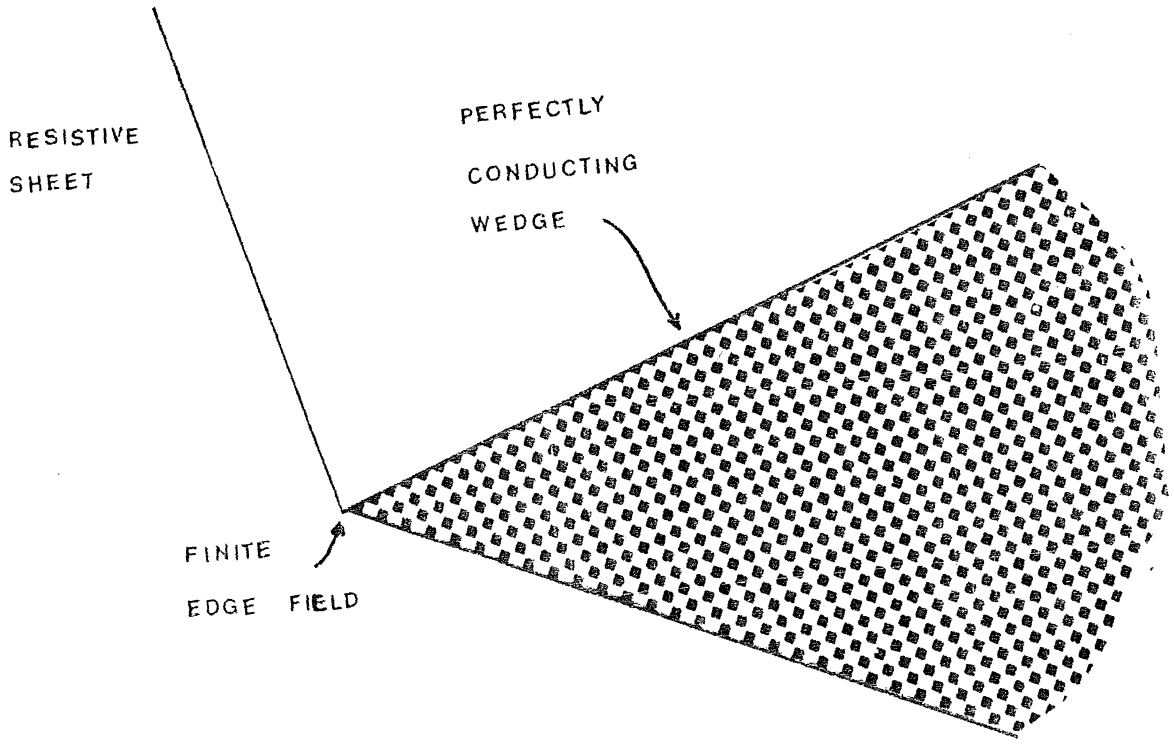

FIGURE 4.5 Conducting wedge and an infinitely thin sheet characterised by an impedance boundary condition (cf. Section 1.3.1).

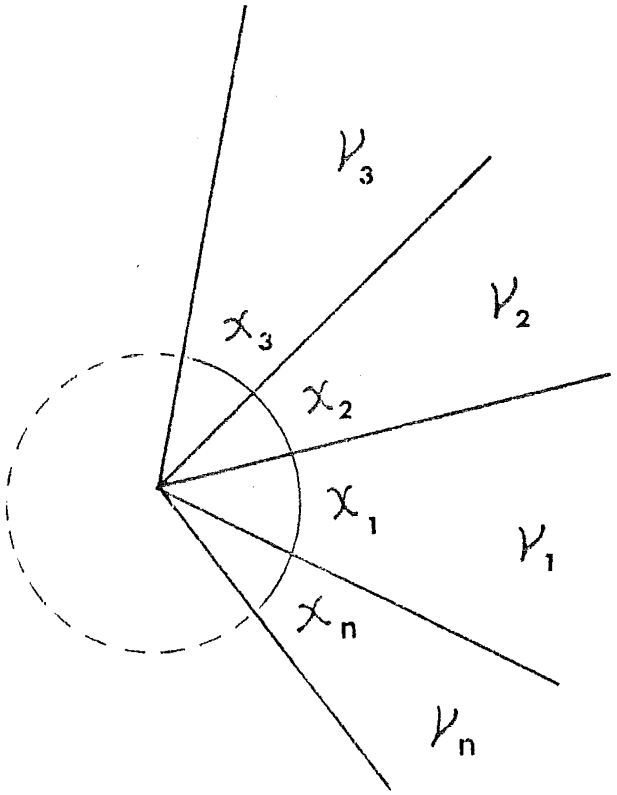

FIGURE 4.6 Configuration of multi-dielectric wedges. The space is divided into N sectors (or wedges). The nth sector, where n = 1, 2, 3, ... , N, has a wedge angle χ_n and refractive index ν_n.

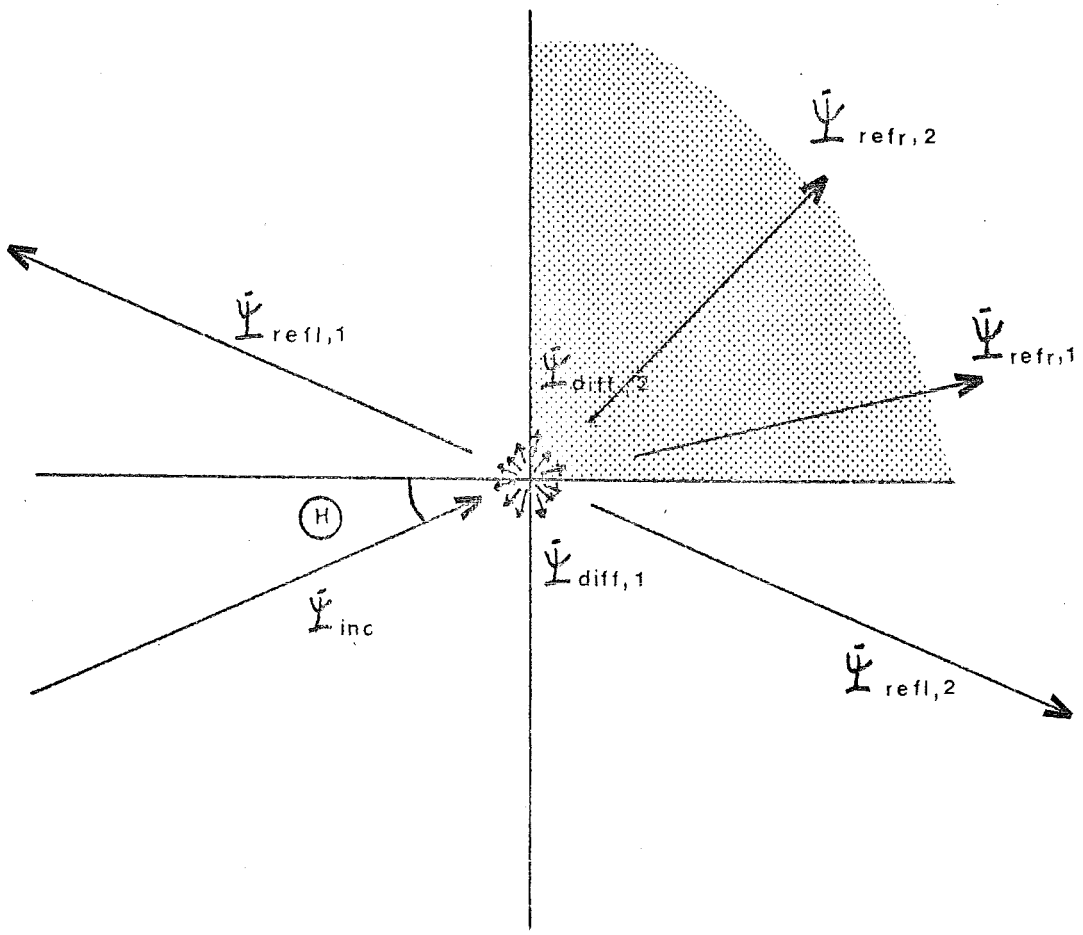

FIGURE 4.7 Diffraction by right-angled wedge. Geometry of which as used by Rawlins (1977a).

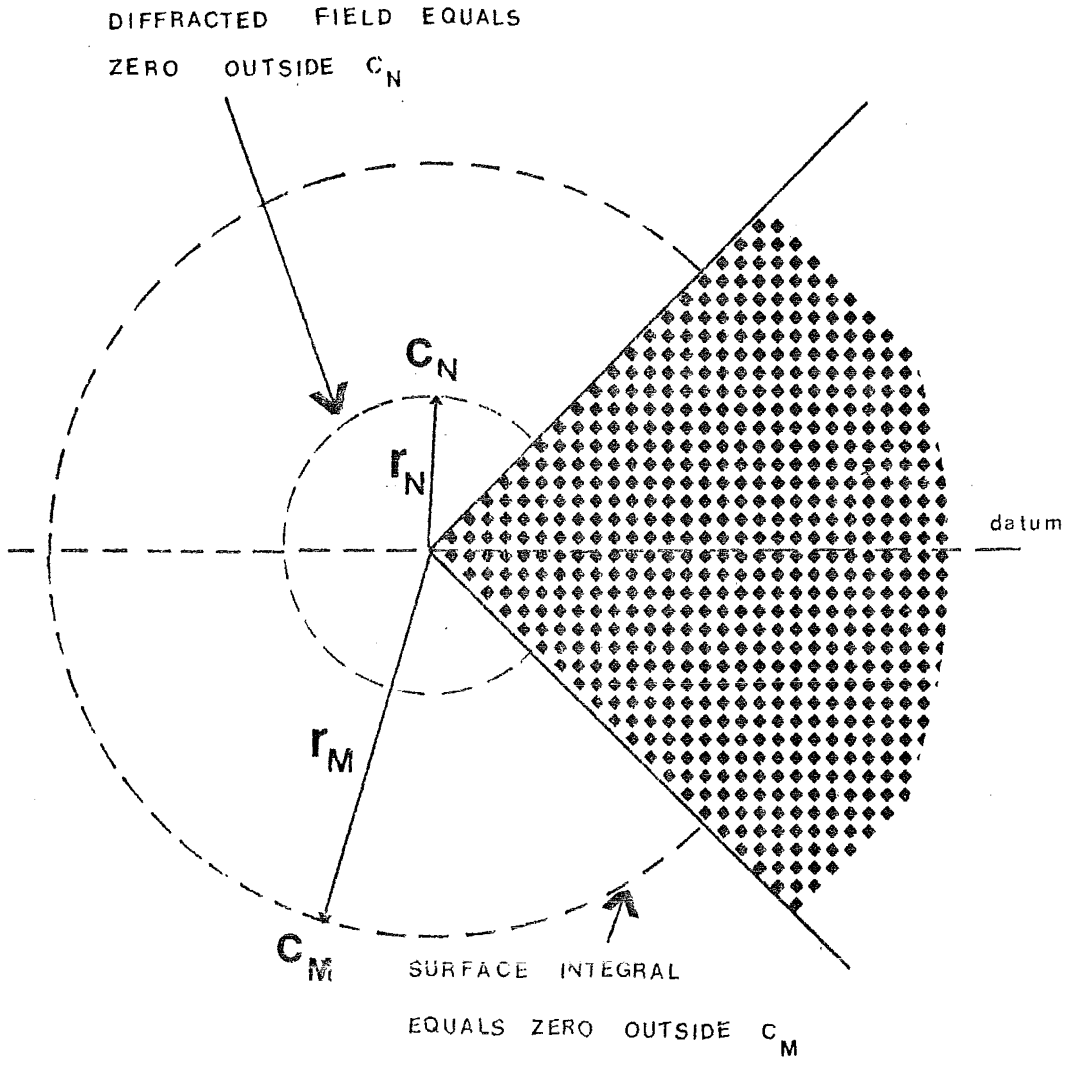

FIGURE 4.8 Regions of existence of various series of Wu and Tsai (1977).

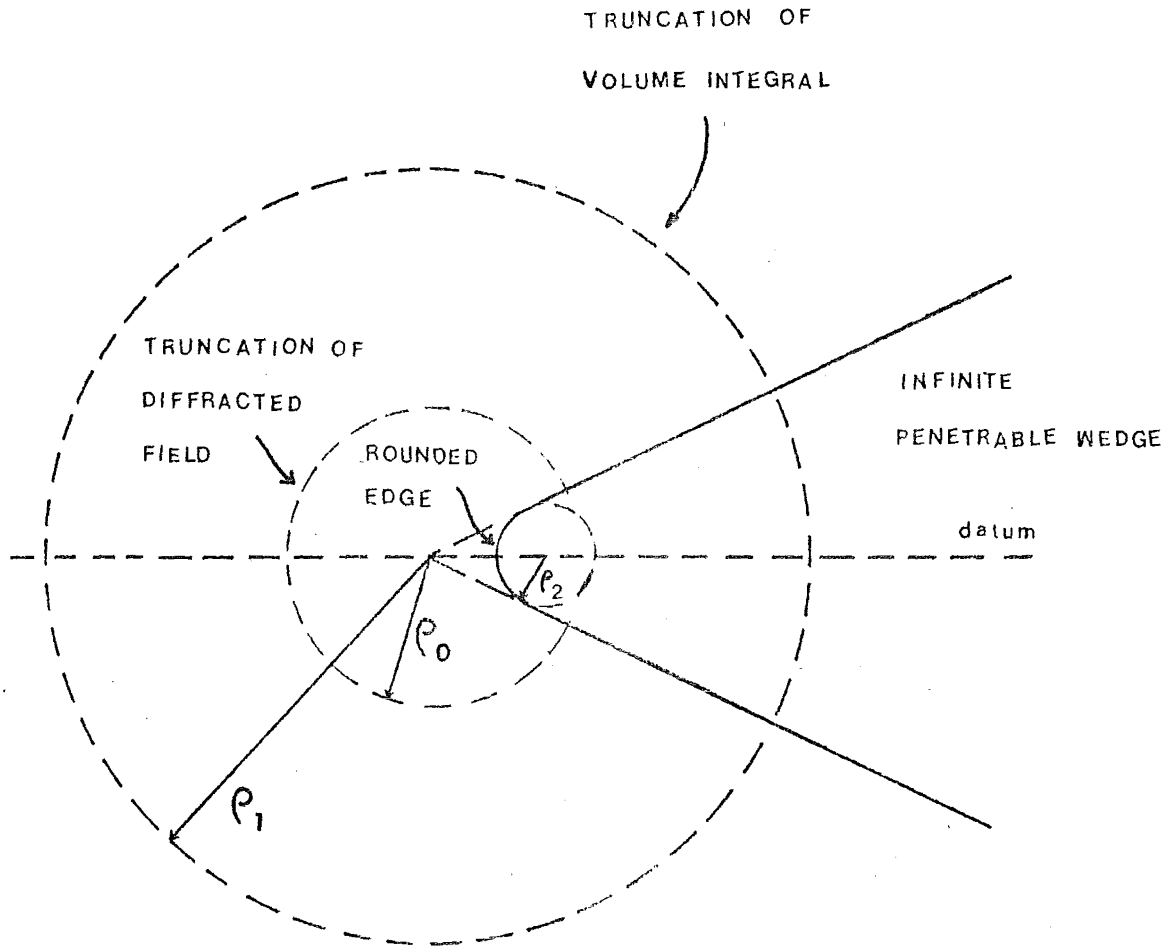

FIGURE 4.9 Rounded wedge of Vasil'ev and Solodoukhov (1971). The 'apex' of the wedge is part of a circle of radius ρ_2.

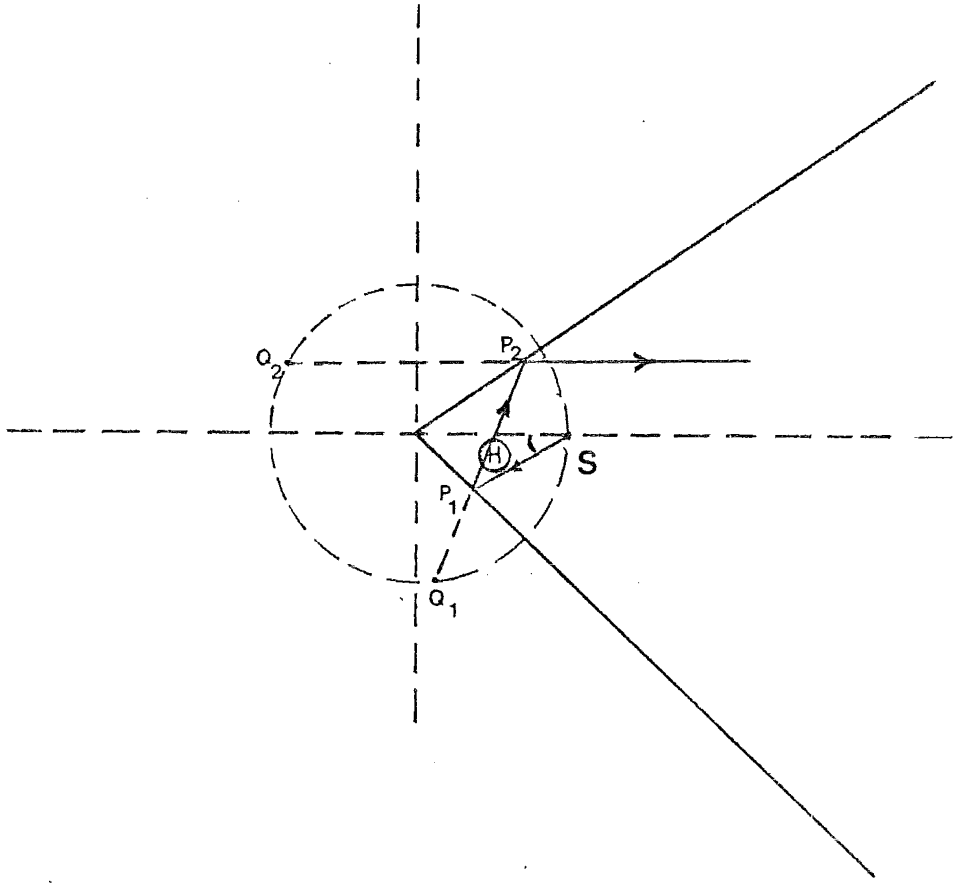

FIGURE 4.10 Dielectric wedge excited by line sources at S. The images (multiple-reflected in the faces of the wedge) of the source are at Q_1, Q_2, ...

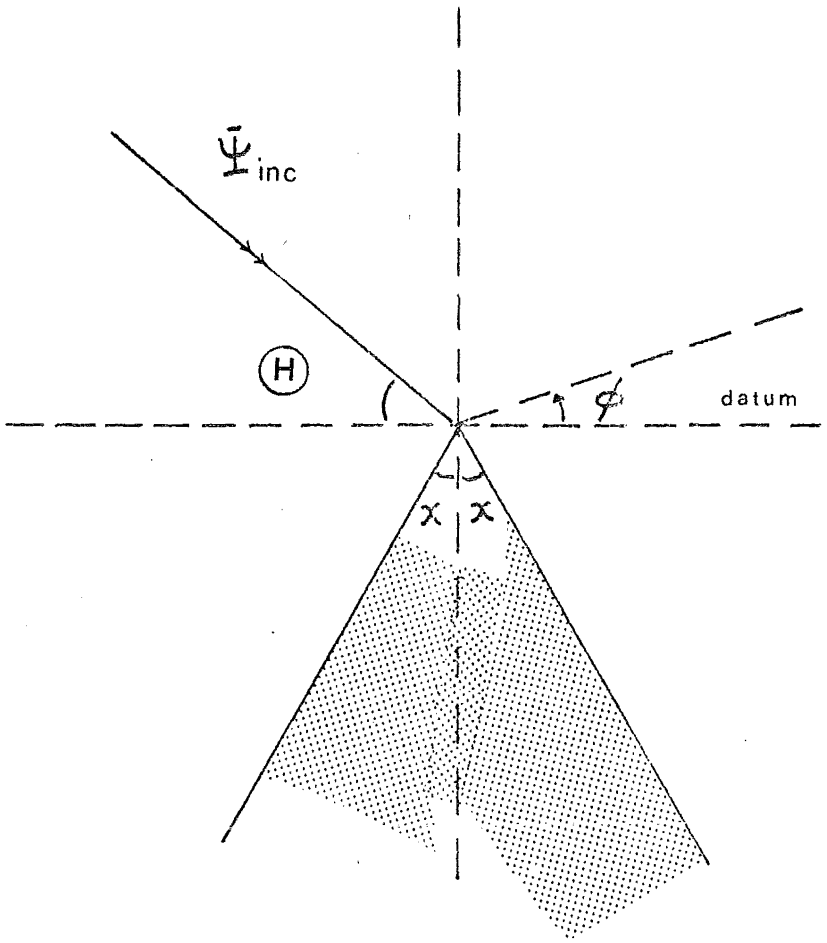

FIGURE 4.11 Geometry of infinite wedge used by Kaminetzky and Keller (1975).

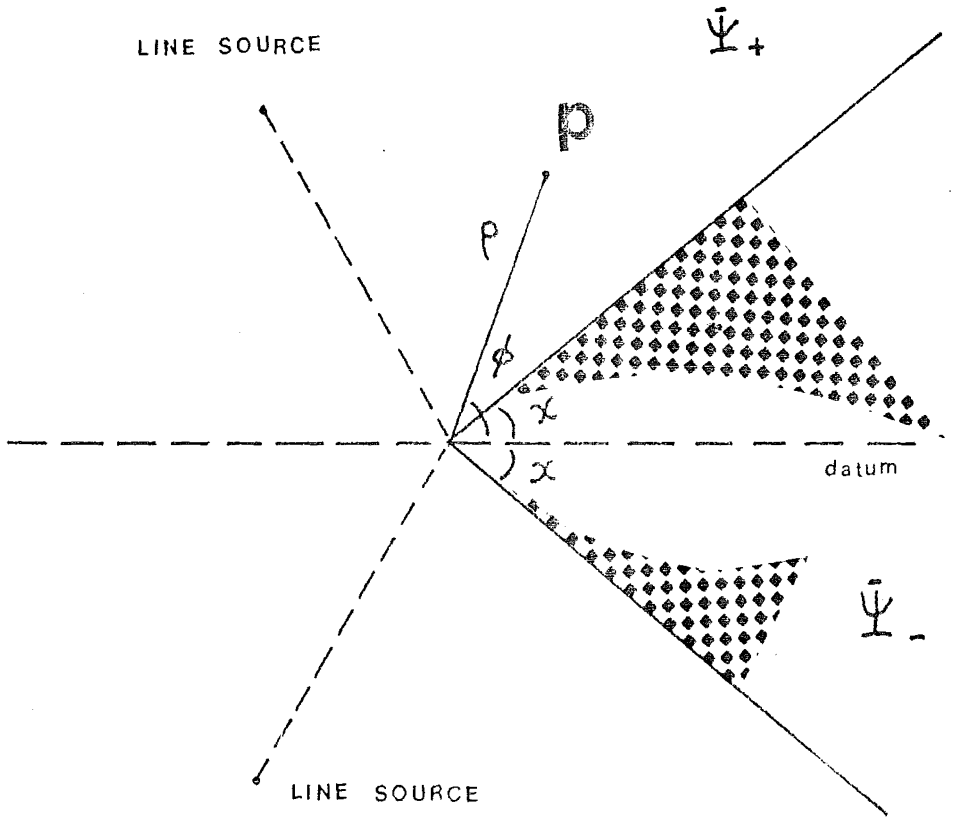

FIGURE 4.12 Dielectric wedge excited by double line sources.

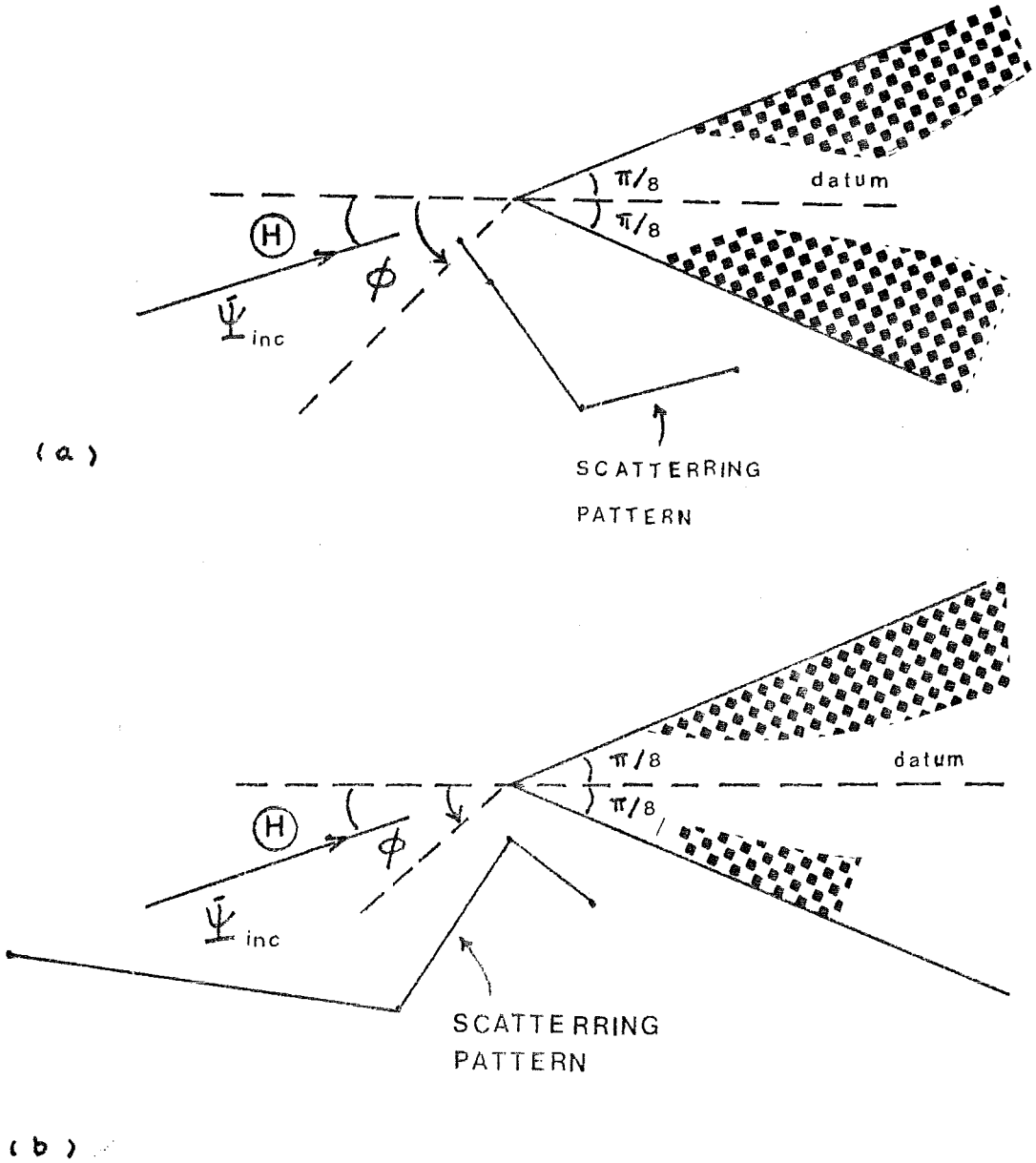

FIGURE 4.13 Diffraction pattern generated from Table I of Berntsen (1983) (a) $\varepsilon_r = 2$ and $\theta = 0.315$, (b) $\varepsilon_r = 5$ and $\theta = 0.315$.

CHAPTER FIVE

BATES' APPROACH TO THE INFINITE PENETRABLE WEDGE DIFFRACTION PROBLEM

A general method of constructing solutions to problems concerning diffraction by a penetrable wedge is presented in this chapter. It is due to Bates (1973, 1980a). The solutions given here are valid for a homogeneous wedge of arbitrary wedge angle and refractive index excited by an arbitrarily positioned line source, provided that the field does not vary in the direction perpendicular to the cross-section of the wedge.

The complete diffracted field is built up from basic wave functions, which are defined in Section 5.2, developed in Section 5.4, shown to be unique in Section 5.3 and demonstrated to exist in Section 5.5. The significance of the work reported here is assessed in Section 5.8. The edge behaviour of the diffracted field is further examined in Chapter 6. The class of solutions discussed in this chapter is not useful by itself, because of extreme numerical difficulties (as explained in Section 5.7). When combined with other approaches (see Chapter 6), however, it does lead to significant improvements in computational efficiency.

5.1 PRELIMINARIES

Fig. 5.1 depicts a penetrable wedge of angle 2χ. The incident wave Ψ_{inc} is due to a two-dimensional point source (i.e. a line source in three dimensions) situated at $(r;\Theta)$. The fields are Ψ and ψ respectively outside (Ω_+) and inside (Ω_-) the wedge. Furthermore, penetrable boundary conditions (cf. Section 1.3.1) apply; i.e.

$$\Psi(\rho;\pm\chi^+) = a\,\psi\,(\rho;\pm\chi^-)$$

$$\partial\Psi(\rho;\pm\chi^+)/\partial\phi = b\,\partial\psi(\rho;\pm\chi^-)/\partial\phi \qquad (5.1)$$

where

$$\Psi = \Psi_{inc} + \Psi_{sc} \qquad (5.2)$$

and Ψ_{sc} is the scattered field, and a, b are complex constant as defined in Section 1.3.1.

5.2 BASIC WAVE FUNCTIONS

It is convenient to build up Ψ and ψ from basic wave functions (or eigenfunctions cf. Section 1.4.) that have (comparatively) simple forms in Ω_+ and Ω_- respectively. The basic wave function in Ω_+, denoted by u, is matched across the faces (of the wedge) to the basic wave function in Ω_-, denoted by w. And the fields Ψ, Ψ_{inc}, Ψ_{sc} and ψ are built up from u, u_o, v and w respectively via

$$\begin{aligned} \Psi_{inc} &= \sum_{\alpha} u_o(\rho;\phi,\alpha) \\ \Psi_{sc} &= \sum_{\alpha} v(\rho;\phi,\alpha) \\ \psi &= \sum_{\alpha} w(\rho;\phi,\alpha) \end{aligned} \tag{5.3}$$

where $\sum_{\alpha}$ is the Schiff's (1949) symbol introduced in Section 1.3. Furthermore, it is seen from Section 1.4. that an appropriate expression for u_o is

$$u_o(\rho;\phi,\alpha) = J_\alpha(k\rho)\cos(\alpha[\pi-\phi+\theta]), \tag{5.4}$$

for some α within the complex plane.

5.3 UNIQUENESS

In this section it is shown that, when $a\neq 0$ and $b\neq 0$ (a and b are defined by (5.1)) and when χ/π is a rational number, u and w must necessarily be zero if u_o is set to zero, i.e. there are no free modes. Consequently, when u_o is given the form of the RHS(5.4), it follows that u and w are unique because it is impossible to add to u and w any further terms that satisfy both the wave equations and the boundary conditions.

The analysis presented in this section is restricted to the case for which u and w are even functions of ϕ. The kind of analysis required for odd functions is identical in all important aspects.

The form of the multiplication formula (cf. Watson 1966, Section 5.21) suggests that, when $u_o = 0$, the simplest forms for v and w, that are regular within Ω_+ and Ω_- respectively, and that satisfy the wave equations, are:

$$v = \sum_{n=o}^{\infty} A_m(\alpha)\ J_{\alpha+2m}(k\rho)\ \cos(\lceil\alpha+2m\rceil\phi),\ |\phi| < \chi \qquad (5.5)$$

and

$$w = \sum_{m=o}^{\infty} B_m(\alpha)\ J_{\alpha+2m}(\nu k\rho)\ \cos(\lceil\alpha+2m\rceil\lceil\pi-\phi\rceil),\ |\pi-\phi| < \pi-\chi \qquad (5.6)$$

Substituting (5.5) and (5.6) into the boundary conditions (5.1) and comparing the coefficients of the Bessel functions $J_{\alpha+2m}(k\rho)$ with the aid of the multiplication theorem (cf. Watson 1966 , Section 5.21), one gets;

(i) for m = 0,

$$(a+b)\ \sin\alpha\pi = (a-b)\ \sin\alpha(\pi-2\chi) \qquad (5.7)$$

(ii) for m > 0,

$$B_m(\alpha) = (-1)^{m+1}(a-b)\ \cos(\lceil\alpha+2m\rceil\lceil\pi-2\chi\rceil)/\sin 2m\chi$$
$$\sum_{n=o}^{m-1} B_n(\alpha)\ F_{m-n}(\alpha+2m,\nu)\nu^{-\alpha}\lceil a\ \cos(\lceil\alpha+2n\rceil\lceil\pi-\chi\rceil)$$
$$\sin(\lceil\alpha+2m\rceil\chi) + ((\alpha+2n)b/(\alpha+2m))\ \sin(\lceil\alpha+2n\rceil\lceil\pi-\chi\rceil)$$
$$\cos(\lceil\alpha+2m\rceil\chi)\rceil \qquad (5.8)$$

It is seen that (5.7) is the so-called static edge condition of Meixner (1972) and Andersen and Solodoukhov (1978). However, the term $\sin(2m\chi)$ in the denominator of RHS(5.8) is necessarily zero for a denumerably infinite number of values of the integer m, when χ/π is rational. It therefore follows that RHS(5.8) cannot exist. Bates (1973, 1980a) therefore concludes that free modes do not exist for penetrable wedges.

5.3.1 Travelling Mode of Felsen (1967)

Maurer and Felsen (1967) write, 'A mode in a general guiding system must satisfy the source-free equations and relevant boundary conditions. When a resonant mode (or cavity mode, or free mode) is considered, the resulting field structure exhibits periodicities throughout the spatial volume (Fig. 5.2a) whereas for a travelling mode (or propagating mode or guided mode), the spatial periodicity descriptive of a given mode occurs in a plane or surface transverse to the selected guiding or propagating direction (Fig. 5.2b).'

This transverse spatial periodicity maintains its characteristics throughout the guiding structure, distinguishes one mode from all others, and forms the basis of orthogonality relations satisfied by the mode set. In its most elementary form, such an identification of modes is tied to the mathematical notation of separability of the field equations and boundary conditions with respect to guiding and transverse coordinates. However, in the penetrable wedge problem, such simple separation of modes is not possible as indicated by Bates (1973, 1980a). Unlike in a conventional free mode situation, one cannot determine the guiding (or cutoff) characteristic by simply equating each 'mode' of u and w. However, one might consider each $J_{\alpha+2m}(\nu k\rho)\cos([\alpha+2m]\phi)$ as a travelling mode propagating from a particular caustic (Fig. 5.2b) and the final solution can therefore be obtained by summing (or integrating) over all modes (or caustics).

The concept of travelling mode can be made clear when one examines the formation of such a mode. A localised source, as in Fig. 5.3, emits rays whose starting intensities in various directions are determined by the source characteristics; upon striking a boundary, these rays are specularly reflected (and refracted) with amplitude prescribed by the surface reflection (refraction) coefficients. The ray structure is therefore determined by the initial conditions at the source and the boundary conditions on the walls. When the source is absent the ray system must, however, still satisfy constraints expressed by closure upon reflection (refraction) and by whatever phase and amplitude consistency relation. Finally, it must be emphasised that the concept of a travelling mode does not contradict Bates' (1973c, 1980a) suggestion that no free mode can exist in a penetrable wedge, since it is only a terminological difference.

5.4 DIFFRACTED BASIC WAVE FUNCTIONS

The matching of u and w across the faces of the wedge is simplified if the basic wave functions are first separated into their even and odd parts. Application of the boundary conditions, with the aid of the multiplication theorem, thus leads to

(i) for m = 0,

$$A_o^p(\alpha) = \pm \left[(a-b)/2\right]\sin 2\alpha(\pi-\chi)\ \mathrm{osi}(\alpha\theta)\left[f_{o,o}^{p}(\alpha,a,b,\chi)\right]^{-1}$$

$$B_o^p(\alpha) = \pm \nu^{-\alpha}\sin\alpha\pi\ \mathrm{osi}(\alpha\theta)\left[f_{o,o}^{p}(\alpha,a,b,\chi)\right]^{-1} \qquad (5.9)$$

where

$$f^{p}_{m,n}(\alpha,a,b,\chi) = a\ \mathrm{osi}(\lceil\alpha+2m-2n\rceil\lceil\pi-\chi\rceil)\ \mathrm{iso}(\lceil\alpha+2m\rceil\chi)$$

$$+ \lceil(\alpha+2m-2n)b/(\alpha+2m)\rceil\mathrm{iso}(\lceil\alpha+2m-2n\rceil\lceil\pi-\chi\rceil)\mathrm{osi}(\lceil\alpha+2m\rceil\chi) \qquad (5.10)$$

and where p indicates the even/odd parts of the wave functions. When p = even, the upper sign in (5.9) is taken, osi = cos, and iso = sin. When p = odd, the lower sign is taken and osi = sin, iso = cos.

(ii) for $m > 0$,

$$A^{p}_{m}(\alpha) = \sum_{n=o}^{m} B^{p}_{m-n}(\alpha)\ F_n(\alpha+2m-2n,\nu)\ g^{p}_{m,n}(\alpha,a,b,\chi) \qquad (5.11)$$

$$B^{p}_{m}(\alpha) = -\nu^{\alpha+2m}/f^{p}_{m,0}(\alpha,a,b,\chi) \sum_{n-1}^{m} B^{p}_{m-n}(\alpha)\ F_n(\alpha+2m-2n,\nu)$$

$$f^{p}_{m,n}(\alpha,a,b,\chi) \qquad (5.12)$$

where

$$g^{p}_{m,n}(\alpha,a,b,\chi) = a\ \mathrm{osi}(\lceil\alpha+2m-2n\rceil\lceil\pi-\chi\rceil)\ \mathrm{osi}(\lceil\alpha+2m\rceil\chi)$$

$$- (\lceil\alpha+2m-2n\rceil\ b/\lceil\alpha+2m\rceil)\ \mathrm{iso}(\lceil\alpha+2m-2n\rceil\lceil\pi-\chi\rceil)$$

$$\mathrm{iso}(\lceil\alpha+2m\rceil\chi) \qquad (5.13)$$

and $F_n(\ell,0)$ is as defined in (1.36).

5.5 EXISTENCE OF DIFFRACTED WAVE FUNCTIONS

In Section 5.6 the actual wave functions are presented as contour integrals over α. However, these integral representations are useful if and only if the series on RHS(5.5) and RHS(5.6) converge appropriately, except at the poles of u and w (considered as functions of α).

A detailed analysis (cf. Bates 1980a) shows that

$$\lim_{m\to\infty} B^{p}_{m+1}(\alpha)/B^{p}_{m}(\alpha) \longrightarrow m \qquad (5.14)$$

However, from (1.31),

$$\lim_{m\to\infty} J_{\alpha+2m-2}(\nu k\rho)/J_{\alpha+2m}(\nu k\rho) \longrightarrow m^{-2} \qquad (5.15)$$

It follows from (5.14) and (5.15) that RHS(5.6) is absolutely convergent. Comparison of (5.5) and (5.6) shows that $A_m^p(\alpha)$ grows asymptotically with m in the same way as $B_m^p(\alpha)$, which implies that RHS(5.5) is also absolutely convergent.

5.6 SATISFYING THE RADIATION CONDITION

Consider the following integral formulas:

$$\Psi = \int_\Gamma \zeta(\alpha)\ u(\alpha,\theta,\rho,\phi)\ d\alpha \tag{5.16}$$

and

$$\psi = \int_\Gamma \zeta(\alpha)\ w(\alpha,\theta,\rho,\phi)\ d\alpha \tag{5.17}$$

where Γ is an appropriate contour in the complex α-plane and $\zeta(\alpha)$ is a weighting function. The actual incident field Ψ_{inc}, is given by (5.16) with u replaced by u_o. i.e.

$$\begin{aligned}\Psi_{inc} &= \int_\Gamma \zeta(\alpha)\ u_o(\alpha,\theta,\rho,\phi)\ d\alpha \\ &= \int_\Gamma \zeta(\alpha)\ J_\alpha(k\rho)\ \cos(\alpha[\pi-|\phi-\theta|])\ d\alpha\end{aligned} \tag{5.18}$$

Since Ψ_{inc} is the field due to a two-dimensional point source at Q (Fig. 5.1), it follows (cf. Jones 1964) that

$$\Psi_{inc} = -j/4\ H_o^{(2)}\ (kR) \tag{5.19}$$

By choosing Γ as the imaginary axis, and

$$\zeta(\alpha) = -H_\alpha^{(2)}\ (kr)/4\ \sin\alpha\pi \tag{5.20}$$

RHS(5.18) represents a Kontorowich-Lebedev integral transform (cf. Section 3.2). When $\rho<r$, the contour Γ can be closed at infinity in the right-half plane. The resulting residue series, due to the poles of α which occur at the zeros of $\sin(\alpha\pi)$, is seen to have the form specified by the addition theorem (cf. Watson 1966, Section 11.3) for RHS(5.19). i.e. The formulation completely determines the source at Q.

Since RHS(5.19) and hence RHS(5.18) satisfy the radiation condition, it transpires that the actual wave functions defined by (5.16) and (5.17) must necessarily satisfy the radiation condition.

5.7 FIELD BEHAVIOUR NEAR THE APEX

It follows from Section 5.6 that solutions to penetrable wedge diffraction problems can be obtained by evaluating the integrals (5.16) and (5.17), i.e.

$$\psi^p(\rho;\phi) = \int_{-j\infty}^{j\infty} -\frac{H_\alpha^{(2)}(kr)}{4\sin\alpha\pi} J_\alpha(k\rho)\cos\alpha(\pi-\phi)\frac{(\pm)\nu^{-\alpha}\sin\alpha\pi\ \mathrm{osi}\alpha\theta}{f_{o,o}^p(\alpha,a,b,\chi)}\,d\alpha$$

$$+\int_{-j\infty}^{j\infty} -\frac{H_\alpha^{(2)}(kr)}{4\sin\alpha\pi}\sum_{m=1}^{\infty} J_{\alpha+2m}(\nu k\rho)$$

$$\cos\left(\left[\alpha+2m\right]\left[\pi-\phi\right]\right)\frac{(-)\ \nu^{\alpha+2m}}{f_{m,o}^p(\alpha,a,b,\chi)}$$

$$\sum_{n=1}^{m} B_{m-n}^p(\alpha)\ F_n(\alpha+2m-2n,\nu)\ f_{m,n}^p(\alpha,a,b,\chi)\,d\alpha,$$

$$|\pi-\phi| < \pi-\chi \qquad (5.21)$$

$$\psi^p(\rho;\phi) = \int_{-j\infty}^{j\infty} -\frac{H_\alpha^{(2)}(kr)}{4\sin\alpha\pi} J_\alpha(k\rho)\cos\alpha\phi\frac{(\pm)(a-b)\ \sin2\alpha(\pi-\chi)\ \mathrm{osi}\alpha\theta}{2\ f_{o,o}^p(\alpha,a,b,\chi)}\,d\alpha$$

$$+\int_{-j\infty}^{j\infty} -\frac{H_\alpha^{(2)}(kr)}{4\sin\alpha\pi}\sum_{m=o}^{\infty} J_{\alpha+2m}(k\rho)$$

$$\cos(\alpha+2m)\phi\sum_{n=o}^{m} B_{m-n}^p(\alpha)$$

$$F_n(\alpha+2m-2n,\nu)\ g_{m,n}^p(\alpha,a,b,\chi)\,d\alpha, \quad |\phi| < \chi \qquad (5.22)$$

However, it would be a formidable task to attempt to evaluate the residue series, even with the aid of computer-aided symbol manipulation facilities (cf. Decken 1983).

Note that close examination of (5.21) reveals that:

(i) for m = 0, the poles are the zeros of $f^{p}_{o,o}$,

(ii) for m = 1, the highest order poles are the zeros of $f^{p}_{1,o} \cdot f^{p}_{o,o}$,

(iii) for m = m_o, the highest order poles are the zeros of $\prod_{m=o}^{m_o} f^{p}_{m,o}$

Similarly, close examination of (5.22) reveals that the highest order poles of the m_o term coincide with the zeros of $\sin(\alpha\pi) \prod_{m=o}^{m_o} f^{p}_{m,o}$. It is clear from (5.21) and (5.22) that these poles determine the orders of the Bessel and Hankel functions in the resultant residue series, and hence the order of the singularities at the apex of the wedge. The fact that the singularities at the apex are completely determined by the values of α at these poles is made even more obvious when the Hankel functions in (5.21) and (5.22) are replaced by their asymptotic forms for $r \to \infty$ (1.32). They then reduce to the form for an incident plane wave, when appropriately normalised.

Rearranging (5.10), one sets,

$$f^{p}_{m,o}(\alpha,a,b,\chi) = \left[a\ \mathrm{osi}(\left[\alpha+2m\right]\left[\pi-\chi\right])\ \mathrm{iso}(\left[\alpha+2m\right]\chi) + b\ \mathrm{iso}(\left[\alpha+2m\right]\left[\pi-\chi\right])\right.$$

$$\left.\mathrm{osi}(\left[\alpha+2m\right]\chi)\right] \qquad (5.23)$$

It must also be emphasised that (5.23) is a more general form of the edge conditions than the forms derived by Meixner (1972) and Andersen and Solodoukhov (1978). Consider the case of uniform boundary conditions (cf. Section 1.3.1) where a = b = 1, then $f^{p}_{m,o}$ becomes

$$f^{p}_{m,o}(\alpha,a,b,\chi) = \mathrm{osi}(\left[\alpha+2m\right]\left[\pi-\chi\right])\ \mathrm{iso}(\left[\alpha+2m\right]\chi) + \mathrm{iso}(\left[\alpha+2m\right]\left[\pi-\chi\right])$$

$$\mathrm{osi}(\left[\alpha+2m\right]\chi) = \sin(\alpha+2m)\pi \qquad (5.24)$$

It is obvious from (5.24) that the zeros of $f^{p}_{m,o}$ are $\alpha = 0,1,2, \ldots .$ (for $m > 0$, $\alpha > 0$).

Two important observations can be drawn from the above results for uniform boundary conditions.

(i) The field at the apex is regular, and the wave function can be expanded by Bessel functions of integer orders.

(ii) The m = 0 term in (5.21) has poles at $\alpha = 0,1,2, \ldots$ The m = 1 term has poles at α^2, $\alpha(\alpha-1)$, $\alpha(\alpha-2)$, . . ., $\alpha(\alpha-n)$, . . . , $(\alpha-1)^2$ $(\alpha-1)(\alpha-2)$, . . ., $(\alpha-1)(\alpha-n)$, . . ., $(\alpha-2)^2$, . . . $(\alpha-2)(\alpha-n)$, . . . , $(\alpha-n)^2$, . . . The m = 2 term has poles at α^3, $\alpha^2(\alpha-1)$, $\alpha^2(\alpha-2)$, . . ., $\alpha(\alpha-1)^2$, $\alpha(\alpha-1)(\alpha-2)$, . . . , $\alpha(\alpha-2)^2$, . . ., $(\alpha-1)^3$, . . . plus other double poles.

The m = 3 term has quadruple, triple and double poles, ... etc. To evaluate the residue of a function $g(\alpha)$ with poles of, say, $(\alpha-p)^m$ $(\alpha-q)^n$, one first factorises the function $g(\alpha)$ such that:

$$g(\alpha) = \sum_{\ell=1}^{m} g_{1\ell}(\alpha) + \sum_{\ell=1}^{n} g_{2\ell}(\alpha)$$

The function $g_{i\ell}^{(\alpha)}$, i = 1, 2 has an ℓth order pole of $(\alpha-s)$, where s = p when i = 1 and s = q when i = 2. Then the residues of $g(\alpha)$ can be determined by the formula:

$$2\pi j \frac{1}{\ell-1} \frac{d^{\ell-1}}{d\alpha^{\ell-1}} \left[(\alpha-s)^{\ell} g_{i\ell}(\alpha)\right]_{\alpha=s} \qquad (5.25)$$

It should now be clear that it would be virtually impossible to evaluate the residue series implicit in (5.21) and (5.22). A serious difficulty arises from the need for differentiating the Bessel and Hankel functions with respect to their orders. Furthermore, when the Bessel functions are differentiated with respect to their orders, their asymptotic behaviour, as $\rho \to 0$ is significantly altered. Therefore, the contribution to the edge field comes not only from the m = 0 term, but also from terms which m > 0.

The most significant aspect of the analysis presented in this chapter, however, is not the possibility of a general solution to the penetrable wedge diffraction problem. The essential point is that it allows one to determine the order of singularities at the apex of the wedge. Furthermore, a complete solution of $f_{m,o}^{p}(\alpha,a,b,\chi) = 0$ enables one to choose the proper eigenfunctions $\{J_{\alpha+2m}(\cdot)\cos([\alpha+2m][\cdot])\}$ when constructing series solutions for scattering problems involving penetrable edges. This is particularly important with regard to numerical solutions of scattering problems. It is mentioned briefly in the next section, while Chapter 6 is entirely devoted to the exploration of computational consequences.

5.8 COMPUTATIONAL ADVANTAGE ARISING FROM THE KNOWLEDGE OF EDGE BEHAVIOUR

It is now well appreciated (cf. Bates and Wall 1977 and many references quoted therein) that the overall efficiency of numerical evaluations of diffracted fields are improved markedly when the functions used to represent quantities that is initially unknown accord with the physical-cum-mathematical requirements of the underlying theory. The point is that the number of basis functions needed to represent the field to a particular accuracy is least when the chosen basis functions are the theoretically correct ones. That this is very significant is readily appreciated when one remembers that the amount of computer time required is usually proportional to the cube of the number of basis functions. The results presented in this chapter should therefore allow numerical solutions of diffraction problems involving penetrable bodies with edges to be evaluated more efficiently and accurately than has been possible heretofore.

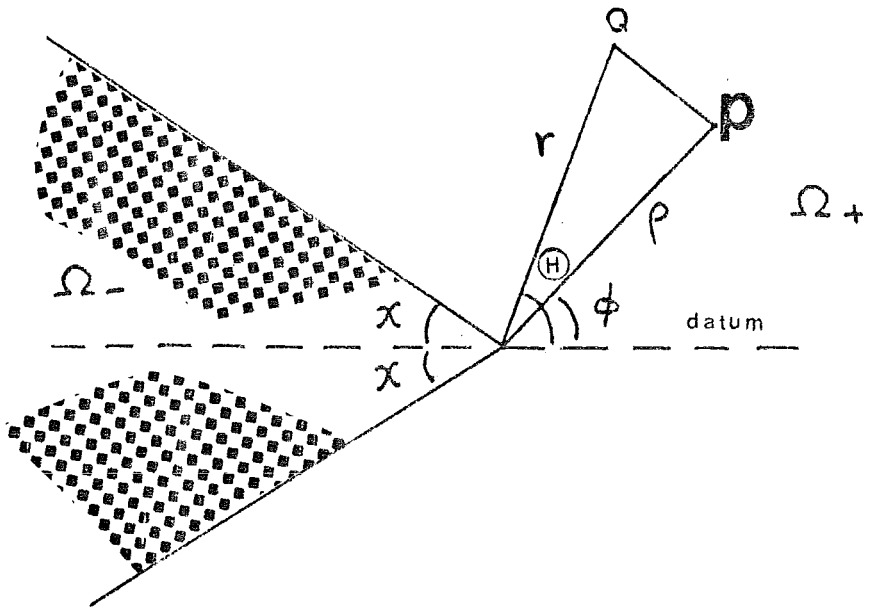

FIGURE 5.1 The geometry of an infinite penetrable wedge used by Bates (1980a). The region inside the wedge is denoted by Ω_- while the region outside the wedge is denoted by Ω_+. The wedge surfaces coincide with $\phi = \pi-\chi$ and $\pi + \chi$. An arbitrary point P in space has the coordinate $(\rho;\phi)$. The wedge is excited by a line source at $Q(r;\theta)$.

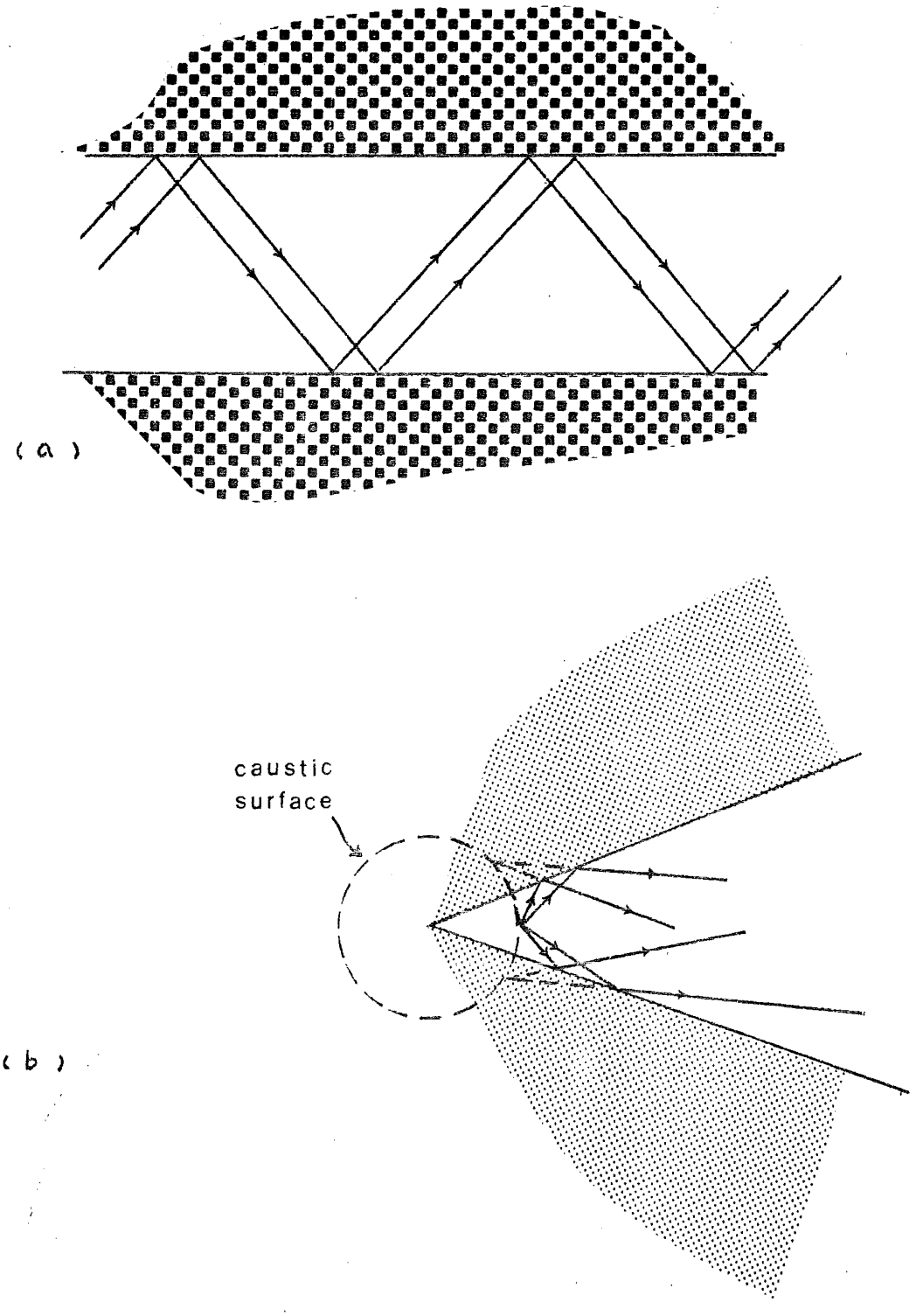

FIGURE 5.2 Modal ray configuration suggested by Maurer and Felsen (1967).
(a) Conventional, periodic ray in a rectangular waveguide.
(b) Nonperiodic ray in a conducting wedge.

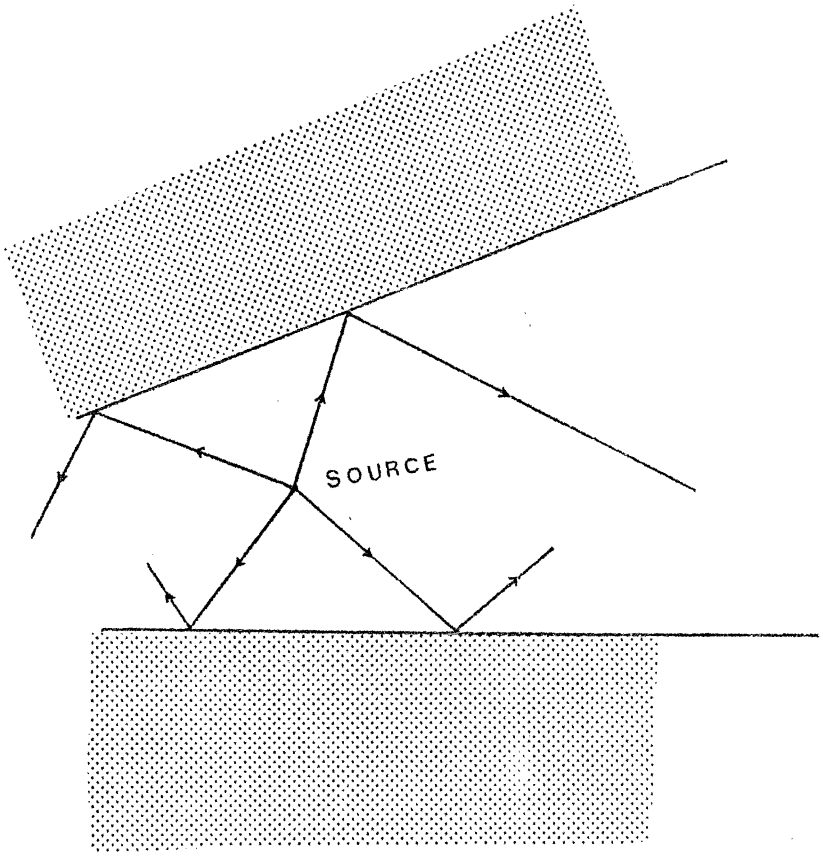

FIGURE 5.3 Formation of a propagation mode.

CHAPTER SIX

SCATTERING BY A PENETRABLE WEDGE-CYLINDER

6.1 INTRODUCTION

It has been mentioned in Section 5.7 and reiterated in Section 5.8 that the main significance of the theory introduced in Chapter 5 is that it leads to a better understanding of the field behaviour close to the apex. Furthermore, as is pointed out in Section 5.8, the computational efficiency of numerical solutions of diffraction by penetrable bodies with edges can be greatly improved by using this knowledge of the edge behaviour.

In this chapter, computational examples are presented to support the argument given in Section 5.8. The problem of scattering by a dielectric wedge-cylinder is solved using the null-field method based on the 'proper' field representation developed in Section 5.7. For comparison, the same problem is solved using improper field representations. This emphasises how the use of proper representations improves computational efficiency. This same point is reinforced by a final example, which is based on an extended formulation due to Morita (1979) - see also Wong (1972) and Bates (1980b).

Furthermore, when the size of the wedge cylinder is large enough, the scattered field approaches that scattered by an infinite wedge. This is especially so in the back-scattered region. Comparisons between the back-scattered field calculated for wedge-cylinders and infinite wedges are made in Chapter 8.

6.2 SCATTERING BY WEDGE-CYLINDER

6.2.1 Preliminaries

Fig. 6.1 depicts a cross-section of a wedge-cylinder. Define

$$\begin{aligned} \Omega &= \Omega_- U \Omega_+ U C \\ \Omega_- &= \Omega_{--} U \Omega_{-+} \\ C &= C_1 U C_2 \\ C_2 &= C_{2-} U C_{2+} \end{aligned} \qquad (6.1)$$

where

Ω_+ = all areas outside wedge-cylinder,

Ω_- = all areas inside wedge-cylinder,

Ω_{--} = $0 \leq r \leq a, \quad 0 \leq \theta \leq 2\pi$

C_{-+} = all areas $\varepsilon\ \Omega_-, \notin \Omega_{--}$,

C_1 = the curve from A to B,

C_{2+} = the straight line from B to 0_1,

C_{2-} = the straight line from 0_1 to A.

The null-field equation (1.95a) is

$$\int_C \left[\Psi_- \, \partial g/\partial\hat{n} - g\partial\Psi_-/\partial\hat{n}\right] dC = -\Psi_{inc} \tag{1.95a}$$

The field $\Psi(\rho)$, $P\varepsilon\Omega_-$ can be expanded (cf. Section 1.4.2) as

$$\Psi_- = \sum_{n=o}^{\infty} A_n \, J_{\mu_n}(\nu k\rho) \begin{matrix}\cos \\ \sin\end{matrix} \mu_n\phi \tag{6.2a}$$

and

$$\Psi_- = \sum_{n=o}^{\infty} A_n \sum_{\ell=-\infty}^{\infty} J_{\mu_n+\ell}(\nu kb) \, J_\ell(\nu ka) \begin{matrix}\cos \\ \sin\end{matrix} \ell(\pi-\theta) \tag{6.2b}$$

with the aid of the Addition theorem for Bessel functions (cf. (1.35)).

Furthermore, the incident plane wave Ψ_{inc} can be written as (cf. Section 1.4.2)

$$\Psi_{inc} = \sum_{m=-\infty}^{\infty} \exp(jm(\phi-\theta)) \, J_m(k\rho) \tag{6.3}$$

Substituting (6.3) and (6.2) into (1.95a), the latter becomes (c.f. also Fig. 5.1)

$$\sum_{n=o}^{\infty} A_n(I_{11} + I_{12} + I_{21} + I_{22}) = 4j(j)^m \begin{matrix}\cos \\ \sin\end{matrix} (m\theta) \tag{6.4}$$

where

$$I_{11}(m,n) = \int_{-\beta}^{\beta} aH_m^{(2)}(kr) \cos m\theta \, \partial\left[J_{\mu_n}(\nu k\rho)\cos(\mu_n\phi)\right]/\partial r \, d\theta$$

$$= \nu ka/2 \, H_m^{(2)}(ka) \sum_{\ell=-\infty}^{\infty} (-1)^\ell J_{\mu_n+\ell}(\nu kb)$$

$$\left[J_{\ell-1}(\nu ka) - J_{\ell+1}(\nu ka)\right] \left[\frac{\sin(\ell-m)\beta}{\ell-m} + \frac{\sin(\ell+m)\beta}{\ell+m}\right] \tag{6.5}$$

$$I_{12}(m,n) = \int_{-\beta}^{\beta} -aJ_{\mu_n}(\nu k\rho)\cos\mu_n\phi\ \partial\left[H_m^{(2)}(kr)\cos(m\phi)\right]/\partial r\ d\theta$$

$$= -ka/2\left[H_{m-1}^{(2)}(ka) - H_{m+1}^{(2)}(ka)\right] \sum_{\ell=-\infty}^{\infty} (-1)^{\ell} J_{\mu_n+\ell}(\nu kb)\ J_{\ell}(\nu ka)$$

$$\left[\frac{\sin(\ell-m)\beta}{\ell-m} + \frac{\sin(\ell+m)\beta}{\ell+m}\right] \qquad (6.6)$$

$$I_{21}(m,n) = 2 \int_{o}^{d} \rho^{-1} H_m^{(2)}(kr)\cos m\theta\ \partial\left[J_{\mu_n}(\nu k\rho)\cos(\mu_n\phi)\right]/\partial\phi\ d\rho \Big|_{\phi=\chi}$$

$$= -2\mu_n \sin(\mu_n\chi)(-1)^m \sum_{\ell=-\infty}^{\infty} H_{m+\ell}^{(2)}(kb)\cos(\ell\chi)\ I_o(n,\ell) \qquad (6.7)$$

$$I_{22}(m,n) = -2 \int_{o}^{d} J_{\mu_n}(\nu k\rho)\cos(\mu_n\phi)\ \rho^{-1}\partial\left[H_m^{(2)}(kr)\cos(m\theta)\right]/\partial\phi\ dp \Big|_{\phi=\chi}$$

$$= 2(-1)^m \cos(\mu_n\chi) \sum_{\ell=-\infty}^{\infty} \ell\sin(\ell\chi)\ H_{m+\ell}^{(2)}(kb)\ I_o(n,\ell) \qquad (6.8)$$

where

$$I_o(n,\ell) = \int_{o}^{d} \rho^{-1} J_{\mu_n}(\nu k\rho)\ J_{\ell}(k\rho)\ d\rho \qquad (6.9)$$

and the choice of μ_n are determined by the proper singularities discussed in Chapter 5.

The far scattered field can be expressed (cf. Section 1.4.2) by

$$\Psi_{sc} = \sum_{m=o}^{\infty} B_m\ \varepsilon_m(-j)^m \cos m\phi\ H_m^{(2)}(k\rho) \qquad (6.10)$$

where the far field scattering coefficients B_m are given by LHS(6.4) with all $H_m^{(2)}(\cdot)$ replaced by $J_m(\cdot)$. Using the asymptotic expansion of Hankel functions (1.32), it is seen that (6.10) can be written as

$$\Psi_{sc} = (2/\pi k\rho)^{\frac{1}{2}} \exp(-jk\rho)\ \exp(j\pi/4) \sum_{m=o}^{\infty} \varepsilon_m\ B_m \cos m\phi$$

$$= (2/\pi k\rho)^{\frac{1}{2}} \exp(-jk\rho)\ \exp(j\pi/4)\ \Psi_o(\phi) \qquad (6.11)$$

where

$$\Psi_o(\phi) = \sum_{m=o}^{\infty} \varepsilon_m\ B_m \cos m\phi \qquad (6.12)$$

The scattering cross-section is defined (cf. Bowman et al. 1969, Section 1.2 as

$$\sigma(\phi) = 4/k\left|\Psi_o(\phi)\right|^2 = 4/k\left|\sum_{m=o}^{\infty} \varepsilon_m\ B_m \cos m\phi\right|^2 \qquad (6.13)$$

and the forward-scattering cross-section (cf. Bowman et al. 1969, Section 1.2) is

$$\sigma_T = 1/2\pi \int_0^{2\pi} \sigma(\phi)\,d\phi = 4/k \sum_{m=0}^{\infty} \varepsilon_m |B_m|^2 \qquad (6.14)$$

Bowman et al. (1969, Section 1.2) indicate that the forward scattering cross-section must equal $-4/k$ Real $(\Psi_o(\Theta-\pi))$. Therefore

$$4/k \sum_{m=0}^{\infty} \varepsilon_m |B_m|^2 = -4/k \text{ Real } (\Psi_o(\Theta-\pi)) \qquad (6.15)$$
$$= -4/k \text{ Real } \left(\sum_{m=0}^{\infty} \varepsilon_m B_m (-1)^m \cos m\Theta \right)$$

And finally, the error ε, in satisfying the forward-scattering theorem is given by

$$\varepsilon = \sum_{m=0}^{\infty} \varepsilon_m \left[|B_m|^2 + (-1)^m \text{ Real } (B_m) \right] \qquad (6.16)$$

which can therefore be used as an effective check on the accuracy of the numerical solution.

6.2.2 E-Polarised Incident Wave

6.2.2.1 Preliminaries

As already mentioned in Section 5.7, the field at the apex of a penetrable wedge is regular when the incident wave is E-Polarised. Consequently, the choice of μ_u in (6.2) is (cf. Section 5.7)

$$\mu_u = n \qquad (6.17)$$

To illustrate the improvement in computational efficiency associated with using the 'proper' eigenvalues, solutions are presented in 6.2.2.2 for both $\mu_n = n$ and $\mu_n = n\,\pi/2(\pi-\chi)$. It should be noted that the latter are the proper eigenvalues for a perfectly conducting wedge.

6.2.2.2 Computational Results

When the series in (6.2) is truncated to $n \in [0,N]$ and the number of equations in (6.4) is truncated to $m \in [0,N]$, the A_n can be calculated using an appropriate numerical scheme (cf. Section 1.5.1). Table 6.1 shows the convergence of the magnitude of the surface field with respect to N. The parameters used are: $\chi=20^o$, $\nu=1.5$, $a=0.2\lambda$ and $\Theta=\pi$ and the accuracy used in numerical integration of I_{21} and I_{22} is 0.0001. It is seen that the surface field converges to better than 1% accuracy when N = 9, Fig. 6.2 shows the

surface field plots for various values of N, while Fig. 6.3 gives the convergence of the surface field expansion coefficient A_o and for field scattering coefficient B_o. The error ε in satisfying the forward-scattering theorem (6.16) is plotted in Fig. 6.4. From the rapid convergence of Figs 6.2 and 6.3 and the (extremely) small error (ε) in Fig. 6.4, it seems clear that the wedge-cylinder diffraction problem has been effectively solved, and to an accuracy adequate for most practical purposes.

On the other hand, when the values of μ_n chosen are $\mu_n = n\pi/2(\pi-\chi)$ = 0.65n, with all other parameters remaining unchanged, the calculated surface field exhibits the effects of significant numerical instability. Fig. 6.5 shows that, although the surface field does converge on the smoother part (i.e. C_1) of the wedge-cylinder, it oscillates and fails to settle down near the apex. This clearly indicates the importance of incorporating the correct 'singular behaviour' into the expansion of the edge field when attempting to obtain numerical solutions. Further evidence of numerical inefficiency when improper edge behaviour is used is presented in Figs 6.6 and 6.7. The convergence of the expansion coefficients thus calculated (Fig. 6.6) is evidently inferior to that of Fig. 6.2. Furthermore, the residue (error) ε plotted in Fig. 6.7 is always at least an order larger than those plotted in Fig. 6.4.

TABLE 6.1 Convergence of Surface Field (Magnitude). The Parameters of the Wedge-Cylinder are $a=0.2\lambda$, $\nu=1.5$, $\theta=\pi$, $\chi=20^{\circ}$ and $\mu_n = n$.

	(rad.)	N = 8	N = 9	% Deviation
edge field	0.0000E+0	0.1904E+1	0.1892E+1	0.63
	0.3491E+0	0.1092E+1	0.1094E+1	0.18
	0.6981E+0	0.1058E+1	0.1061E+1	0.28
	0.1047E+1	0.8054E+0	0.8092E+0	0.47
	0.1369E+1	0.8106E+0	0.8118E+0	0.15
	0.1745E+1	0.1061E+1	0.1062E+1	0.09
	0.2094E+1	0.1373E+1	0.1376E+1	0.22
	0.2443E+1	0.1589E+1	0.1592E+1	0.19
	0.2792E+1	0.1697E+1	0.1701E+1	0.23
	0.3142E+1	0.1728E+1	0.1732E+1	0.23

6.2.2.3 Morita's Method

Kirchoff's (cf. Section 1.5.5.1) principle states that the scattered field is completely determined by the total field (and its derivatives) on the scattering surface. The surface integral equation (1.95b)

$$\Psi_{sc}(P) = \int_C -\left[\partial\Psi_-/\partial\hat{n}\; g - \Psi_-\; \partial g/\partial\hat{n}\right]\, dC,\; P \in \Omega_+ \qquad (1.95b)$$

is a good example of the above statement. It is, therefore, appropriate to evaluate the surface field and its normal derivative viz, say, the null-field equation (1.95a)

$$-\int_C \left[\partial\Psi_-/\partial\hat{n}\; g - \Psi_-\; \partial g/\partial\hat{n}\right]\, dC = -\Psi_{inc},\; P \in \Omega_- \qquad (1.95a)$$

In principle, at least, there is no other restriction imposed on Ψ_-. i.e. It can be expanded in any eigenfunctions which are convenient. Then its normal derivative $\partial\Psi_-/\partial\hat{n}$ is evaluated. However, as is shown in Section 6.2.2.2, when Ψ_- is not expressed as an expansion which is physically correct, $\partial\Psi/\partial\hat{n}$ significantly misrepresents the actual surface behaviour of the field. The resulting solution (if one is able to obtain it) is inferior and the computations are inefficient. It has, therefore, been the aim of some authors (Wong 1972, Morita 1979, Bates 1980b to circumvent this difficulty, especially in those cases for which the correct representation for Ψ_- is not known.

Morita (1979) suggests (also see Wong 1972, Bates 1980b a combination of (1.95a) and (1.95c) of the null-field equations, i.e.

$$j/4 \int_C \left[\partial\Psi_-/\partial\hat{n}\; g_f - \Psi_-\; \partial g_f/\partial\hat{n}\right]\, dC = -\Psi_{inc}(P),\; P \in \Omega_- \qquad (1.95a)$$

$$j/4 \int_C \left[\partial\Psi_-/\partial\hat{n}\; g_d - \Psi_-\; \partial g_d/\partial\hat{n}\right]\, dC = 0,\; P \in \Omega_+ \qquad (1.95c)$$

where

$g_f = H_o^{(2)}(KR)$, $g_d = H_o^{(2)}(\nu kR)$ and $R = \left[\underline{P} - \underline{Q}\right]$, $\underline{P}$, $\underline{Q}$ and position vectors of field and source points respectively. The two equations then enable one to expand Ψ_- and $\partial\Psi_-/\partial\hat{n}$ in two independent series

$$\Psi_- = \sum_{n=o}^{\infty} A_n\, J_n\,(\nu kp) \begin{matrix}\cos\\ \sin\end{matrix} n\phi \qquad (6.18a)$$

$$\partial\Psi_{-}/\partial n = \sum_{n=o}^{\infty} B_n \, k \, J_n(\nu k\rho) \begin{matrix}\cos \\ \sin\end{matrix} n\phi \tag{6.18b}$$

Substituting (6.18) into (1.95a) and (1.95c) and manipulating in the normal manner enables one to obtain the following matrix equations:

$$C_{11} \, B + C_{12} \, A = D \tag{6.19a}$$

$$C_{21} \, B + C_{22} \, A = 0 \tag{6.19b}$$

where C_{11}, C_{12}, C_{21}, C_{22} and D have elements $c_{11}(m,n)$, $c_{12}(m,n)$, $c_{21}(m,n)$ $c_{22}(m,n)$, $d(m)$ respectively.

$$c_{11}(m,n) = Ka \, H_m^{(2)}(Ka) \sum_{\ell=-\infty}^{\infty} (-1)^{\ell}$$

$$J_{n+\ell}(\nu kb) \, J_{\ell}(\nu ka) \left[\frac{\sin(\ell-m)\beta}{\ell-m} + \frac{\sin(\ell+m)\beta}{\ell+m} \right]$$

$$+ 2 \int_o^1 H_m^{(2)'}(kr) \, J_n(\nu kr)(kd) \cos(m\theta) \cos(n\phi) \, dq \Big|_{\phi=\chi} \tag{6.20a}$$

$$c_{12}(m,n) = -ka \, H_m^{(2)'}(ka) \sum_{\ell=-\infty}^{\infty} (-1)^{\ell} \, J_{n+\ell}(\nu kb)$$

$$J_{\ell}(\nu ka) \left[\frac{\sin(\ell-m)\beta}{\ell-m} + \frac{\sin(\ell+m)\beta}{\ell+m} \right]$$

$$- 2 \int_o^1 J_n(\nu k\rho) \cos(n\phi) \, \rho^{-1} \left[H_m^{(2)'}(kr) \right.$$

$$k \cos(m\theta) \, \partial r/\partial\phi - H_m^{(2)}(kr)$$

$$\left. m \sin(m\theta) \, \partial\theta/\partial\phi \right] (d) \, dq \Big|_{\phi=\chi} \tag{6.20b}$$

$$c_{21}(m,n) = ka \, J_m(ka) \sum_{\ell=-\infty}^{\infty} (-1)^{\ell} J_{n+\ell}(\nu kb)$$

$$J_{\ell}(\nu ka) \left[\frac{\sin(\ell-m)\beta}{\ell-m} + \frac{\sin(\ell+m)\beta}{\ell+m} \right]$$

$$+ 2 \int_o^1 J_m(\nu kr) J_n(\nu k\rho)(kd) \cos(m\theta) \cos(m\phi) \, dq \Big|_{\phi=\chi} \tag{6.20c}$$

$$c_{22}(m,n) = -\nu ka\, J'_m(\nu ka) \sum_{\ell=-\infty}^{\infty} (-1)^{\ell}$$

$$J_{n+\ell}(\nu kb) \left[\frac{\sin(\ell-m)\beta}{\ell-m} + \frac{\sin(\ell+m)\beta}{\ell+m}\right]$$

$$- 2 \int_0^1 J_n(\nu k\rho) \cos(n\phi)\, \rho^{-1} \left[J'_m(\nu kr)\, \nu k \cos(m\theta)\, \partial r/\partial\phi - J_m(\nu kr)\right.$$

$$\left. m \sin(m\theta)\, \partial\theta/\partial\phi\right] (d)\, dq \qquad \phi=\chi \tag{6.20d}$$

$$q = \rho/d \tag{6.20e}$$

$$r^2 = \rho^2 + b^2 - 2\rho b \cos(\phi) \tag{6.20f}$$

$$\partial r/\partial\phi = r^{-1} \rho b \cos(\phi) \tag{6.20g}$$

$$\partial\theta/\partial\phi = \left[\sin(\tau-\theta)\, \partial r/\partial\phi - \rho \cos\phi\right]\left[r \cos(\pi-\theta)\right]^{-1} \tag{6.20h}$$

and

$$d(m) = 4j(j)^m \cos(m\theta) \tag{6.20i}$$

Multiplying (6.19b) by the inverse of C_{21} (i.e. C_{21}^{-1}) transforms (6.19b) into

$$C_{21}^{-1} C_{21} B + C_{21}^{-1} C_{22} A = B + C_{21}^{-1} C_{22} A = 0$$

$$\text{i.e.} \quad B = - C_{21}^{-1} C_{22} A \tag{6.21}$$

Substituting (6.21) into (6.19a) gives

$$C_{11}(-C_{21}^{-1} C_{22} A) + C_{12} A = D$$

$$\text{i.e.} \quad (C_{12} - C_{11} C_{21}^{-1} C_{22})\, A = D \tag{6.22}$$

The expansion coefficients A_n of the surface field can therefore be calculated from (6.22). The surface field thus calculated is plotted in Fig. 6.8.

6.2.2.4 Advantage of Using Proper Field Representation

Table 6.2 compares condition numbers (defined in Section 1.5.1), CPU times (of a Prime 750 computer) and memory requirement for different surface field representations.

TABLE 6.2 Comparison of efficiencies between three methods: (i) integer μ_n, (ii) fractional μ_n and (iii) Morita's method. The parameters of the wedge-cylinder are $a=0.2\lambda$, $\chi=20$, $\nu=1.5$ and $\theta=180^{\circ}$. The computer used is a Prime 750.

Parameters \ μ_n	Integer	Fractional	Morita's Method
Condition number	11870	150000	378000
CPU time (sec.)	116	158	209
Memory requirement (normalised)	1	1	4

It is clear from Table 6.2 that more CPU time and memory space are required to arrive at an acceptable far field solution for an 'improperly' represented surface field and its normal derivative. It is also worth emphasising that no numerical convergence is manifest for this solution close to the apex of the wedge-cylinder. When the proper representation is used, the edge field converges rapidly (cf. Fig. 6.2). Furthermore, use of the proper representation results in significantly greater numerical efficiency (cf. Table 6.2).

The concept of using a physically correct field representation to improve the convergence and stability of numerical calculations, and to reduce computer time and memory storage, is well known (cf. Hunter 1974, Vassallo 1976 and Bates and Wall 1977). This argument is reinforced by the results presented in Section 6.2.2.2. Fig. 6.8, which displays results calculated from Morita's (1979) method, and Fig. 6.2 which relates to straightforward use of a proper edge representation, further emphasises the significance of the theory developed in Chapter 5.

6.2.3 H-Polarised Incident Field

Since integers represent the proper choise of μ_n for E-polarised incident fields in Section 6.2.2, one might argue that the efficiency achieved arises from the fact that Bessel functions of integer orders can be evaluated more easily than those of non-integer order. Furthermore, one might argue that the instability and inefficiency in the 'improper' representation solutions could be due to the routines which have to be invoked to handle the more intricate formulas that are involved. Finally, one might conclude that both representations may well be incorrect, and one solution is better than the other not because of using the proper edge behaviour but because of the way the routines are written.

In order to help quench such doubts, an example is now given for which integers do not represent the proper choice of μ_n. The same parameters as the example given in Section 6.2.2 (i.e. $\chi=20^{\circ}$, $\nu=1.5$, $a=0.2\lambda$, $\Theta=\pi$) are employed, but an H-polarised incident wave is treated. The boundary conditions are

$$\Psi_+(C_+) = \Psi_-(C_-) \tag{6.23}$$

$$\partial\Psi_+(C_+)/\partial\hat{n} = 1/\nu^2\ \partial\Psi_-(C_-)/\partial\hat{n} \tag{6.24}$$

and the null-field equation (1.95a) is

$$\int_C \left[\Psi_-\ \partial g/\partial\hat{n} - g\partial\Psi_-/\partial\hat{n}/\nu^2\right] dC = -\Psi_{inc} \tag{6.25}$$

where the Ψ_- is again given by (6.2).
However, as indicated by (5.23), the μ_n are not integers. The proper choice of each μ_n, calculated from (5.23), is tabulated in Table 6.3.

TABLE 6.3 The first twenty properly chosen μ_n for a wedge-cylinder (ν=1.5, χ=20°) and an H-polarised incident wave.

n	μ_n	n	μ_n
0	0.000	10	4.942
1	0.563	11	5.064
2	1.064	12	5.878
3	1.688	13	6.189
4	2.114	14	6.888
5	2.814	15	7.314
6	3.123	16	7.938
7	3.939	17	8.439
8	4.059	18	9.002
9	4.502	19	9.563

Figs 6.9 and 6.10 show surface fields calculated, for several values of N, when the μ_n are, respectively, properly chosen (cf. Table 9.3) and taken to be given by μ_n=n. The latter choice, while correct for E-polarisation, is incorrect here. It is clear that the surface field calculated from the proper choice of μ_n (Fig. 6.9) converges faster than the surface field calculated with integer μ_n (Fig. 6.10).

6.2.4 Conclusions

Two important conclusions can be drawn from the examples given in this chapter.

(i) The theory developed in Chapter 5, enables one to determine the correct field behaviour near the apex of a penetrable wedge-cylinder of arbitrary angle and refractive index.

(ii) This knowledge of edge behaviour, when incorporated into the formulation of a numerical solution, markedly improves the efficiency and stability of the numerical procedure.

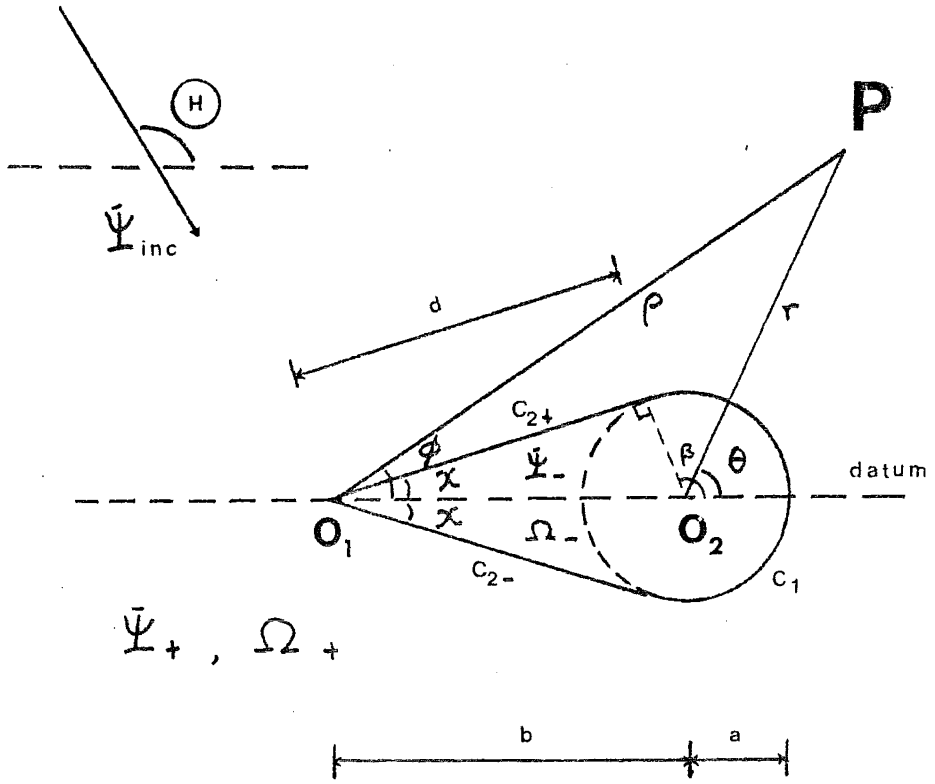

FIGURE 6.1 Geometry of wedge-cylinder with refractive index ν. The right-handed cylindrical coordinate of an arbitrary point P are either $(\rho;\phi)$ or $(r;\theta)$ which have the points O_1 and O_2 respectively as origin. Ψ_- is the total field inside (denoted by Ω_-) while Ψ_+ is the total field outside (denoted by Ω_+).

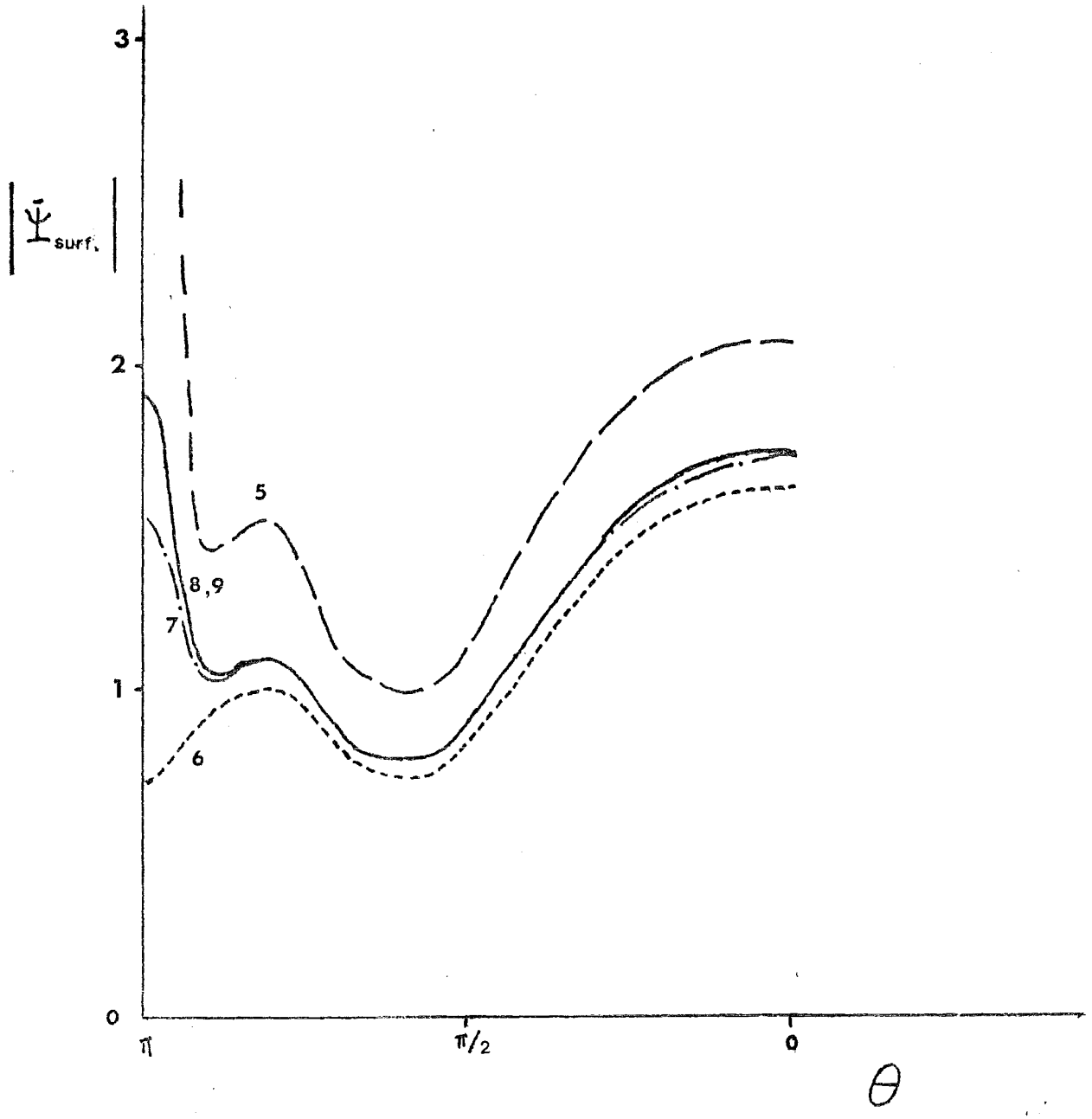

FIGURE 6.2 Plot of surface field magnitudes versus θ (as defined in Fig. 6.1). The variable is N, the number of surface field expansion coefficients used. The parameters of the wedge-cylinder are $\chi = 20^{\circ}$, $a = 0.2\lambda$, $\nu = 1.5$ and $\mu_n = n$. The E-polarised field is incident at an angle $\theta = \pi$.

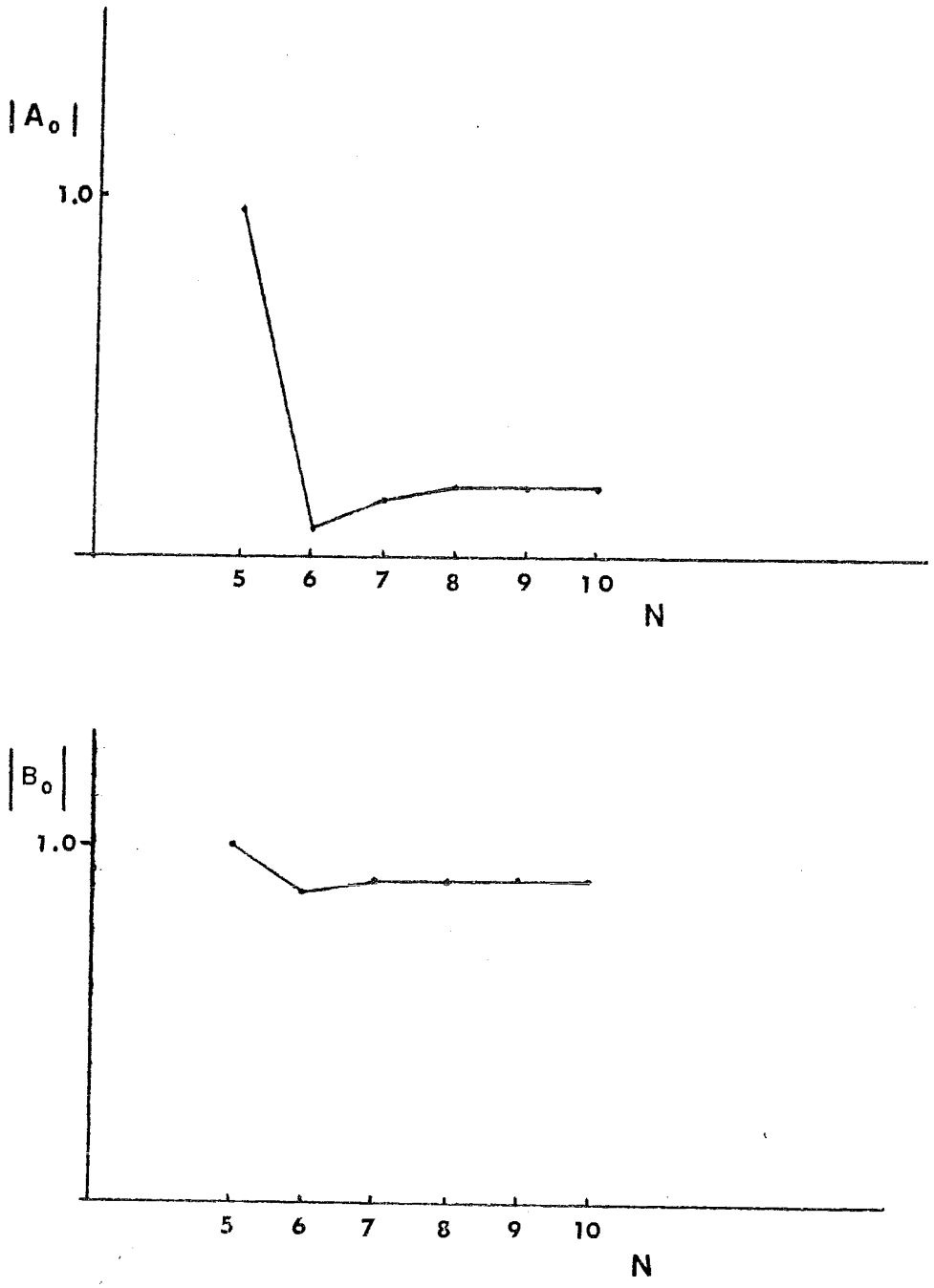

FIGURE 6.3 Plot of A_o, the first surface field expansion coefficient, and B_o, the first far field scattering coefficient, with respect to N, the number of expansion coefficients used. The parameters of the wedge-cylinder are $\chi = 20^o$, $a = 0.2\lambda$, $\nu = 1.5$ and $\mu_n = n$. The E-polarised field is incident at an angle $\Theta = \pi$.

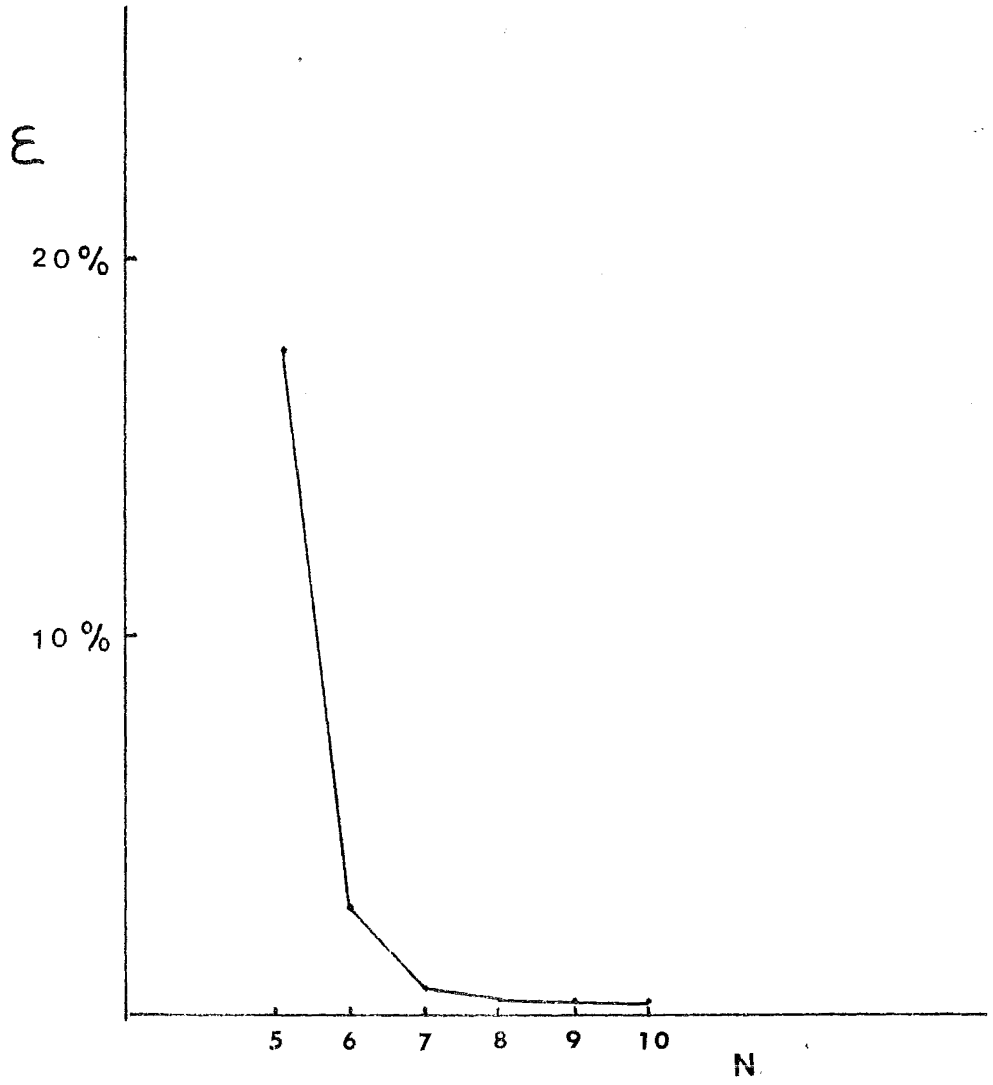

FIGURE 6.4 The error ε in satisfying the forward scattering theorem (6.16) is plotted against N, the number of surface field expansion coefficients used. The parameters of the wedge-cylinder are $\chi = 20^{\circ}$, $a = 0.2\lambda$, $\nu = 1.5$ and $\mu_n = n$. The E-polarised field is incident at an angle $\theta = \pi$.

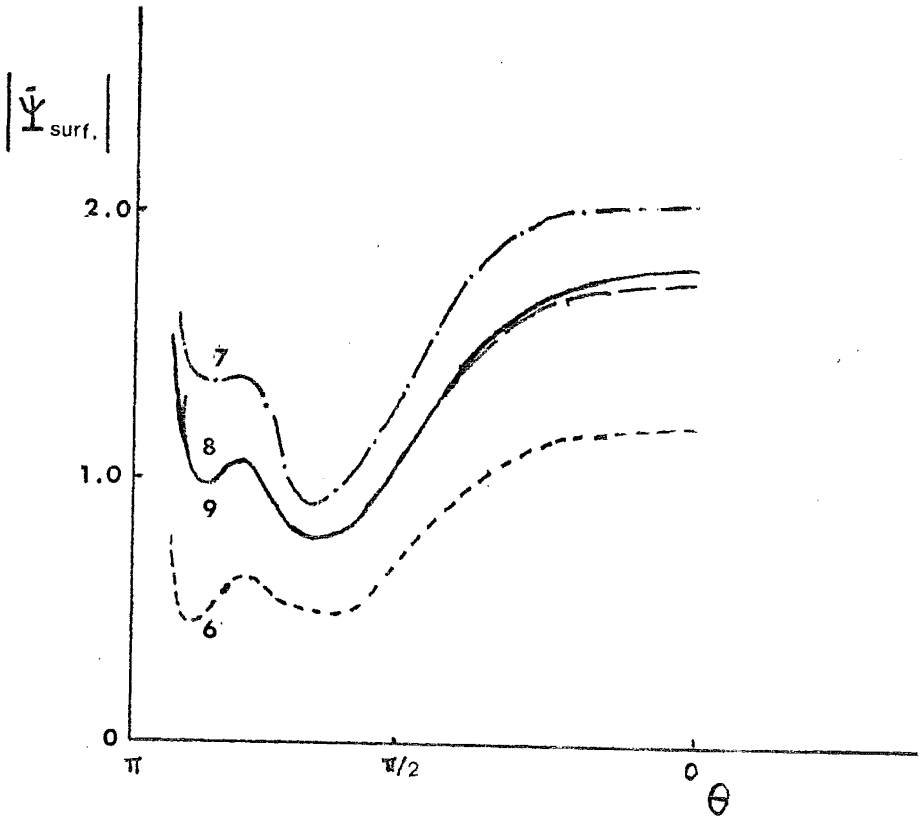

FIGURE 6.5 Plot of surface field magnitudes verses θ (as defined in Fig. 6.1). The variable is N, the number of surface field expansion coefficients used. The parameters of the wedge-cylinder are $\chi = 20^{\circ}$, $a = 0.2\lambda$, $\nu = 1.5$ and $\mu_n = 0.65n$. The E-polarised field is incident at an angle $\theta = \pi$.

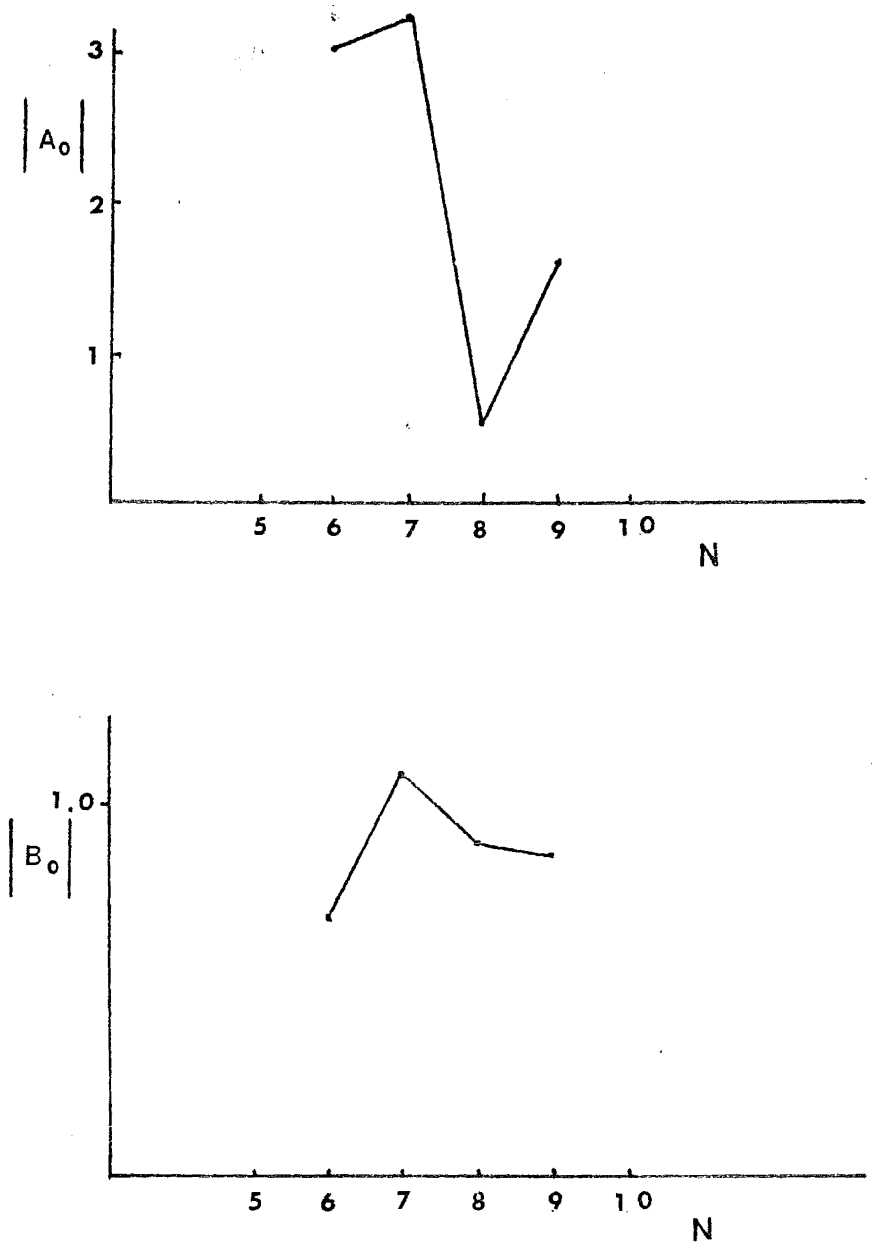

FIGURE 6.6 Plot of A_o, the first surface field expansion coefficient, and B_o, the first far field scattering coefficient, with respect to N, the number of expansion coefficients used. The parameters of the wedge-cylinder are $\chi = 20^o$, $a = 0.2\lambda$, $\nu = 1.5$ and $\mu_n = 0.65n$. The E-polarised field is incident at an angle $\theta = \pi$.

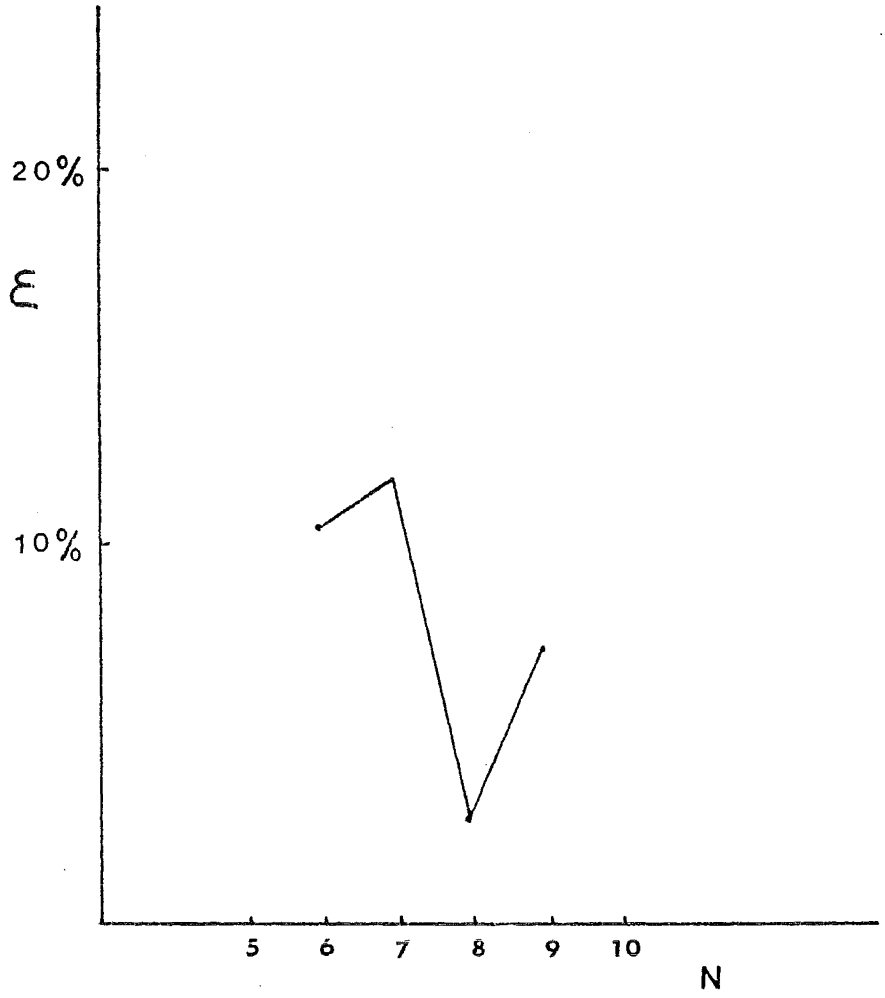

FIGURE 6.7 The error ε in satisfying the forward scattering theorem (6.16) is plotted against N, the number of surface field expansion coefficients used. The parameters of the wedge-cylinder are $\chi = 20^{\circ}$, $a = 0.2\lambda$, $\nu = 1.5$ and $\mu_n = 0.65n$. The E-polarised field is incident at an angle $\theta = \pi$.

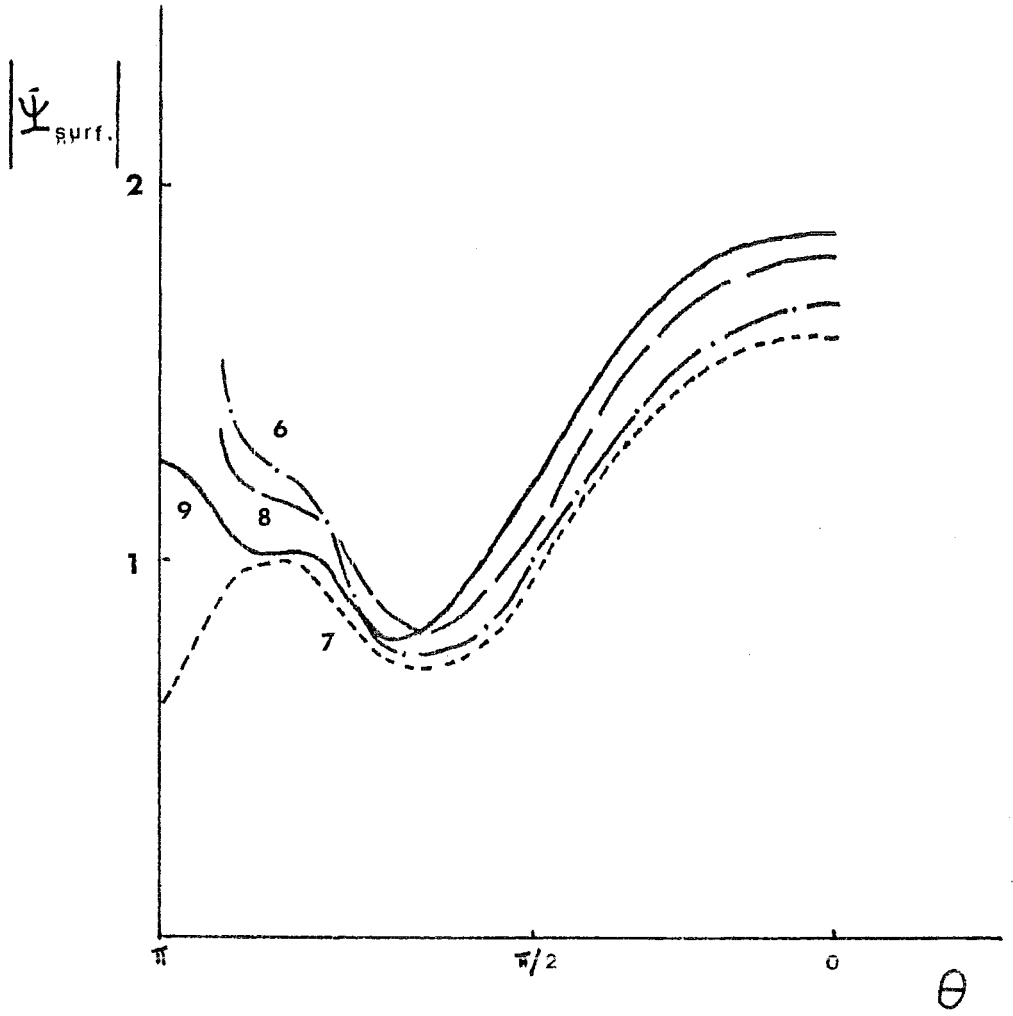

FIGURE 6.8 Plot of surface field magnitudes versus θ (as defined in Fig. 6.1). The variable is N, the number of surface field expansion coefficients used. The parameters of the wedge-cylinder are $\chi = 20^{\circ}$, $a = 0.2\lambda$, $\nu = 1.5$ and $\mu_n = n$. The E-polarised field is incident at an angle $\Theta = \pi$. The field is calculated from the method of Morita (1979).

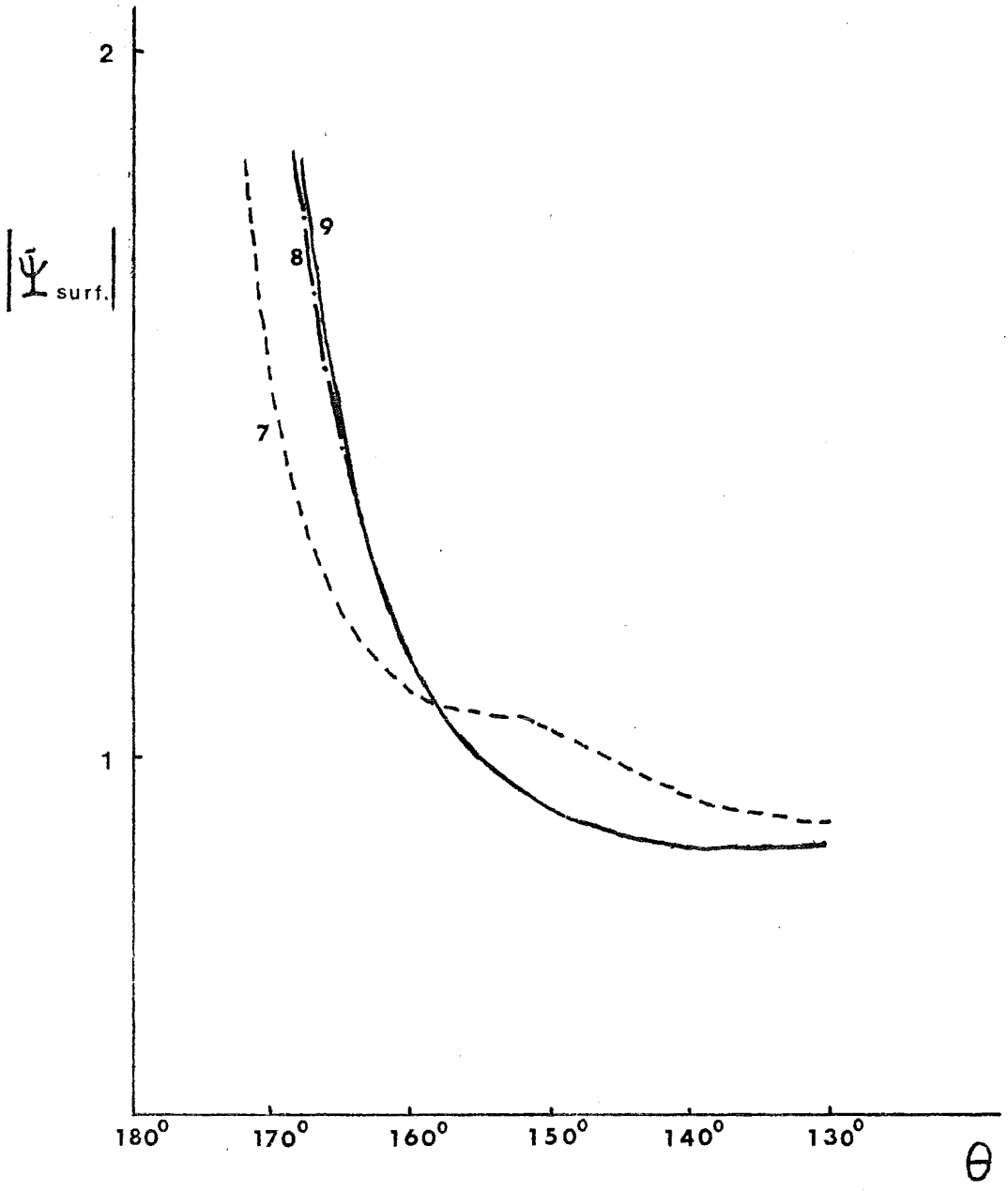

FIGURE 6.9 Plot of surface field magnitudes versus θ (as defined in Fig. 6.1). The variable is N, the number of surface field expansion coefficients used. The parameters of the wedge-cylinder are $\chi = 20^{\circ}$, $a = 0.2\lambda$ and $\nu = 1.5$. The values of μ_n are as given in Table 6.3. The H-polarised field is incident at an angle $\theta = \pi$.

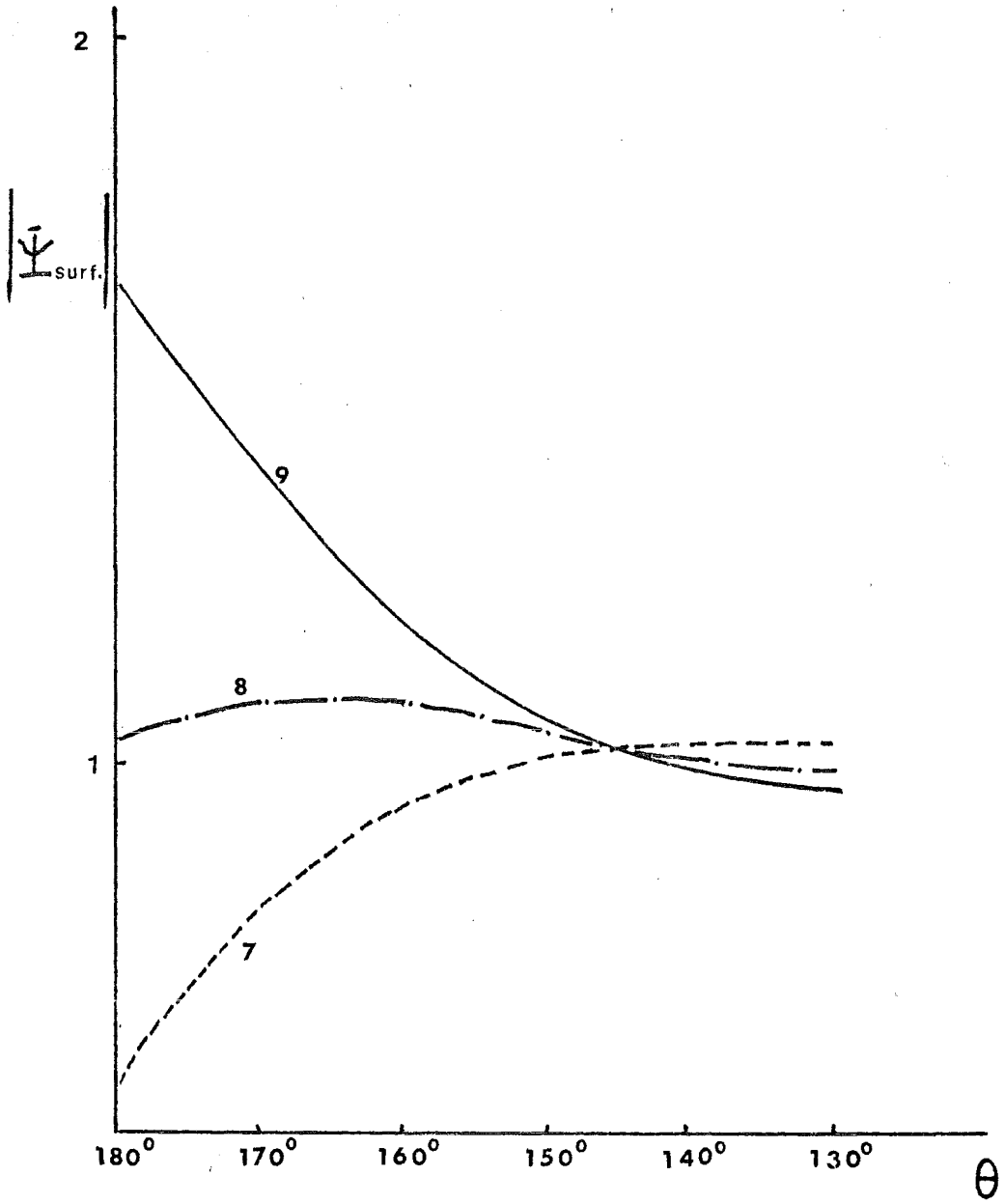

FIGURE 6.10 Plot of surface field magnitudes versus θ (as defined in Fig. 6.1). The variable is N, the number of surface field expansion coefficients used. The parameters of the wedge-cylinder are $\chi = 20^{\circ}$, $a = 0.2\lambda$, $\nu = 1.5$ and $\mu_n = n$. The H-polarised field is incident at an angle $\Theta = \pi$.

CHAPTER SEVEN

SPECIALISED SOLUTIONS FOR INFINITE PENETRABLE WEDGES

7.1 INTRODUCTION

A comprehensive approach to electromagnetic scattering by penetrable wedges is introduced in Chapter 5 and its significance is examined in Chapter 6. Based on the results and experience so gained, the general solution is specialised in this chapter to scattering of an E-polarised wave incident symmetrically (see Fig. 7.1) on a dielectric wedge with wedge angle 2χ, with $\pi/2 \leq 2\chi \leq \pi$.

Bessel functions of integer order, and argument $\zeta k\rho$, where $\zeta = 1$ when outside the wedge and $\zeta = \nu$ when inside the wedge, are used as the radially-dependent parts of the basis wave functions for the expansion of incident, reflected, refracted and diffracted fields. Different expansions are used for each of the regions shown in Fig. 7.1. The multiplication theorem (cf. Watson 1966, Section 5.21) is then invoked to match the fields across the boundaries. However, before the resultant system of linear equations can be solved, the radiation condition must be imposed. This is done in two different ways:

(i) The radiation condition is explicitly imposed by requiring the far scattered field to be outgoing.

(ii) The Bessel function expansions are restricted to $\rho > \rho_o$ (Fig. 7.2). For $\rho > \rho_o$, Hankel function expansions are used. The fields are point-matched on $\rho = \rho_o$.

Unfortunately, the solutions so constructed suffer from a special case of 'relative convergence' (cf. Section 7.5). Although it has not been found possible to perfect these methods, they are presented because the results are informative and some of them are reasonably accurate.

7.2 PRELIMINARIES

The geometry of a two-dimensional infinite wedge is depicted in Fig. 7.1 The two-dimensional Ω plane is partitioned into Ω_-, L, Ω_+ accordingly where L is the intercept of the wedge with Ω plane, Ω_- represents the region within the wedge for which $|\phi| < \chi$, and Ω_+ represents the region outside the wedge for which $\chi < |\phi| < \pi$. An arbitrary point in Ω is given the polar coordinate $(\rho;\phi)$. A scalar monochromatic plane wave is incident at the angle $\Theta = \pi$. The reflected wave boundaries (c.f. Section 4.1.1) L_+, consist of the two radial lines defined by $\phi = \pm 2\chi$, $0 < \rho < \infty$, while the refracted wave boundaries L_- consist of the two radial lines defined by $\phi = \pm \gamma$, $0 < \rho < \infty$, with γ given by Snell's law, i.e.

$$\cos \chi = \nu \cos(\chi+\gamma) \tag{7.1}$$

where ν is the refractive index of the wedge Ω_-. The refractive index of free space Ω_+ is unity.

7.3 FIELD CLOSE TO THE APEX

7.3.1 Formulation

Due to the symmetry of the problem, from now on only the upper half of the Ω plane is considered. Referring to Fig. 7.1, the four regions of interest are:

$$\Omega_1 = 0 < \rho < \infty, \quad 2\chi < \phi < \pi$$

$$\Omega_2 = 0 < \rho < \infty, \quad \chi < \phi < 2\chi$$

$$\Omega_3 = 0 < \rho < \infty, \quad \gamma < \phi < \chi$$

$$\Omega_4 = 0 < \rho < \infty, \quad 0 < \phi < \gamma$$

where

$$\Omega_+ = \Omega_1 \cup \Omega_2, \quad \Omega_- = \Omega_3 \cup \Omega_4 ,$$

Denoting Ψ_{inc}, $\Psi_{refl.}$, $\Psi_{refr.upper}$ and $\Psi_{refr.\ lower}$ as the incident wave, the reflected wave from the upper wedge surface, the refracted wave from the upper wedge surface and the refracted wave from the lower wedge surface, respectively, then

$$\Psi_{inc} = \sum_{m=o}^{\infty} \varepsilon_m (-j)^m \cos(m\phi)\ J_m(k\rho) \tag{7.2}$$

$$\Psi_{refl.} = G \sum_{m=o}^{\infty} \varepsilon_m (-j)^m \cos\, m(2\chi-\phi)\ J_m(k\rho) \tag{7.3}$$

$$\Psi_{refr.upper} = H \sum_{m=o}^{\infty} \varepsilon_m (-j)^m \cos\, m(\phi+\gamma)\ J_m(\nu k\rho) \tag{7.4}$$

and

$$\Psi_{refr.lower} = H \sum_{m=o}^{\infty} \varepsilon_m (-j)^m \cos\, m(\phi-\gamma)\ J_m(\nu k\rho) \tag{7.5}$$

where

$$G = \frac{\sin\chi - (\nu^2-\cos^2\chi)^{\frac{1}{2}}}{\sin\chi + (\nu^2-\cos^2\chi)^{\frac{1}{2}}} \tag{7.6}$$

$$H = \frac{2\sin\chi}{\sin\chi + (\nu^2-\cos^2\chi)^{\frac{1}{2}}} \tag{7.7}$$

The total field in each of these four regions is given by (7.8) to (7.11) below:

$$\Psi_1(\varepsilon\Omega_1) = \sum_{m=o}^{\infty} E_m \cos\, m(\pi-\phi)\ J_m(k\rho) + \Psi_{inc.} \tag{7.8}$$

$$\Psi_2\ (\varepsilon\Omega_2) = \sum_{m=o}^{\infty} (A_m \cos m\phi + D_m \sin m\phi)\ J_m(k\rho) + \Psi_{inc.} + \Psi_{refl.} \tag{7.9}$$

$$\Psi_3(\varepsilon\Omega_3) = \sum_{m=o}^{\infty} (B_m \cos m\phi + Z_m \sin m\phi)\ J_m(\nu k\rho) + \Psi_{refr.upper} \tag{7.10}$$

$$\Psi_4(\varepsilon\Omega_4) = \sum_{m=o}^{\infty} F_m \cos m\phi\ J_m(\nu k\rho) + \Psi_{refr.upper} + \Psi_{refr.lower} \tag{7.11}$$

The fields and their derivatives are matched across L_+, L and L_-. The multiplication theorem (cf. (1.36)) is invoked. After equating the coefficients of the Bessel functions, the variables A_m, D_m, B_m, Z_m and F_m are eliminated. One then arrives at a set of simultaneous equations:

$$\sum_{\ell=o}^{\infty} (-1)^{\ell} E_{\ell}\ g(\ell,m,\chi)\ F_{\frac{m-\ell}{2}}(\ell,\nu^{-1}) = -\sum_{\ell=o}^{\infty} \varepsilon_{\ell}\ (-1)^{\ell}\ g(\ell,m,\chi)\ F_{\frac{m-\ell}{2}}(\ell,\nu^{-1}),$$

$$m \in [0,\infty] \tag{7.12}$$

where

$$g(\ell,m,\chi) = m \sin(m\chi) \cos(\ell\chi) - \ell \cos(m\chi) \sin(\ell\chi) \tag{7.13}$$

and $F_m(\ell,\nu^{-1})$ is as defined in (1.36).

However, before (7.12) can be solved for the E_ℓ, the radiation condition must be imposed. It is worth mentioning, in passing, that if one attempts to generate a solution without imposing the radiation condition, one always seems to end up with a trivial solution. The diffracted field completely cancels the incident wave, so that the total field is zero everywhere.

In Ω_1, the diffracted field is

$$\Psi_{diff.1} = \sum_{m=o}^{\infty} E_m \cos m(\pi-\phi) \; J_m(k\rho) \tag{7.14}$$

which can be written as

$$\Psi_{diff.1} = 1/2 \sum_{m=o}^{\infty} E_m \cos m(\pi-\phi) \left[H_m^{(1)}(k\rho) + H_m^{(2)}(k\rho)\right] \tag{7.15}$$

Substituting the asymptotic forms of the Hankel functions (1.32) into (7.15), the latter becomes

$$\Psi_{diff.1} = (1/2\pi k\rho)^{\frac{1}{2}} \left[\exp(jk\rho) \exp(-j\pi/4) \sum_{m=o}^{\infty} E_m \cos(m\phi)(j)^m \right.$$
$$\left. + \exp(-jk\rho) \exp(j\pi/4) \sum_{m=o}^{\infty} E_m \cos(m\phi)(-j)^m \right] \tag{7.16}$$

It is clear from (7.16) that if $\Psi_{diff.1}$ is to behave like an outgoing wave at infinity, then

$$\Psi^+(\phi) = \sum_{m=o}^{\infty} E_m \cos(m\phi)(j)^m = 0, \quad |\phi| > 2\chi \tag{7.17}$$

is necessary in Ω_1. Together with appropriate radiation constraints in each of the four regions, (7.12) can be solved. The results are presented in the next section.

The above analysis is only valid for

$$\pi \geq 2\chi \geq \pi/2 \tag{7.18}$$

as can be seen from the following argument. Since from (7.16), the magnitude of the outgoing part of the diffracted field is

$$\Psi^{++}(\phi) = \sum_{m=o}^{\infty} E_m \cos(m\phi)(-j)^m \tag{7.19}$$

Note that (7.17) and (7.19) exist only in Ω_1, where $2\chi<\phi<2\pi-\chi$.

Let ϕ_o be a value of ϕ such that $2\chi<\phi_o<\pi-2\chi$, then $\Psi^{++}(\phi_o)$ has the value

$$\begin{aligned}\Psi^{++}(\phi_o) &= \sum_{m=o}^{\infty} E_m \cos(m\phi_o)(-j)^m \\ &= \sum_{m=o}^{\infty} E_m \cos m(\phi_o+\pi)(j)^m \\ &= \Psi^{+}(\phi_o+\pi)\end{aligned} \tag{7.20}$$

If $2\chi<\pi/2$, then $\phi_o+\pi<2\pi-\chi$. Therefore $\Psi^{+}(\phi_o+\pi)$ must equal zero from (7.17), which then implies that $\Psi^{++}(\phi_o) = 0$ for $2\chi<\phi_o<\pi-2\chi$. However, because of analytic continuation (cf. Section 1.4.3), $\Psi^{+}(\phi)$ must be zero everywhere for $2\chi<\phi<2\pi-2\chi$. The condition (7.18) thus eliminates this contradiction.

7.3.2 Computational Results

Figs. 7.3(a to d) and 7.4(a to d) display the variation of the diffracted field with respect to distance away from the apex of the wedge. The wedge angle 2χ is 100^o and the refractive index ν is 2.0. The incoming (E-polarised) plane wave is incident at 180^o. The number M of eigenfunctions used is 5 for Fig. 7.3 and 6 for Fig. 7.4. The diffracted field variations (both magnitude and phase) are plotted against ρ/λ for several values of ϕ. The values of ϕ are (a) 180^o, (b) 170^o, (c) 160^o and (d) 150^o. Figs 7.3 and 7.4 suggest very strongly that the diffracted fields are outgoing for $\rho > \lambda$.

Figs 7.5 and 7.6 display the variation of the diffracted field for M = 7 and M = 8 respectively. All other parameters are identical to those applying for Figs 7.3 and 7.4. It is seen that the fields plotted in Figs 7.5 and 7.6 no longer resemble outgoing waves. The reason for this pathological behaviour is that the way in which the problem has been formulated is markedly unstable.

It has already been pointed out in Section 7.3.1 that the radiation condition (7.17) must be imposed explicitly when solving (7.12). The computer routine employed to generate the results presented in this section is written in such a way that half of the number of equations are taken from (7.12) while the other half is taken from (7.17). The (M/2) equations chosen from (7.12) are those corresponding to m = 0,1,2, . . ., M/2. The (M/2) equations chosen from (7.17) are $\phi = \pi, \pi - \phi_o, \pi - 2\phi_o, \ldots$, where $\phi_o = 2(\pi-2\chi)/M$, e.g. when M = 10 five equations are taken from (7.12) with m = 0, 1, 2, 3, 4, 5. The other five equations are taken from (7.17) with $\phi = 180^o, 152^o, 124^o, 96^o$, and 68^o with $\chi = 20^o$.

It seems, from the results shown in this section, that there is some connection between the efficiency of the solutions and the choice of the equations. Several computer experiments have been carried out in an attempt to determine this connection. If M_1 is the number of equations taken from (7.12) and M_2 is the number of equations taken from (7.17), where $M_1 + M_2 = M$, several combination of M_1 and M_2 are used in the experiments. Furthermore, the M_1 equations taken from (7.12) are chosen randomly, i.e. they do not correspond to m = 0, 1, 2, . . ., M_1. Similarly, the M_2 equations taken from (7.17) are chosen in random with respect to ϕ, $2\chi<\phi<\pi$.

It is found that a special case of 'relative convergence' does exist and the efficiency of the solutions depends on how the equations are chosen. Unfortunately, it has not been found possible to determine a set ratio of the number of equations to be chosen from (7.12) and (7.17), or a suitable way of choosing the variables m in (7.12) and ϕ in (7.17), to arrive at an optimal solution.

7.4 FAR SCATTERED FIELD

7.4.1 Formulation

As mentioned in Section 7.1, the radiation condition can be imposed by expanding the far scattered field in Hankel functions. Referring to Fig. 7.2, the upper Ω plane is now divided into six regions.

$$\Omega_1 = \rho_o < \rho < \infty, \qquad 2\chi < \phi < \pi$$

$$\Omega_2 = \rho_o < \rho < \infty, \qquad \chi < \phi < 2\chi$$

$$\Omega_3 = \rho_o < \rho < \infty, \qquad \gamma < \phi < \chi$$

$$\Omega_4 = \rho_o < \rho < \infty, \qquad 0 < \phi < \gamma$$

$$\Omega_5 = 0 < \rho < \rho_o, \qquad \chi < \phi < \pi$$

$$\Omega_6 = 0 < \rho < \rho_o, \qquad 0 < \phi < \chi$$

Furthermore, in addition to the boundaries L, L_-, L_+ defined as in Section 7.3, the further boundary L_o, at $\rho = \rho_o$ for $0 \leq \phi \leq 2\pi$, is introduced. The fields in the various regions are:

$$\Psi_1(\varepsilon\Omega_1) = \sum_{m=o}^{\infty} E_m \cos m(\pi-\phi)\, H_m^{(2)}(k\rho) + \Psi_{inc.} \tag{7.21}$$

$$\Psi_2(\varepsilon\Omega_2) = \sum_{m=o}^{\infty} (A_m \cos m\phi + D_m \sin m\phi)\, H_m^{(2)}(k\rho) + \Psi_{inc.} + \Psi_{refl.} \tag{7.22}$$

$$\Psi_3(\varepsilon\Omega_3) = \sum_{m=o}^{\infty} (B_m \cos m\phi + Z_m \sin m\phi)\, H_m^{(2)}(\nu k\rho) + \Psi_{refr.upper} \tag{7.23}$$

$$\Psi_4(\phi\Omega_4) = \sum_{m=o}^{\infty} F_m \cos m\phi\, H_m^{(2)}(\nu k\rho) + \Psi_{refr.upper} + \Psi_{refr.lower} \tag{7.24}$$

$$\Psi_5(\varepsilon\Omega_5) = \sum_{m=o}^{\infty} P_m \cos m(\pi-\phi)\, J_m(k\rho) \tag{7.25}$$

$$\Psi_6(\varepsilon\Omega_6) = \sum_{m=o}^{\infty} Q_m \cos m\phi\, J_m(\nu k\rho) \tag{7.26}$$

The fields and their normal derivatives have to be matched across the boundaries L, L_-, L_+ and L_o. Since there does not seem to be a multiplication theorem (cf. Watson 1966, Section 5.21) for Hankel functions of integer order, point-matching is invoked. Typical results are presented in Section 7.4.2.

7.4.2 Computational Results

Fig. 7.7 shows the diffracted fields calculated from the procedure described in Section 7.4.1. The parameters used are $\nu = 2.0$, $\chi = 50^o$, $\Theta = 180^o$ and (a) $M = 3$, $\rho_o = 1.0\lambda$, (b) $M = 4$, $\rho_o = 1.0\lambda$, (c) $M = 3$, $\rho_o = 1.2\lambda$, where M is the number of eigenfunctions used in (7.21) through (7.26). Figs. 7.7(a), (b) correspond to increasing value of M while Fig. 7.7(a), (c) correspond to increasing values of ρ_o.

It is seen that (a) is the best solution among those displayed in Fig. 7.7 because the (diffracted) field resembles an outgoing wave for $\rho/\lambda < 1$. Furthermore, increasing values of M or ρ_o do not lead to a better solution. This is again due to the problem of 'relative convergence', where the optimal solution can be obtained only when a specific combination of parameters is used. Furthermore, the solution plotted in Fig. 7.7(a) is seen to be worse

than those plotted in Figs 7.3 and 7.4 in Section 7.3 because of the instability of the (diffracted) field plotted. This is probably due to the limited number of eigenfunctions (M = 3) used for Fig. 7.7. This small number (3) of eigenfunctions, incidentally, is believed to be insufficient to completely represent the diffracted field. This brings out a further difficulty in the formulation described in Section 7.4.1. As there are eight different sets of variables which have to be solved simultaneously, the size of the matrix which has to be inverted is then (8 X M) X (8 X M). It has been noted (cf. Section 1.5.4) that the computer storage and execution time are proportional to N^2 and N^3 respectively, when the matrix to be inverted is of the size N X N. It is therefore difficult to have larger values of M, since N = 8 X M in this case. The convergence of the series expansion for the diffracted field is then difficult to demonstrate. The method described in Section 7.4.1 is therefore useful only when a very large computing facility is available.

7.5 RELATIVE CONVERGENCE, LEAST SQUARES SOLUTION AND THE METHOD OF SINGULAR VALUE DECOMPOSITION

There are, basically, three ways of overcoming the difficulties associated with relative convergence.

(i) Try to determine, analytically, a theoretical condition which leads to an optimal solution of a particular problem. This is similar to what Mittra and Lee (1971, also see Section 1.5.1.2) have done for the problem of the bifurcated waveguide. However, it does not seem to be an easy task to obtain an analytical solution for the infinite penetrable wedge diffraction problem. Therefore, this method must remain an ideal only, for the present at least.

(ii) Scan all possible combinations of the parameters until an optimal solution is found. Unfortunately, this is extremely computationally intensive and there is no guarantee of getting the desired result.

(iii) Use a large number of contraint equations (i.e. the equations which imposed the radiation condition). Of course, the number of equations would then be larger than the number of expansion coefficients used. Such a system of equations cannot be solved by the usual method of matrix inversion (cf. Section 1.5.1.3). However, a least squares solution can be obtained by, for example, employing the method of singular value decomposition (cf. Section

1.5.1.3). Therefore, provided that a sufficiently large computing facility is available, it may be possible to obtain an acceptable solution in this manner.

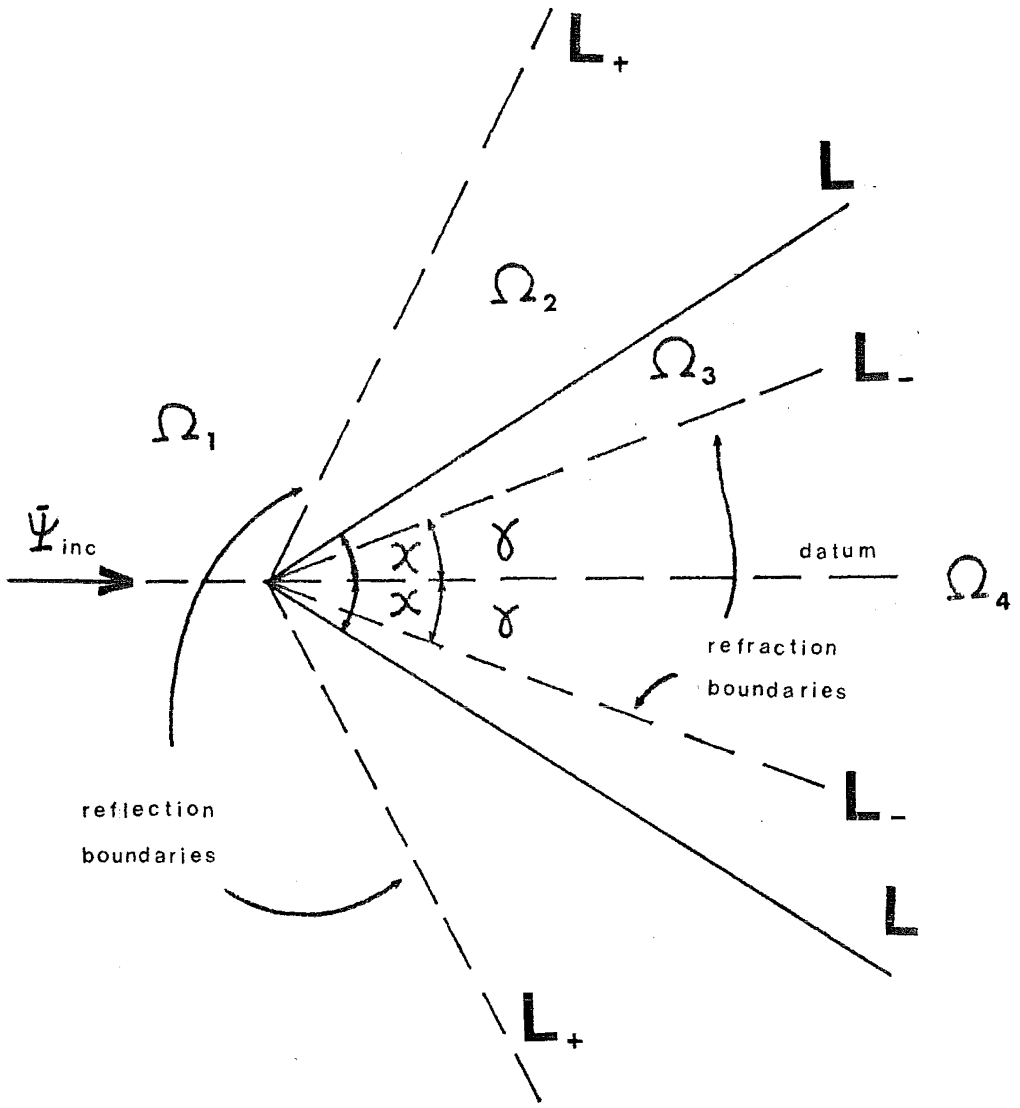

FIGURE 7.1 Reflection and refraction boundaries of an infinite penetrable wedge illuminated symmetrically, i.e. the incoming field is incident at $\phi = \pi$ while the wedge surface L coincide with the lines $\phi = \pm\chi$. The reflection boundaries are denoted by L_+ (cf. Section 4.1.1) while the refraction boundaries are denoted by L_-.

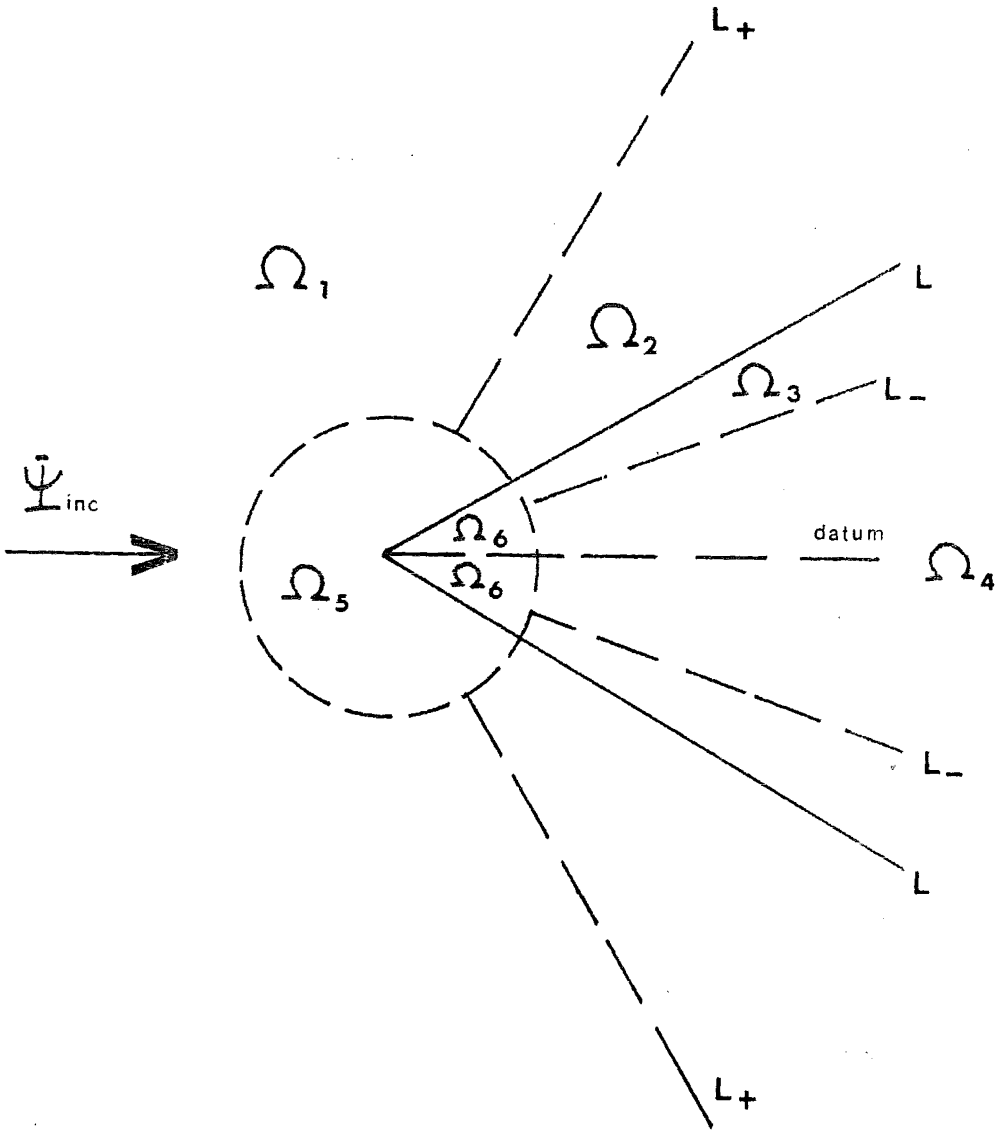

FIGURE 7.2 Different regions of interest for the infinte wedge scattering problem. The nth region is denoted by Ω_n.

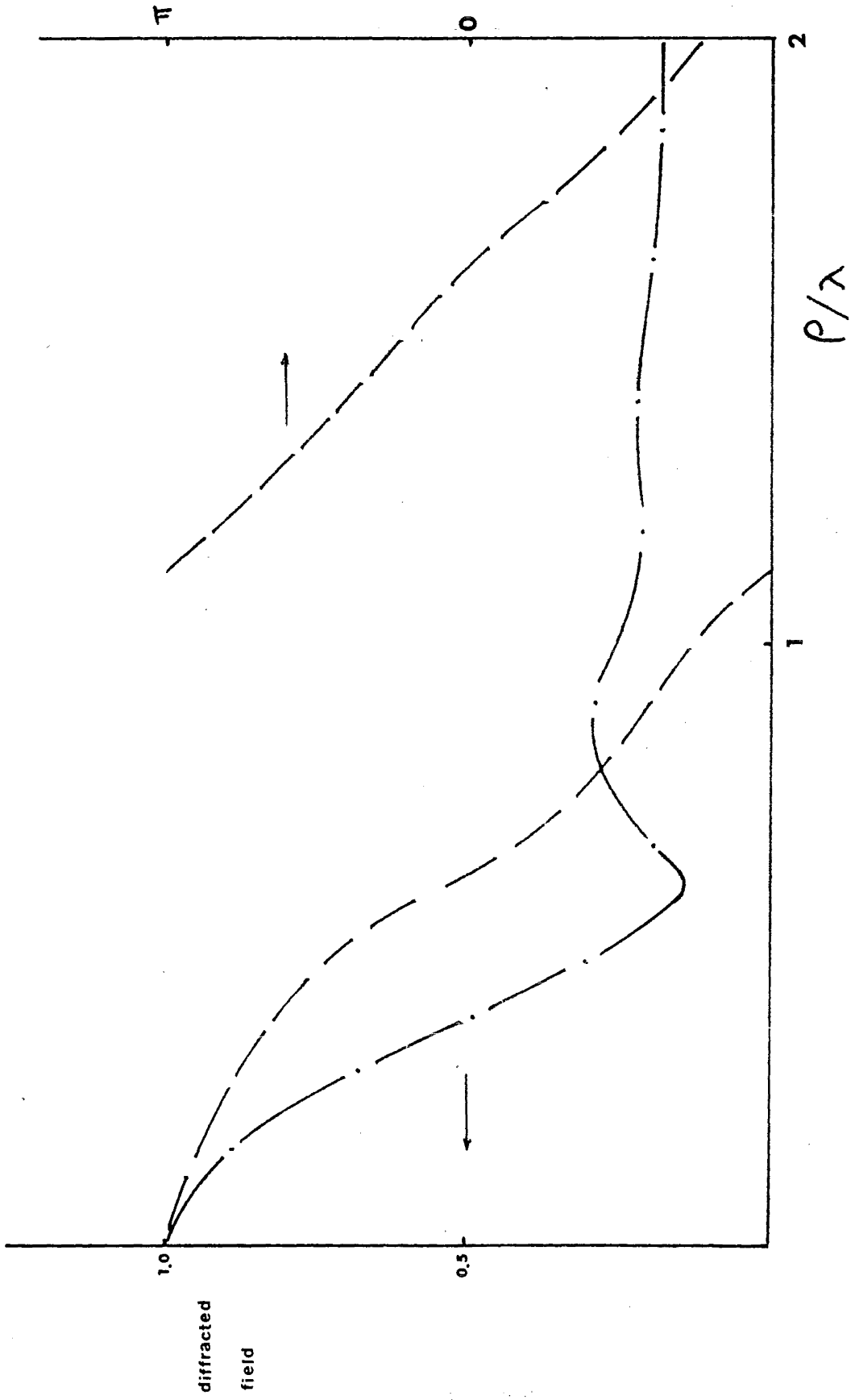

FIGURE 7.3a Plots of magnitudes (——·· —— · ——) and phases (- - - - - -), versus ρ/λ, of fields diffracted by an infinite penetrable wedge in the ϕ-direction. The parameters of the wedge are $\chi = 50^{\circ}$ and $\nu = 2.0$. The number of expansion coefficients used is 5.
(a) $\phi = 180^{\circ}$, (b) $\phi = 170^{\circ}$, (c) $\phi = 160^{\circ}$ and (d) $\phi = 150^{\circ}$.

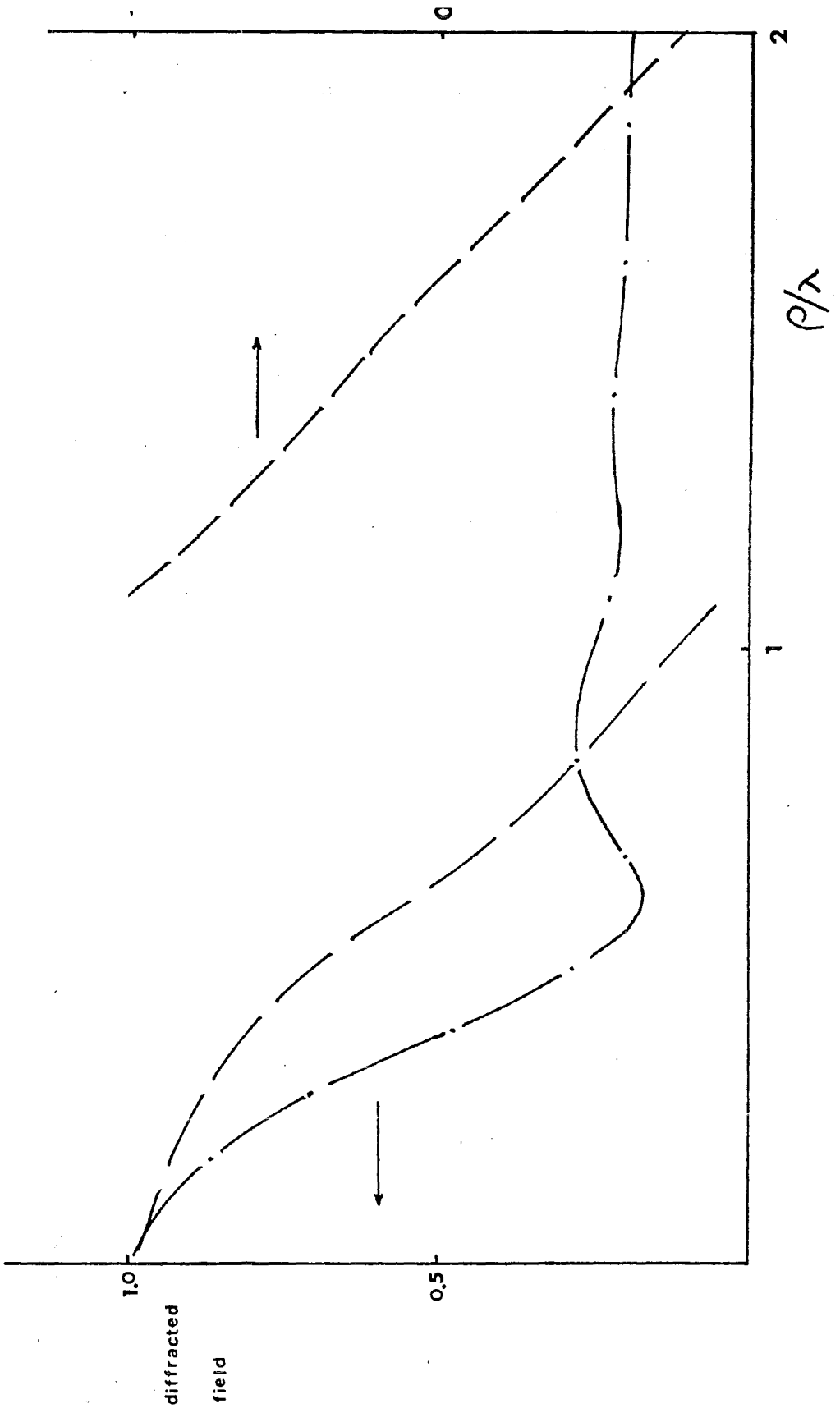

FIGURE 7.3b Plots of magnitudes (——· —— · ——) and phases (- - - - - -), versus ρ/λ, of fields diffracted by an infinite penetrable wedge in the ϕ-direction. The parameters of the wedge are $\chi = 50^{\circ}$ and $\nu = 2.0$. The number of expansion coefficients used is 5.

(a) $\phi = 180^{\circ}$, (b) $\phi = 170^{\circ}$, (c) $\phi = 160^{\circ}$ and (d) $\phi = 150^{\circ}$.

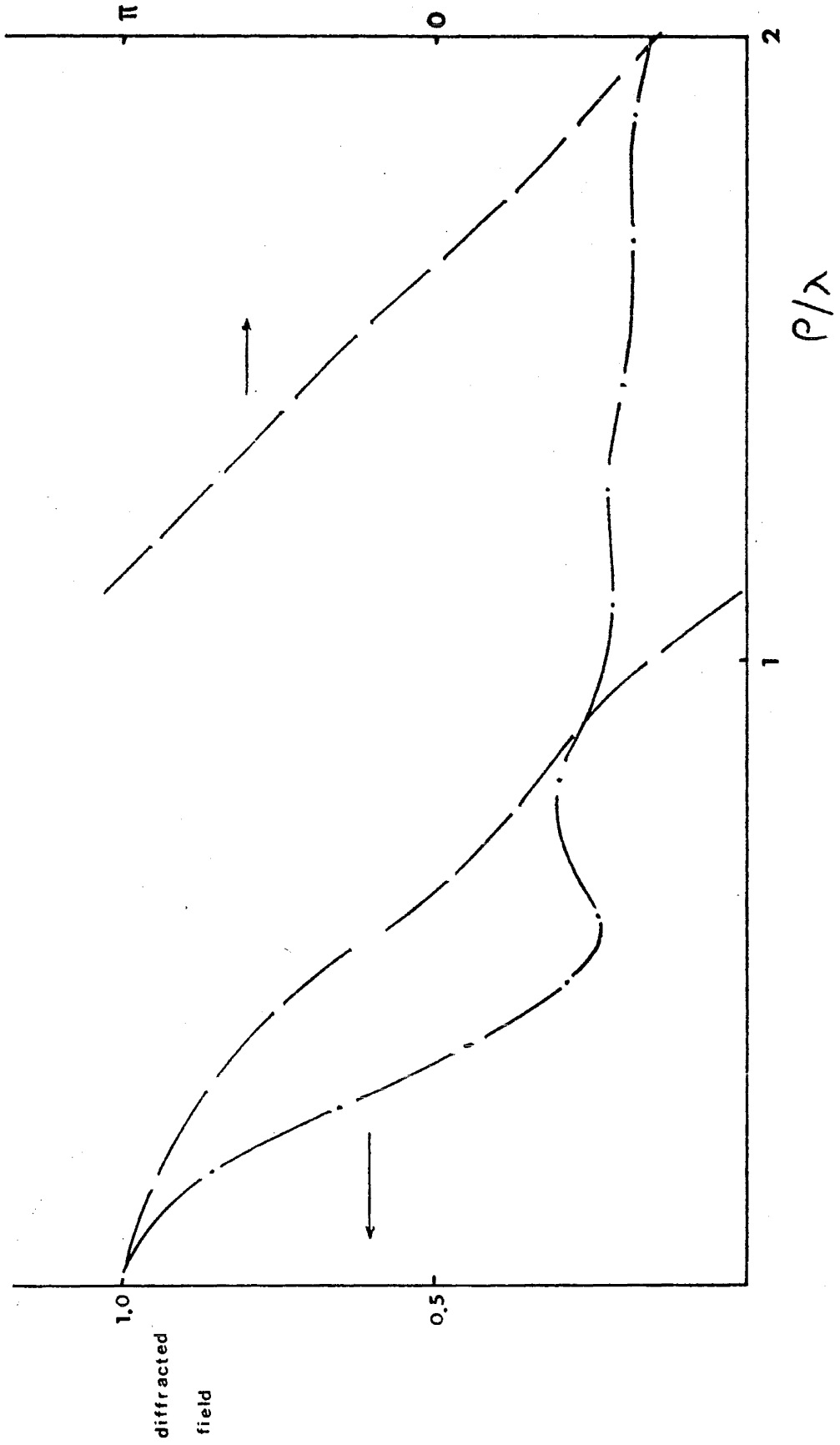

FIGURE 7.3C Plots of magnitudes (——· —— · ——) and phases (- - - - - -), versus ρ/λ, of fields diffracted by an infinite penetrable wedge in the ϕ-direction. The parameters of the wedge are $\chi = 50^{\circ}$ and $\nu = 2.0$. The number of expansion coefficients used is 5.
(a) $\phi = 180^{\circ}$, (b) $\phi = 170^{\circ}$, (c) $\phi = 160^{\circ}$ and (d) $\phi = 150^{\circ}$.

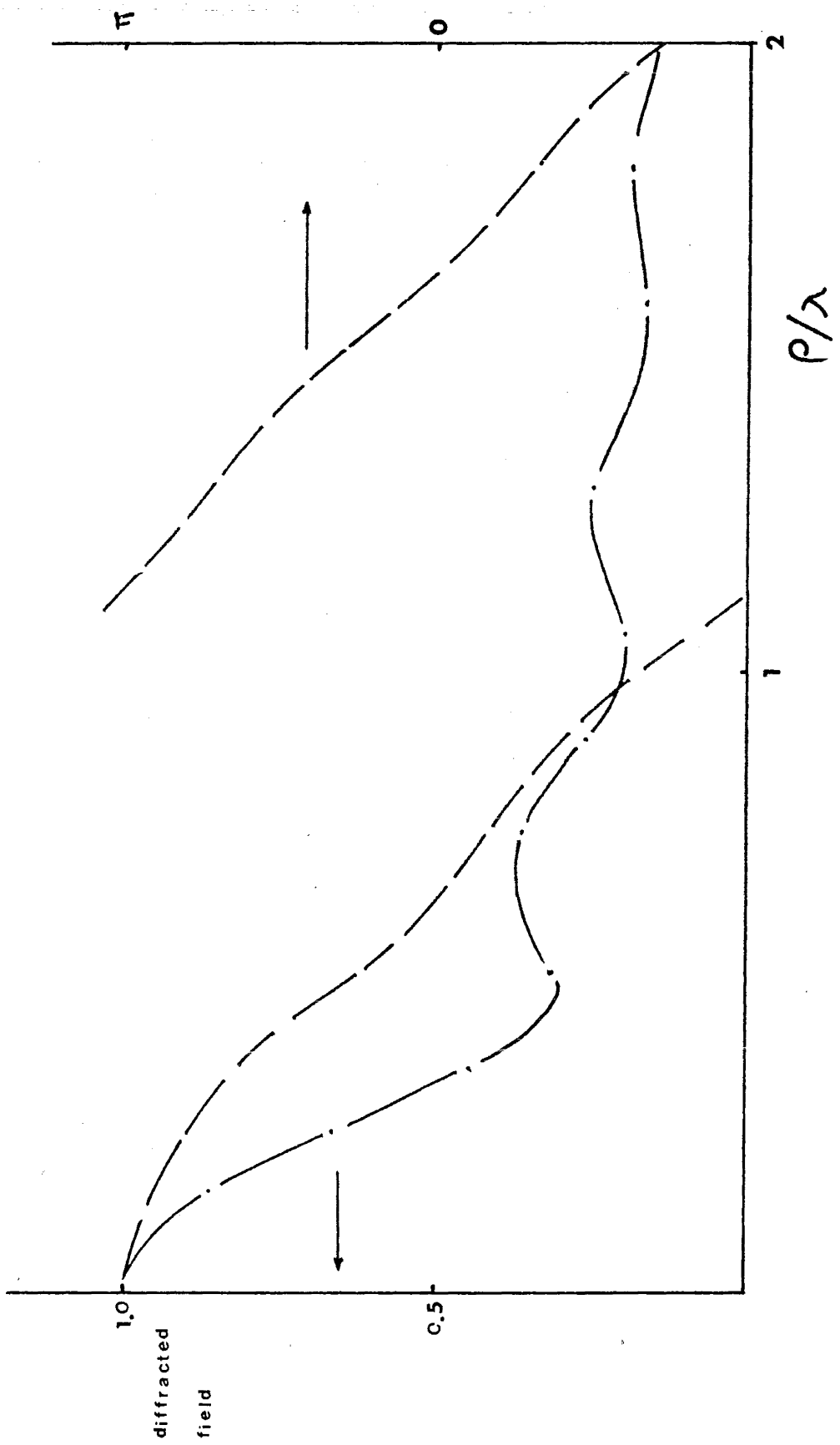

FIGURE 7.3d Plots of magnitudes (——· —— · ——) and phases (- - - - - -), versus ρ/λ, of fields diffracted by an infinite penetrable wedge in the ϕ-direction. The parameters of the wedge are $\chi = 50^\circ$ and $\nu = 2.0$. The number of expansion coefficients used is 5.
(a) $\phi = 180^\circ$, (b) $\phi = 170^\circ$, (c) $\phi = 160^\circ$ and (d) $\phi = 150^\circ$.

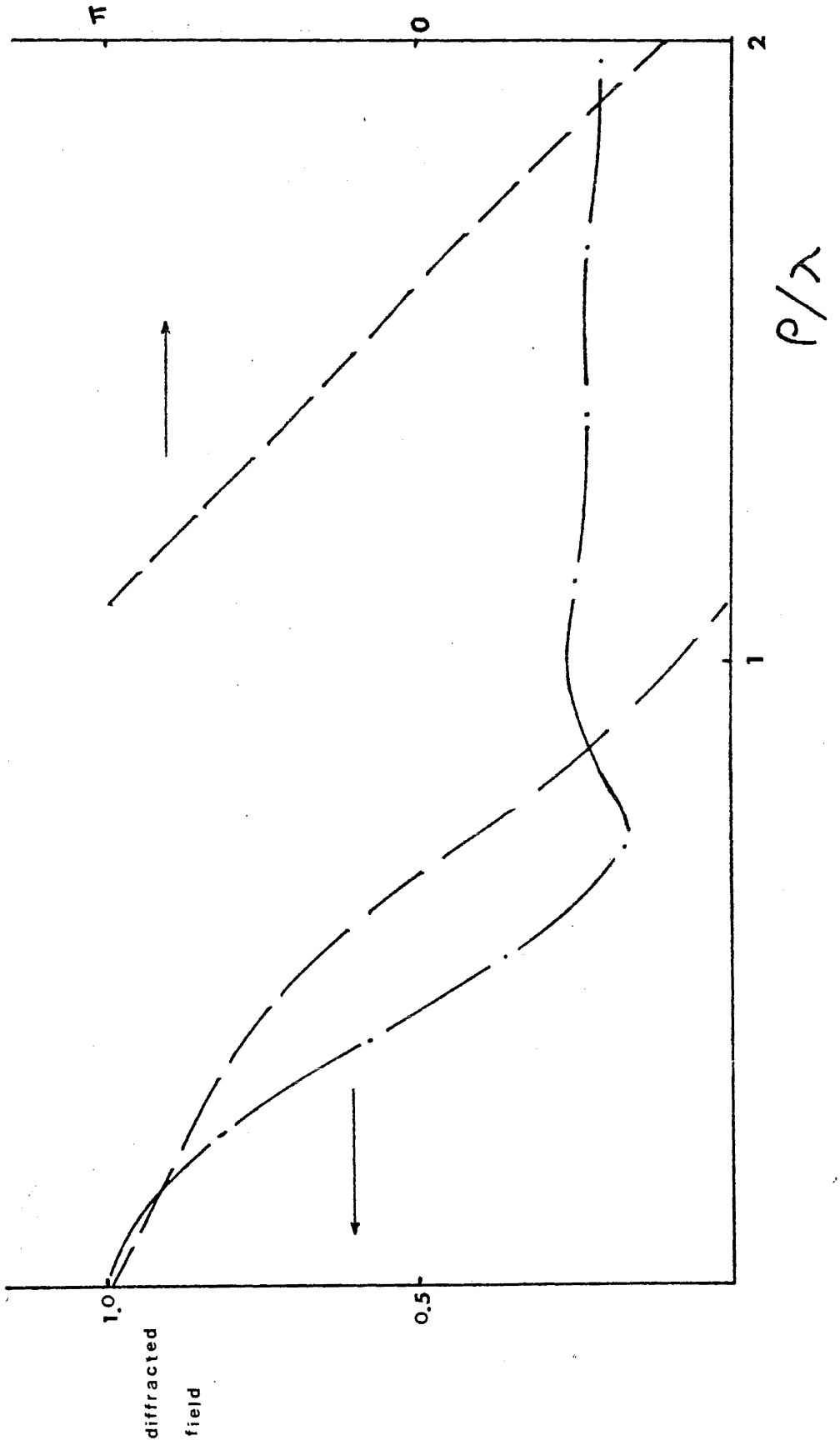

FIGURE 7.4a Plots of magnitudes (—— · —— · ——) and phases (- - - - - -), versus ρ/λ, of fields diffracted by an infinite penetrable wedge in the ϕ-direction. The parameters of the wedge are $\chi = 50^{\circ}$ and $\nu = 2.0$. The number of expansion coefficients used in 6.
(a) $\phi = 180^{\circ}$, (b) $\phi = 170^{\circ}$, (c) $\phi = 160^{\circ}$ and (d) $\phi = 150^{\circ}$.

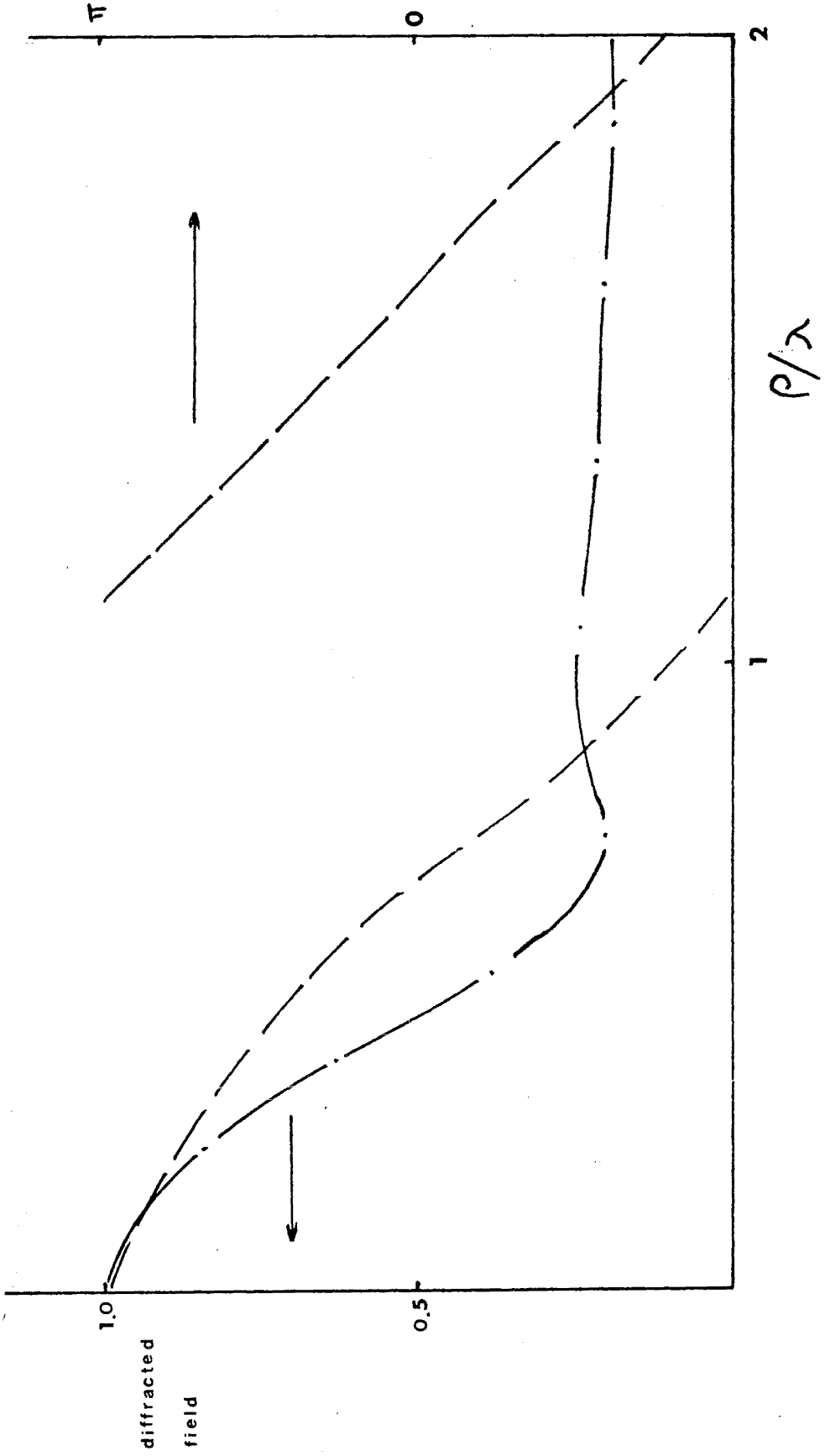

FIGURE 7.4b Plots of magnitudes (—— · —— · ——) and phases (- - - - - -), versus ρ/λ, of fields diffracted by an infinite penetrable wedge in the ϕ-direction. The parameters of the wedge are $\chi = 50^{\circ}$ and $\nu = 2.0$. The number of expansion coefficients used in 6.

(a) $\phi = 180^{\circ}$ (b) $\phi = 170^{\circ}$, (c) $\phi = 160^{\circ}$ and (d) $\phi = 150^{\circ}$.

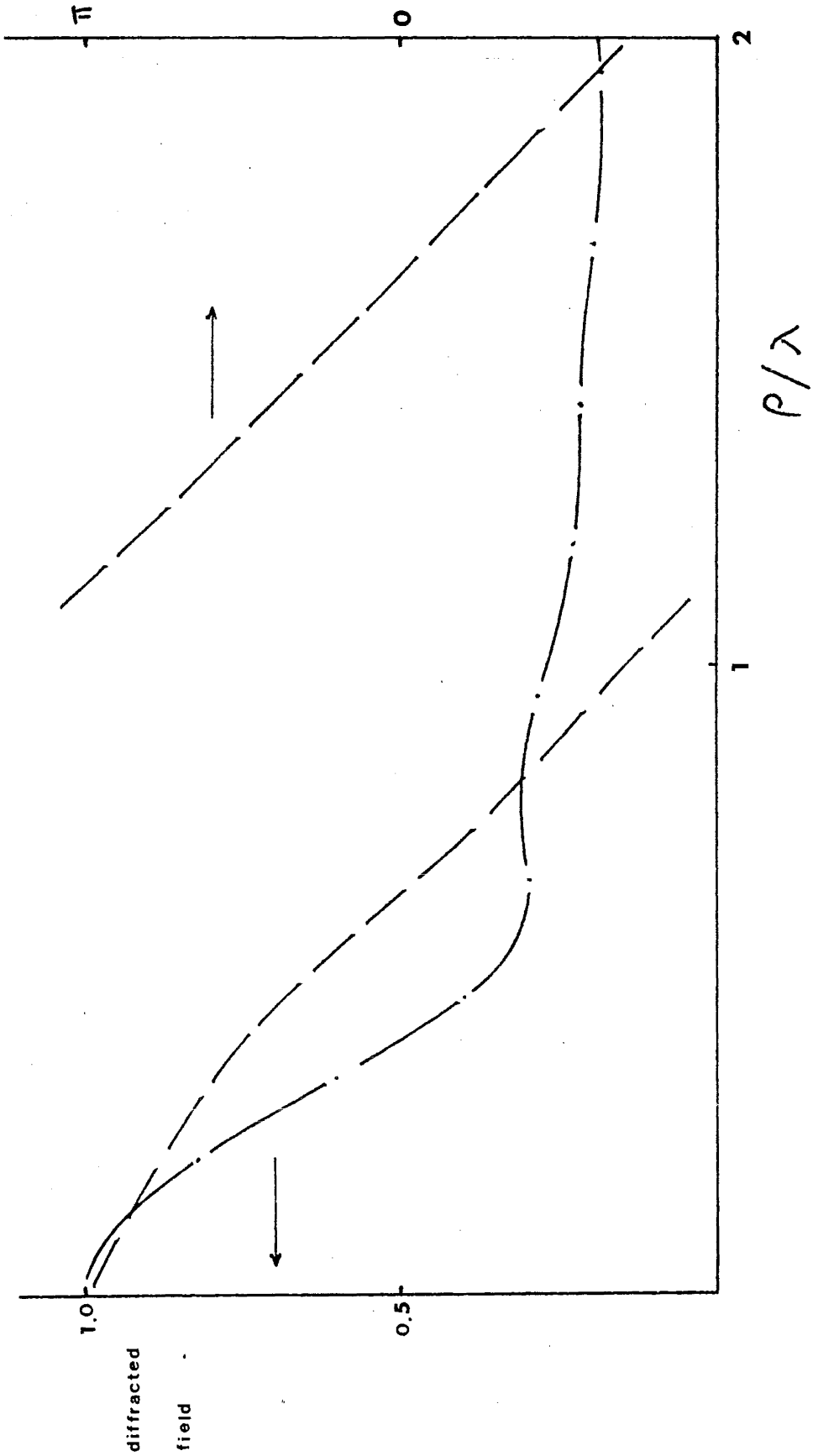

FIGURE 7.4c Plots of magnitudes (—— · —— · ——) and phases (- - - - - -), versus ρ/λ, of fields diffracted by an infinite penetrable wedge in the ϕ-direction. The parameters of the wedge are $\chi = 50^{\circ}$ and $\nu = 2.0$. The number of expansion coefficients used in 6.
(a) $\phi = 180^{\circ}$, (b) $\phi = 170^{\circ}$, (c) = 160° and (d) $\phi = 150^{\circ}$.

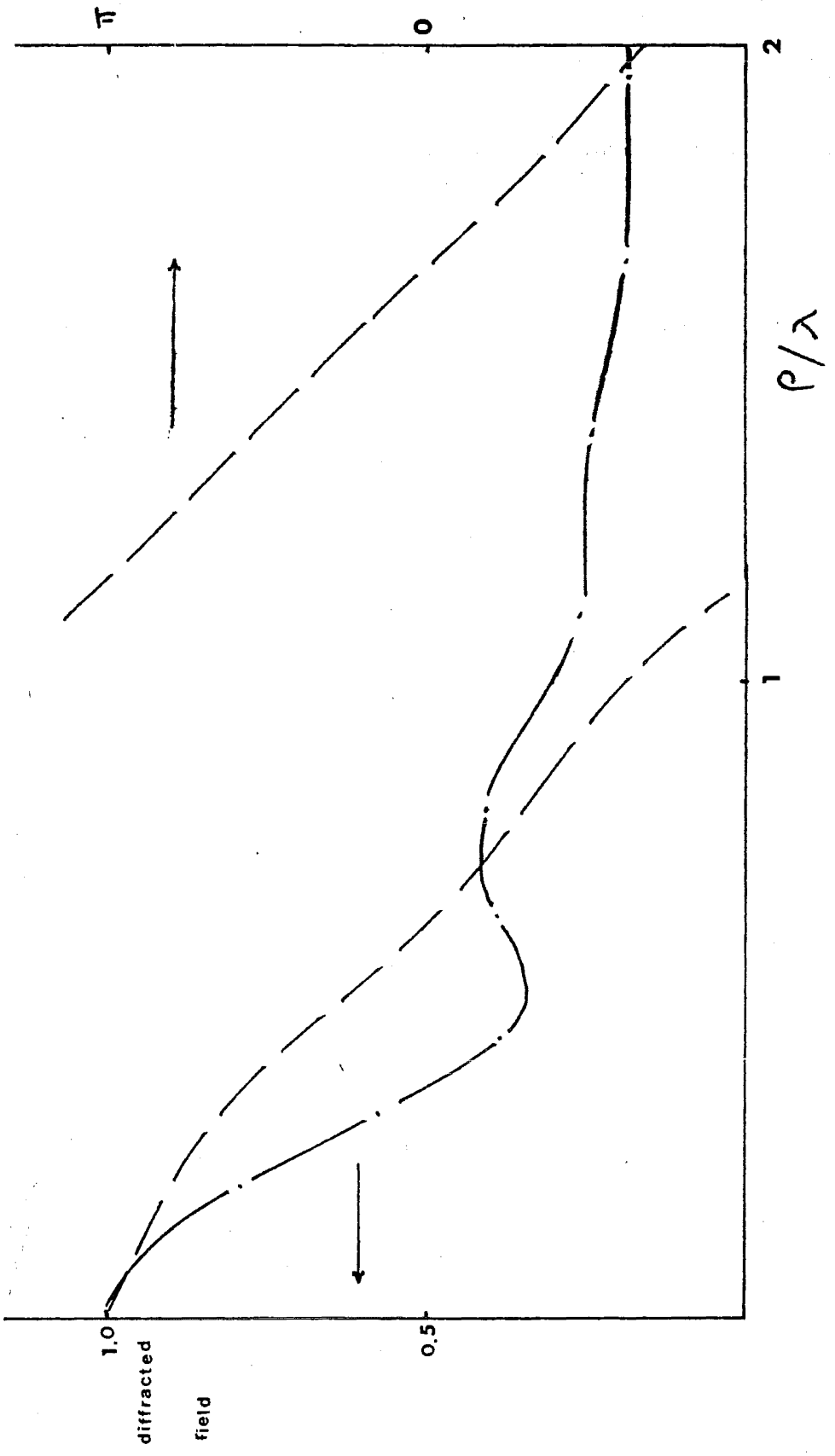

FIGURE 7.4d Plots of magnitudes (—— · —— · ——) and phases (- - - - - -), versus ρ/λ, of fields diffracted by an infinite penetrable wedge in the ϕ-direction. The parameters of the wedge are $\chi = 50^{\circ}$ and $\nu = 2.0$. The number of expansion coefficients used in 6.
(a) $\phi = 180^{\circ}$, (b) $\phi = 170^{\circ}$, (c) $\phi = 160^{\circ}$ and (d) $\phi = 150^{\circ}$.

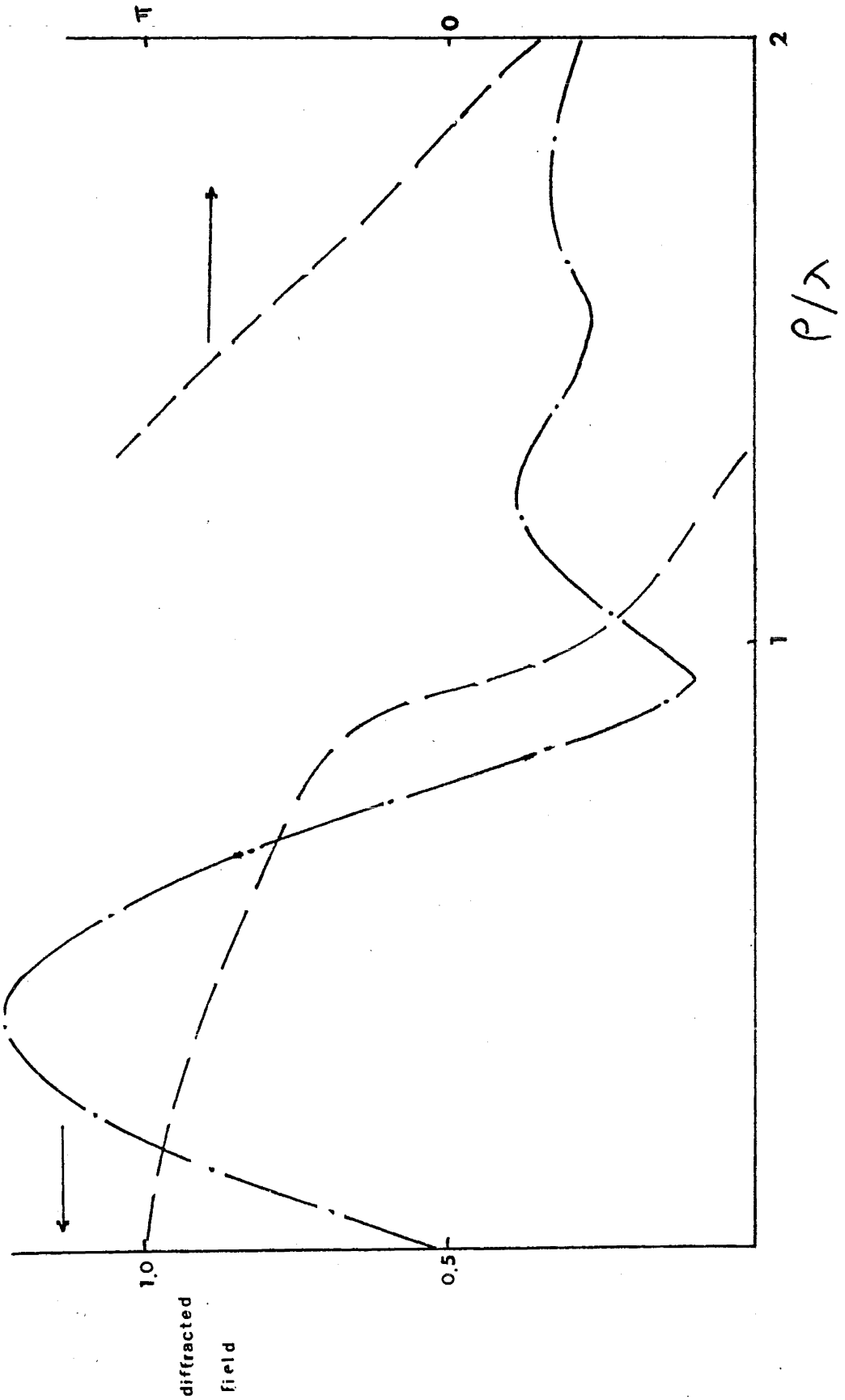

FIGURE 7.5 Plots of magnitude (—— · —— · ——) and phase (- - - - - -), versus ρ/λ, of field diffracted by an infinite penetrable wedge in the ϕ = 180 - direction. The parameters of the wedge is $\chi = 50^{\circ}$ and $\nu = 2.0$. The number of expansion coefficients used is 7.

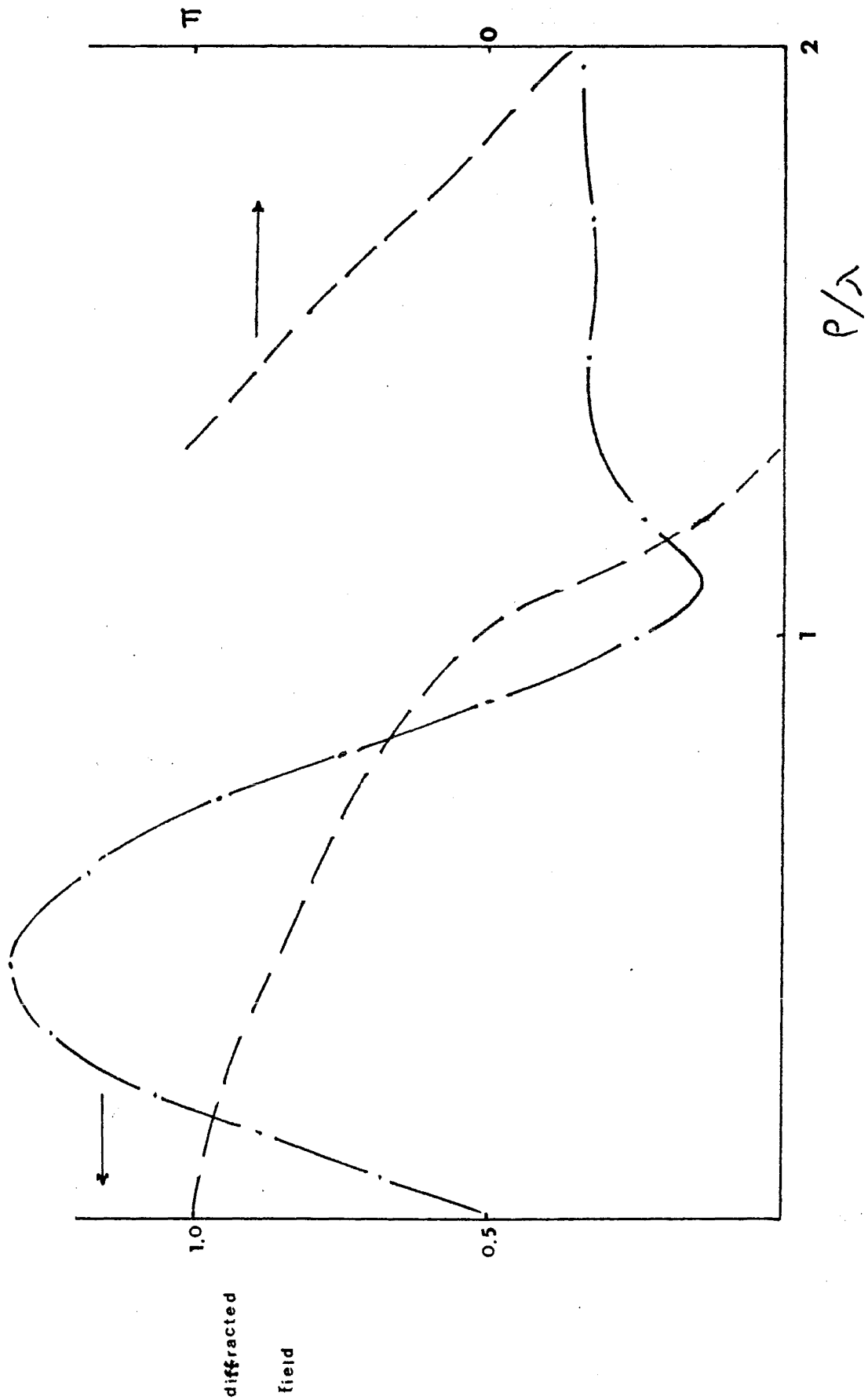

FIGURE 7.6 Plots of magnitude (—— · —— · ——) and phase (- - - - - -), versus ρ/λ, of field diffracted by an infinite penetrable wedge in the ϕ = 180 - direction. The parameters of the wedge is $\chi = 50^{\circ}$ and ν = 2.0. The number of expansion coefficients used is 8.

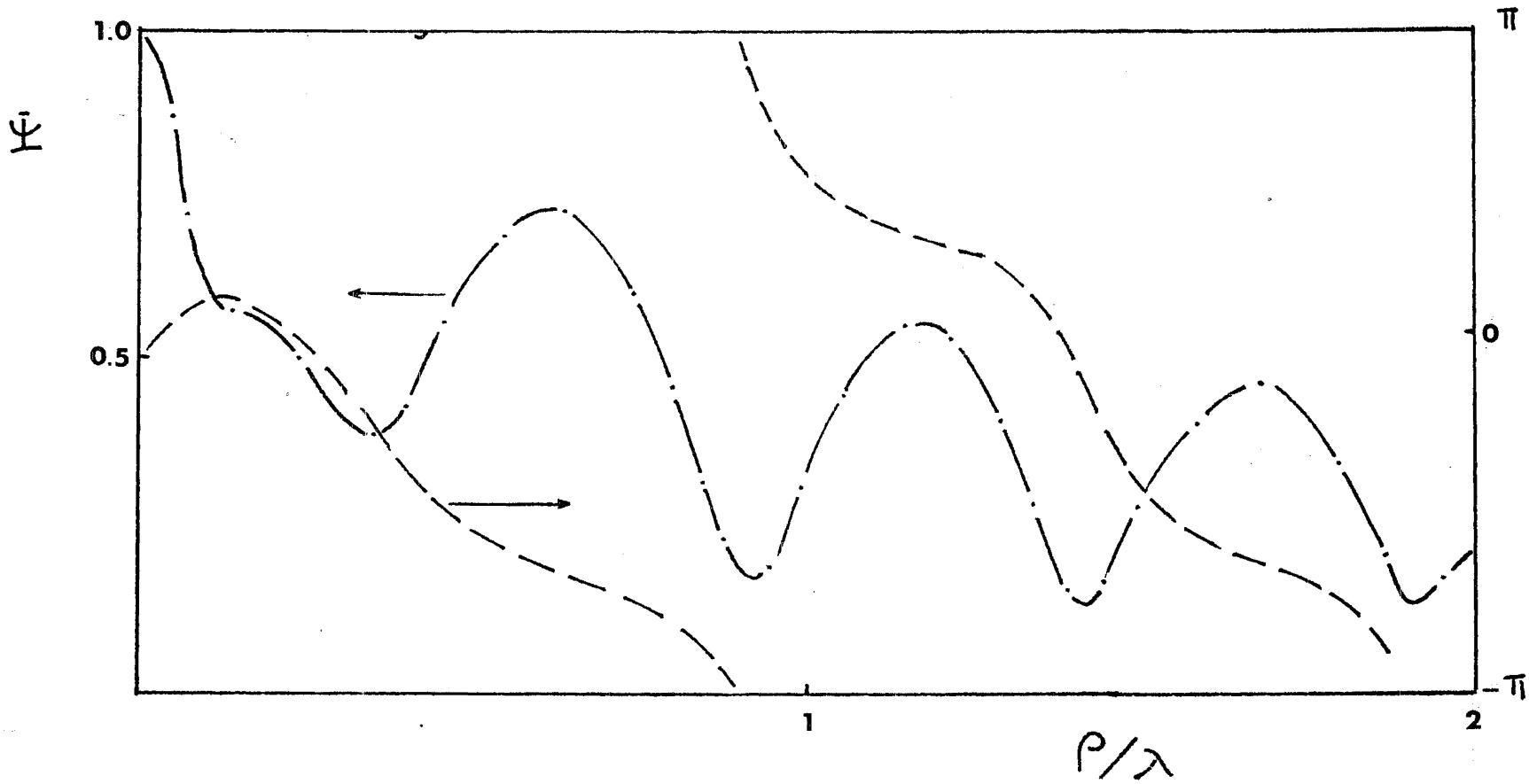

FIGURE 7.7a Plots of magnitude (—— · —— ·) and phase (- - - -), versus ρ/λ, of field diffracted by an infinite penetrable wedge in the $\phi = 180-$ direction. The parameters of the wedge are $x = 50^{\circ}$ and $\nu = 2.0$, (a) $m = 3$, $\rho = 1.0\lambda$, (b) $m = 4$, $\rho = 1.0\lambda$ and (c) $m = 3$, $\rho = 1.2\lambda$.

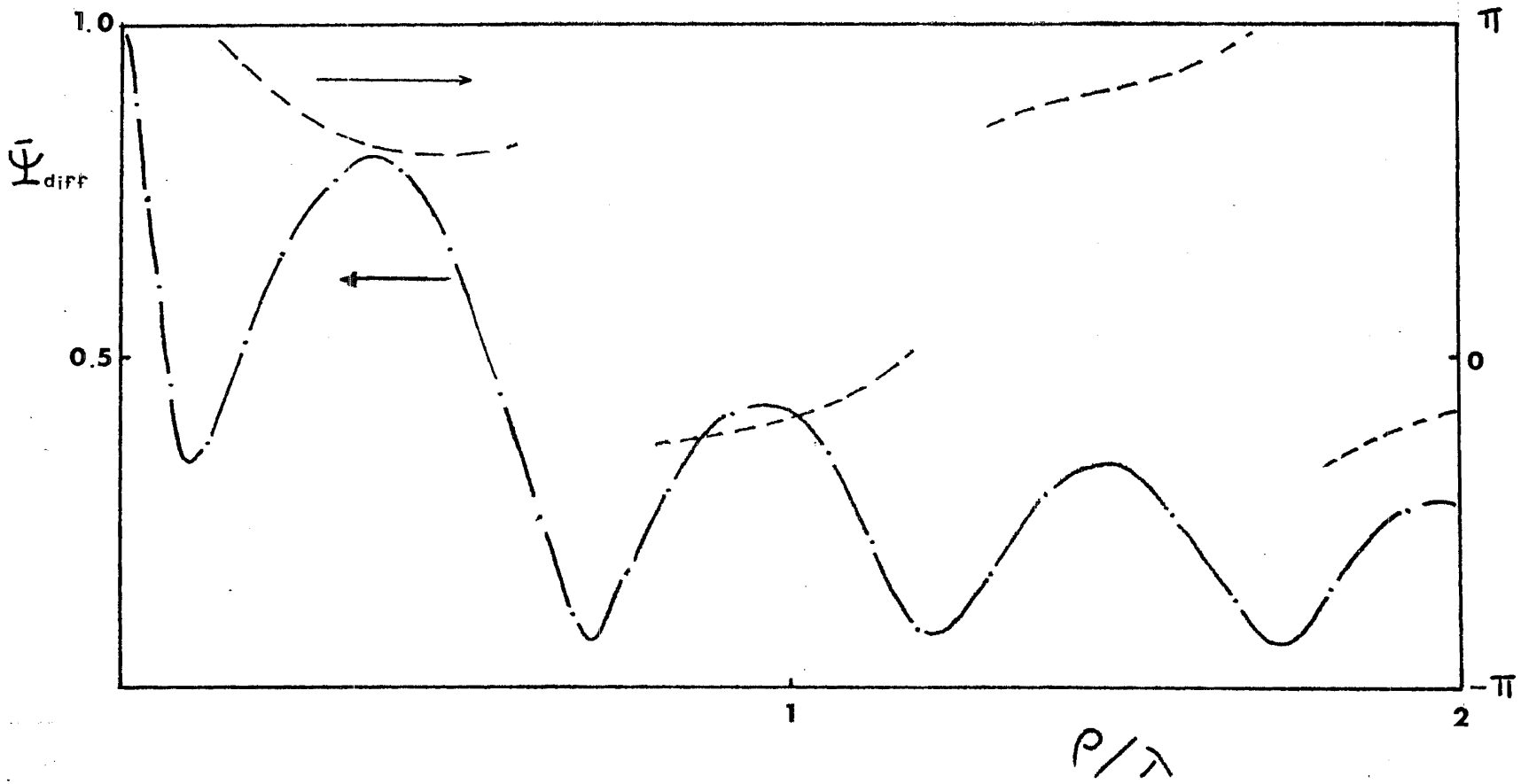

FIGURE 7.7b Plots of magnitude (—— · —— ·) and phase (- - - -), versus ρ/λ, of field diffracted by an infinite penetrable wedge in the ϕ = 180- direction. The parameters of the wedge are $x = 50^{o}$ and $\nu = 2.0$, (a) $m = 3$, $\rho = 1.0\lambda$, (b) $m = 4$, $\rho = 1.0\lambda$ and (c) $m = 3$, $\rho = 1.2\lambda$.

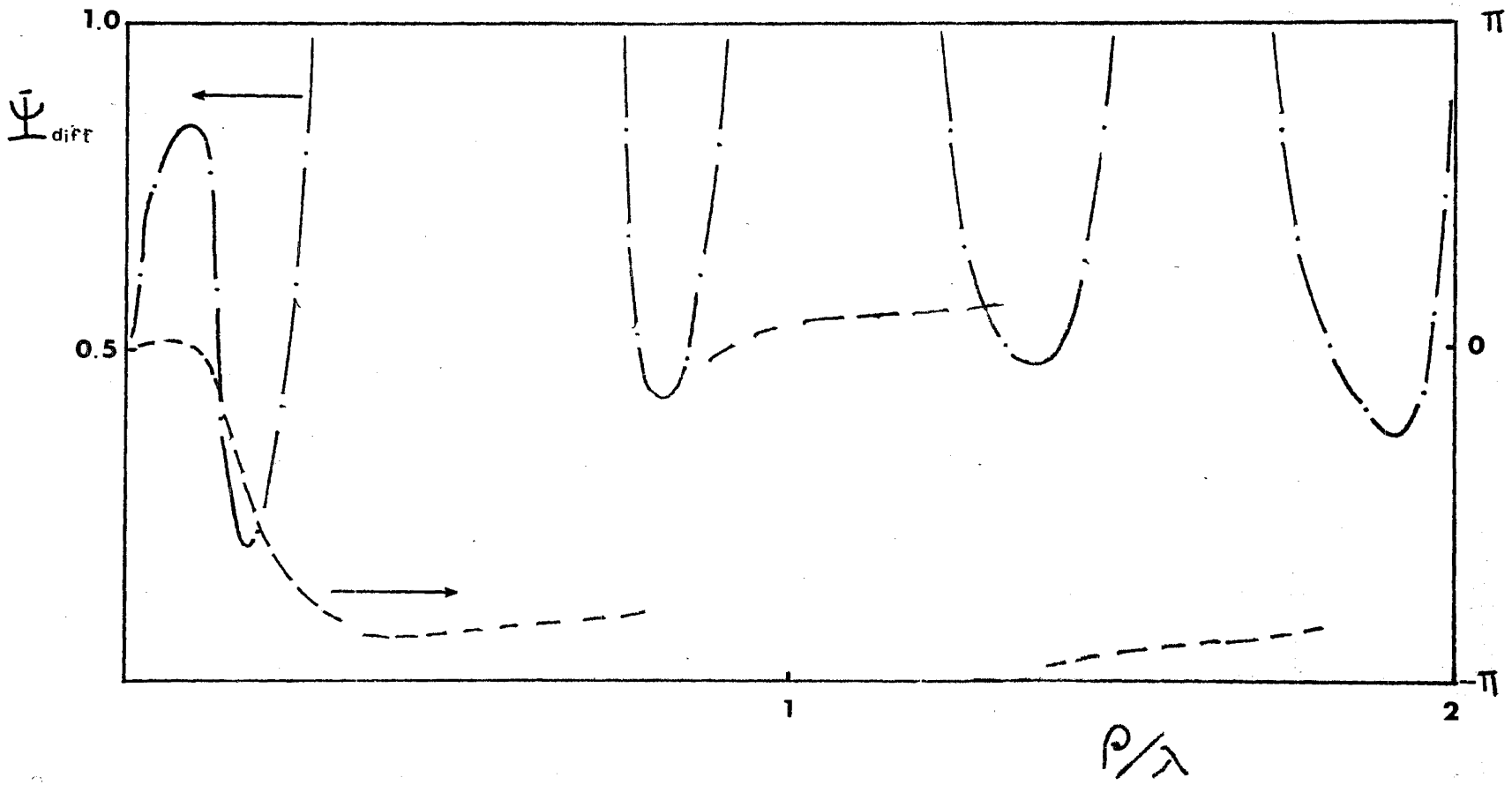

FIGURE 7.7c Plots of magnitude (—— · —— ·) and phase (- - - - -), versus ρ/λ, of field diffracted by an infinite penetrable wedge in the ϕ = 180- direction. The parameters of the wedge are $x = 50^{o}$ and $\nu = 2.0$, (a) $m = 3$, $\rho = 1.0\lambda$, (b) $m = 4$, $\rho = 1.0\lambda$ and (c) $m = 3$, $\rho = 1.2\lambda$.

CHAPTER EIGHT

THE NULL-FIELD METHOD APPLIED TO THE INFINITE PENETRABLE WEDGE DIFFRACTION PROBLEM

The null-field method introduced in Section 1.5.5 has been shown to be useful in solving many practical scattering problems (cf. Bates 1975a, Bates and Wall 1977, Bates 1980b and the many references quoted therein). However, as pointed out in Section 1.5.5.5, the conventional (circular) null-field method is unsuitable for solving the infinite wedge scattering problem. Details of some of the difficulties encountered in applying the null-field method to infinite penetrable wedge diffraction are outlined in Section 8.1.

On the other hand, it has been shown (cf. Bates 1974 and also Section 3.3) that the null-field method can still be applied to infinite bodies, when appropriate precautions are taken. In this chapter, the null-field method is applied to the penetrable wedge diffraction problem. Computational results are included and comparisons are made with those obtained by other authors.

8.1 PRELIMINARIES

8.1.1 The Radial Null-Field Method

The conventional way of applying the null-field method to scattering problems - the circular null-field method (cf. Section 1.5.5.4- is to impose the null-field condition explicitly within a circle inscribed by the scatterer (cf. Fig. 8.1). However, computational experience (cf. Bates and Wall 1977) has indicated that this conventional approach is not suitable for problems of scattering by infinite bodies. This is because the numerical stability of the resultant null-field equations (cf. Section 1.5.5.5) is proportional to the ratio ζ, which is defined in (1.102) as (cf. Fig. 8.1).

$$\zeta = \text{area of circle } \overset{\frown}{C} \text{ /area of scatter } C \tag{1.102}$$

When applied to the infinite wedge problems (cf. Fig. 8.2), it is clear that the ratio ζ defined by (1.102) is always infinitesimal. It is worth noting in passing that the author has actually attempted to apply the circular null-field method to the infinite penetrable wedge diffraction problem. The resulting numerical instabilities have prov too difficult to overcome.

On the other hand, it has been argued in Section 3.3 that it is reasonable to expect that the null-field method can be applied successfully, to the infinite (conducting) wedge diffraction problem, by imposing the null-field condition on radial lines inside the infinite wedge (cf. Fig. 8.3). This 'radial' null-field method (cf. Fig. 8.3) is here invoked to attack the infinite penetrable wedge diffraction problem. Details are presented in Sections 8.2.

8.1.2 The Role of Surface Field in the Null-Field Method

Kirchoff's Principle (cf. Section 1.5.5.1) states thatthe scattered field can be completely determined by the (total) field and its normal derivative on the surface of a scatterer. It is, therefore, important to evaluate the surface field and its derivatives. There is an exception, of course, when the scatterer is perfectly conducting. In that case either the surface field or its normal derivative must be zero, for E- and H-polarised fields respectively. For a penetrable body, however, knowledge of both the surface field and its normal derivative are needed to completely determine the scattered field.

There are two different ways of evaluating the surface field and its normal derivative. As already mentioned in Section 6.2 (cf. also Morita 1979, Wong 1972 and Bates 1980b), one can expand the surface field and its normal derivative in two independent expansions (cf. (6.18a) and (6.18b)). Two coupled integral equations are then needed to evaluate the (two sets of) expansion coefficients. On the other hand, if the field behaviour on the surface of the scatterer is known, one needs only to expand the surface field. The normal derivative can then be calculated by performing an analytical differentiation (see e.g. Bates 1980b). This latter method forms the basis of the analysis developed in this chapter.

Since one knows the general form of the field inside a penetrable wedge (cf. Chapter 5), the surface field can be deduced from it, i.e.

$$\Psi_{surface} = \lim_{P \to Q} \Psi_{-}(P) \tag{8.1}$$

where Ψ_{-} is the total field inside the wedge. It can be expanded (cf. Section 1.4) as

$$\Psi_{-} = \sum_{n=0}^{\infty} A_n J_{\mu_n}(\nu k \rho) \begin{matrix} \cos \\ \sin \end{matrix} (\mu_n \phi) \tag{8.2}$$

The μ_n in (8.2) are the properly chosen eigenvalues calculated from (5.23).

After substituting (8.1) and (8.2) into the null-field equation (1.95a), one obtains an infinite series of infinite integrals, a typical one of which is

$$H_m^{(2)}(k\rho) \int_o^\rho r^{-1} J_{\mu_n}(\nu kr)\, J_m(kr)\, dr + J_m(k\rho) \int_\rho^\infty r^{-1} J_{\mu_n}(\nu kr)\, H_m^{(2)}(kr)\, dr \tag{8.3}$$

It has not been found possible to evaluate the integrals in (8.3) analytically when ν differs from unity. It is also impracticable to attempt to carry out these integrations numerically. It is worth noting that infinite integration is a pervading difficulty encountered in infinite wedge diffraction problems, whether one uses the null-field method or the methods of surface and volume integral equations. Many authors try to overcome this difficulty by truncating the infinite integrals (cf. Wu and Tsai 1977, Vasil'ev and Solodoukhov 1971 and also Chapter 4 of this thesis). However, this unavoidably involves approximations which are difficult to justify. Furthermore, any attempt to choose an 'effective finite upper limit', ρ_o say, leads to unmanageable relative convergence problems (cf. Chapter 7).

It is noted that (cf. Watson 1966, Section 5.12), (8.3) can be evaluated analytically if all of the Bessel and Hankel functions have the same argument. So, one might think that invocation of the multiplication theorem (1.36), so as to express each $J_{\mu_n}(\nu kr)$ as a sum of terms, the ℓth being proportional to $J_{\mu_n+2\ell}(kr)$, might overcome the aforesaid difficulty. Unfortunately, though, the kinds of problem discussed in Section 4.1 are then encountered. It therefore seems that the only sensible way of overcoming all these difficulties is to deduce the surface field from the field outside the wedge, i.e.

$$\Psi_{\text{surface}} = \lim_{P \to Q} \Psi_+(P) \tag{8.4}$$

where Ψ_+ is the total field outside the wedge and can be expanded (cf. Section 1.4) as

$$\Psi_+ = \sum_{n=o}^{\infty} B_n J_{\mu_n}(k\rho) \begin{matrix}\cos \\ \sin\end{matrix} (\mu_n \phi) \tag{8.5}$$

However, this approach turns out to be over-simplistic. When the total surface field is expressed as in (8.4) and (8.5), there is nothing in the

formulation specifying the value of the refractive index of the wedge. It is worth noting in passing that the author has attempted to obtain solutions in such a simplistic way. They turned out to be trivial, however, i.e. the solution always turned out to correspond to the case for $\nu = 1$, the incident wave propagates freely in space as if there is no wedge.

In order to incorporate the vital piece of information (i.e. the value of the refractive index ν), the problem must be formulated more subtly. The external field must be expanded in a form which takes explicit cognisance of the presence of the wedge and the value of ν. A convenient way of doing this is to write

$$\Psi_{+} = \Psi_{inc.} + \Psi_{refr.} + \Psi_{diff.} \tag{8.6}$$

where $\Psi_{inc.}$ is the incident field, $\Psi_{refr.}$ represents the two geometrical optics fields reflected from the upper and lower wedge surfaces and $\Psi_{diff.}$ represents the remainder field due to multiple reflection/refraction at the wedge surfaces and to diffraction at the apex of the wedge.

The incident field, $\Psi_{inc.}$, can be written as (cf. Section 1.4)

$$\Psi_{inc.} = \exp(jk\rho \cos(\Theta-\phi)) = \sum_{m=o}^{\infty} \varepsilon_m j^m \cos m(\Theta-\phi)\, J_m(k\rho)$$

$$\begin{cases} \chi < \phi < \Theta + \pi, & \chi < \Theta < \pi - \chi \\ \chi < \phi < 2\pi - \chi, & \pi - \chi < \Theta < \pi + \chi \\ \Theta - \pi < \phi < 2\pi - \chi, & \pi + \chi < \Theta < 2\pi - \chi \end{cases} \tag{8.7}$$

where Θ is the angle of incidence (cf. Fig. 8.3). The reflected field $\Psi_{refl.}$ is the geometrical optics field which would be generated if the incoming field was incident on an infinite interface:

$$\Psi_{refl.(upper\ surface)} = G_1 \exp(-jk\rho \cos(\pi+2\chi-\Theta-\phi))$$

$$= G_1 \sum_{m=o}^{\infty} \varepsilon_m (-j)^m \cos m(\pi+2\chi-\Theta-\phi)\, J_m(k\rho),$$

$$\chi < \phi < \pi + 2\chi - \Theta \tag{8.8a}$$

$$\Psi_{\text{refl.(lower surface)}} = G_2 \exp(-jk\rho\cos(\pi-2\chi-\theta-\phi))$$

$$= G_2 \sum_{m=o}^{\infty} \varepsilon_m (-j)^m \cos m(\pi-2\chi-\theta-\phi)\ J_m(k\rho),$$

$$3\pi - 2\chi - \theta < \phi < 2\pi - \chi \qquad (8.8b)$$

where G_1 and G_2 are the reflection coefficients given by (1.5), i.e.

$$G_1 = \frac{\sin(\theta-\chi) - (\nu^2-\cos^2(\theta-\chi))^{\frac{1}{2}}}{\sin(\theta-\chi) + (\nu^2-\cos^2(\theta-\chi))^{\frac{1}{2}}}$$

$$G_2 = \frac{\sin(\theta-\pi+\chi) - (\nu^2-\cos^2(\theta-\pi+\chi))^{\frac{1}{2}}}{\sin(\theta-\pi+\chi) + (\nu^2-\cos^2(\theta-\pi+\chi))^{\frac{1}{2}}}$$

Referring back to (8.6), it is seen that the 'incident' and 'reflected' parts of the surface field are the geometrical optics field and they extend from the apex to infinity. On the other hand, the part of the surface field arising from diffraction at the apex of the wedge must necessarily decay with distance away from the apex. If this were not so, the diffracted field re-radiated from the surface would contradict the established results of Keller (1962). Therefore, one can safely assume that this 'diffracted' part of the surface field is important only within some moderate distance of the apex. An expansion for this 'diffracted' part of the surface field, therefore, needs only to represent the field within such a distance.

Bates (1975a, see also Section 1.5.5) indicates that, in the case where the (internal or external) Rayleigh hypotheses (cf. Section 1.4.4) is not valid, the null-field method can still be used to evaluate the surface field. This is because, even when the Rayleigh hypotheses is not valid so that the infinite series

$$f(\rho;\phi) = \sum_{n=o}^{\infty} A_n J_n(k\rho) \begin{matrix}\cos\\ \sin\end{matrix} (n\phi) \qquad (8.10)$$

does not correspond to the actual field behaviour close to the surface of the scatterer, the truncated series

$$\tilde{f}(\rho;\phi) = \sum_{n=o}^{N} A_n J_n(k\rho) \begin{matrix}\cos\\ \sin\end{matrix} (n\phi) \qquad (8.11)$$

can nevertheless present a meaningful solution to the scattering problem (cf. Ikuno and Yasuura 1973). Bates (1975a) further indicates that the scattered field evaluated through the Green's integral (1.95b), using the approximate representation (8.11), can be a useful approximation to the correct field.

8.2 RADIAL NULL-FIELD METHOD APPLIED TO INFINITE PENETRABLE WEDGE DIFFRACTION PROBLEMS

In order to illustrate the feasibility of applying the radial null-field method to the infinite penetrable wedge diffraction problems, a specialised solution is derived in this section. The computational results for this specialised solution are reported in Section 8.3. Comparisons are also made with the results obtained by other authors. The viability of the radial null-field method applied to infinte (conducting) bodies has already been demonstrated in Section 3.3. The possible extension of the specialised methods of solution derived in this section to general penetrable wedge diffraction problems is discussed in Section 8.3.

8.2.1 Preliminaries

As shown in Fig. 8.4, the apex of the wedge is at the origin 0. A point in space is given the polar coordinates $(\rho;\phi)$. The wedge surfaces coincide with the radial lines $\phi = \pm\chi$. The incoming wave is incident symmetrically at $\phi = 180^{\circ}$. Furthermore, the wedge angle is 2χ and the refractive index ν is such that $\gamma \leq \chi$, where γ, (the angle made by the refraction boundaries with respect to the datum line (Fig. 8.4)), is given by the Snell's law (cf. Section 1.2.2) as;

$$\cos\chi = \nu\cos(\chi+\gamma) \tag{8.12}$$

The four regions in Fig. 8.4 are defined as

$\Omega_+ = \Omega_1 \cup \Omega_2$

$\Omega_- = \Omega_3 \cup \Omega_4$

$\Omega_+ : 0<\rho<\infty, \quad \chi<|\phi|<\pi.$

$\Omega_- : 0<\rho<\infty, \quad 0<|\phi|<\chi.$

$\Omega_1 : 0<\rho<\infty, \quad 2\chi<|\phi|<\pi.$

$\Omega_2 : 0<\rho<\infty, \quad \chi<|\phi|<2\chi.$

$$\Omega_3 : 0<\rho<\infty, \qquad \gamma<|\phi|<\chi.$$

$$\Omega_4 : 0<\rho<\infty, \qquad 0<|\phi|<\gamma. \tag{8.13}$$

and the respective (total) fields are:

$$\Psi_1(\varepsilon\Omega_1) = \Psi_{inc.} + \Psi_{diff.1}$$

$$\Psi_2(\varepsilon\Omega_2) = \Psi_{inc.} + \Psi_{refl.} + \Psi_{diff.2}$$

$$\Psi_3(\varepsilon\Omega_3) = \Psi_{refr.3} + \Psi_{diff.3}$$

$$\Psi_4(\varepsilon\Omega_4) = \Psi_{refr.4} + \Psi_{diff.4} \tag{8.14}$$

The incident field $\Psi_{inc.}$ is

$$\Psi_{inc.} = \sum_{n=o}^{\infty} \varepsilon_n (-j)^n \cos n\phi \; J_n(k\rho) \tag{8.15}$$

The reflected field $\Psi_{refl.}$ is

$$\Psi_{refl.} = G \sum_{n=o}^{\infty} \varepsilon_n (-j)^n \cos n(2\chi-\phi) \; J_n(k\rho), \quad \chi<\phi<2\chi$$

$$= G \sum_{n=o}^{\infty} \varepsilon_n (-j)^n \cos n(2\chi+\phi) \; J_n(k\rho), \quad 2\pi-2\chi<\phi<2\pi-\chi \tag{8.16}$$

The refracted field $\Psi_{refr.3}$ is

$$\Psi_{refr.3} = H \sum_{n=o}^{\infty} \varepsilon_n (-j)^n \cos n(\phi-\gamma) \; J_n(\nu k\rho), \quad \gamma<\phi<\chi$$

$$= H \sum_{n=o}^{\infty} \varepsilon_n (-j)^n \cos n(\phi+\gamma) \; J_n(\nu k\rho), \quad 2\pi-\chi<\phi<2\pi-\gamma \tag{8.17}$$

The refracted field $\Psi_{refr.4}$ is

$$\Psi_{refr.4} = H \sum_{n=o}^{\infty} \varepsilon_n (-j)^n \cos n(\phi-\gamma) \; J_n(\nu k\rho)$$

$$+ H \sum_{n=o}^{\infty} \varepsilon_n (-j)^n \cos n(\phi+\gamma) \; J_n(\nu k\rho), \quad |\phi| < \gamma \tag{8.18}$$

where G and H are the respective refraction and reflection coefficients given by

$$G = \frac{\sin\chi - (\nu^2-\cos^2\chi)^{\frac{1}{2}}}{\sin\chi + (\nu^2-\cos^2\chi)^{\frac{1}{2}}}$$

$$H = \frac{2\sin\chi}{\sin\chi + (\nu^2-\cos^2\chi)^{\frac{1}{2}}} \qquad (8.19)$$

There are three important points one must keep in mind when attempting to write down an expansion for the diffracted field:

(i) The reflection and refraction boundaries are only artificial idealisations. The total field must be continuous across these boundaries. Since the geometrical optics fields (8.16) to (8.18) are discontinuous across these boundaries, the diffracted field must compensate for these discontinuities.

(ii) One needs only the surface field and its normal derivative in the null-field formulation.

(iii) The 'diffracted' part of this surface field is only important reasonably close to the apex of the wedge. Therefore, one needs only to model the 'diffracted' field for the moderate value of ρ/λ.

Bearing in mind the three above-mentioned points, the diffracted field in (8.14) can be expanded as

$$\Psi_{diff.1} = \sum_{n=o}^{\infty} E_n \cos n(\pi-\phi)\ J_n(k\rho)$$

$$\Psi_{diff.2} = \sum_{n=o}^{\infty} (A_n \cos n\phi + B_n \sin n\phi)\ J_n(k\rho)$$

$$\Psi_{diff.3} = \sum_{n=o}^{\infty} (F_n \cos n\phi + R_n \sin n\phi)\ J_n(\nu k\rho)$$

$$\Psi_{diff.4} = \sum_{n=o}^{\infty} S_n \cos n\phi\ J_n(\nu k\rho) \qquad (8.20)$$

By matching the total fields and their derivatives across their respective reflection and refraction boundaries, the surface field is then obtained as

$$\Psi_{surface} = \lim_{\phi\to\chi} \sum_{n=o}^{\infty} (A_n + \varepsilon_n(-j)^n + \varepsilon_n(-j)^n G \cos 2n\chi) \cos n\phi\ J_n(k\rho) \qquad (8.21a)$$

or

$$\Psi_{surface} = \lim_{\phi \to \chi} \sum_{n=o}^{\infty} (F_n + \varepsilon_n (-j)^n H \cos n\gamma) \cos n\phi \, J_n(\nu k\rho) \qquad (8.21b)$$

8.2.2 The Outside-In Formulation

Substituting (8.21a) and (8.15) into the null-field equation (1.95a), the latter becomes

$$-j/4 \left[I_1 - I_2 - I_3 + I_4\right] = - \sum_{m=o}^{\infty} \varepsilon_m (-j)^m \cos m\phi \, J_m(k\rho) \qquad (8.22)$$

where

$$I_1 = \int_o^{\infty} \Psi_{surface} \, \partial H_o^{(2)}(kR)/\partial\theta \, (1/r) \, dr \Big|_{\theta=\chi}$$

$$= \sum_{n=o}^{\infty} (A_n + \varepsilon_n (-j)^n + \varepsilon_n (-j)^n G \cos 2n\chi) \cos n\chi \sum_{m=o}^{\infty} m \, \varepsilon_m \sin m(\phi-\chi) \, I_{m,n} \qquad (8.23a)$$

$$I_2 = \int_o^{\infty} \partial\Psi_{surface}/\partial\theta \, H_o^{(2)}(kR) \, (1/r) \, dr \Big|_{\theta=\chi}$$

$$= -\sum_{n=o}^{\infty} (A_n + \varepsilon_n (-j)^n + G \, \varepsilon_n (-j)^n \cos 2n\chi) \, n \sin n\chi \sum_{m=o}^{\infty} \varepsilon_m \cos m(\phi-\chi) \, I_{m,n} \qquad (8.23b)$$

$$I_3 = \int_o^{\infty} \Psi_{surface} \, \partial H_o^{(2)}(kR)/\partial\theta \, (1/r) \, dr \Big|_{\theta=2\pi-\chi}$$

$$= \sum_{n=o}^{\infty} (A_n + \varepsilon_n (-j)^n + G \, \varepsilon_n (-j)^n \cos 2n\chi) \cos n\chi \sum_{m=o}^{\infty} m \, \varepsilon_m \sin m(\chi+\phi) \, I_{m,n} \qquad (8.23c)$$

$$I_4 = \int_o^{\infty} \partial\Psi_{surface}/\partial\theta \, H_o^{(2)}(kR) \, (1/r) \, dr \Big|_{\theta=2\pi-\chi}$$

$$= \sum_{n=o}^{\infty} (A_n + \varepsilon_n (-j)^n + G \, \varepsilon_n (-j)^n \cos 2n\chi) \, n \sin n\chi \sum_{m=o}^{\infty} \varepsilon_m \cos m(\chi+\phi) \, I_{m,n} \qquad (8.23d)$$

where $I_{m,n}$ is defined in Section 3.3.1.

After substituting (8.23) and the value of $I_{m,n}$ into (8.22), the latter becomes

$$-\pi^{-1} \sum_{\substack{m,n=o \\ m\neq n}}^{\infty} \varepsilon_m \cos m\phi \; (A_n + \varepsilon_n(-j)^n + \varepsilon_n(-j)^n \, G \cos 2n\chi)(m^2-n^2)^{-1}$$

$$\exp(-jn\pi/2)(n \sin n\chi \cos m\chi - m \sin m\chi \cos n\chi)$$

$$(\exp(jm\pi/2) \; J_m(k\rho) - \exp(jn\pi/2) \; J_n(k\rho))$$

$$= - \sum_{m=o}^{\infty} \varepsilon_m(-j)^m \, J_m(k\rho) \cos m\phi \qquad (8.24)$$

Since Bessel functions of argument $k\rho$ with $0 < \rho < \infty$ are independent, one can equate the coefficients of $J_\ell(k\rho)$ in (8.24) and obtain

$$\pi^{-1} \sum_{\substack{m=o \\ m\neq \ell}}^{\infty} \varepsilon_m \cos m\phi \; (A_\ell + \varepsilon_\ell(-j)^\ell + \varepsilon_\ell(-j)^\ell \cos 2\ell\chi)(m^2-\ell^2)^{-1}$$

$$\exp(-j\ell\pi/2)(\ell \sin \ell\chi \cos m\chi - m \sin m\chi \cos \ell\chi)(-\exp(j\ell\pi/2))$$

$$+ \pi^{-1} \sum_{\substack{n=o \\ n\neq \ell}}^{\infty} \varepsilon_\ell \cos \ell\phi \; (A_n + \varepsilon_n(-j)^n + \varepsilon_n(-j)^n G \cos 2n\chi)(\ell^2-n^2)^{-1}$$

$$\exp(-jn\pi/2)(n \sin n\chi \cos \ell\chi - \ell \sin \ell\chi \cos n\chi) \exp(j\ell\pi/2)$$

$$= \varepsilon_\ell(-j)^\ell \cos \ell\phi, \qquad \ell=0,1,2, \ldots \infty$$
$$|\phi| < \chi \; . \qquad (8.25)$$

By choosing a suitable value of ϕ, with $|\phi| < \chi$, the set of simultaneous equations (8.25) can be solved, in principle, using an appropriate numerical method. However, certain steps must be taken in order to achieve numerical efficiency and stability of the solution.

(i) As mentioned earlier in Section 1.5.5.5 and reiterated in Section 8.1, the null-field condition, in principle, can be imposed within any part of the scattering body. This argument is reinforced in Section 3.3 where the null-field condition is imposed on a radial line within a perfectly conducting wedge. However, the analysis presented in Section 3.3 is entirely analytical. Moreover, it is mentioned in Section 1.5.5.5 and Section 8.1 that extra considerations must be taken into account when a numerical solution is required.

The numerical efficiency of the solutions improves directly with the value ζ, which is defined by

ζ = area of region within which the null-field condition is imposed/area of interior of scatterer.

The value ζ is always infinitesimal when the conventional (circular) null-field method is invoked for the infinite wedge problem. On the other hand, if one chooses (randomly) a value of ϕ, with $|\phi| < \chi$, for (8.25), then the null-field condition is applied only along a radial line. Such a line has no area so that ζ is zero. Numerical evaluation of (8.25) is then unstable.

One might try to overcome this difficulty by using more than one value of ϕ in (8.25). For instance, if 20 equations are required from (8.25), then the equations chosen are $\phi \in [\phi_1, \phi_2, \phi_3, \phi_4]$ and $\ell \in [0,1,2,3,4]$. Unfortunately, this does not overcome the problem just mentioned, for two reasons. First of all, the value of ζ is still zero, since the area of a finite number of lines is always zero. Also, the random choice of ϕ creates a 'relative convergence' problem. One must then try and find an optimal way for choosing the most suitable values of ϕ.

The most sensible way to overcome the above problem, it seems, is to multiply (8.25) by $\cos \tilde{\ell}\pi\phi/\chi$ and integrate from $-\chi$ to χ. The integration process effectively imposes the null-field condition on the entire interior of the infinite wedge. Furthermore, it transforms the dependence of (8.25) on the variable ϕ and index ℓ to the indices $\tilde{\ell}$ and ℓ. A set of simultaneous equations are then chosen (from 8.25) in the following manner. For the, say, 20 equations required, the index ℓ runs from 0 to 19. Then for each ℓ^*, $\ell^* \in [0,19]$, the index $\tilde{\ell}^*$ is chosen such that the value $\tilde{\zeta}_{\tilde{\ell}}$ is maximum, i.e.

$$\tilde{\zeta}_{\tilde{\ell}^*} = \text{max.} \ |\tilde{\zeta}_{\tilde{\ell}}| \tag{8.26}$$

with the value of $\tilde{\zeta}_{\tilde{\ell}}$ defined by

$$\tilde{\zeta}_{\tilde{\ell}} = |C_{\ell^*,\ell^*}(\tilde{\ell})| / \sum_n |C_{\ell^*,n}(\tilde{\ell})| \tag{8.27}$$

where the $C_{\ell,n}(\tilde{\ell})$ are the coefficients of the A_n in (8.25) with $\ell = \ell^*$.

(ii) It is found that a change of variable in (8.25) can help to rearrange terms which can be summed analytically. Therefore, numerical convergence can be improved as such. The variable change is effected by setting

$$a_o = A_o$$

$$n\, a_n = A_n \quad , \; n \neq 0 \tag{8.28}$$

Implementing (i) and (ii) above in (8.25) and re-arranging terms gives

$$a_o \begin{cases} -2(j)^{\ell} \sin \ell\chi \; \tilde{I}_{\ell,\tilde{\ell}}/\ell, & \ell \neq 0 \\ 2\, I_A \quad , & \ell = 0 \end{cases}$$

$$+ \varepsilon_\ell \sum_{\substack{n=1 \\ n\neq\ell}}^{\infty} a_n \tilde{I}_{\ell,\tilde{\ell}} \exp(j(\ell-n)\pi/2)\, n^2 (\sin n\chi \cos \ell\chi - \ell \sin \ell\chi \cos n\chi)/(\ell^2-n^2)$$

$$- a_\ell \ell^2 (\sin \ell\chi \; I_B - \cos \ell\chi \; I_C/\ell)$$

$$= \pi\varepsilon_\ell (-j)^{\ell} \tilde{I}_{\ell,\tilde{\ell}} - \varepsilon_\ell \tilde{I}_{\ell,\tilde{\ell}} (j)^{\ell} \cos \ell\chi \; I_D$$

$$- G\, \varepsilon_\ell \tilde{I}_{\ell,\tilde{\ell}} (j)^{\ell} \cos \ell\chi \; I_E$$

$$+ \varepsilon_\ell \tilde{I}_{\ell,\tilde{\ell}} (j)^{\ell} \ell \sin \ell\chi \; I_F + G\, \varepsilon_\ell \tilde{I}_{\ell,\tilde{\ell}} (j)^{\ell} \ell \sin \ell\chi \; I_G$$

$$+ (1+G \cos 2\ell\chi)\, \varepsilon_\ell (-j)^{\ell} \ell \sin \ell\chi \; I_B$$

$$- (1+G \cos 2\ell\chi)\, \varepsilon_\ell (-j)^{\ell} \cos \ell\chi \; I_C \tag{8.29}$$

where

$$\tilde{I}_{\ell,\tilde{\ell}} = \frac{\sin(\ell-\tilde{\ell}\pi/\chi)\chi}{\ell - \tilde{\ell}\pi/\chi} + \frac{\sin(\ell+\tilde{\ell}\pi/\chi)\chi}{\ell + \tilde{\ell}\pi/\chi} \tag{8.30a}$$

$$I_A = \sum_{m=1}^{\infty} \sin m\chi \; \tilde{I}_{m,\tilde{\ell}}/m$$

$$= \begin{cases} \chi(\pi-\chi) \; , & \tilde{\ell} = 0 \\ 0 \quad , & \text{otherwise} \end{cases} \tag{8.30b}$$

$$I_B = \sum_{\substack{m=o \\ m\neq\ell}}^{\infty} \varepsilon_m \cos m\chi \; \tilde{I}_{m,\tilde{\ell}}/(m^2-\ell^2)$$

$$\begin{cases} -2\chi/\ell^2 + 3\sin 2\ell\chi/2\ell^3 + (\pi-2\chi)(\cos 2\ell\chi-1)/\ell^2, & \tilde{\ell} = 0 \\ 0, & \tilde{\ell}\pi/\chi = \ell \\ (\pi-2\chi)\cos n\chi\,(\cos 2\ell\chi-1) - 2\chi\cos n\chi & \\ \quad + \cos n\chi\cos 2\ell\chi\,(2\ell/(\ell^2-n^2) - 1/2\ell)/(\ell^2-n^2), & \tilde{\ell}\pi/\chi = n \neq \ell \\ \cos(\tilde{\ell}\pi)(\sin 2\ell\chi/2\ell + (\pi-2\chi)\cos\ell\chi - \pi\cos(\tilde{\ell}\pi))/(\ell^2-(\tilde{\ell}\pi/\chi)^2) & \\ \quad + 2\ell\cos(\tilde{\ell}\pi)\sin 2\ell\chi/(\ell^2-(\tilde{\ell}\pi/\chi)^2)^2, & \text{otherwise} \end{cases} \tag{8.30c}$$

$$I_C = \sum_{\substack{m=o \\ m\neq\ell}}^{\infty} \varepsilon_m \tilde{I}_{m,\tilde{\ell}}\, m \sin m\chi/(m^2-\ell^2)$$

$$\begin{cases} \sin^2\ell\chi/\ell^2 + (\pi-2\chi)\sin 2\ell\chi/\ell, & \tilde{\ell} = 0 \\ \chi(\pi-\chi)\cos\ell\chi, & \tilde{\ell}\pi/\chi = \ell \\ (2\ell(\pi-2\chi)\cos\ell\chi + (\ell^2+3n^2)\sin\ell\chi/(\ell^2-n^2))\cos n\chi\sin\ell\chi/(\ell^2-n^2), & \\ \qquad\qquad \tilde{\ell}\pi/\chi = n \neq \ell & \\ ((\pi-2\chi)\ell\sin 2\ell\chi + \sin^2\ell\chi)\cos(\tilde{\ell}\pi)/(\ell^2-(\tilde{\ell}\pi/\chi)^2) & \\ \quad + (\tilde{\ell}\pi/\chi)^2\sin^2\ell\chi\cos(\tilde{\ell}\pi)/(\ell^2-(\tilde{\ell}\pi/\chi)^2)^2, & \text{otherwise} \end{cases} \tag{8.30d}$$

$$I_D = \sum_{\substack{n=o \\ n\neq\ell}}^{\infty} \varepsilon_n\, n \sin n\chi\,(-1)^n/(\ell^2-n^2)$$

$$= \begin{cases} \chi, & \ell = 0 \\ (-1)^\ell\,(\sin\ell\chi/2\ell + \chi\cos\ell\chi), & \text{otherwise} \end{cases} \tag{8.30e}$$

$$I_E = \sum_{\substack{n=o \\ n\neq\ell}}^{\infty} \varepsilon_n\, n \sin n\chi\cos 2n\chi\,(-1)^n/(\ell^2-n^2)$$

$$= \begin{cases} \chi, & \pi > 3\chi, \quad n = 0 \\ -\pi/6, & \pi = 3\chi, \quad n = 0 \\ \chi-\pi, & \pi < 3\chi, \quad n = 0 \\ (-1)^{\ell} \sin \ell\chi \cos 2\ell\chi/2\ell & \\ \quad -(-1)^{\ell} \chi \cos \ell\chi/2 & \end{cases}$$

$$+ \begin{cases} (-1)^{\ell} 3\chi \cos 3\ell\chi/2, & \pi > 3\chi, \quad n \neq 0 \\ 0 \quad , & \pi = 3\chi, \quad n \neq 0 \\ (-1)^{\ell}(3\chi/2-\pi) \cos 3\ell\chi, & \pi < 3\chi, \quad n \neq 0 \end{cases} \tag{8.30f}$$

$$I_F = \sum_{\substack{n=o \\ n\neq\ell}}^{\infty} \varepsilon_n (-1)^n \cos n\chi/(\ell^2-n^2)$$

$$= \begin{cases} \pi^2/6 - \chi^2/2 \quad , & n = 0 \\ -(-1)^{\ell} \cos \ell\chi/2\ell^2 & \\ -\chi(-1)^{\ell} \sin \ell\chi/\ell, & \text{otherwise} \end{cases} \tag{8.30g}$$

$$I_G = \sum_{\substack{n=o \\ n\neq\ell}}^{\infty} \varepsilon_n (-1)^n \cos n\chi \cos 2n\chi/(\ell^2-n^2)$$

$$= \begin{cases} (\pi^2 - 15\chi^2)/6, & \pi > 3\chi, \quad n = 0 \\ -\pi^2/9, & \pi = 3\chi, \quad n = 0 \\ -(5\pi^2 - 18\chi\pi + 15\chi^2)/6, & \pi < 3\chi, \quad n = 0 \\ -(-1)^{\ell} \cos 2\ell\chi \cos \ell\chi/2\ell^2 & \\ \quad -(-1)^{\ell} \chi \sin \ell\chi/2\ell & \end{cases}$$

$$+ \begin{cases} -3\chi(-1)^{\ell} \sin 3\ell\chi/2\ell, & \pi > 3\chi, \quad n \neq 0 \\ 0 \quad , & \pi = 3\chi, \quad n \neq 0 \\ (2\pi-3\chi) \sin 3\ell\chi/2\ell, & \pi < 3\chi, \quad n = 0 \end{cases} \tag{8.30h}$$

8.2.3 The Scattered Fields

The field scattered by the infinite penetrable wedge can be determined from the Green's integral (1.95b) as

$$\Psi_{SC}(P) = -\pi^{-1} \sum_{\substack{m,n=o \\ m\neq n}}^{\infty} \varepsilon_m \cos m\phi \; (a_n(-j)^n + \varepsilon_n(-1)^n + G\,\varepsilon_n(-1)^n \cos 2n\chi)$$

$$(m^2-n^2)^{-1} \; (n \sin n\chi \cos m\chi - m \sin m\chi \cos n\chi)$$

$$(\exp(jm\pi/2)\, J_m(k\rho) - \exp(jn\pi/2)\, J_n(k\rho))$$

$$= -\pi^{-1} \sum_{m=o}^{\infty} \varepsilon_m \cos m\phi \, \exp(jm\pi/2) \, Jm(k\rho) \sum_{\substack{n=o \\ n\neq m}}^{\infty} a_n(-j)^n \, (m^2-n^2)^{-1}$$

$$(n \sin n\chi \cos m\chi - m \sin m\chi \cos n\chi)$$

$$- \chi \, J_o(k\rho)/\pi$$

$$- 2/\pi \sum_{m=1}^{\infty} \cos m\phi \, \exp(jm\pi/2) \, J_m(k\rho)((-1)^m \sin 2m\chi/2m + \chi(-1)^m$$

$$\cos m\chi) \cos m\chi$$

$$+ 2/\pi \sum_{m=1}^{\infty} \cos m\phi \, \exp(jm\pi/2) \, J_m(k\rho) \, m \sin m\chi \, (-(-1)^m \cos m\chi/2m^2$$

$$-\chi(-1)^m \sin m\chi/m)$$

$$- G/\pi \, J_o(k\rho) \begin{cases} \chi, & \pi > 3\chi \\ -\chi/2, & \pi = 3\chi \\ -\pi+\chi, & \pi < 3\chi \end{cases}$$

$$- 2/\pi \sum_{m=1}^{\infty} \cos m\phi \, \exp(jm\pi/2) \, J_m(k\rho) \, G \cos m\chi$$

$$\Big((-1)^m \, (\sin m\chi - \sin 3m\chi)/4m - \chi(-1)^m \cos m\chi/2$$

$$+ \begin{cases} 3\chi(-1)^m \cos 3m\chi/2, & \pi > 3\chi \\ 0, & \pi = 3\chi \\ -(2\pi-3\chi)(-1)^m \cos 3m\chi/2, & \pi < 3\chi \end{cases} \Big)$$

$$+ 2/\pi \sum_{m=1}^{\infty} \cos m\phi \, \exp(jm\pi/2) \, J_m(k\rho) \, G \, m \sin m\chi$$

$$\Big[-(-1)^m \, (\cos m\chi + \cos 3m\chi)/4m^2 - \chi(-1)^m \sin m\chi/2m$$

$$+ \begin{cases} -3\chi(-1)^m \sin 3m\chi/2m, & \pi > 3\chi \\ 0 \quad , & \pi = 3\chi \\ (2\pi-3\chi)(-1)^m \sin 3m\chi/2m, & \pi < 3\chi \end{cases} \Bigg]$$

$$+ 1/\pi \sum_{n=1}^{N} a_n J_n(k\rho)\, n \sin n\chi\, ((\cos n(\phi-\chi) + \cos n(\phi+\chi))/4n^2$$

$$- ((\pi-\phi+\chi) \sin n(\phi-\chi) + (\pi-\phi-\chi) \sin n(\phi+\chi))/2n)$$

$$+ \chi/\pi\, a_o J_o(k\rho)$$

$$- 1/\pi \sum_{n=1}^{N} a_n J_n(k\rho) \cos n\chi((\sin n(\phi-\chi) - \sin n(\phi+\chi))/4n$$

$$- ((\pi-\phi+\chi) \cos n(\phi-\chi) - (\pi-\phi-\chi) \cos n(\phi+\chi))/2)$$

$$+ 2/\pi \sum_{n=1}^{\infty} (-j)^n J_n(k\rho)\, n \sin n\chi\, ((\cos n(\phi-\chi) + \cos n(\phi+\chi))/4n^2$$

$$- ((\pi-\phi+\chi) \sin n(\phi-\chi) + (\pi-\phi-\chi) \sin n(\phi+\chi))/2n)$$

$$+ \chi/\pi\, J_o(k\rho)$$

$$- 2/\pi \sum_{n=1}^{\infty} (-j)^n J_n(k\rho) \cos n\chi((\sin n(\phi-\chi) - \sin n(\phi+\chi))/4n$$

$$- ((\pi-\phi+\chi) \cos n(\phi-\chi) - (\pi-\phi-\chi) \cos n(\phi+\chi))/2)$$

$$+ 2/\pi \sum_{n=1}^{\infty} G\, (-j)^n \cos 2n\chi\, J_n(k\rho)\, n \sin n\chi\, ((\cos n(\phi-\chi) + \cos n(\phi+\chi))/4n^2$$

$$- ((\pi-\phi+\chi) \sin n(\phi-\chi) + (\pi-\phi-\chi) \sin n(\phi+\chi))/2n)$$

$$+ G\, \chi/\pi\, J_o(k\rho)$$

$$- 2/\pi \sum_{h=1}^{\infty} (-j)^n G \cos 2n\chi\, J_n(k\rho) \cos n\chi((\sin n(\phi-\chi) - \sin n(\phi+\chi))/4n$$

$$- ((\pi-\phi+\chi) \cos n(\phi-\chi) - (\pi-\phi-\chi) \cos n(\phi+\chi))/2), \quad P \in \Omega_+$$

(8.31)

8.2.4 Far Scattered Fields

The far scattered field of an infinite wedge can be determined by substituting the asymptotic forms for the Bessel functions (1.32) into (8.31), i.e.

$$\Psi_{sc}(P) = -\pi^{-1} \sum_{\substack{m,n=o \\ m\neq n}}^{\infty} \varepsilon_m \cos m\phi \; (a_n(-j)^n + \varepsilon_n(-1)^n + G\,\varepsilon_n(-1)^n \cos 2n\chi)(m^2-n^2)^{-1} \; (n \sin n\chi \cos m\chi - m \sin m\chi \cos n\chi)(\exp(jm\pi/2)\, J_m(k\rho) - \exp(jn\pi/2)\, J_n(k\rho))$$

$$\simeq -\pi^{-1} \sum_{\substack{m,n=o \\ m\neq n}}^{\infty} \varepsilon_m \cos m\phi \; (a_n(-j)^n + G\,\varepsilon_n(-1)^n \cos 2n\chi + \varepsilon_n(-1)^n)(m^2-n^2)^{-1} \; (n \sin n\chi \cos m\chi - m \sin m\chi \cos n\chi)$$

$$(\exp(jm\pi/2)(1/2\pi k\rho)^{\frac{1}{2}} (\exp(j(k\rho - m\pi/2 - \pi/4)) + \exp(-j(k\rho - m\pi/2 - \pi/4)))$$

$$- \exp(jn\pi/2)(1/2\pi k\rho)^{\frac{1}{2}} (\exp(j(k\rho - n\pi/2 - \pi/4)) + \exp(-j(k\rho - n\pi/2 - \pi/4)))$$

$$= -1/2\pi(2/\pi k\rho)^{\frac{1}{2}} \sum_{\substack{m,n=o \\ m\neq o}}^{\infty} \varepsilon_m \cos m\phi \; (a_n(-j)^n + G\,\varepsilon_n(-1)^n \cos 2n\chi + \varepsilon_n(-1)^n)(m^2-n^2)^{-1} (n \sin n\chi \cos m\chi - m \sin m\chi \cos n\chi)$$

$$(\exp(jk\rho)\exp(-j\pi/4) + \exp(-jk\rho)\exp(jm\pi)\exp(j\pi/4) - \exp(jk\rho)\exp(-j\pi/4) - \exp(-jk\rho)\exp(jn\pi)\exp(j\pi/4))$$

$$= (1/k\rho)^{\frac{1}{2}} \exp(-jk\rho)(-1/2\pi)(2/\pi)^{\frac{1}{2}} \exp(j\pi/4) \sum_{\substack{m,n=o \\ m\neq o}}^{\infty} \varepsilon_m \cos m\phi \; (a_n(-j)^n + G\,\varepsilon_n(-1)^n \cos 2n\chi + \varepsilon_n(-1)^n)(m^2-n^2)^{-1}$$

$$(\exp(jm\pi) - \exp(jn\pi))(n \sin n\chi \cos m\chi - m \sin m\chi \cos n\chi)$$

$$= (1/k\rho)^{\frac{1}{2}} \exp(-jk\rho)(-1/2\pi)(2/\pi)^{\frac{1}{2}} \exp(j\pi/4)$$

$$\Bigg[- (a_o + G + 1) \begin{cases} -\chi, & \phi+\chi>\pi \\ (\phi-\chi)/2, & \phi+\chi=\pi \\ \pi-\chi, & \phi+\chi<\pi \end{cases} - \chi (a_o + G + 1)$$

$$+ \sum_{n=1}^{\infty} (a_n(-j)^n + G\,\varepsilon_n(-1)^n \cos 2n\chi + \varepsilon_n(-1)^n)\, n \sin n\chi$$

$$\Bigg((-1)^n (\cos n(\phi-\chi) + \cos n(\phi+\chi))/4n^2 -$$

$$\begin{cases} (-1)^n ((\phi-\chi) \sin n(\phi-\chi) + (\phi+\chi) \sin n(\phi+\chi))/2n, & \phi+\chi>\pi \\ (-1)^n (\phi-\chi) \sin n(\phi-\chi)/2n, & \phi+\chi=\pi \\ (-1)^n ((\phi-\chi) \sin n(\phi-\chi) - (2\pi-\phi-\chi) \sin n(\phi+\chi))/2n, & \phi+\chi<\pi \end{cases} \Bigg)$$

$$- \sum_{n=1}^{\infty} (a_n(-j)^n + G\,\varepsilon_n(-1)^n \cos 2n\chi + \varepsilon_n(-1)^n) \cos n\chi \Bigg((-1)^n$$

$$(\sin n(\phi-\chi) - \sin n(\phi+\chi))/4n -$$

$$\begin{cases} (-1)^n ((\phi-\chi) \cos n(\phi-\chi) - (\phi+\chi) \cos n(\phi+\chi))/2, & \phi+\chi>\pi \\ (-1)^n (\phi-\chi) \cos n(\phi-\chi)/2, & \phi+\chi=\pi \\ (-1)^n ((\phi-\chi) \cos n(\phi-\chi) + (2\pi-\phi-\chi) \cos n(\phi+\chi))/2, & \phi+\chi<\pi \end{cases} \Bigg) \Bigg] \tag{8.32}$$

8.2.5 The Inside-Out Formulation

The radial null-field method described in Section 8.2.2, where the surface field is taken from outside the wedge (8.21a) and the null-field condition is imposed inside the wedge (1.95a) is called the Outside-In formulation. On the other hand, an inside-out formulation can be derived in a similar manner, taking the surface field from inside the wedge (8.21b) and imposing the null-field condition outside the wedge (1.95c).

On substituting (8.21b) into (1.95c), and manipulating in a way similar to the procedure described in Section 8.2.2, one arrives at

$$f_o \begin{cases} -2\,(j)^{\ell} \sin \ell\chi\, \tilde{I}^*_{\ell,\tilde{\ell}}/\ell & \ell \neq 0 \\ 2\,\tilde{I}_A & \ell = 0 \end{cases}$$

$$+ \varepsilon_\ell \sum_{\substack{n=1 \\ n\neq\ell}}^{\infty} f_n \, (\tilde{I}^*_{\ell,\tilde{\ell}} \exp(j(\ell-n)\pi/2) \, n^2 \, (\sin n\chi \cos \ell\chi - \ell \sin \ell\chi \cos n\chi/n) / (\ell^2-n^2)$$

$$- f_\ell \, \ell^2 \, (\sin \ell\chi \, \tilde{I}_B - \cos \ell\chi \, \tilde{I}_C/\ell)$$

$$= -H \, \varepsilon_\ell \, \tilde{I}^*_{\ell,\tilde{\ell}} \, (j)^\ell \cos \ell\chi \, \tilde{I}_E + H \, \varepsilon_\ell \, \tilde{I}^*_{\ell,\tilde{\ell}} (j)^\ell \, \ell \sin \ell\chi \, \tilde{I}_G$$

$$+ H \cos \ell\gamma \, \varepsilon_\ell (-j)^\ell \, \ell \sin \ell\chi \, I_B - H \cos \ell\gamma \, \varepsilon_\ell (-j)^\ell \cos \ell\chi \, I_C \qquad (8.33)$$

$$\tilde{I}^*_{\ell,\tilde{\ell}} = \frac{\cos(\ell-\tilde{\ell}\pi/(\pi-\chi))\pi \sin(\ell-\tilde{\ell}\pi/(\pi-\chi))(\pi-\chi)}{\ell - \tilde{\ell}\pi/(\pi-\chi)}$$

$$+ \frac{\cos(\ell+\tilde{\ell}\pi/(\pi-\chi))\pi \sin(\ell+\tilde{\ell}\pi/(\pi-\chi))(\pi-\chi)}{\ell + \tilde{\ell}\pi/(\pi-\chi)} \qquad (8.34a)$$

$$\tilde{I}_A = \sum_{m=1}^{\infty} \sin m\chi \, \tilde{I}^*_{m,\ell}/m$$

$$= \begin{cases} -\chi(\pi-\chi) \, , & \tilde{\ell} = 0 \\ 0 \, , & \text{otherwise} \end{cases} \qquad (8.34b)$$

$$\tilde{I}_B = \sum_{\substack{m=0 \\ m\neq\ell}}^{\infty} \varepsilon_m \, \tilde{I}^*_{m,\tilde{\ell}} \cos m\chi/(m^2-\ell^2)$$

$$= \begin{cases} -2(\pi-\chi)/\ell^2 - 3 \sin 2\ell\chi/2\ell^3 - (\pi-2\chi)(\cos 2\ell\chi - 1)/\ell^2 \, , & \tilde{\ell} = 0 \\ 0 \, , & \tilde{\ell}\pi/(\pi-\chi) = \ell \\ -(\pi-2\chi) \cos n\chi(\cos 2\ell\chi - 1) - 2(\pi-\chi) \cos n\chi & \\ \quad - \cos n\chi \cos 2\ell\chi(2\ell/(\ell^2-n^2) - 1/2\ell)/(\ell^2-n^2), & \tilde{\ell}\pi/(\pi-\chi) = n\neq\ell \\ -\cos(\tilde{\ell}\pi^2/(\pi-\chi))(\sin 2\ell\chi/2\ell + (\pi-2\chi) \cos 2\ell\chi)/(\ell^2-(\tilde{\ell}\pi/(\pi-\chi))^2) & \\ \quad - 2\pi \cot(\tilde{\ell}\pi^2/(\pi-\chi)) \sin(\tilde{\ell}\pi\chi/(\pi-\chi))/(\ell^2-(\tilde{\ell}\pi/(\pi-\chi))^2) & \\ \quad + 2\ell \cos \ell\chi \cos(\ell-\tilde{\ell}\pi/(\pi-\chi))\pi \sin(\ell-\tilde{\ell}\pi/(\pi-\chi))(\pi-\chi) & \\ \quad /(\ell^2-(\tilde{\ell}\pi/(\pi-\chi))^2) \, , & \text{otherwise} \end{cases} \qquad (8.34c)$$

$$\tilde{I}_C = \sum_{\substack{m=o \\ m\neq\ell}}^{\infty} \varepsilon_m \tilde{I}^*_{m,\tilde{\ell}}\, m \sin m\chi/(m^2-\ell^2)$$

$$= \begin{cases} -\sin^2 \ell\chi/\ell^2 - (\pi-2\chi)\sin 2\ell\chi/\ell\,, & \tilde{\ell} = 0 \\ -\chi(\pi-\chi)\cos\ell\chi\,, & \tilde{\ell}\pi/(\pi-\chi) = \ell \\ -(2\ell(\pi-2\chi)\cos\ell\chi + (\ell^2+3n^2)\sin\ell\chi/(\ell^2-n^2)) & \\ \qquad \cos n\chi \sin\ell\chi/(\ell^2-n^2), & \tilde{\ell}\pi/(\pi-\chi) = n \neq \ell \\ -\cos(\tilde{\ell}\pi^2/(\pi-\chi))\cos(\tilde{\ell}\pi)(\sin^2\ell\chi + \ell(\pi-2\chi)\sin 2\ell\chi)/(\ell^2-(\tilde{\ell}\pi/(\pi-\chi))^2) & \\ \qquad + 4(\tilde{\ell}\pi/(\pi-\chi))^2 \sin\ell\chi\cos(\ell-\tilde{\ell}\pi/(\pi-\chi))\pi & \\ \qquad \sin(\ell-\tilde{\ell}\pi/(\pi-\chi))(\pi-\chi)/(\ell^2-(\tilde{\ell}\pi/(\pi-\chi))^2)^2\,, & \text{otherwise} \end{cases}$$

(8.34d)

$$\tilde{I}_E = \sum_{\substack{n=o \\ n\neq\ell}}^{\infty} \varepsilon_n\, n \sin n\chi \cos n\gamma\, (-1)^n/(\ell^2-n^2)$$

$$= \begin{cases} \pi - \chi\,, & n = 0 \\ \sin\ell\chi\cos\ell\gamma/2\ell + (\pi-\gamma-\chi)\cos\ell(\chi+\gamma)/2 & \\ \qquad -(\pi-\chi+\gamma)\cos\ell(\chi-\gamma)/2\,, & n \neq 0 \end{cases} \qquad (8.34e)$$

$$\tilde{I}_G = \sum_{\substack{n=o \\ n=\ell}}^{\infty} \varepsilon_n (-1)^n \cos n\chi \cos n\gamma/(\ell^2-n^2)$$

$$= \begin{cases} \pi^2/3 - \pi\chi + (\gamma^2+\chi^2)/2\,, & n = 0 \\ -\cos\ell\chi\cos\ell\chi/2\ell^2 + (\pi-\gamma-\chi)\sin\ell(\chi+\gamma)/2\ell & \\ \qquad +(\pi-\chi+\gamma)\sin\ell(\chi-\gamma)/2\ell\,, & n \neq 0 \end{cases} \qquad (8.34f)$$

8.2.6 Accelerated Outside-In Formulation

Meaningful results have been obtained from the formulation described previously in Section 8.2.2. Reasonable numerical efficiency has also been achieved. However, the calculation of the coefficient matrix of (8.29) is somewhat (CPU-) time consuming. In this section, an accelerated formulation is described.

This new formulation is obtained by substituting the integral formula

$$J_n(k\rho) = (-j)^n/2\pi \int_o^{2\pi} \exp(jk\rho\cos\alpha) \cos n\alpha \, d\alpha \tag{8.35}$$

for the Bessel function $J_n(k\rho)$ into (8.21a). Comparing

$$\Psi_{surface} = \lim_{\phi\to\chi} \sum_{n=o}^{\infty} z_n \cos n\phi \, J_n(k\rho)$$

$$= \lim_{\phi\to\chi} \sum_{n=o}^{\infty} z_n \cos n\phi \int_o^{2\pi} (-j)^n/2\pi \exp(jk\rho\cos\alpha) \cos n\alpha \, d\alpha$$

$$= \lim_{\phi\to\chi} \sum_{n=o}^{\infty} 1/4\pi \, z_n(-j)^n \int_o^{2\pi} \exp(jk\rho \cos\alpha)(\cos n(\phi+\alpha) + \cos n(\alpha-\phi)) \, d\alpha$$

$$= \lim_{\phi\to\chi} 1/4\pi \sum_{n=o}^{\infty} z_n(-j)^n \int_o^{2\pi} (\exp(jk\rho\cos(\alpha-\phi)) + \exp(jk\rho\cos(\alpha+\phi))) \cos n\alpha \, d\alpha$$

$$= \lim_{\phi\to\chi} \int_o^{2\pi} 1/2 \left[\exp(jk\rho\cos(\alpha-\phi)) + \exp(jk\rho\cos(\alpha+\phi))\right] 1/2\pi \sum_{n=o}^{\infty} z_n(-j)^n \cos n\alpha \, d\alpha$$

$$= \lim_{\phi\to\chi} \int_o^{2\pi} 1/2 \left[\exp(jk\rho\cos(\alpha-\phi)) + \exp(jk\rho\cos(\alpha+\phi))\right] z(\alpha) \, d\alpha$$

$$= \lim_{\phi\to\chi} \int_o^{2\pi} \sum_{n=o}^{\infty} \varepsilon_n (j)^n \cos n\alpha \cos n\phi \, J_n(k\rho) \, z(\alpha) \, d\alpha$$

$$= \lim_{\phi\to\chi} \sum_{n=o}^{\infty} \varepsilon_n (j)^n \int_o^{2\pi} z(\alpha) \cos n\alpha \, d\alpha \cos n\phi \, J_n(k\rho) \tag{8.36}$$

with (8.21a), indicates that $z(\alpha)$ must be given by

$$z(\alpha) = A(\alpha) + \delta(\alpha-\pi) + G \, \delta(\alpha-\pi+2\chi) \tag{8.37}$$

Substituting (8.36) and (8.37) into (1.95c) and manipulating in a similar way to the procedure described in previous sections, gives

$$-1/\pi \int_0^{2\pi} d\alpha\ z(\alpha) \sum_{\ell=1}^{4} \tilde{J}_\ell(\alpha) = -\exp(-jk\rho\cos\phi), \qquad |\phi|<\chi \tag{8.38}$$

where

$$\tilde{J}_1(\alpha) = -J_o(k\rho) \begin{cases} -(\pi-\alpha+\chi)/2, & \alpha>\chi \\ 0, & \alpha=\chi \\ (\pi-\chi+\alpha)/2, & \alpha<\chi \end{cases}$$

$$+ J_o(k\rho) \begin{cases} (\pi-\chi-\alpha+2\pi)/2, & \alpha>2\pi-\chi \\ 0, & \alpha=2\pi-\chi \\ (\pi-\chi-\alpha)/2, & \alpha<2\pi-\chi \end{cases}$$

$$- \sum_{m=1}^{\infty} \varepsilon_m \cos m\phi \cos m\chi (j)^m J_m(k\rho)$$

$$\left[-\sin m\chi \cos m\alpha/4m + \begin{cases} -(\pi-\alpha+\chi)\cos(\alpha-\chi)/2, & \alpha>\chi \\ 0, & \alpha=\chi \\ (\pi-\chi+\alpha)\cos m(\chi-\alpha)/2, & \alpha<\chi \end{cases} \right.$$

$$\left. + \begin{cases} (\pi-\chi-\alpha+2\pi)\cos m(\chi+\alpha)/2, & \alpha>2\pi-\chi \\ 0, & \alpha=2\pi-\chi \\ (\pi-\chi-\alpha)\cos m(\chi+\alpha)/2, & \alpha<2\pi-\chi \end{cases} \right] \tag{8.39a}$$

$$\tilde{J}_2(\alpha) = \sum_{m=1}^{\infty} \varepsilon_m \cos m\phi (j)^m m \sin m\chi J_m(k\rho)$$

$$\left[\cos m\chi \cos m\alpha/4m^2 + \begin{cases} -(\pi-\alpha+\chi)\sin m(\alpha-\chi)/2m, & \alpha>\chi \\ 0, & \alpha=\chi \\ -(\pi-\chi+\alpha)\sin m(\chi-\alpha)/2m, & \alpha<\chi \end{cases} \right.$$

$$\left. + \begin{cases} -(\pi-\chi-\alpha+2\pi)\sin(\alpha+\chi)/2m, & \alpha>2\pi-\chi \\ 0, & \alpha=2\pi-\chi \\ -(\pi-\chi-\alpha)\sin(\chi+\alpha)/2m, & \alpha<2\pi-\chi \end{cases} \right] \tag{8.39b}$$

$$\tilde{J}_3(\alpha) = - \sum_{n=1}^{\infty} \varepsilon_n (j)^n \cos n\alpha \; n \sin n\chi \; J_n(k\rho)$$

$$\left[\cos n\phi \cos n\chi/4n^2 - (\pi-\chi+\phi) \sin n(\chi-\phi)/2n \right.$$

$$\left. - (\pi-\chi-\phi) \sin n(\chi+\phi)/2n \right] \qquad (8.39c)$$

$$\tilde{J}_4(\alpha) = J_o(k\rho)((\pi-\chi+\phi)/2 + (\pi-\phi-\chi)/2) + \sum_{n=1}^{\infty} \varepsilon_n (j)^n \cos n\alpha \cos n\chi \; J_n(k\rho)$$

$$\left[- \sin n\chi \cos n\phi/4n + (\pi-\chi+\phi) \cos n(\chi-\phi)/2 + (\pi-\phi-\chi) \cos n(\chi+\phi)/2\right]$$

$$(8.39d)$$

Further manipulation of (8.38) leads to

$$\sum_{m=o}^{\infty} \varepsilon_m (j)^m \left[\int_{\chi}^{2\pi-\chi} d\alpha \; A(\alpha) \cos m\alpha + G \cos m(\pi-2\chi) \right] \cos m\phi \; J_m(k\rho) = 0$$

$$|\phi| < \chi$$

$$0 < \rho < \infty \qquad (8.40)$$

Since all Bessel functions in (8.40) must be independent, one obtains

$$\int_{\chi}^{2\pi-\chi} d\alpha \; A(\alpha) \cos m\alpha = - G \cos m(\pi-2\chi) \qquad m = 0, 1, 2, \ldots \infty \qquad (8.41)$$

8.3 APPRAISAL OF RESULTS

Numerical results have been obtained using the formulations described in Section 8.2 for penetrable wedge solutions. In the first instance, a wedge of angle $2\chi = 40^{\circ}$ and refractive index $\nu = 1.2$ is examined. The E-polarised plane wave is incident at an angle $\phi = 180^{\circ}$. Fig. 8.5 shows the numerical convergence of the surface field expansion coefficients A_o, A_1 and A_2. It is clear that these coefficients converge very well as the number (N) of expansion coefficients is increased. Figs 8.6 and 8.7 are the plots of the magnitudes and phases, respectively, of the fields diffracted by the wedge. The fields are plotted in the back scattering region ($\phi = 180^{\circ}$, 150°, and 135°). It is seen that they closely resemble outgoing waves because the phase varies very nearly as $-k\rho$ with distance from the apex. The fact that the diffracted field becomes more oscillatory with decreasing values of ϕ also corresponds to physical intuition. One would expect stronger interference of purely scattered and quasi-surface-wave fields closer to the wedge surface. In order to evaluate the numerical accuracy of the solution obtained, Fig. 8.8 displays the error in satisfying the null-field condition (1.95a) with respect to ρ/λ. It is seen that the error is well under 3% for $\rho/\lambda \lesssim 1$. The error increases with ρ/λ, as is to be expected since the surface field formulation is only accurate close to the apex. Figs 8.9 to 8.14 are plots of the magnitudes and phases of fields diffracted by wedges of angle 60° and refractive indices of 1.2, 1.3 and 1.4 respectively. They all seem to resemble outgoing waves.

While Figs 8.1 to 8.14 show results obtained by the numerical evaluation of the outside-in formulation described in Section 8.2.2, attempts have also been made to obtain a solution from the inside-out formulation described in Section 8.2.5. Unfortunately, the latter procedure is much more unstable than the outside-in formulation and is only satisfactory when the order of the difference between ν and unity is 0.01 or less. Fig. 8.15 shows surface fields evaluated using both the outside-in and inside-out formulations for a wedge of angle $2\chi = 10^{\circ}$ and refractive index 1.01. The agreement is reasonably clear. A further observation is that the condition number, as defined in (1.67), for the inside-out formulation is at least an order of magnitude higher than that of the outside-in formulation, even for such a small value of $(\nu-1)$.

It is also worth mentioning that the results obtained from the accelerated formulation described in Section 8.2.6 agree to within 1% with the results obtained from the original formulation (described in Section 8.2.2).

In order to confirm the validity of the work described in this Chapter, a comparison between results so evaluated and those obtained by other authors is shown in Figs 8.16 to 8.18. In Fig. 8.16, the wedge angle is 90° while the refractive index is 1.1. The total field outside the wedge at $\rho = 10\lambda$ is plotted from (a) Kaminetzky and Keller's (1975) formulation, (b) Rawlins (1977a) formulation and (c) the radial null-field method with the outside-in formulation (called NULL-IN from now on). It is seen that the agreement is close, except near the reflection boundaries. Fig. 8.17 shows this more clearly by plotting only the diffracted fields.

The confidence in the viability of the results presented in this Chapter is enhanced by the following facts:

(i) The diffracted fields are seen to resemble outgoing waves.

(ii) The diffraction pattern corresponds to that of Kaminetzky and Keller (1975) and Rawlins (1977a).

However, it would be beneficial if one could make further comparisons. Unfortunately, the parallel-plate experiment described in Section 9.2 has not proved capable of producing data of sufficient accuracy for the reasons given in Section 9.2. On the other hand, there is another available means of comparison. The field back-scattered by a wedge-cylinder, as described in Chapter 6, can be expected to resemble that diffracted by a corresponding infinite wedge, provided that the dimensions of the wedge-cylinder are large enough compared to the wavelength. A comparison between the back-scattered fields from a wedge-cylinder and from an infinite wedge are shown in Fig. 8.18. The infinite wedge fields are calculated from (a) Kaminetzky and Keller's (1975) formulation and (b) NULL-IN. Because of the limitations imposed by the large CPU time required for the numerical integration in the wedge-cylinder formulation, it is only possible to calculate diffracted fields for a wedge-cylinder of quite small dimensions and refractive index very close to unity. It is worth noting that the value of the refractive index ($\nu = 1.01$) used allows accurate comparison with Kaminetzky and Keller's (1975) results since the accuracy of the latter increases as $(\nu-1)$ decreases. The wedge angle is 40 and the diffraction patterns are plotted at $\rho = 10\lambda$ and $a = 0.5\lambda$, where a is the radius of the circular part of the wedge-cylinder, as shown in Fig. 6.1. Despite the small dimensions of the wedge cylinder, Fig. 8.18 indicates that

there is indeed close agreement of the three solutions in directions close to the back-scattered direction.

Generally speaking, the results presented in this section are very encouraging and demonstrate the viability of the reported procedure. In Chapter 10 this thesis is concluded with a discussion of possible extensions of the technique to handle incident waves of arbitrary polarisations and incident angles.

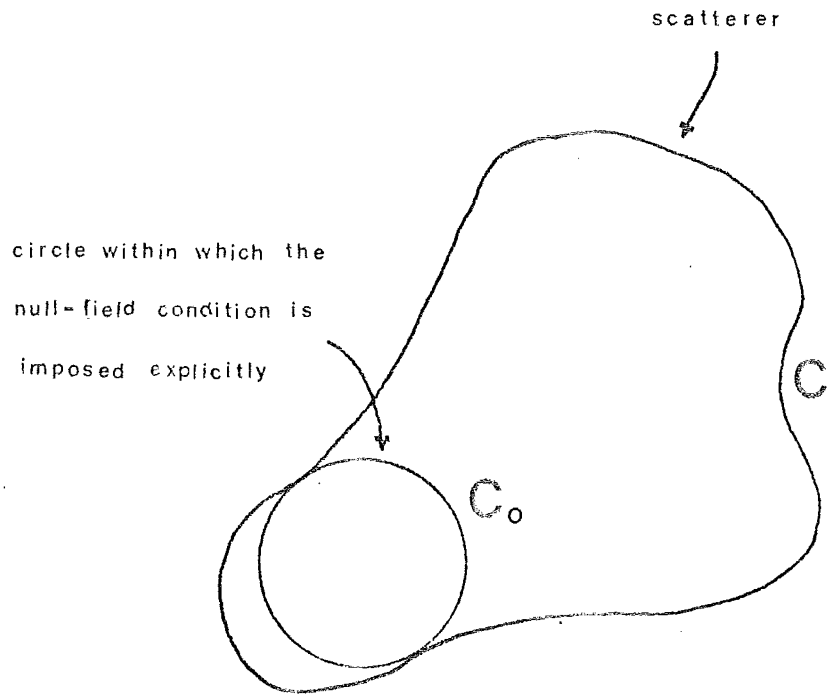

FIGURE 8.1 Circular null-field method. The null-field condition is imposed explicitly within a circle inscribed by the scatterer.

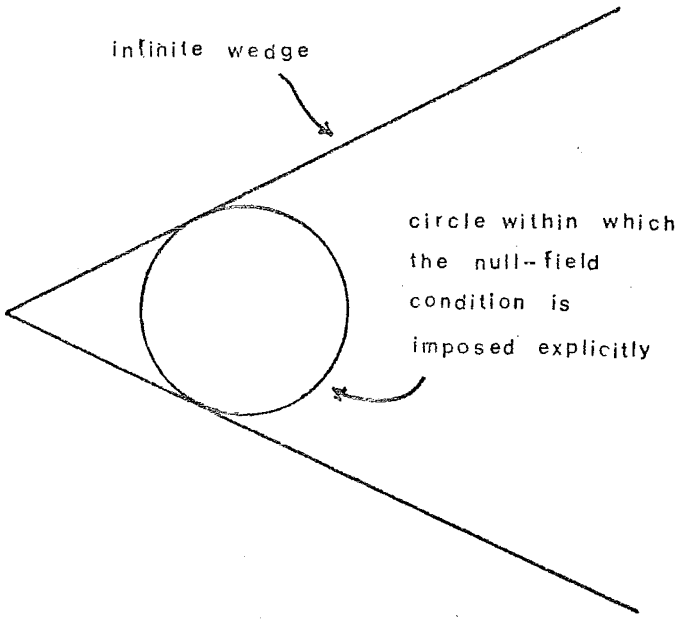

FIGURE 8.2 Circular null-field method applied to an infinite penetrable wedge. The value of ζ defined by (1.102) is always infinitesimal.

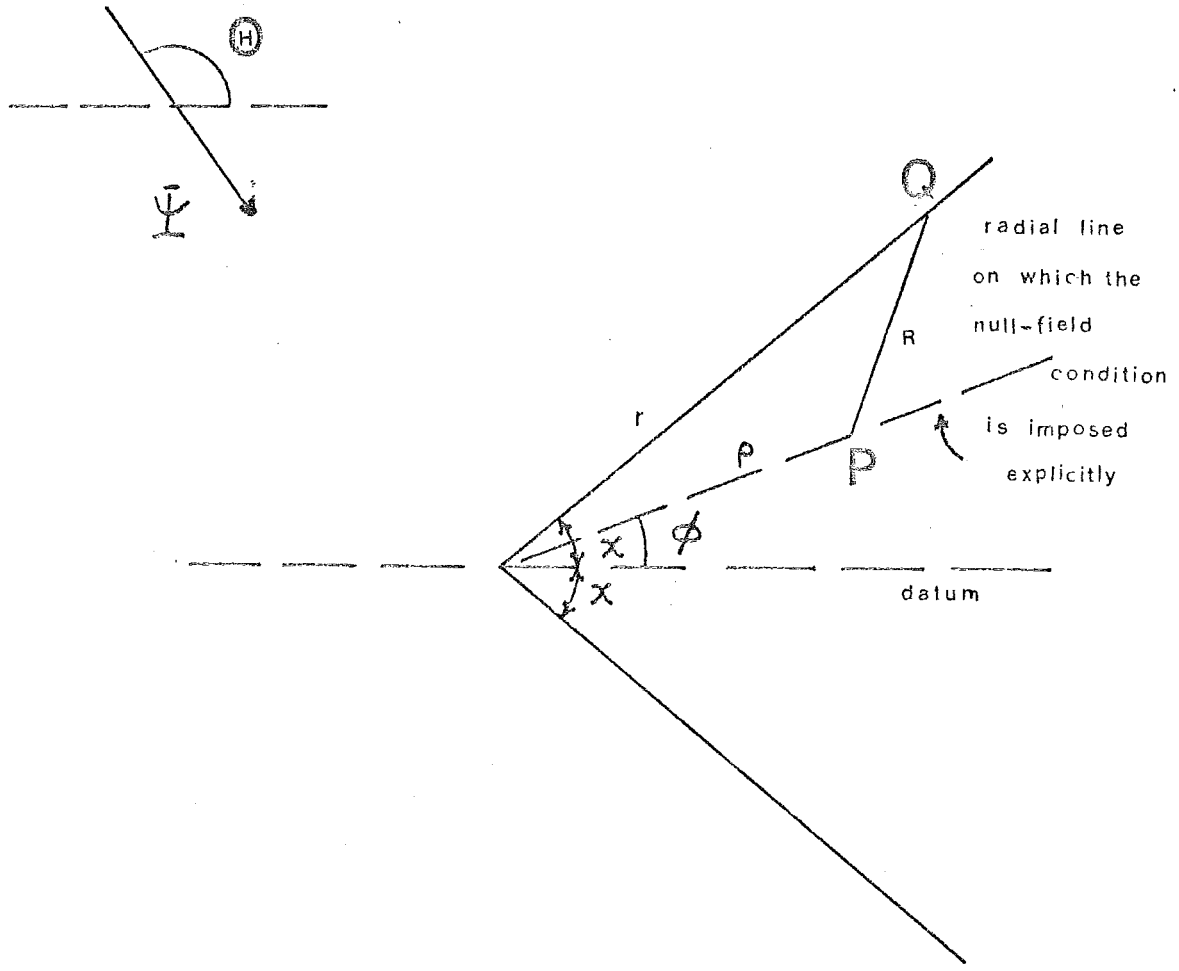

FIGURE 8.3 Radial null-field method. The null-field condition is imposed on radial lines inside the infinite wedge. An arbitrary point P on this line has the coordinate $(\rho;\phi)$ while an arbitrary point Q on the wedge surface has the coordinate $(r;\pm\chi)$. Ψ_- is the total field inside the wedge Ω_- and Ψ_+ is the total field outside the wedge Ω_+.

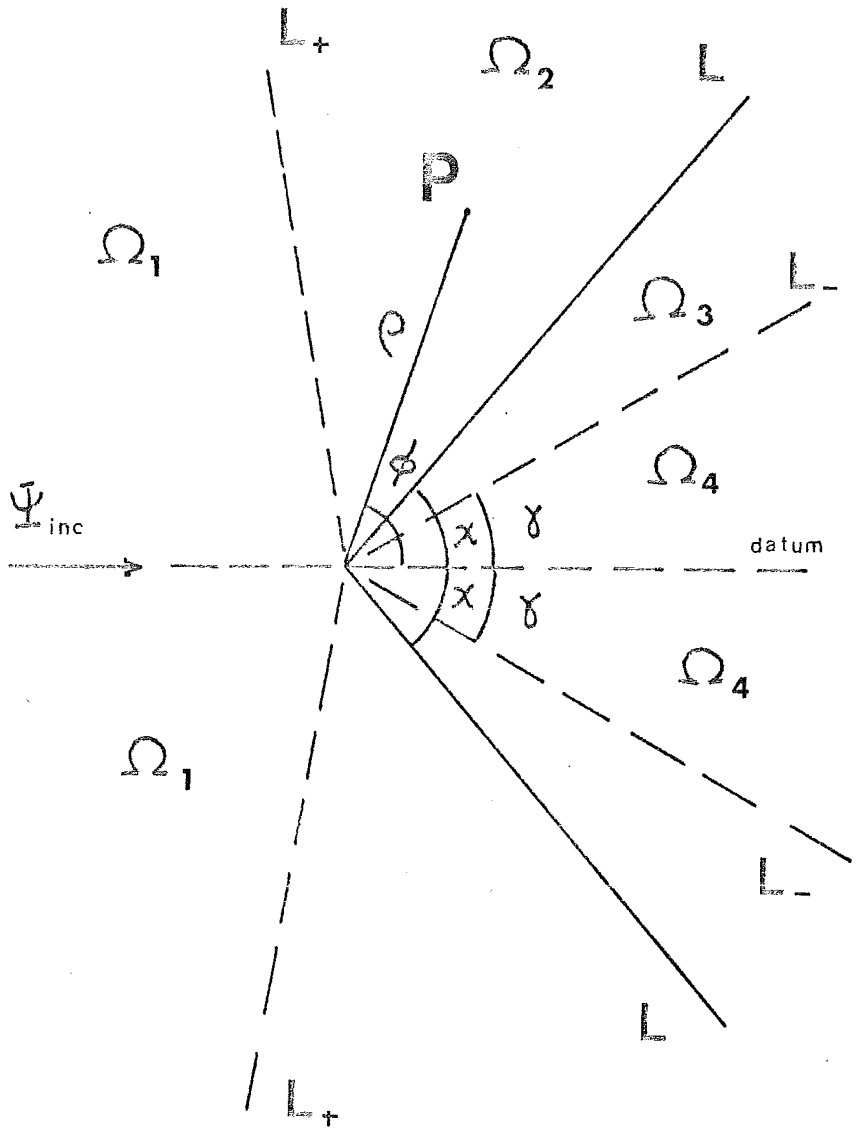

FIGURE 8.4 The different regions of interest in penetrable wedge diffraction problems. The wedge surfaces are denoted by L while the reflection and refraction boundaries are denoted by L_+ and L_- respectively.

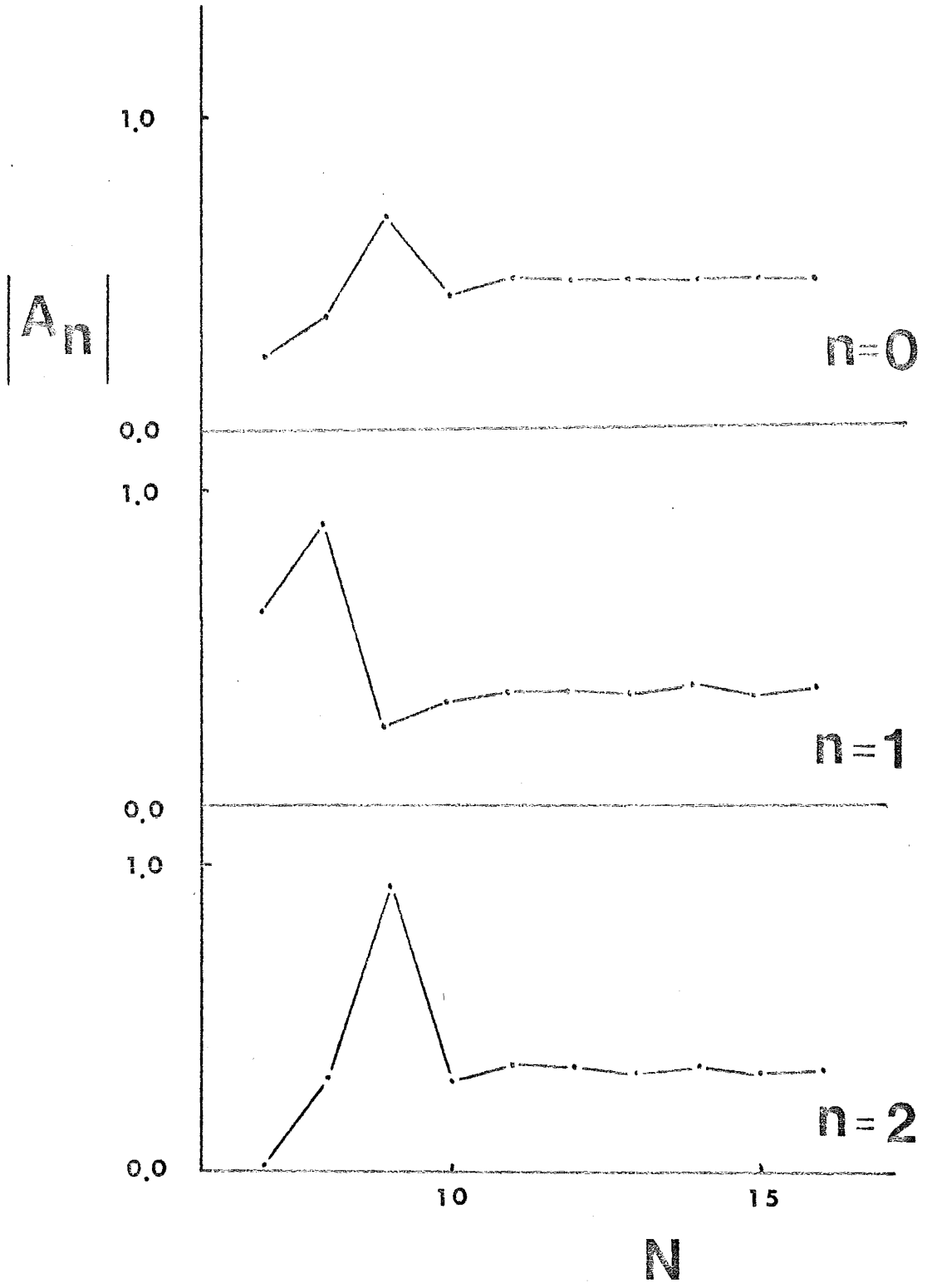

FIGURE 8.5 Plots of the first three surface field expansion coefficients with respect to N, the number of expansion coefficients used.

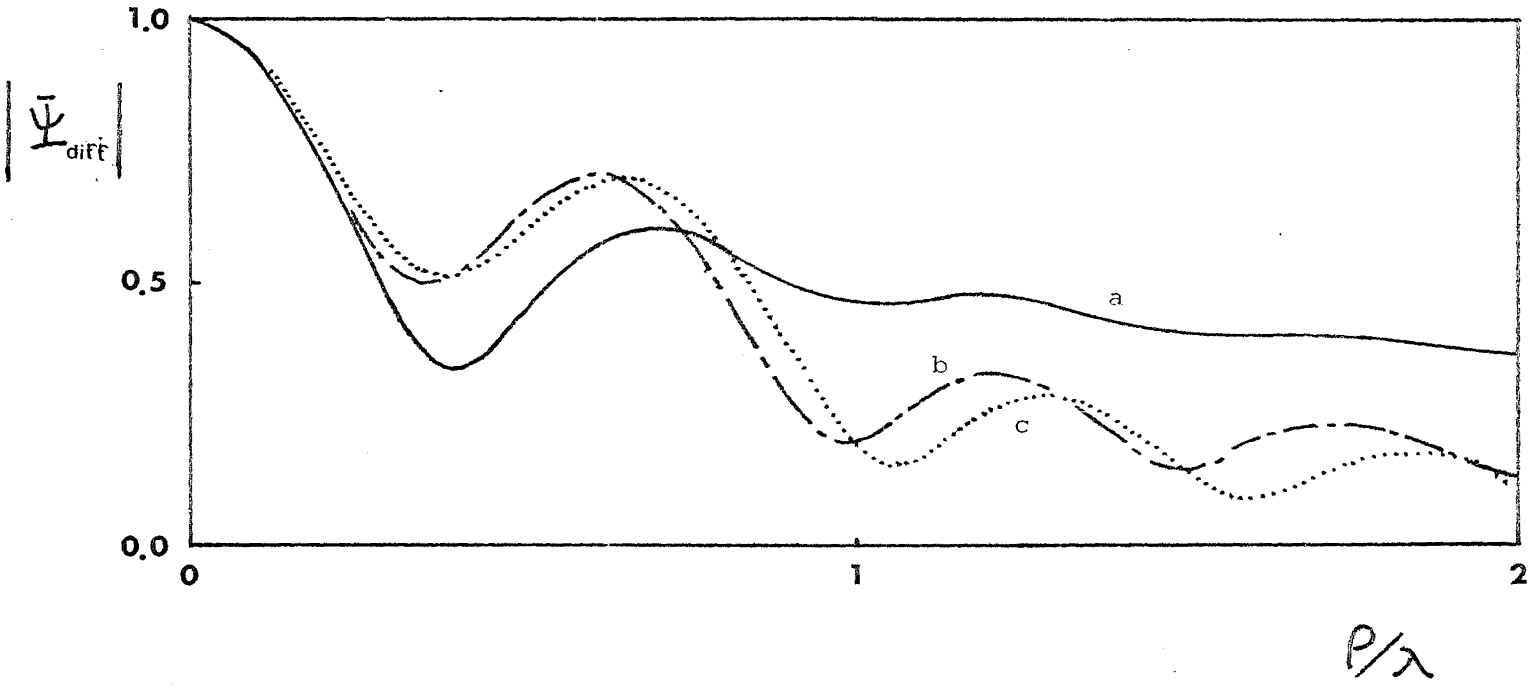

FIGURE 8.6 Plots of the (normalised) magnitudes of fields diffracted by an infinite penetrable wedge. The fields are at (a) $\phi = 180^{\circ}$, (b) $\phi = 150^{\circ}$ and (c) $\phi = 135^{\circ}$. The parameters of the penetrable wedge are $\chi = 20^{\circ}$, $\nu = 1.2$ and $N = 16$. The edge field is 0.098.

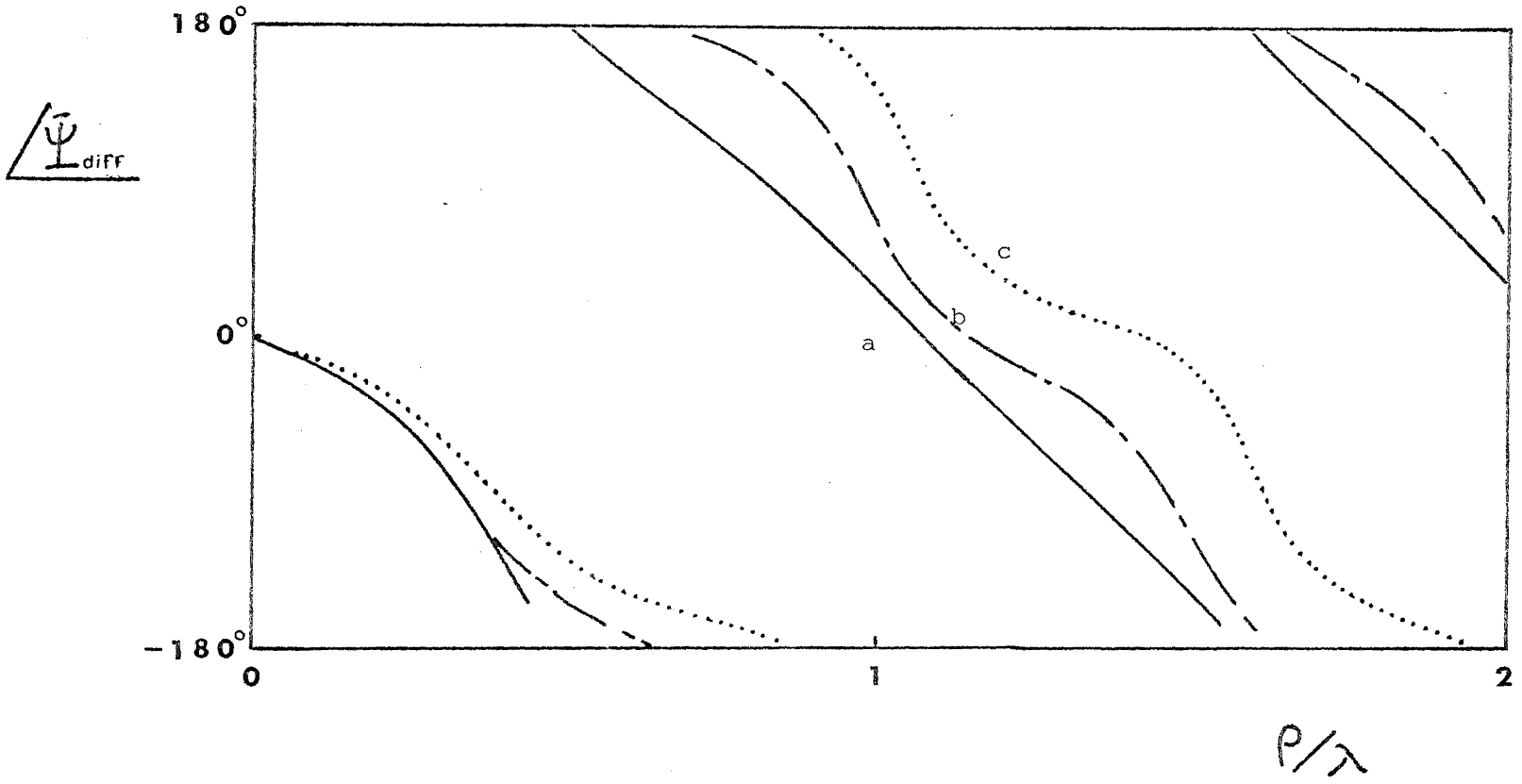

FIGURE 8.7 Plots of phases of diffracted fields described in Fig. 8.6.

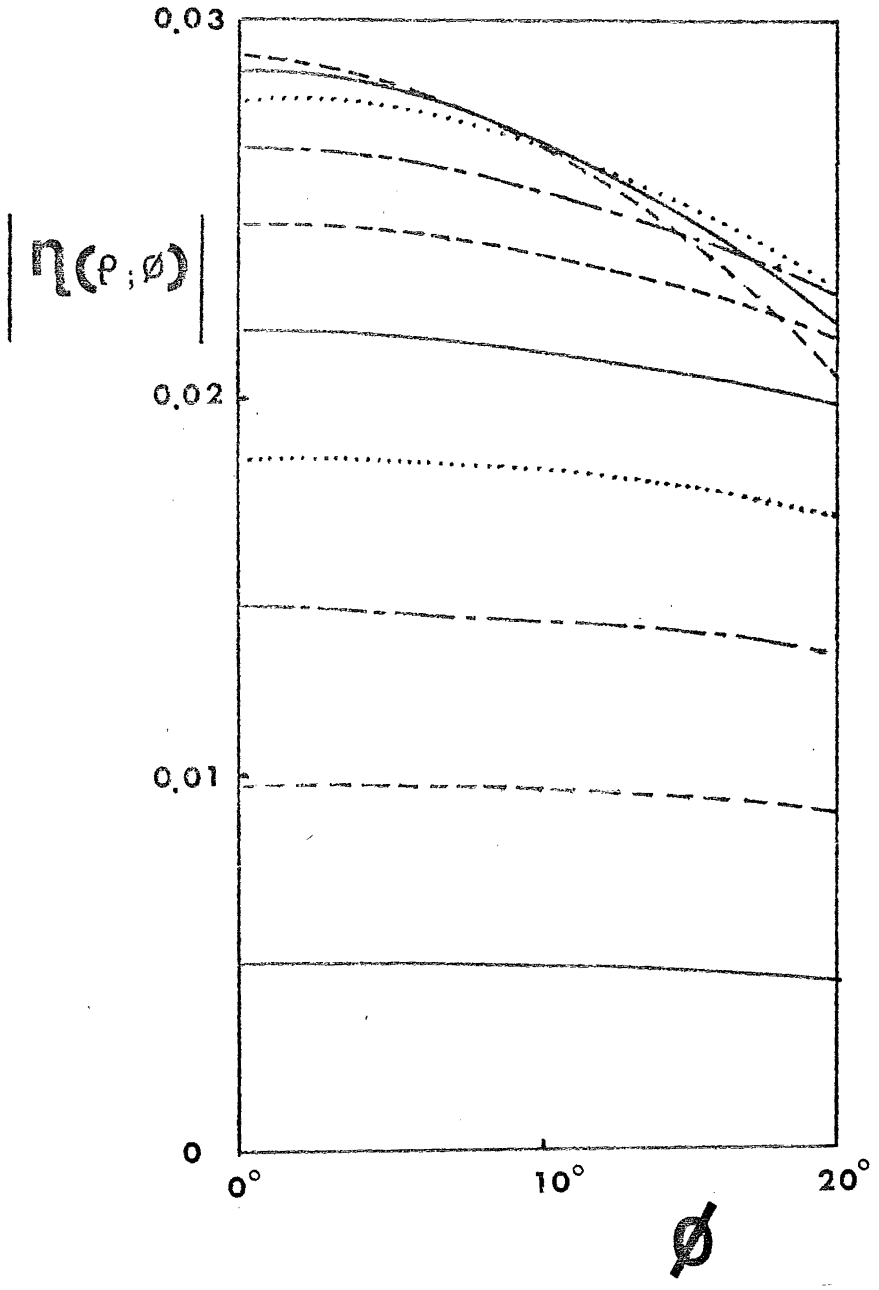

FIGURE 8.8 Plots of $\eta(\rho;\phi)$, the error in satisfying the null-field condition for the scattering calculation reported in Figs 8.5 to 8.7. They are plotted against ϕ, with $0 < \phi < \chi$. The variable in the figure is ρ, starting from $\rho = 0.1\lambda$ (the bottom-most curve), with an increment of 0.1λ. The top-most curve is for $\rho = 1.$

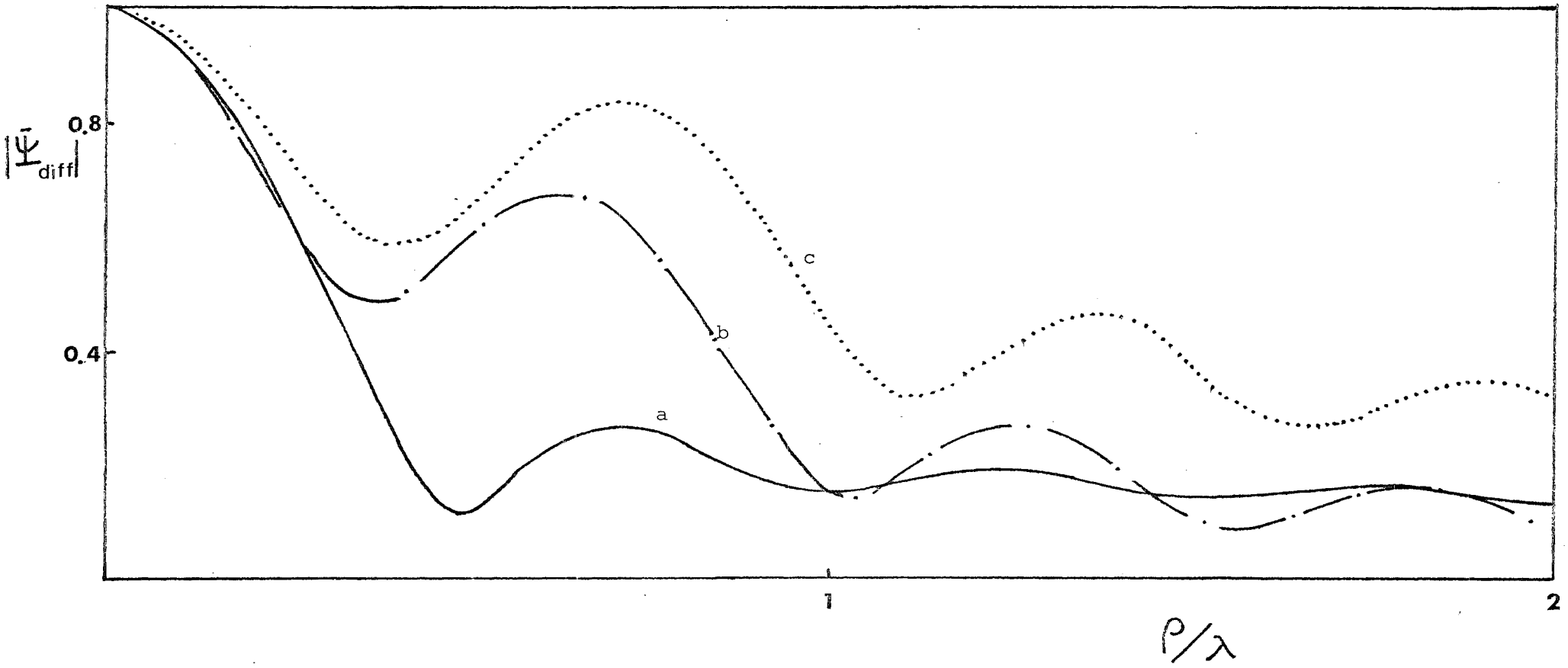

FIGURE 8.9 Plots of the (normalised) magnitudes of fields diffracted by an infinite penetrable wedge. The fields are at (a) $\phi = 180^{\circ}$, (b) $\phi = 150^{\circ}$ and (c) $\phi = 135^{\circ}$. The parameters of the penetrable wedge are $\chi = 30^{\circ}$ and $\nu = 1.2$.

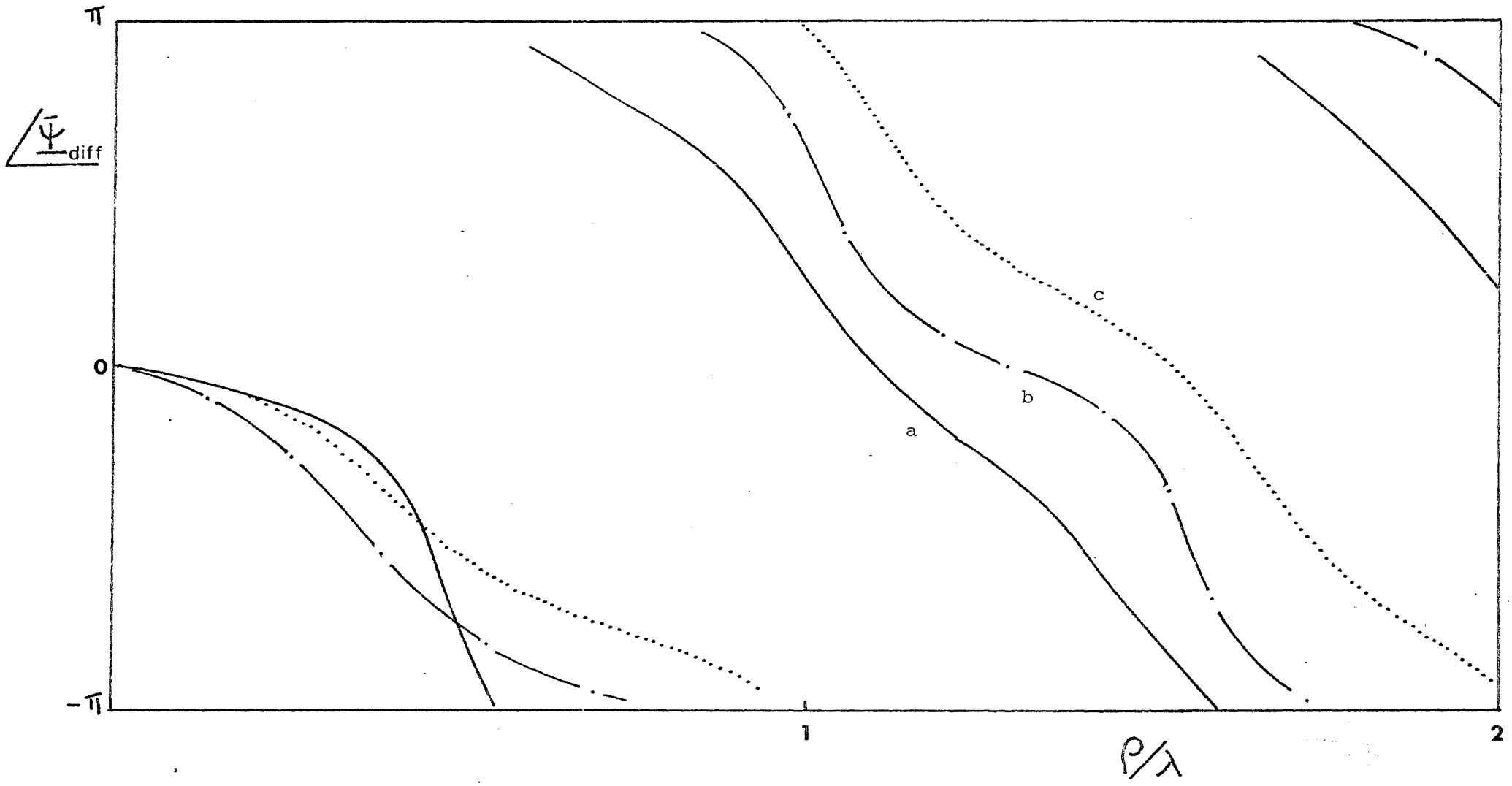

FIGURE 8.10 Plots of phases of diffracted fields described in Fig. 8.9.

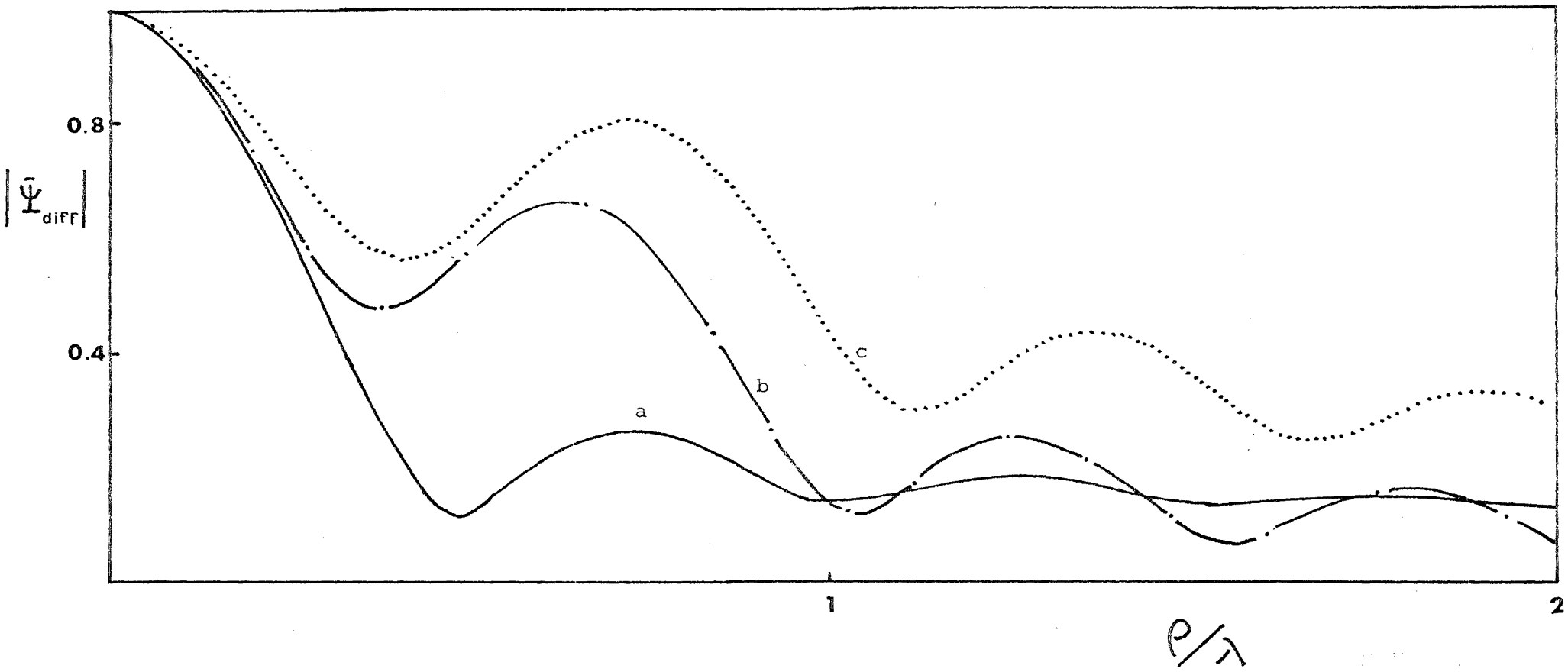

FIGURE 8.11 Plots of the (normalised) magnitudes of fields diffracted by an infinite penetrable wedge. The fields are at (a) $\phi = 180^{\circ}$, (b) $\phi = 150^{\circ}$ and (c) $\phi = 135^{\circ}$. The parameters of the penetrable wedge are $\chi = 30^{\circ}$ and $\nu = 1.3$.

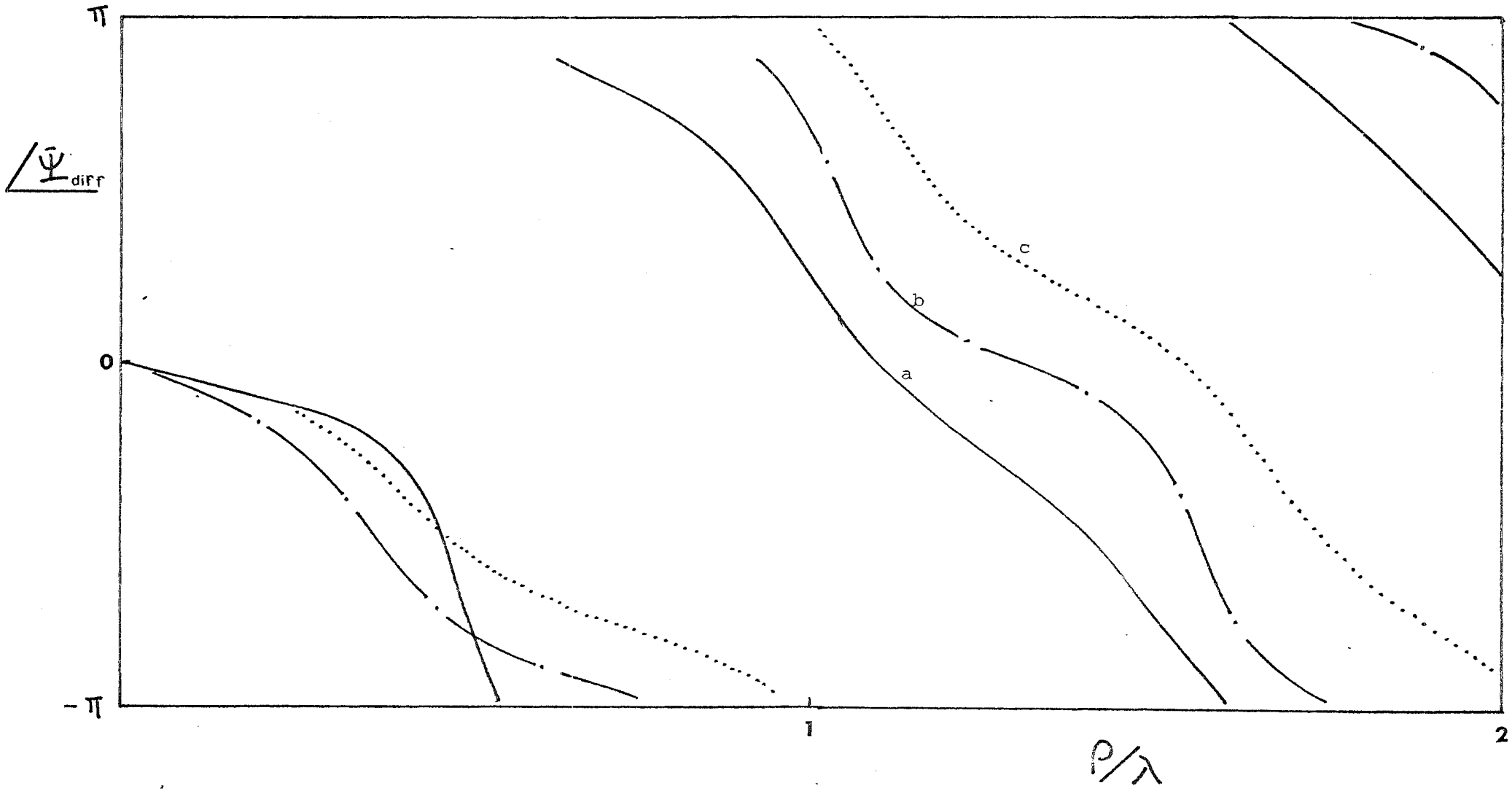

FIGURE 8.12 Plots of phases of diffracted fields described in Fig. 8.11.

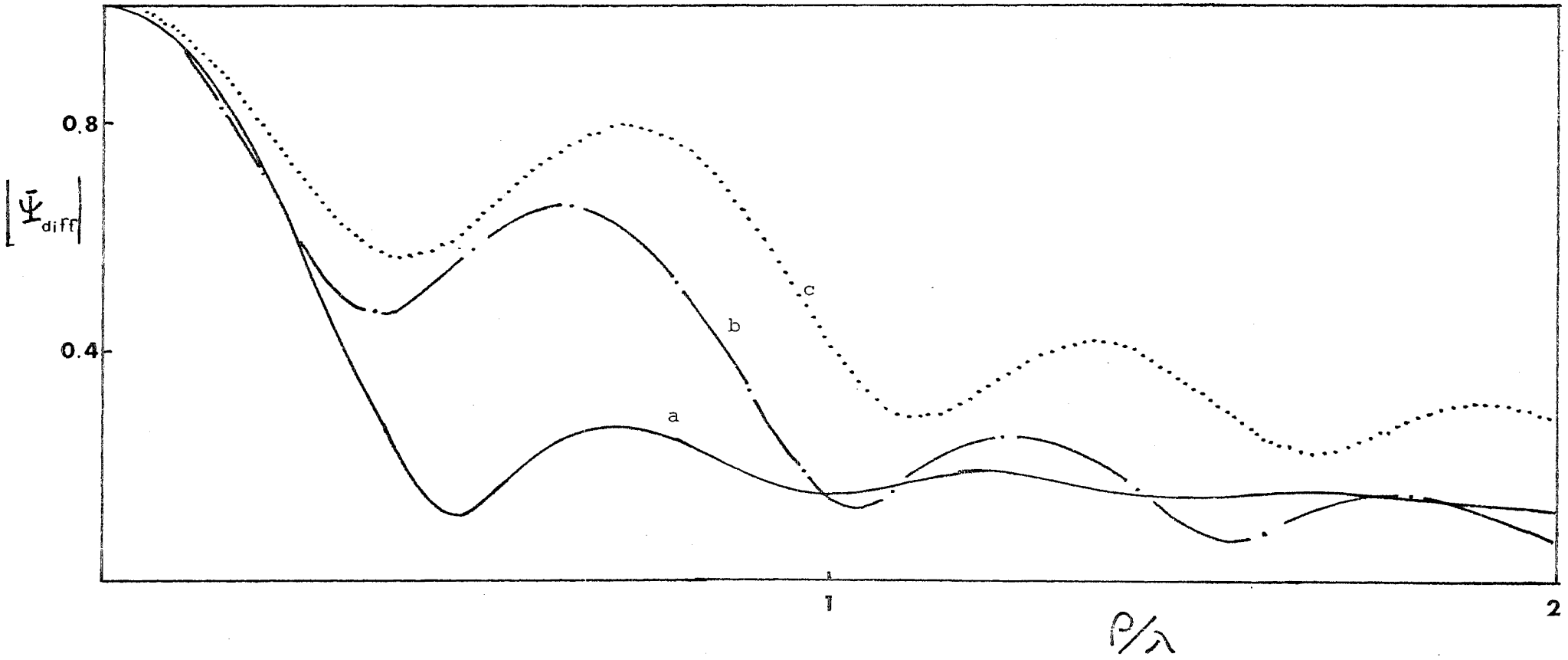

FIGURE 8.13 Plots of the (normalised) magnitudes of fields diffracted by an infinite penetrable wedge. The fields are at (a) $\phi = 180^{\circ}$, (b) $\phi = 150^{\circ}$ and (c) $\phi = 135^{\circ}$. The parameters of the penetrable wedge are $\chi = 30^{\circ}$ and $\nu = 1.4$

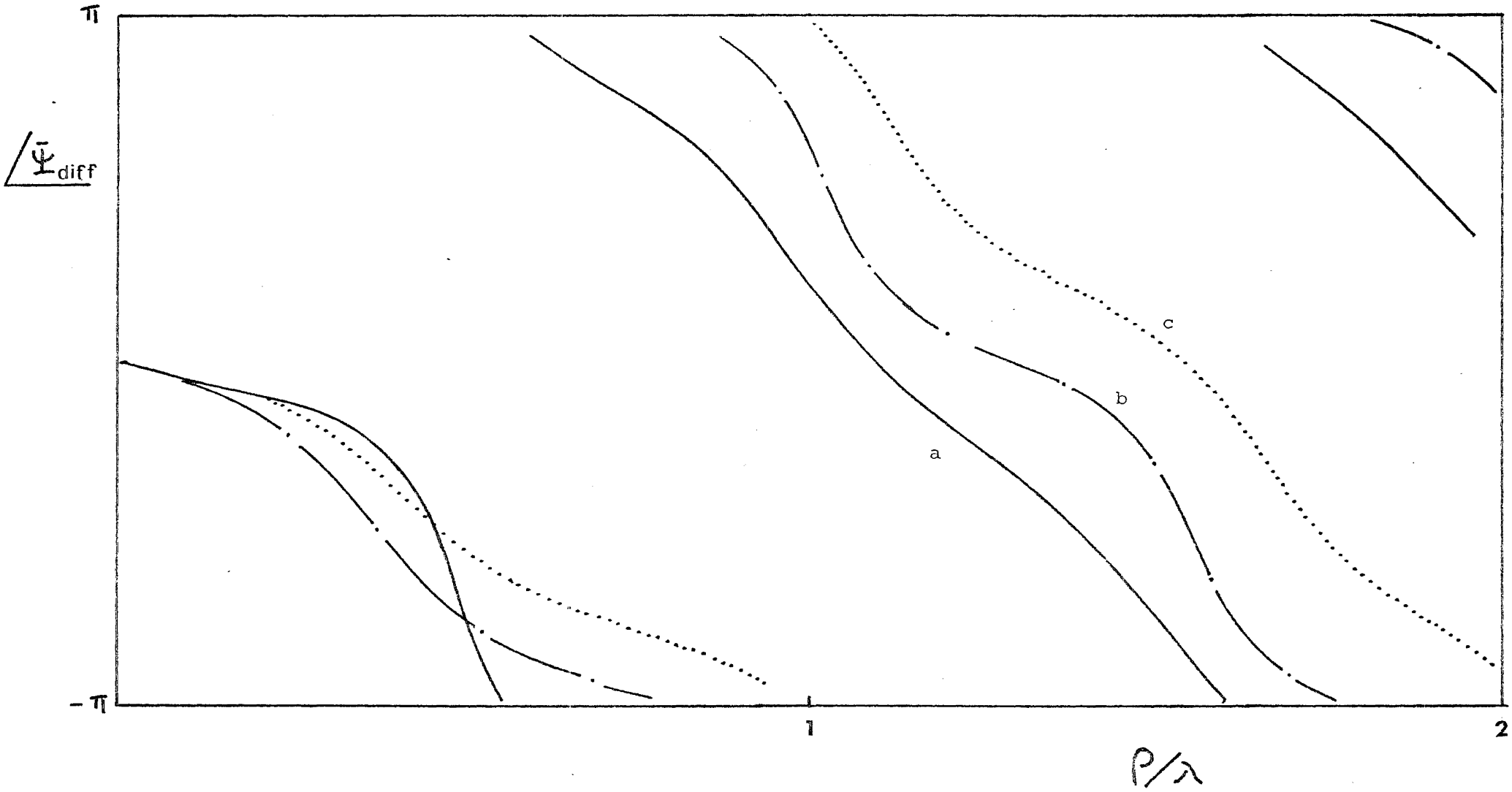

FIGURE 8.14 Plots of phases of diffracted fields described in Fig. 8.13.

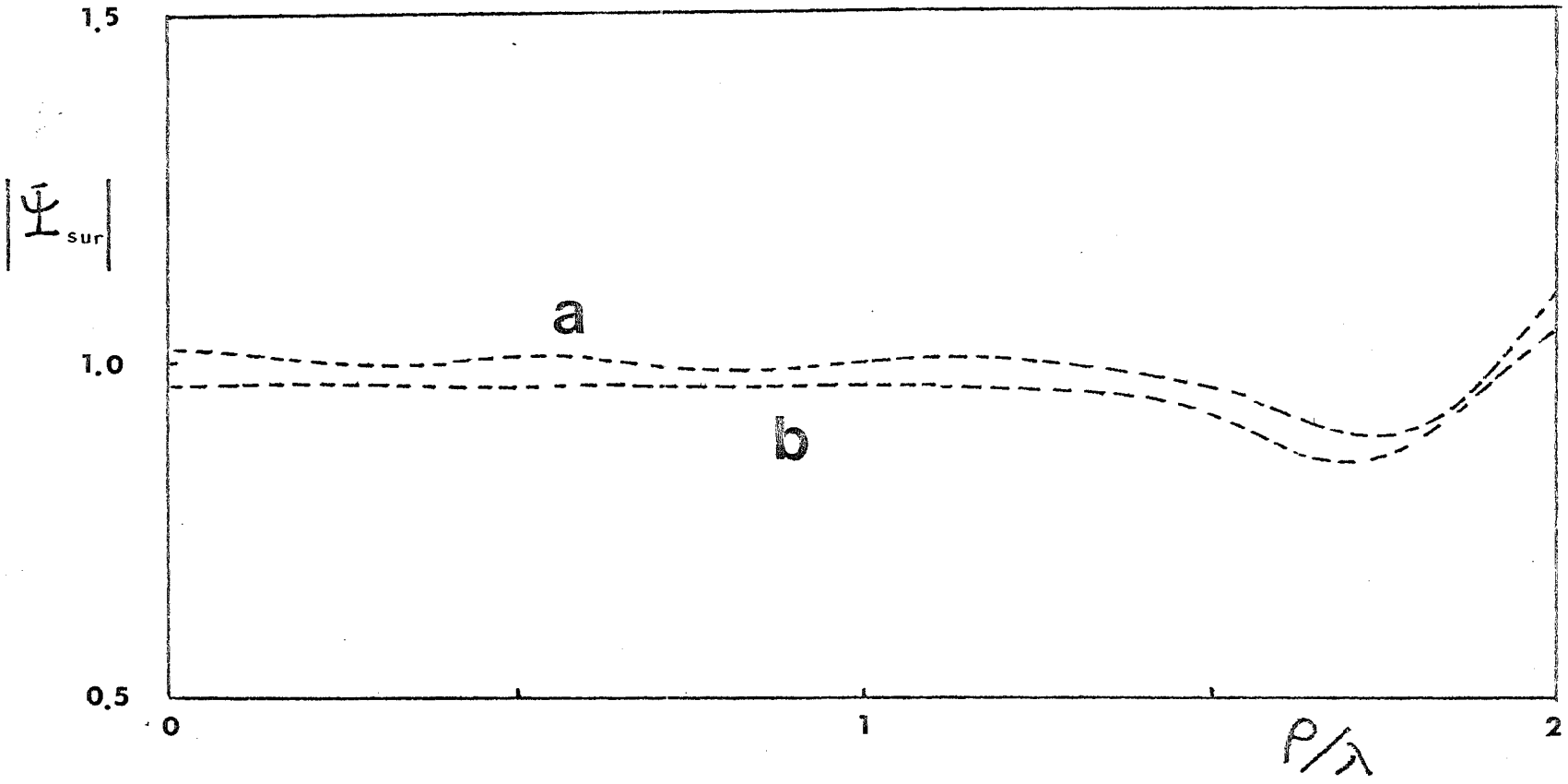

FIGURE 8.15 Plots of surface field magnitudes calculated from (a) outside-in formulation and (b) inside-out formulation.

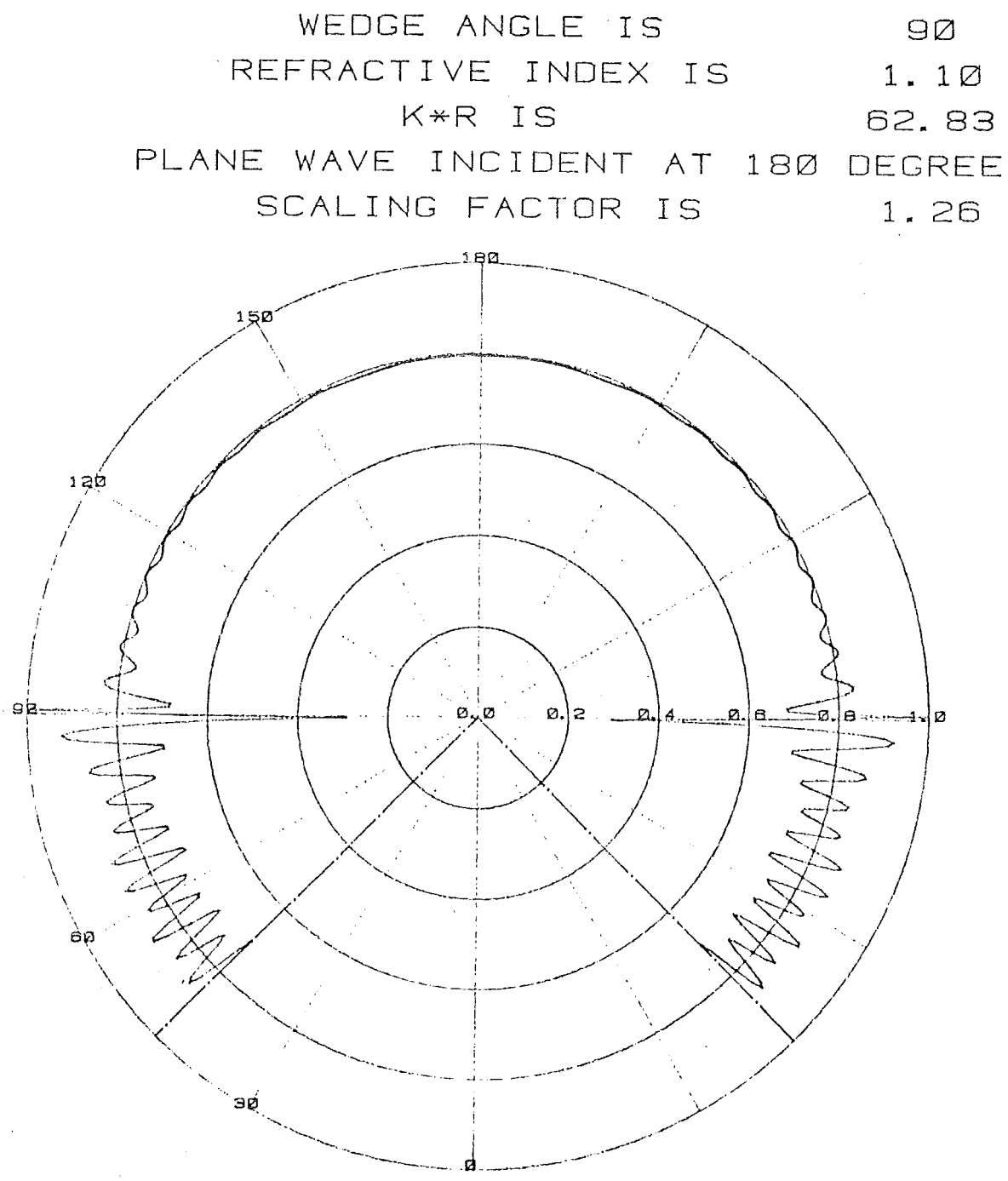

FIGURE 8.16a Plots of (total) field (magnitudes) outside a right-angled penetrable wedge of refractive index $\nu = 1.1$. The fields are plotted at $\rho = 10\lambda$. They are calculated from (a)Kaminetzky & Keller's (1975) formulation, (b) Rawlins' (1977a) formulation and (c) outside-in formulation.

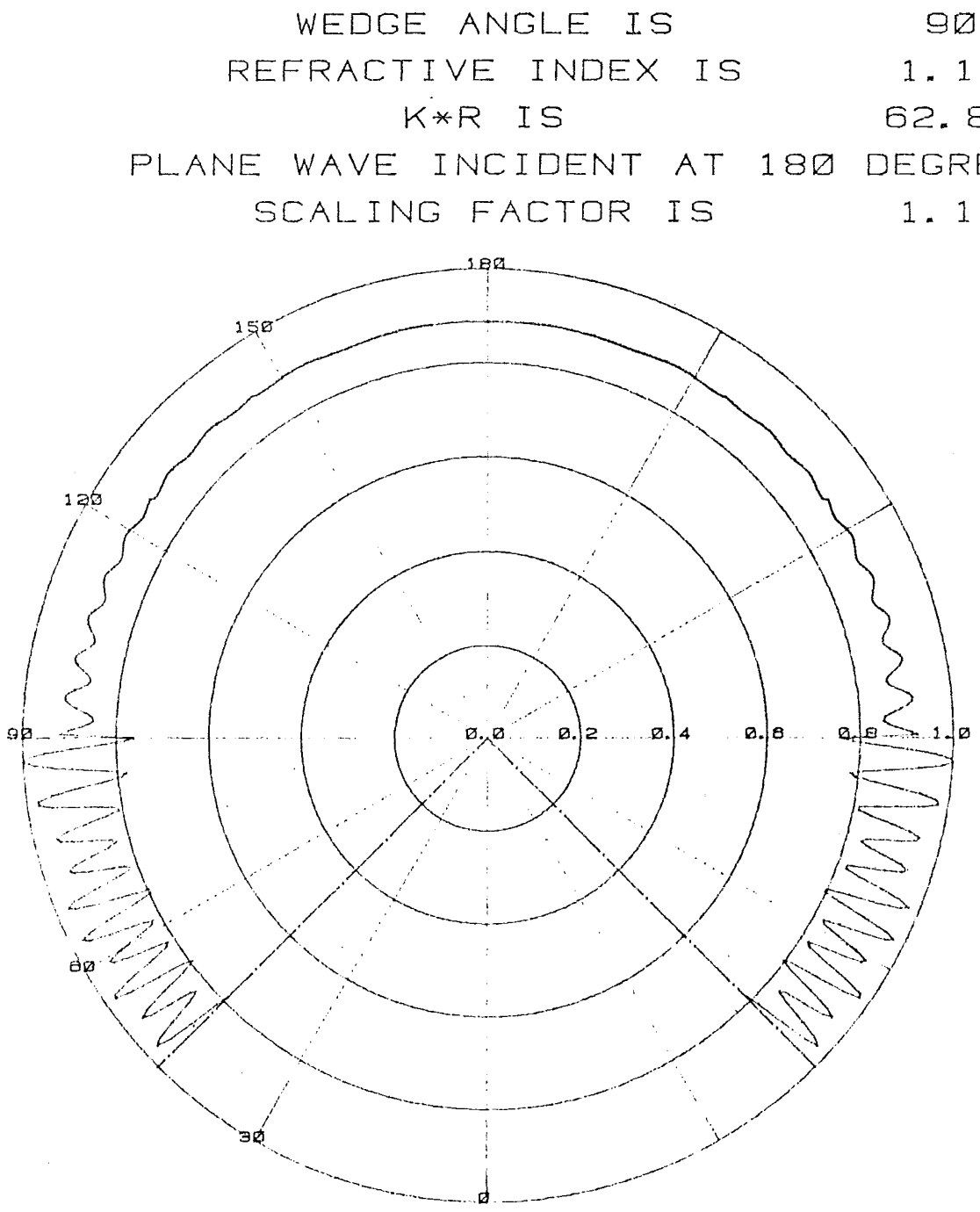

FIGURE 8.16b Plots of (total) field (magnitudes) outside a right-angled penetrable wedge of refractive index $\nu = 1.1$. The fields are plotted at $\rho = 10\lambda$. They are calculated from (a) Kaminetzky & Keller's (1975) formulation, (b) Rawlins' (1977a) formulation and (c) outside-in formulation.

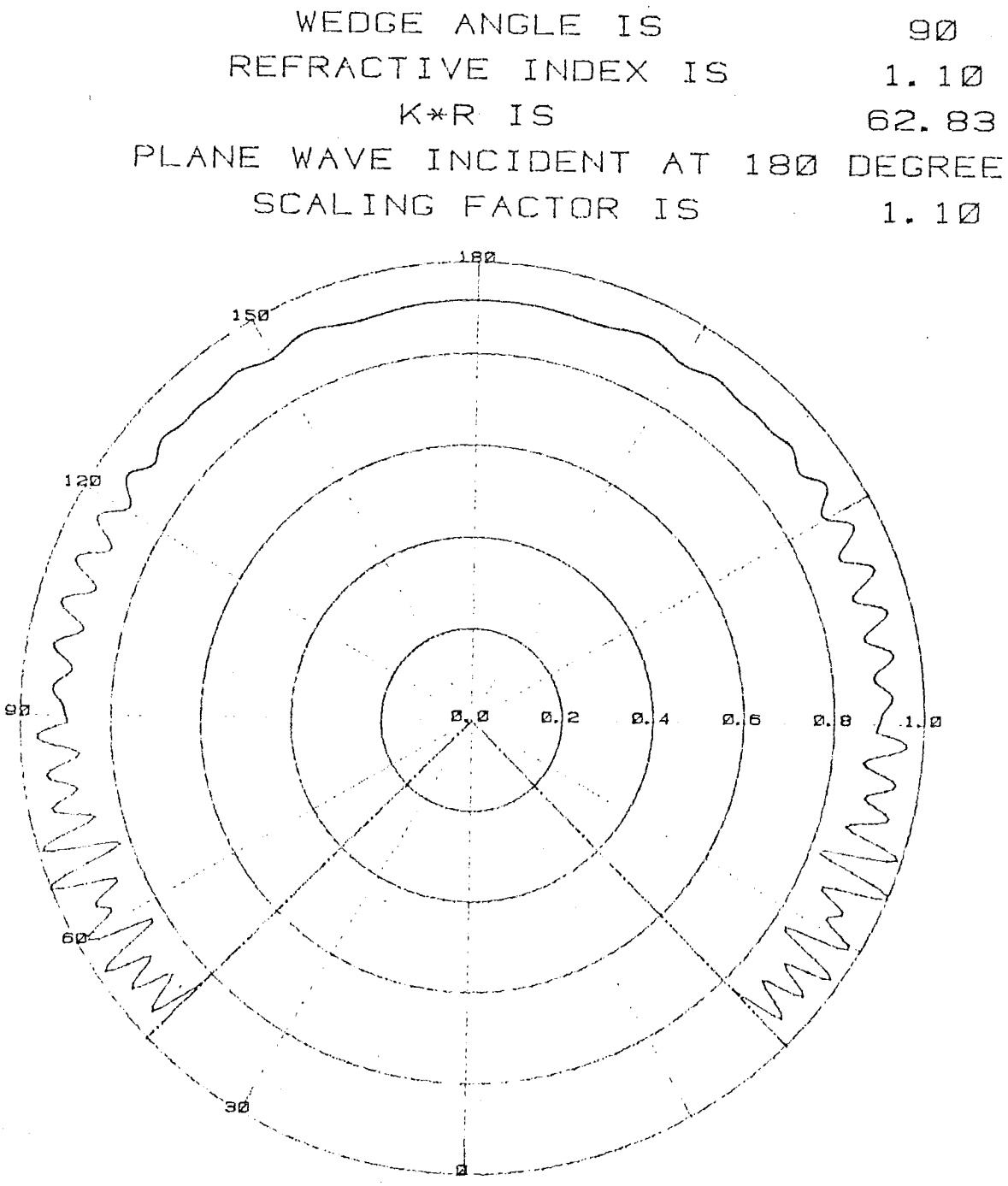

FIGURE 8.16c Plots of (total) field (magnitudes) outside a right-angled penetrable wedge of refractive index $\nu = 1.1$. The fields are plotted at $\rho = 10\lambda$. They are calculated from (a) Kaminetzky & Keller's (1975) formulation, (b) Rawlins' (1977a) formulation and (c) outside-in formulation.

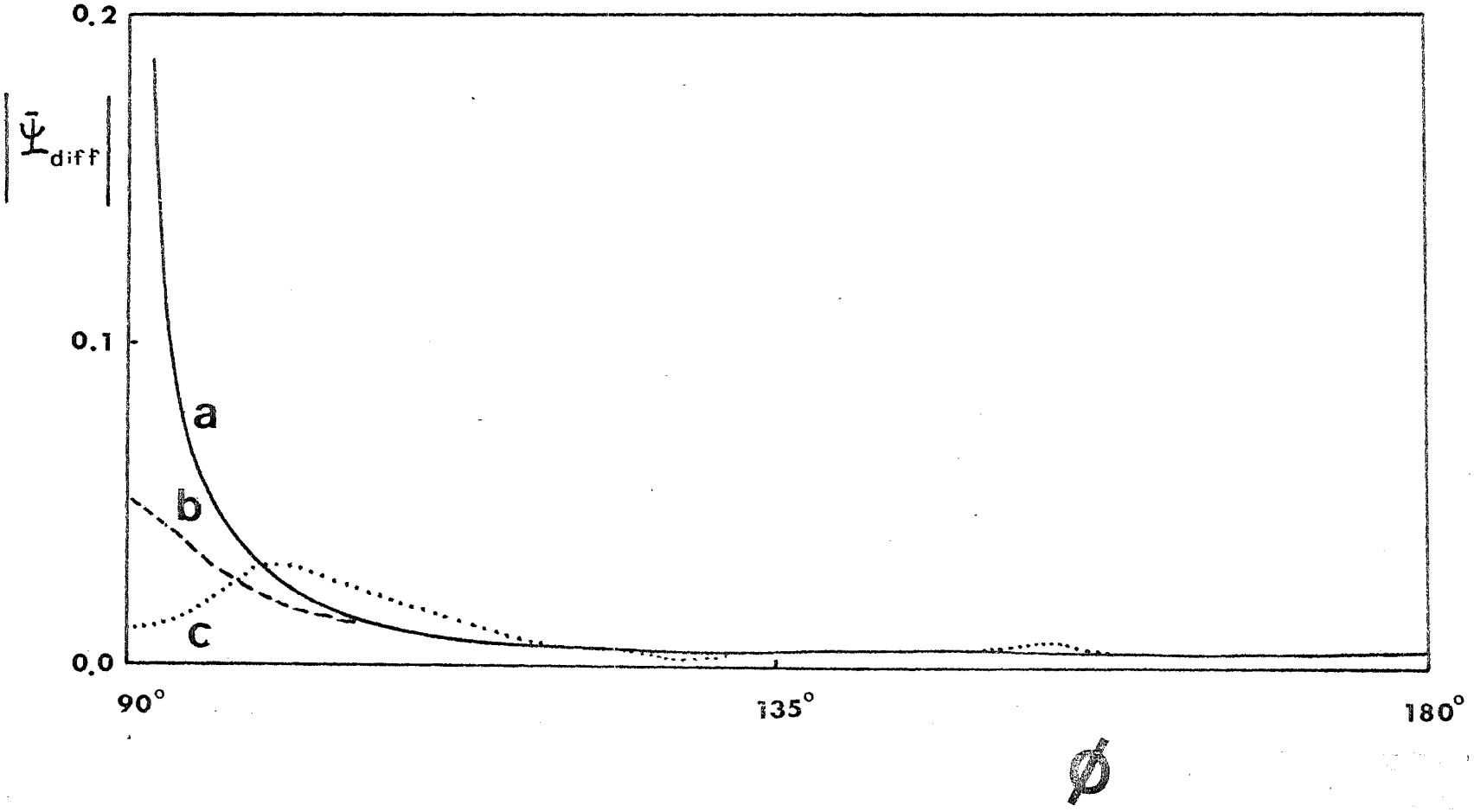

FIGURE 8.17 Plots of (diffracted) fields magnitudes of Fig. 6.16 against ϕ.

No page 274 in original

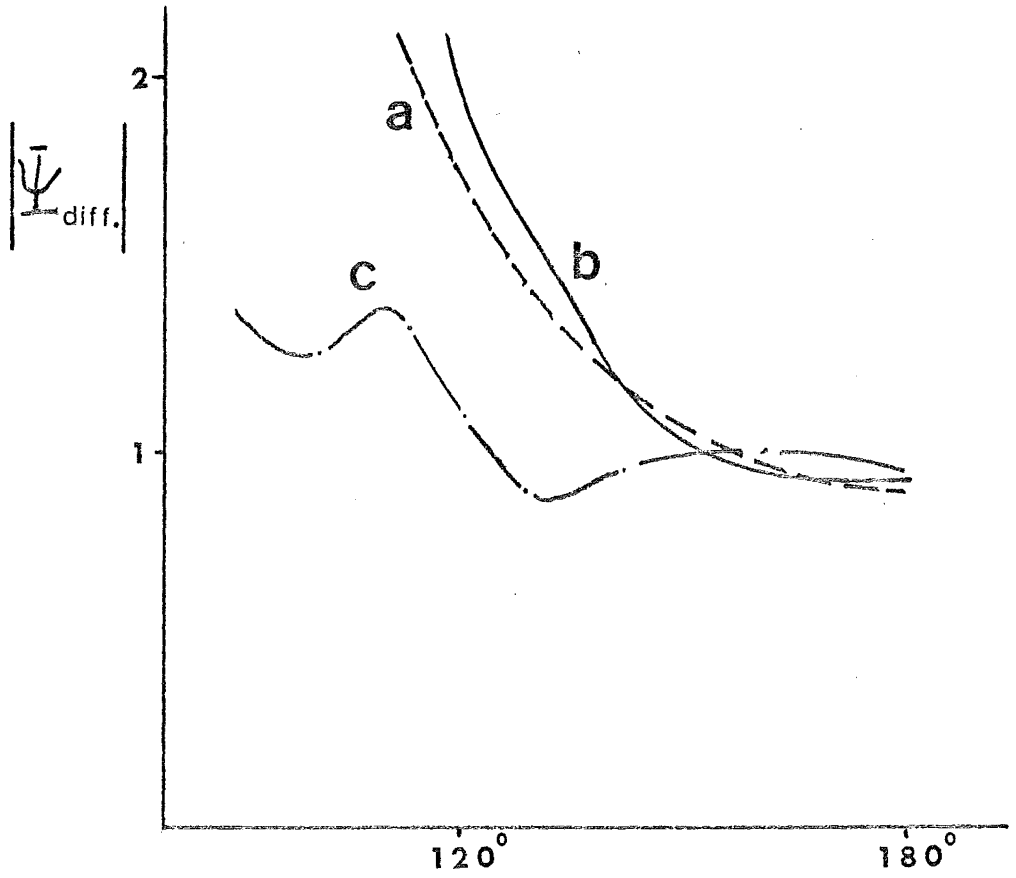

FIGURE 8.18 Comparison between back-scattered fields of
(a) an infinite penetrable wedge of angle $2\chi = 40^\circ$ and refractive index $\nu = 1.01$, as calculated from Kaminetzky and Keller's (1975) formulation,
(b) an infinite penetrable wedge of angle $2\chi = 40^\circ$ and refractive index $\nu = 1.01$, as calculated from NULL-IN,
(c) a wedge-cylinder, of wedge angle $2\chi = 40^\circ$, refractive index $\nu = 1.01$ and $a = 0.5$, where a is as defined in FIG 6.1.

CHAPTER NINE

EXPERIMENTAL RESULTS

It has been established in Chapter 6 that knowledge of the field behaviour close to edges of penetrable bodies can increase the efficiencies of computational solutions to practical problems. In this chapter, experimental results are presented to support this argument. Cutoff wave numbers of circular-cylindrical cavities loaded with dielectric sectors have been measured (Section 9.1) and they are in substantial agreement with the computed results.

A parallel plate scattering experiment has also been designed in order to attempt to measure diffraction coefficients for infinite wedges. Unfortunately, with the limited resources available, it was not possible to make measurements to an adequate accuracy. Since the results were not completely useless, however, they are reported in this chapter, mainly for the purpose of indicating the kind of improvements needed to make them really useful. The experimental procedure is described in Sections 9.2.1 and 9.2.2, while suggestions for further work are made in Section 9.2.3.

9.1 E-MODE CUTOFF WAVE NUMBER OF A CIRCULAR-CYLINDRICAL CAVITY LOADED WITH SECTORAL DIELECTRIC

9.1.1 Preliminaries

The problem - determination of the cutoff wave number of a circular-cylindrical cavity loaded with sectoral dielectric - is chosen because of the ease with which experimental and computational results can be compared. In this section, the equations from which cutoff wave numbers can be calculated, are derived. The experimental setup and the procedures employed are described in the next section.

The geometry of a 'circular-cylindrical cavity loaded with sectoral dielectric' is depicted in Fig. 9.1

Define

C_1 = curve AB (in the anti-clockwise sense)

C_2 = curve BA (in the anti-clockwise sense).

$C_3 = C_{3+} \cup C_{3-}$

C_{3+} = line BO

C_{3-} = line OA

Let $\Psi_-(\rho;\phi)$ be the (total) field inside the dielectric sector and $\Psi_+(\rho;\phi)$ be the (total) field in the empty sector of the cavity. The null-field method (cf. Section 1.5.5) then stipulates that, at any point P outside the cavity (e.g. Fig. 9.1),

$$\int_{C_3} \left[\Psi_- \, \partial g/\partial\hat{n} - g \, \partial\Psi_-/\partial\hat{n}\right] dC - \int_{C_1} \partial\Psi_-/\partial\hat{n} \; g \; dC - 2\int_{C_2} \partial\Psi_+/\partial\hat{n} \; g \; dC = 0 \tag{9.1}$$

where $g = g(P,Q)$ is the Green's function relating the source point Q on either C_1, C_2 or C_3 and the field point P.

Expanding Ψ_- and Ψ_+ in terms of Bessel functions of integer order, and considering only the fields which are even functions of ϕ, one gets,

$$\Psi_- = \sum_{n=o}^{\infty} A_n \cos n\phi \; J_n(\nu k\rho) \tag{9.2}$$

and

$$\Psi_+ = \sum_{n=o}^{\infty} B_n \cos n(\pi-\phi) \; J_n(k\rho) \tag{9.3}$$

Substituting (9.2) and (9.3) into (9.1), and manipulating the latter in the normal way (cf. Section 1.5.5.4), it becomes

$$\sum_{n=o}^{\infty} A_n \; 2[m \cos n\chi \sin m\chi - n \sin n\chi \cos m\chi]$$

$$- \sum_{n=o}^{\infty} A_n \, \nu ka \, J_n'(\nu ka) \; I_1 + 2\sum_{n=o}^{\infty} B_n \, ka \, J_n'(ka) \; I_2 = 0 \tag{9.4}$$

where

$$I_o = \int_o^a \rho^{-1} \, J_n(\nu k\rho) \, J_n(k\rho) \, d\rho \tag{9.5}$$

and

$$I_i = \begin{cases} 2\chi & , \; m = n = 0, \; i = 1 \\ 2\chi - 2\pi & , \; m = n = 0, \; i = 2 \\ \sin(2m)\chi/2m + \chi & , \; m = n \neq 0, \; i = 1 \\ \sin(2m\chi)/2m + \chi - \pi & , \; m = n \neq 0, \; i = 2 \\ \sin(m+n)\chi/(m+n) + \sin(m-n)\chi/(m-n) & , \; m \neq n \quad , \; i = 1,2 \end{cases} \tag{9.6}$$

An additional set of equations can be obtained by point-matching Ψ_- and Ψ_+ on C_3, i.e.

$$\sum_{n=o}^{\infty} A_n J_n(\nu k\rho) \cos n\chi - \sum_{n=o}^{\infty} B_n J_n(k\rho) \cos n(\pi - \chi) \tag{9.7}$$

Combining (9.4) and (9.7), the matrix equation (cf. Section 1.5.1)

$$\begin{bmatrix} \underline{\underline{K}} \end{bmatrix} \quad \begin{bmatrix} \underline{A} \\ \underline{B} \end{bmatrix} = 0 \tag{9.8}$$

is obtained. The cutoff wave number can then be determined by setting the determinant of $\underline{\underline{K}}$ to zero. This is done using the method of Regula Falsi (cf. Kreyszig 1972, Section 18.2)

$$k_{n+1} = \frac{k_c f(k_n) - k_n f(k_c)}{f(k_n) - f(k_c)} \tag{9.9}$$

where k_c is the cutoff wave number of the empty waveguide, which serves as the initial guess, $f(k_o)$ is the determinant of $\underline{\underline{K}}$ when $k = k_o$, and k_n, k_{n+1} are the nth and the n+1th iterations for k. A solution is said to have converged if $|k_{n+1} - k_n| < \varepsilon$, where ε is an arbitrarily chosen small constant.

9.1.2 Cavity Configuration and Experimental Setup

9.1.2.1 Cavity Construction

A circular-cylindrical cavity was constructed from a section of brass tube and was coupled to two sections of X-band waveguide through coupling holes. Construction details and important dimensions are shown in Fig. 9.2. The top and bottom covers were fastened to the cavity with screws. These covers were removable so that a dielectric sector (see insert of Fig. 9.2) could be easily inserted and removed.

9.1.2.2 Experimental Setup

The refractive indices of the dielectrics used in this experiment were measured using the method of Von Hippel (1954), the experimental setup for which is not shown here, because it was standard (cf. Sucher and Fox 1963). The refractive indices measured are listed in Table 9.1. The measurement error was estimated to be about 1% (cf. Mnyama 1983).

Dielectric sectors (of various angles and refractive indices, see insert in Fig. 9.2) were loaded into the cavity (cf. Fig. 9.2). The experiment was set up as indicated in Fig. 9.3. The power input to and output from the cavity were sensed by the detectors and fed into the comparator. The comparator was an electronic circuit built by Mnyama (1983), a block diagram of which is shown in Fig. 9.4. The output from the comparator was arranged to be the logarithm of the ratio of the power output to the power input to the cavity (cf. Fig. 9.4) and was registered by the voltmeter. This setup overcame difficulties associated with power level fluctuations from the generator.

TABLE 9.1 Refractive Indices of the Dielectrics Used in the Experiments

Material	Refractive Index ν
Ultra wear	1.90
Acetal	2.05

9.1.3 Results and Conclusions

TABLE 9.2 Comparison of Computed and Measured E-mode Cutoff Wave Number k_c. The angle of the dielectric sector was 2χ while its refractive index was ν. The radius of the circular-cylindrical cavity was 2.5 cm. The depth of the cavity was 1.5 cm.

Material	ν	2χ	k_c (computed)	k_c (measured)	% error
Ultra wear	1.90	60°	91.10	89.60	1.65
		90°	86.88	87.14	0.30
Acetal	2.05	60°	87.46	86.36	1.25
		90°	79.58	81.28	2.13

The cutoff wave numbers of a circular-cylindrical cavity loaded with various dielectric sectors are listed in Table 9.2. The theoretical values were calculated using the method described in Section 9.1.1 while the experimental values were measured as outlined in Section 9.1.2. The dielectrics used were 'ultra wear', which has a refractive index of 1.90, and 'acetal',

which has a refractive index of 2.05 (cf. Table 9.1). The angles of the dielectric sectors were 60° and 90° respectively. As can be seen from Table 9.2, the computed and measured cutoff wave numbers agree to within about 2%, and in two cases to within about 1% or better. Since this is of the order of the estimated error (cf. Mnyama 1983), the agreement is encouraging. Therefore, it may be concluded that knowledge of field behaviour close to the apex of a penetrable body (as discussed in Chapter 5) can lead to efficient numerical solutions (as indicated in Chapter 6) of practical problems (as indicated in Table 9.2).

9.2 SCATTERING COEFFICIENTS FOR INFINITE WEDGES

In an attempt to produce experimental results to verify some of the theoretical computation reported in Chapters 6, 7 and 8, a parallel plate scattering experiment was designed. This experimental arrangement (described in Section 9.2.1) was chosen because of its relative convenience. Unfortunately, due to limitations of available resources, it was not possible to obtain data of adequate accuracy. The difficulties which were experienced, and possible ways of overcoming them, are discussed in Section 9.2.3.

9.2.1 Experimental Setup - The Parallel Plate in Time Domain

The experimental setup is shown in Fig. 9.5, while details of the construction of the parallel plate scattering range are shown in Fig. 9.6.

The parallel plate scattering range (cf. Fig. 9.6) consisted of two flat aluminium plates, 2.5 cm apart. The spacing of the plates was kept as constant as possible by the presence of the wedge and also by six spacers placed around the periphery of the range. The apex of the wedge was positioned at the centre of the plates. The input and output signals were fed to and from the range through terminals, the construction of each of which was identical. A typical terminal, when connected to the scattering range, is shown in Fig. 9.7.

The input terminal was positioned 50 cm from the apex. The receiving terminals were positioned 20 cm from the apex. The angular separation of the receiving terminals was 10° for $2\chi < \phi < \pi$. The receiving terminals were removable and could be replaced by metal plugs which fitted snugly into the holes (into which the terminals were inserted) flush with the plate. The depth of insertion of the brass rod at each receiving terminal was adjustable.

The time-domain reflectometer (TDR) produced a step output (of 350 psec rise time), which was converted into a (approximately 0.7 nsec duration) pulse by the T-junction. The pulse was fed into the scattering range, and the output waveform sampled by the TDR (Tan 1984). The waveform accepted at each receiving terminal was fed (through the TDR and an A/D converter) to the Vax 11/750 computer which stored samples of it (cf. Fig. 9.5). Further signal processing, effected with the aid of the VAX computer, is described in the next section.

9.2.2 Signal Processing Procedure

Let the waveform arriving at a particular receiving terminal, when the wedge is removed from the scattering range, be $f_1(t)$. Also let the waveform received at the same terminal, with the wedge in place, be $f_2(t)$. The waveform $f_1(t)$ consists mainly of the input pulse (of 0.7 nsec duration). The waveform $f_2(t)$ consists not only of the input pulse, which travels directly from the transmitter to the receiver, but also of the signals which are reflected and diffracted from the wedge. The experiment was designed such that the reflected/diffracted part of $f_2(t)$ arrived at the receiver after the input pulse. This time lag was needed to ensure the $f_1(t)$ and $f_2(t)$ could be accurately aligned (cf. Fig. 9.8). The alignment was done, automatically in the computer, by minimising $|f_1(t) - Af_2(t-\tau)|^2$ over the interval $0 < t < 0.7$ nsec., where the time origin coincides with the earliest detectable arrival of $f_1(t)$. This interval is chosen because the first 0.7 nsec of the received signal can be expected to have the same form as $f_1(t)$. The values of A and τ are varied (using a gradient routine) to effect the minimisation. Finally, $f_1(t)$ was subtracted from $f_2(t)$ to obtain $f_3(t)$, i.e.

$$f_3(t) = Af_2(t-\tau) - f_1(t) \tag{9.10}$$

which was the best available estimate of the field scattered by the wedge. The Fourier transforms of $f_1(t)$ and $f_3(t)$ were then obtained as $F_1(\omega)$ and $F_3(\omega)$ respectively. The ratio $G(\omega) = |F_3(\omega)/F_1(\omega)|$ was then calculated for a range of values of ω. This procedure was repeated for each receiving terminal so that the scattering pattern of the wedge could be estimated over the aforesaid range of values of ω.

9.2.3 Appraisal of Results

The aluminium plates described in Section 9.2.1 was left over from a previous research project. No funds were available for making major alterations to this range. Unfortunately, the dimensions of the range, taken together with the shortest pulse which could be generated at a useful amplitude, implied that only a small portion of a typical received signal (see Fig. 9.8) contained information (concerning diffraction by the wedge) which was not contaminated by unwanted reflections. This meant that the waveforms $f_1(t)$ and $f_2(t)$ were useful only for the time $t_1 < t < t_2$, where t_1 is the time taken for the signal to arrive at the receiving terminal and t_2 is the time of first arrival of unwanted reflections. These latter can be either reflection from the edges of the scattering range, or secondary reflections from the wedge surfaces. From the dimensions of the scattering range (shown in Fig. 9.6), it is easy to deduce that, on average, $t_1 \simeq 1.3$ nsec and $t_2 \simeq 2.5$ nsec. Therefore, the useful duration of $f_3(t)$, as shown in Fig. 9.8, is only 0.5 nsec. This interval is, in fact, less than the duration of the incident pulse.

Therefore, the calculated value of $G(\omega)$ cannot be very accurate. The useful duration of $f_3(t)$ should at least equal the duration of the input pulse, for meaningful results to be obtained. The longer this duration, the better the signal-to-noise ratio, and therefore the results, should be.

It is seen from Fig. 9.8 that the useful duration t_3 of $f_3(t)$ is $t_3 = t_2 - t_1$ - input pulse width. To achieve a large useful t_3, one can either reduce the input pulse width, or enlarge the scattering range (since t_2 increases with the linear dimensions of the scattering range). The pulse width is unfortunately limited by the rise time of the TDR. (The shortest pulse available has a width of twice the rise time of the TDR). On the other hand, the dimensions of the required scattering range should be, ideally, as large as possible.

Using a larger scattering range seems to be the most feasible solution to the difficulties encountered in this experiment. However, due to limitations of time and resources, it was not possible to construct such a scattering range while the research reported in this thesis was in progress. Nevertheless, it is the intention of this author to take up the task as soon as possible after returning to the National University of Singapore.

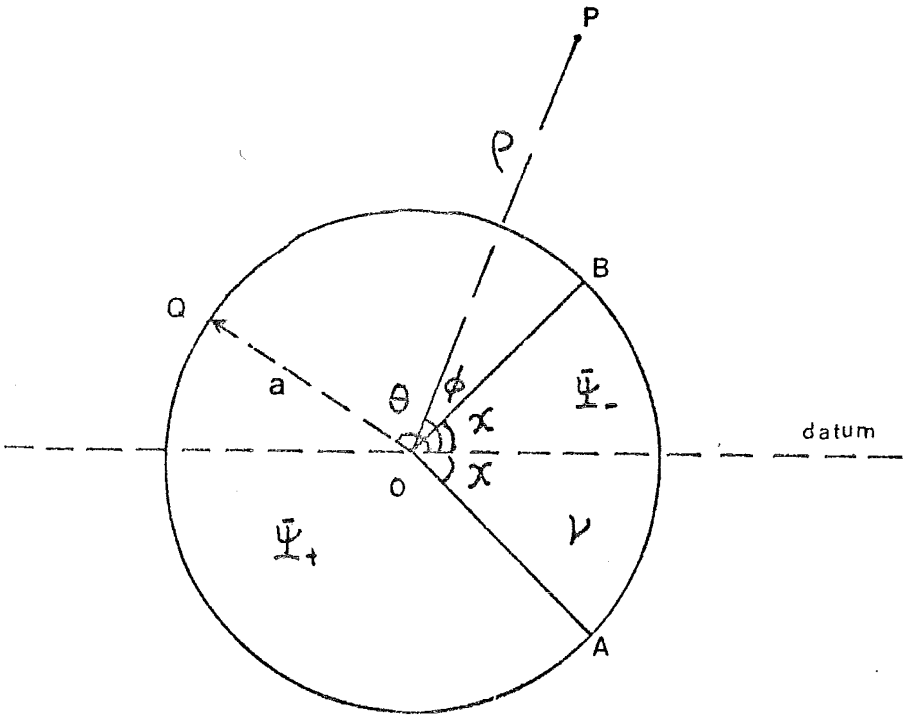

FIGURE 9.1 Circular-cylindrical cavity loaded with sectoral dielectric. The cavity has a radius a. The angle of the dielectric sector is 2χ and the sector has a refractive index ν.

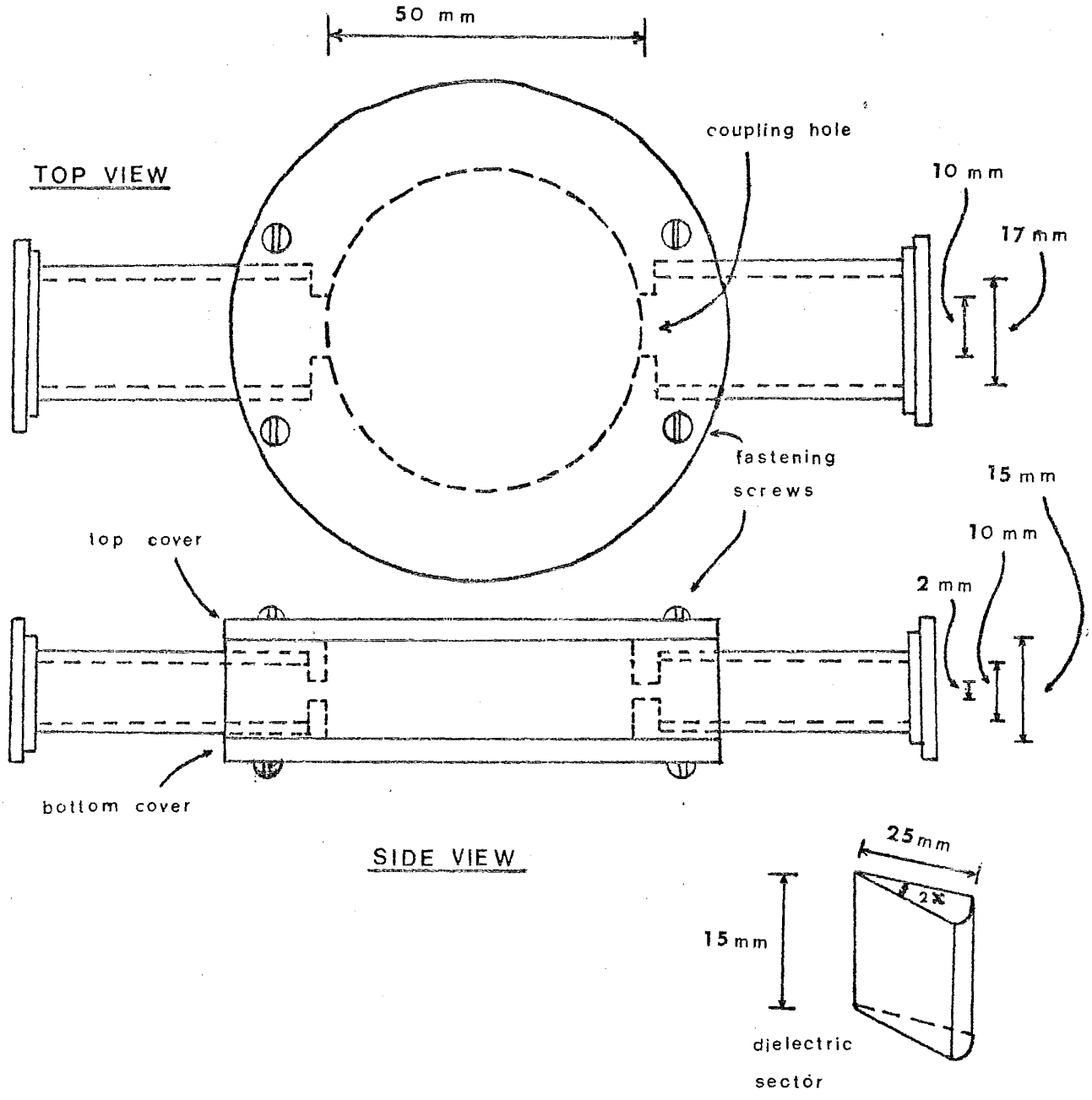

FIGURE 9.2 Top and side views of circular-cylindrical cavity. It is made from a section of brass tube and is coupled to two sections of standard (British WG 16) X-band waveguide through coupling holes. The various dimensions of the cavity, holes and waveguide are indicated in the figure. The insert is a sketch of a dielectric sector.

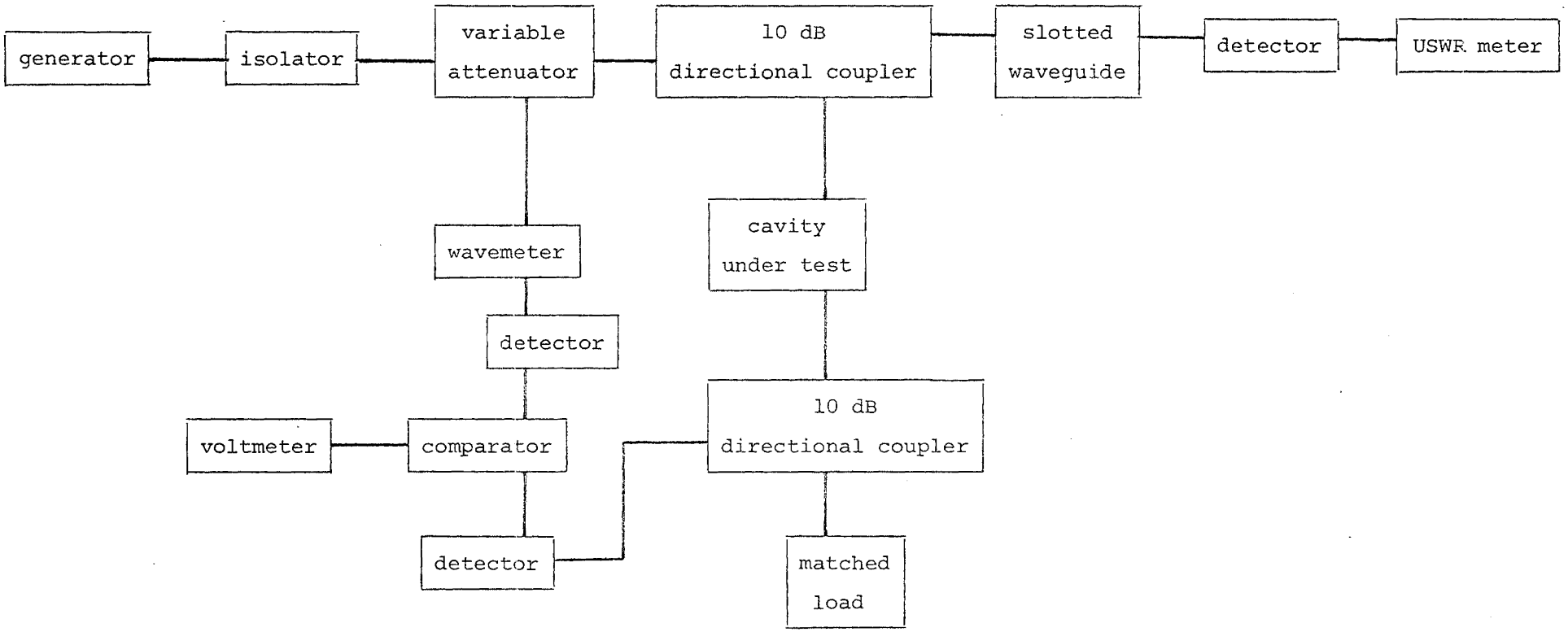

FIGURE 9.3 Experimental setup for the measurement of cutoff wave number for a circular-cylindrical cavity loaded with a dielectric sector. The ratio of the input and output powers was determined by the comparator and displayed on the voltmeter.

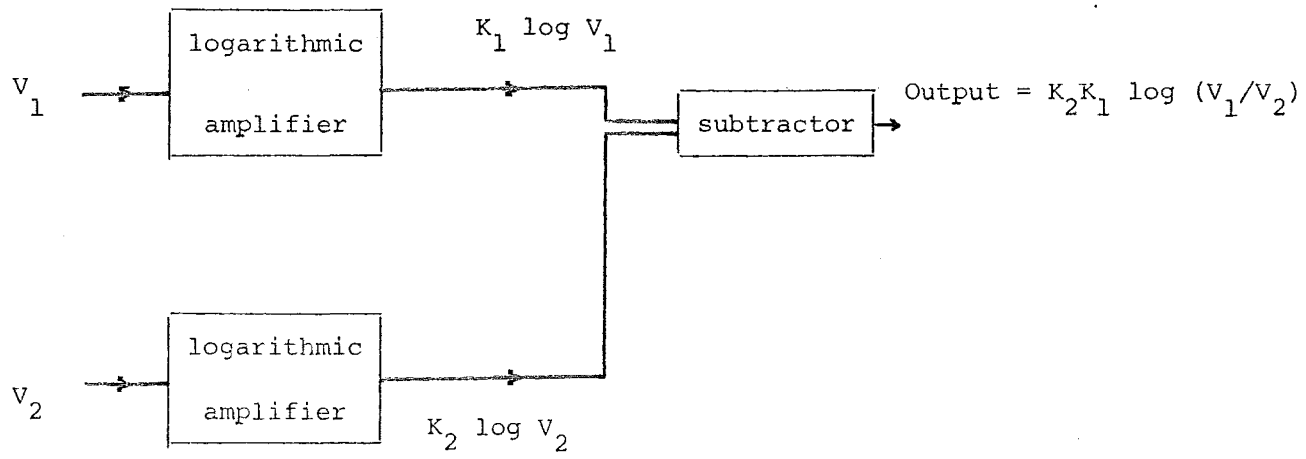

FIGURE 9.4 Block diagram of comparator circuit (cf. Mnyama 1983). The amplification factors of the logarithmic amplifiers are, identically, K_1. The amplification factor of the subtractor is K_2.

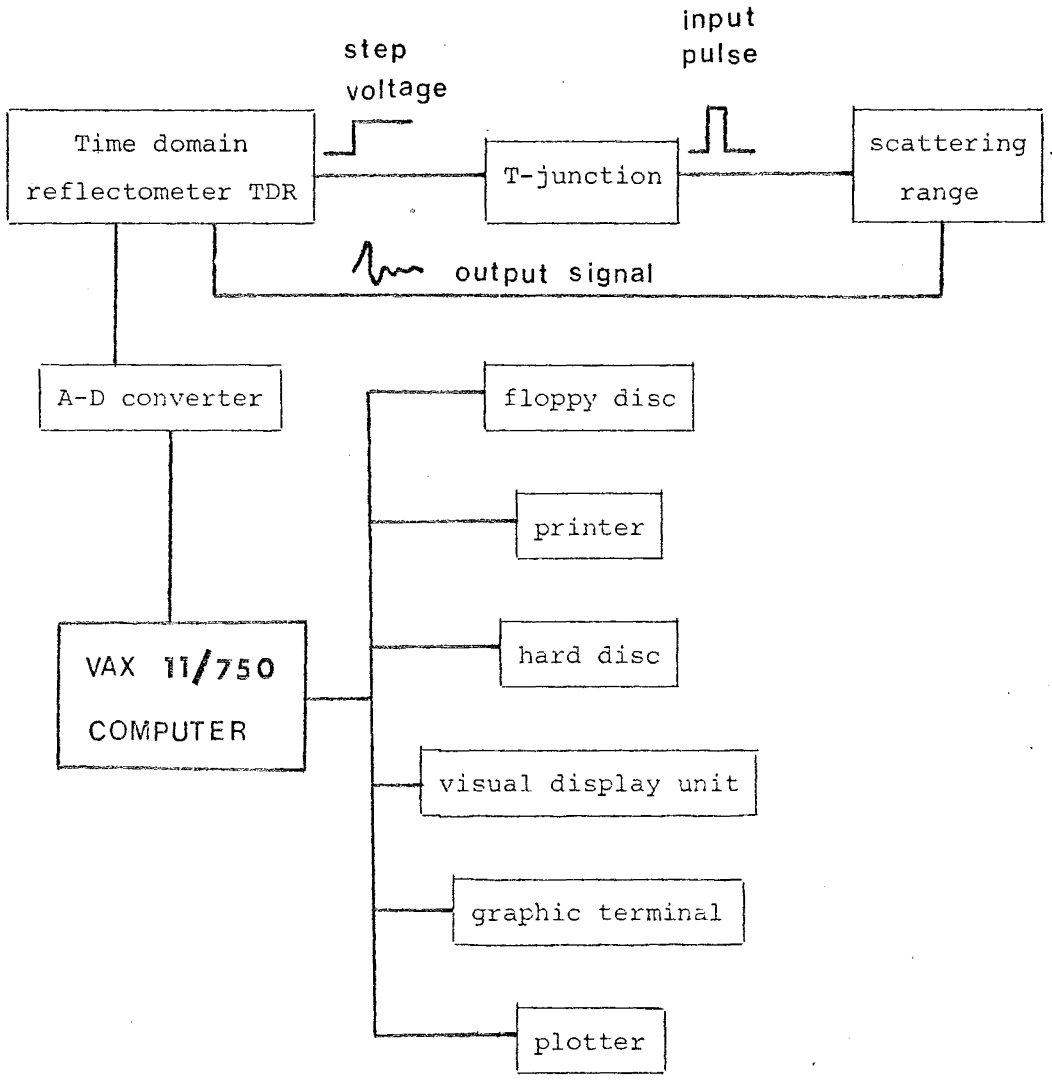

FIGURE 9.5 Experimental setup of parallel-plate, time domain scattering measurement. A pulse was generated by the TDR/T-junction and fed into the scattering range. The output waveform was sampled and stored in the VAX computer.

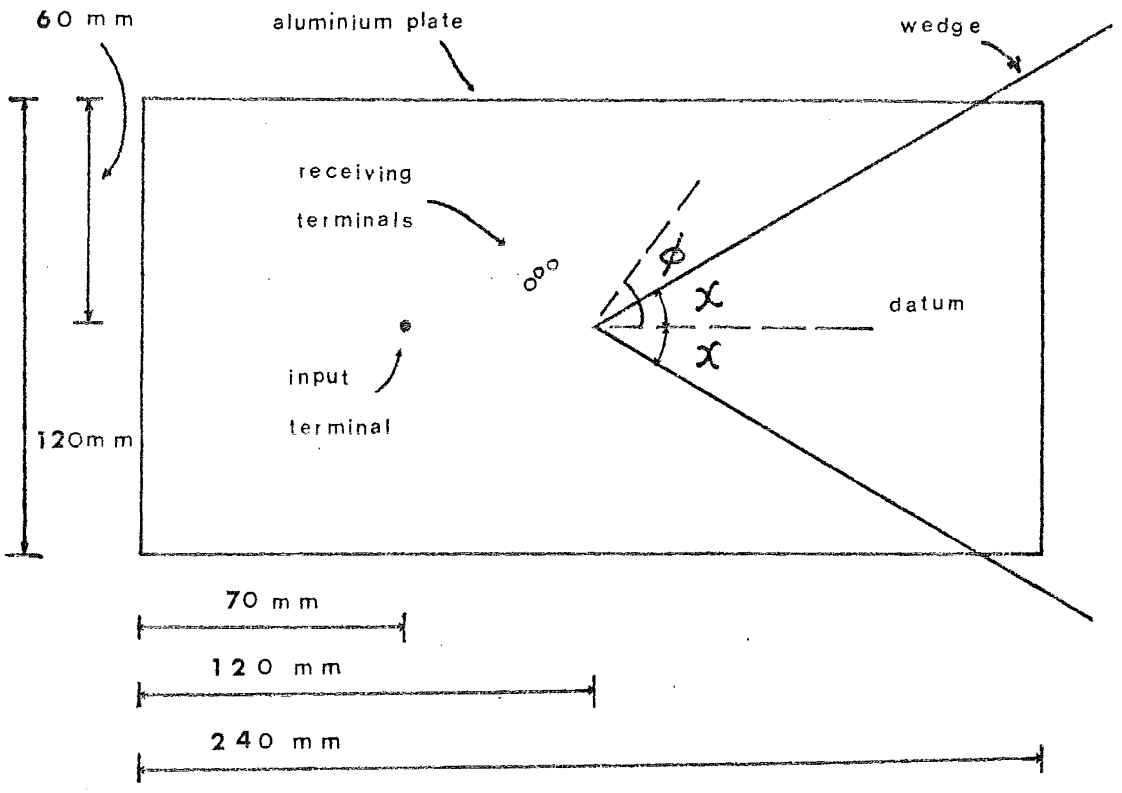

FIGURE 9.6 Parallel-plate scattering range. The input terminal was positioned 50 cm from the apex of the wedge while the output terminals were positioned 20 cm from the apex. The angular displacement between each receiving terminal was 10° for $2\chi < \phi < \pi$.

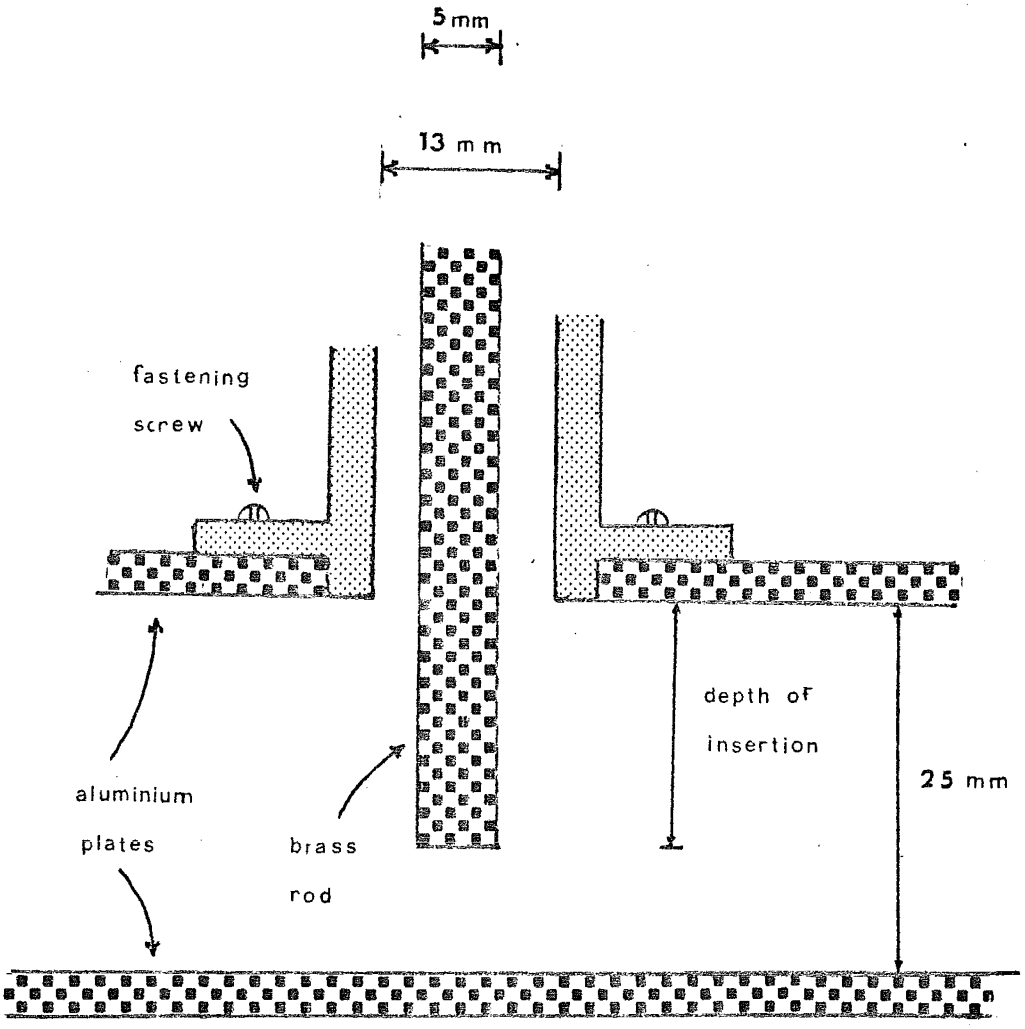

FIGURE 9.7 Input-output terminal. The terminal was fastened to the aluminium plates by screws. It could be removed and replaced by an aluminium plug. The depth of insertion of the centre brass rod was adjustable.

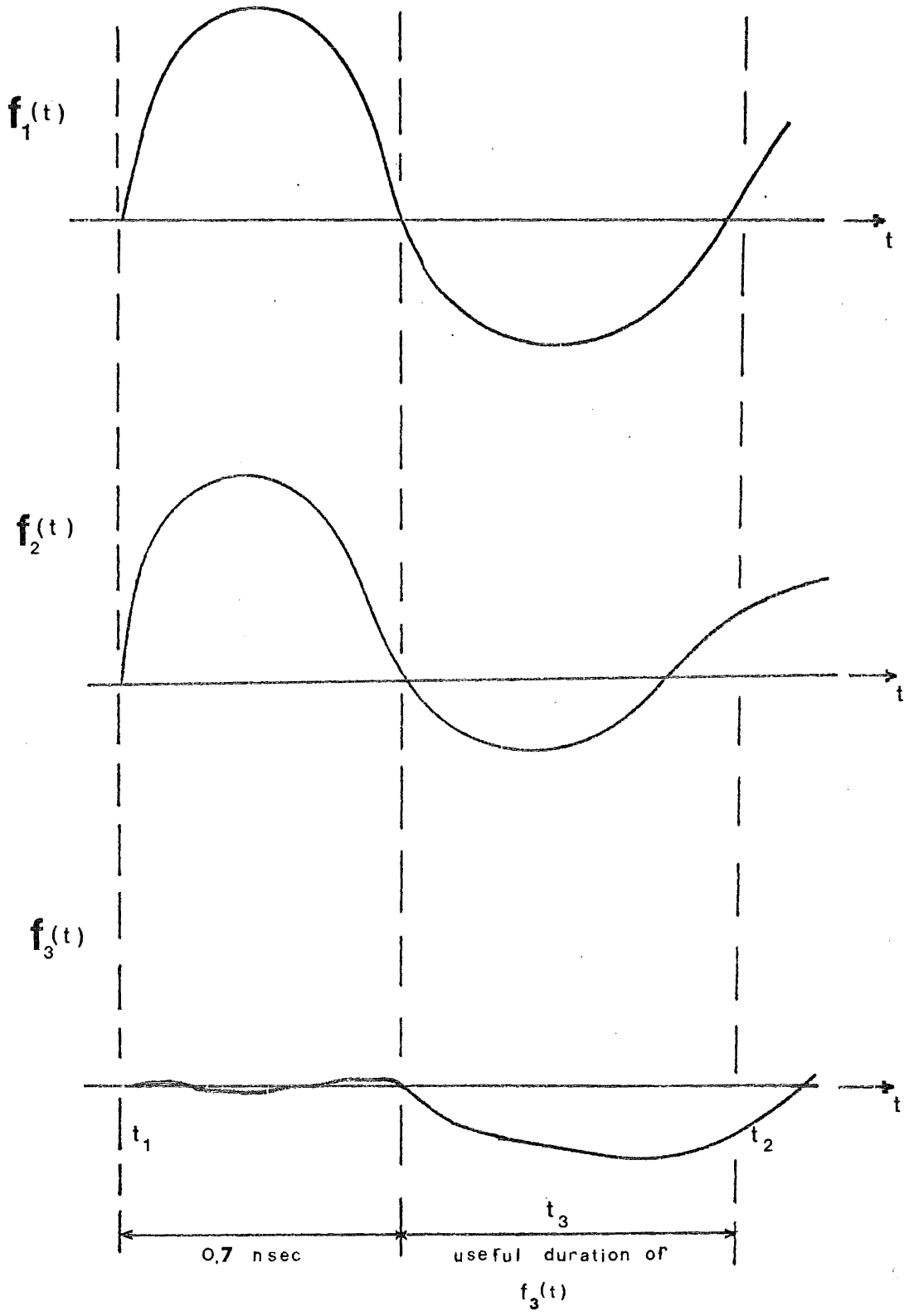

FIGURE 9.8 The field $f_3(t)$, scattered by the wedge was obtained by subtracting $f_1(t)$, field received without the wedge present, from $f_2(t)$, field received with the wedge in place.

PART III

CONCLUSIONS

CHAPTER TEN

CONCLUSIONS AND SUGGESTIONS FOR FURTHER RESEARCH

In this chapter, general conclusions are drawn from the results reported in this thesis and comments and suggestions for further research are given where applicable. Section 10.1 deals with general inverse scattering problems, Section 10.2 deals with general direct scattering problems and finally Section 10.3 deals specifically with penetrable wedge diffraction problems.

10.1 GENERAL INVERSE PROBLEMS

Special solutions, or solutions applicable to a specific problem, and approximations, abound in the literature on inverse problems (cf. Chapter 2). Unfortunately, it has not been possible, to date, to construct a general algorithm. However, two approaches, reported by Bates (1975b, 1984), Roger (1981), Johnson et. al. (1983, 1984) and Wall (1984) have shown to be most encouraging.

The first approach, called model-fitting in this thesis, involves modelling the scattering parameters and calculating the scattered fields so that they can be compared with measured data. The initial model is then modified accordingly. This approach is implemented either through the polarisation source formulation (cf. Johnson et. al. 1983, 1984) the null-field formulation (cf. Wall 1984) or a complex differential operator (cf. Roger 1981). The advantage of this approach is its generality. One can attempt to reconstruct any scattering parameters from whatever information is available, at least in principle. The drawback of this approach is that one requires a greater amount of prior knowledge (of the scattering parameters), when fewer scattering data are available.

When the model is good in the sense that it resembles the actual scatterer, fast converging results can be obtained. On the other hand, if the model is bad, the numerical procedure may diverge, or converge to a wrong answer. In other words, uniqueness cannot be guaranteed. Therefore, the most immediate problem, other than convincing other researchers of the worthwhileness of this approach, is to find a general goodness measure required

for the initial model, i.e. one must be able to say confidently, when given a certain amount of prior information, what is the probability of reconstructing the scatterer faithfully.

One possible way of arriving at a reasonably accurate model, surprisingly stems from an inverse source formulation reported in this thesis (cf. Section 2.5). It seems that one may be able to estimate the positions of scattering centres to a useful accuracy. A fair model could then be constructed by joining the scattering centres.

The second approach, on the other hand, introduces no assumption or approximation. It has already been shown (cf. Section 2.4.2) that one can deduce theoretical resolution limits from this formulation. The problem, at present, is to devise a numerical procedure which is able to extract, efficiently, a stable solution from the complicated non-linear equations derived (cf. Bates 1984).

10.2 GENERAL DIRECT PROBLEMS

10.2.1 Rayleigh Hypotheses

Besides the need for building bigger and faster computers which is, incidentally, beyond the scope of this thesis, the most pressing problem is to investigate, analytically, the consequences of the failure of the Rayleigh hypotheses. There has been much argument (cf. Bates et. al. 1973) on whether calculated scattered fields can be analytically correct in situations where the Rayleigh hypotheses do not hold. Details of these arguments have been discussed in Sections 1.5.5.6 and 8.1. Essentially, Bates (1975a) indicates that the scattered field is correct when calculated from the Green's integral of the surface field. Moreover, the surface field need not be derived from the infinite series representations, whose viability depends on the Rayleigh hypotheses. It needs only to be correct on the surface and can therefore be represented as a truncated series (cf. Ikuno and Yasuura 1973). This argument, unfortunately, has not been accepted universally. Therefore, it would be very beneficial if one could show rigorously that the postulate is correct.

10.2.2 Numerical Algorithms

The need for efficient numerical methods which can lead to stable solutions to general scattering problems goes, of course, without saying. Specific problems in this area include:

(i) Handling of large matrices,

(ii) Instability of matrix equations, and

(iii) Relative convergence.

The last problem, shown by Mittra and Lee (1971) to be connected to the physics of the scattering problem, is said to be just a pure numerical difficulty by Shuley (1985) and Leroy (1983). Therefore, the need for a thorough investigation of this is becoming increasingly urgent as more and more researchers (cf. Section 1.5) are encountering 'relative convergence' difficulties.

10.2.3 Bodies of Non-standard Shapes

Three forms of simple bodies are most interesting and warrant immediate attention. Infinite bodies, bodies with corners and concave bodies. These three classes of scatterers present different problems in scattering calculations. The first two cases are discussed in some detail in Section 10.3. Concave bodies, on the other hand, can exhibit instabilities which often relate to the validity or otherwise of the Rayleigh hypotheses. Attempts have been made (cf. Wall 1984) to overcome this numerical stability by expressing the fields in terms of expansions referred to multiple coordinate origins (Fig. 10.1).

In the conventional null-field method, for example, the fields are expanded with respect to a single origin, O_1 say, and the null-field condition is imposed on C_1. However, one can also expand the fields with respect to O_2 and O_3 say. The null-field condition must then be imposed on C_1, C_2 and C_3 simultaneously. This method accords with the spirit of the technique for improving stability through increasing the value ζ defined in (1.102) Limited success has been obtained (cf. Wall 1984). It would therefore, be worthwhile to pursue such an investigation further.

10.3 INFINITE PENETRABLE WEDGES

The problem of infinite penetrable wedge diffraction is, no doubt, the most notable of the remaining unsolved problems for scattering by simple shapes. The solutions to scattering by infinite conducting wedges have long been established (cf. Chapter 3). If its solution could be obtained and formulated useably as a canonical problem, the infinite penetrable wedge problem would be able to broaden the scope of the Geometrical Theory of Diffraction.

10.3.1 Experimental Research

A wise man has once said, 'A picture is worth more than a thousand words'. It is so very true in scientific research of this kind. To avoid future controversy on the penetrable wedge problem, one must seek ways in which to verify results with confidence. There is nothing better than data collected experimentally. Section 9.1 provides a partial experimental verification of the effectiveness of the theory described in Chapter 5. Unfortunately, due to the limitation imposed by available experimental facilities, the parallel plate experiment described in Section 9.2 has not been able to generate data of sufficient accuracy. It should, therefore, be the first task of any further research into penetrable wedge diffraction to obtain experimental data of sufficient accuracy for a proper evaluation of computational results.

10.3.2 Edge Behaviour and its Application

The formulation by Bates (1980a) provides a clear picture of the field behaviour near a penetrable edge. This result, together with those of Meixner (1972) and Andersen and Solodoukhov (1978), when incorporated into the formulation of field expansions, can improve markedly the efficiency of the computational procedure. It would, therefore, be appropriate, when attempting to solve any problem of scattering by a penetrable body with corners, to use the proper edge behaviour.

10.3.3 Null-field Method in Penetrable Wedge Diffraction Problems

It is shown in Chapter 8 that the null-field method can be applied to the penetrable wedge diffraction problem. Stable results have also been obtained. Furthermore, it is shown in Chapter 3 that the procedure is analytically correct when applied to infinite bodies. The following tasks still need to be done:

(i) Verification of results with experimental data.

(ii) Improving the efficiency of the method. This might be effected either by improving the numerical procedure, or by careful re-arrangement of the numerous infinite series appearing in the formulation.

(iii) Extension of the formulation to handle incident fields at arbitrary angles.

When the incident wave impinges on the wedge at arbitrary angles, multiple reflection and refraction (Fig. 10.2) takes place. However, it would not be a difficult task to incorporate all of the geometrical optics fields into the surface field formulation. For instance, in Fig. 10.2, where three refractions take place, the surface field must then be

$$\begin{aligned}\Psi_{surface} = &\lim_{\phi\to\chi}\left[\exp(jk\rho\cos(\phi-\theta))\right]\\ &+\lim_{\phi\to\chi}\left[G_1\exp(-jk\rho\cos(\phi-\theta_1))\right]\\ &+\lim_{\phi\to\chi}\left[H_1H_2\exp(-jk\rho\cos(\phi-\theta_2))\right]\\ &+\lim_{\phi\to\chi}\left[H_1G_2H_2\exp(-jk\rho\cos(\phi-\theta_3))\right]\\ &+\lim_{\phi\to\chi}\left[\Psi_{diff.}\right]\end{aligned} \qquad (10.1)$$

where the first term is the incident field, the second, third and fourth terms are the geometrical optics fields and the last term represents the diffracted field. G_1, G_2, H_1 and H_2 are the corresponding reflection and refraction coefficients found from Snell's law. Furthermore, the first four terms exist only in appropriate regions. The last term ensures the field's continuity across the reflection/refraction boundaries.

The surface field expansion (10.1) might be used in the radial null-field method for penetrable wedge scattering of a wave incident at an arbitrary angle.

(iv) Dielectric wedge scattering of H-polarised incident field. When an H-polarised field is incident on a dielectric wedge, the field expansion must include Bessel functions of non-integer orders μ (cf. Bates 1980a). The values of μ, as indicated by Bates (1980a), take the form

$$\mu = \alpha_n + 2m \qquad m = 0,1,2, \ldots .$$
$$n = 0,1,2, \ldots . \qquad (10.2)$$

The problem is then to choose an appropriate combination of m and n, such that a stable solution can be calculated. Care will be needed to avoid 'relative convergence' difficulties. On the other hand, the surface integral on LHS of the null-field equation (1.95a) produces a series of the form

$$\sum_{\ell,m} A_m \left[f(\nu,\chi,\phi,\ell,m,\alpha_n)\ J_{\alpha_n+2m}(k\rho) + g(\nu,\chi,\phi,\ell,m,\alpha_n)\ J_\ell(k\rho) \right] \qquad (10.3)$$

while the RHS of the null-field equation (1.95a) represents the incident wave which takes the form

$$\sum_{\ell=o}^{\infty} \varepsilon_\ell (j)^\ell \cos \ell(\phi-\theta)\ J_\ell(k\rho) \qquad (10.4)$$

where f and g in (10.3) are some complex functions generated by the surface integral of (1.95a). The A_m are the surface field expansion coefficients. Furthermore, as indicated in Section 3.3, the coefficients of all Bessel functions of non-integer orders must reduce to zero individually, which therefore implies that

$$\sum_{\ell} f(\nu,\chi,\phi,\ell,m,\alpha_n) = 0$$
$$m = 0,1,2, \ldots \qquad (10.5)$$

Moreover, on equating the coefficients of the Bessel functions of integer orders, one gets

$$\sum_{m} A_m\ g(\nu,\chi,\phi,\ell,m,\alpha_n) = \varepsilon_\ell (j)^\ell \cos \ell(\phi-\theta)$$
$$\ell = 0,1,2, \ldots . \qquad (10.6)$$

It may seem that a new difficulty arises due to the extra constraint imposed by (10.5). However, careful examination of (10.2), (10.5) and (10.6) reveals that (10.5) can be used to eliminate the uncertainty introduced by (10.2), i.e. one should choose the appropriate values of α_n and m such that (10.5) is satisfied. Finally, (10.6) can be used to solve for the A_m. Therefore, it seems that the null-field method should be applicable to dielectric wedge scattering of the H-polarised field as well.

(v) The surface field expansion, as argued in Section 8.1, is only valid within a finite distance of the apex. Therefore, it would be beneficial to compare the result represented by (8.25) with the result obtained by using two coupled equations (1.95a) and (1.95c). When two coupled equations are used, the surface field and its derivative can then be expanded as

$$\Psi_{surface} = \sum_{m=o}^{\infty} A_m J_m(k\rho) \cos m\chi \tag{10.7}$$

$$\partial\Psi_{surface}/\partial\hat{n} = \sum_{m=o}^{\infty} B_m J_m(k\rho) \sin m\chi \tag{10.8}$$

The expansion coefficients A_m and B_m can be calculated from (1.95a) and (1.95c) with the aid of the multiplication theorem for Bessel functions (1.36). This is of course a much more inefficient (cf. Section 6.2.2) and numerically unstable (cf. Section 4.1) procedure. However, if all the numerical problems could be overcome, it would provide a distinctly rigorous solution to the penetrable wedge diffraction problem.

10.4 CONCLUSION

Solutions to various direct and inverse scattering problems are presented in this thesis. Some results are shown to have converged numerically. Furthermore, some results are shown to agree reasonably well with experimental data. Comparisons between results obtained by various authors have also been made.

A new, potentially useful, inverse source reconstruction algorithm is described in Section 2.5. The null-field method is formulated for general inverse scattering problems in Section 2.7 and viable preliminary results are obtained. Theoretical resolution limits for inverse scattering calculations are also derived (cf. Section 2.4.2). The advantage (numerical efficiency) of incorporating the proper edge behaviour in field expansions is illustrated in Chapter 6, using the example of wedge-cylinder scattering. Chapter 7 presents specialised solutions to penetrable wedge diffraction problems. Unfortunately, due to difficulties associated with 'relative convergence', it has not been found possible to generalise these solutions.

The solution presented by Joo et al (1980, 1984) and Kim et al (1983) is argued to be incorrect in Section 4.4. In Chapter 9, the measured and calcu-

lated cutoff wave numbers of a circular-cylindrical cavity loaded with dielectric sectors are shown to agree to about 1%. Preliminary results from a parallel-plate scattering range are reported, and it is shown what improvements would be needed to obtain measurements accurate enough to permit computations to be usefully assessed.

Chapter 8 introduces a radial null-field method for the infinite penetrable wedge diffraction problem. This method is shown to be analytically correct for infinite (conducting) wedge scattering in Section 3.3. Combining with a geometrical theory of diffraction type field expansion, this radial null-field method is invoked to derive solutions for penetrable wedge scattering problems. The diffracted fields are shown to be outgoing and they agree reasonably well with results obtained by Kaminetzky and Keller (1975) and Rawlins (1977a), especially in the back scattering region. The diffraction pattern of a long wedge-cylinder is also shown to agree encouragingly well with the corresponding wedge solution.

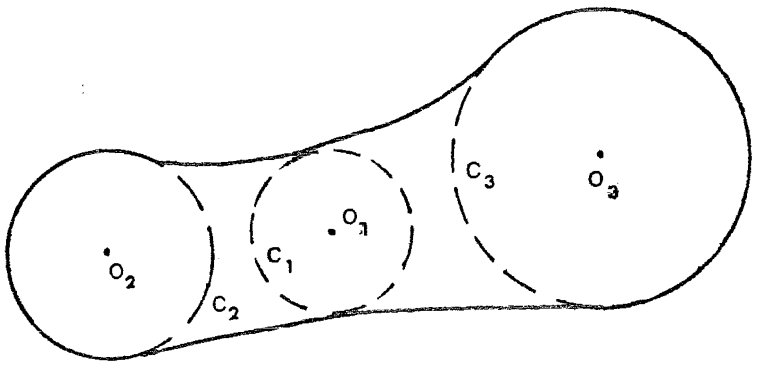

FIGURE 10.1 Use of more than one origin in calculation of scattering by a concave bode. O_1, O_2, and O_3 are the origins while C_1, C_2 and C_3 are circles, within which the null-field condition is imposed.

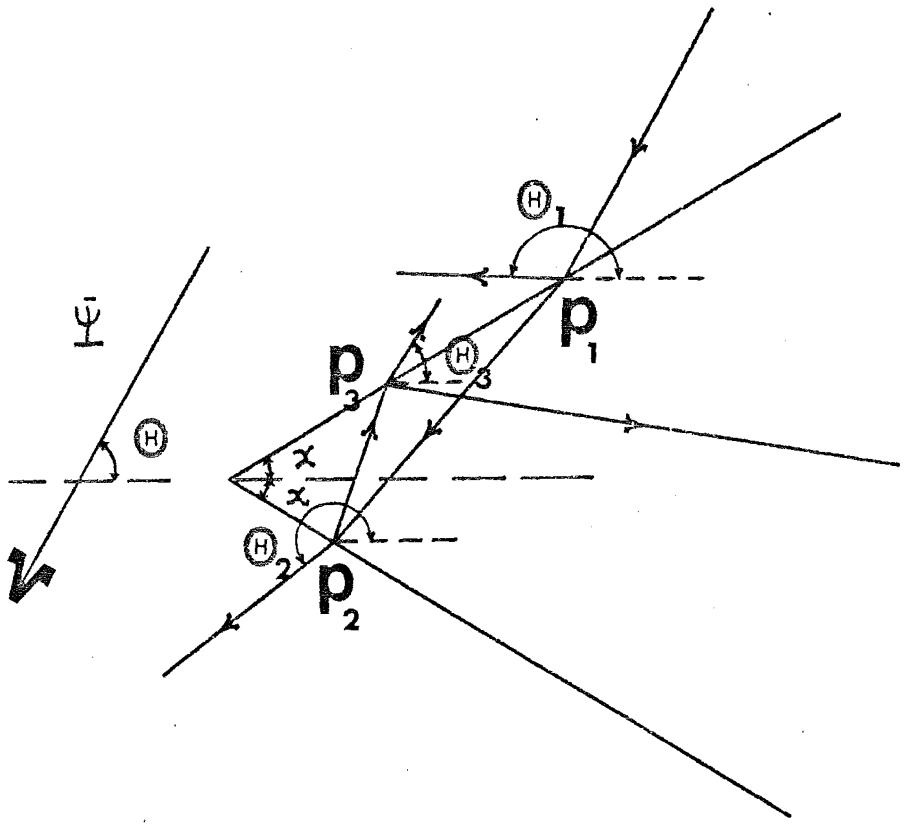

FIGURE 10.2 Multiple reflection and refraction occurs on the wedge surfaces when the incoming field is incident upon the wedge at an arbitrary angle.

REFERENCES

ABRAMOWITZ, M. and STEGUN, I.A. 'Handbook of mathematical functions' Dover Publications, Inc. New York, 1965.

AGARWAL, G.S. Relation between Waterman's extended boundary condition and the generalised extinction theorem. Phys. Rev. D., vol. 14, pp 1168-1171, 1976.

ALBERT, G.E. and SYNGE, J.L. The general problem of antenna radiation and the fundamental interval equation with application to an antenna of revolution, Part I. Quarterly Appl. Math. vol. 6, pp 117-131, 1948.

ALEKSANDROVA, A.A. and KHIZHNYA, N.A. Diffraction of electromagnetic waves by a dielectric wegde. Sov. Phys. Tech. Phys., vol. 19, pp 1385-1389, 1975.

ALEKSANDROVA, A.A. and KHIZHNYAK, N.A. Near field diffracted at a dielectric wedge. J. Appl. Mech. Tech. Phys., vol. 17, pp 594-599, 1976.

ALEKSANDROVA, A.A. and KHIZHNYAK, N.A. Scattering of electromagnetic waves on a dielectric wedge. Radioteknika Kharkov, pp 98-105, 1978.

ANDERSEN, J.B. and SOLODUKHOV, V.V. Field behaviour near a dielectric wedge. IEEE Transactions on Antennas and Propagation, vol. 26, pp 598-602, 1978.

ANDERSON, I. Plane wave diffraction by a thin dielectric half-plane. IEEE Transactions on Antennas and Propagation, vol. 27, pp 584-589, 1979.

BAKER, B.B. and COPSON, E.T. "The mathematical theory of Huygen's principle" Clarendon Press: Oxford, 1953.

BACKUS, G.E. and GILBERT, J.F. Numerical applications of a formalism for geophysical inverse problems. Geophys. J.R. Astr. Soc., vol. 13, pp 247-276, 1967.

BALLING, P. Surface fields on the source-excited dielectric wedge. IEEE Transactions on Antennas and Propagation, vol. 21, pp 113-115, 1973.

BALLING P. On the role of lateral waves in the radiation from the dielectric wedge. IEEE Transactions on Antennas and Propagation, vol. 21, pp 247-248, 1973.

BAMBERGER, A., CHAVENT, G. and LAILLY, P. About the stability of the inverse problem in one-dimensional wave equations - application to the interpretation of seismic profiles. Appl. Math. Optim., vol. 5, pp 1-47, 1979.

BALTES, H.P. 'Inverse source problems in optics'. Springer-Verlag, Berlin, 1978.

BALTES, H.P. 'Inverse scattering problems in optics'. Springer-Verlag: Berlin, 1980.

BATES, R.H.T. Simulation techniques for evaluation of space vehicle identification radar systems, vol. 1 and 2. Sperry Rand Research Centre, Sudbury, Mass., USA, Report No. SRCC 526 - 38, 1965.

BATES, R.H.T. Radiation pattern of line sources on a wedge covered with finite distributions of dielectric. Proc. IEEE, vol. 55, pp 1650-1651, 1967a.

BATES, R.H.T. The point matching method for interior and exterior two-dimensional boundary value problems. IEEE Transactions on Microwave Theory and Techniques, vol. 15, pp 185-187, 1967b.

BATES, R.H.T. Modal expansions for electromagnetic scattering from perfectly conducting cylinders of arbitrary cross-section. Proc. IEEE, vol. 115, pp 1443-1445, 1968.

BATES. R.H.T. The theory of the point matching method for perfectly conducting waveguides and transmission lines. IEEE Transactions on Microwave Theory and Techniques, vol. 17, pp 294-301, 1969a.

BATES, R.H.T. Rayleigh hypotheses, the extended-boundary condition and point matching. Electronics Letters, vol. 5, pp 654-655, 1969b.

BATES, R.H.T. Towards estimating the shapes of radar targets. Elect. Engrg. Trans. Instn. Engrs. Aust., vol. 5, pp 290-294, 1969c.

BATES, R.H.T. and HUNTER, J.D. Scattering from perfectly conducting wedges excited by transversely polarised line sources. Int. J. Electr., vol. 26, pp 91-94, 1969.

BATES, R.H.T. Inverse scattering for totally reflecting objects, Arch. Rational Mech. Anal., vol. 38, pp 123-130, 1970.

BATES, R.H.T. and NG, F.L. Polarisation-source formulation of electro-magnetism and dielectric-loaded waveguides. Proc. IEE, vol. 119, pp 1568-1574, 1972.

BATES, R.H.T., JAMES, J.R., CALLETT, I.N.L. and MILLAR, R.F. An overview of point matching. Radio and Electronic Eng., vol. 43, pp 193-200, 1973.

BATES, R.H.T. and NG, F.L. Point matching computation of transverse resonances. Int. J. Numerical Methods in Eng., vol. 6, pp 155-168, 1973.

BATES, B.H.T. Wavefunctions for prisms. Int. J. Electronics. vol. 34, pp 81-95, 1973.

BATES, B.H.T. New justification for physical optics and the aperture-field method. AGARD Conf. Pub. CPP-14, pp 36-42, 1974.

BATES, B.H.T. Analytic constraints on electromagnetic field computations. IEEE Transactions on Microwave Theory and Techniques, vol. 23, pp 605-623, 1975a.

BATES, B.H.T. Global solution to the scalar inverse scattering problem. J. Phys. A: Math. Gen., vol. 8, pp 80-82, 1975.

BATES, B.H.T., BOERNER, W.M. and DUNLOP, G.R. An extended Rytov approximation and its significance for remote sensing and inverse scattering. Optics Comm., vol. 18, pp 421-423, 1976.

BATES, B.H.T. and WALL, D.J.N. Null field approach to scalar diffraction. I. General methods, II. Aproximate methods, III. Inverse methods. Phil. Trans. R. Soc. Lond. A, vol 287, pp 45-114, 1977.

BATES, B.H.T. Diffraction by a partially transparent wedge. Unpublished report, University of Canterbury, 1980a.

BATES, R.H.T. General introduction to the extended boundary condition in 'Acoustic, electromagnetic and elastic scattering - forcus on the T-matrix approach', VARADAN, V.K. and VARADAN, V.V. eds. Pergamon Press, pp 21-31, 1980b.

BATES, R.H.T., MCKINON, G.C. and SEAGAR, A.D. A limitation on systems for imaging electrical conductivity distribution. IEEE Transactions on Biomedical Engineering, vol. 27, pp 418-420, 1980.

BATES, R.H.T. and MILLANE R.P. Time domain approach to inverse scattering. IEEE Transactions on Antennas and Propagation, vol. 29, pp 309-363, 1981.

BATES R.H.T. Astronomical speckle imaging. Physics Report, vol. 95, pp 204-294, 1982.

BATES R.H.T., GARDEN K.L. and PETERS, T.M. Overview of computerized tomography with emphasis on future developments. Proc. IEEE, vol. 71, pp 356-372, 1983.

BATES, R.H.T. Full wave computed tomography. I : Fundamental theory. IEE Proc. Pt. A, vol. 131, pp 610-615, 1984.

BERNTSEN, S. Diffraction of an electromagnetic wave by a dielectric wedge. IEEE/APS - Symposium Publication, 1978.

BERNTSEN, S. Diffraction of an electric polarized wave by a dielectric wedge. SIAM J. APPL. Math., vol. 43, pp 186-211, 1983.

BERAN, M.J. and PARRENT, G.B. 'Theory of partial coherence'. Society of Photo-optical Instrumentation Engineers, 1974.

BER TERO, M., VIANO, G.A., PASQUALETTI, F., ROUCHI, L. and FRANCIS, G.T.D. The inverse scattering problem in the Born approximation and the number of degrees of freedom. Optica Acta, vol. 27, pp 1011-1024, 1980.

BIGGS, A.W. Asymptotic approximations for surface scattering integrals. IEEE Transactions on Antennas and Propagation, vol. 25, 443-445, 1977.

BIGGS, A.W. Fourier transform in propagation and scattering problems. IEEE Transactions on Antennas and Propagation, vol. 25, pp 585-586, 1977.

BORROVNIKOV, M.S. and ZAMARRAEVA, V.P. On the singularity of the field near a dielectric wedge. Sov. Phys. J., vol. 9, pp 1230-1232, 1973.

BOERNER, W.M., VANDENBERCHE, F.H. and HAMID, M.A.K. Determination of the electrical radius ka of a circular cylindrical scatterer from the scattered field. Candian J. Phys., vol. 49, pp 804-819, 1971.

BOLOMEY, J.C. and WIRGIN, A. Numerical comparision of the Green's function and the waterman and Rayligh theories of scattering from a cylinder with arbitrary cross-section. Proc. IEE, vol. 121, pp 794-904, 1974.

BORN, M. and WOLF, E. 'Principles of optics'. Pergamon Press: Oxford, 1970.

BOSTROM, A. A new expression for the T-matrix in the null field approach. Proc. URSI Int. Symp., Santiago, 1983a.

BOSTROM, A. Passbands stopbands for an electromagnetic waveguid with a periodically varying cross section. IEEE Transactions on Microwave Theory and Techniques, vol. 31, pp 752-756, 1983b.

BOSTROM, A. Scattering of acoustic waves by a layered elastic obstacle in a field - an improved null-field approach. J. Acoust. Soc. Am., vol. 76, pp 588-593, 1984.

BOUWKAMP, C.J. A note on singularities occurring at sharp edges in electromagnetic diffraction theory. Physica, vol. 12, pp 467-474, 1946.

BOUWKAMP, C.J. Diffraction Theory. Reports on Progress in Physics: London, vol. 12, pp 35-100, 1954.

BOWMAN, J.J., SENIOR, T.B.A. and USLENGHI, P.L.E. 'Electromagnetic and acoustic scattering by simple shapes'. North-Holland Publishing Co: Amsterdam, 1969.

BRESSAN, M. and CONCIAURO, G. An optimum inversion method for the remote probing of defective phase shifters in phase arrays. IEEE Transactions on Antennas and Propagation, vol. 30, pp 1184-1190, 1982.

BROMWICH, T.J.I'A. Diffraction of waves by a wedge. Proc. Lond. Math. Soc., vol. 14, pp 450-463, 1915.

BURNSIDE, W.D., YU, C.L., MARHEFKA, R.J. A technique to combine the geometical theory of diffractions and the moment method. IEEE Transactions on Antennas and Propagation, vol. 23, pp 551-558, 1975.

BROOK, G.H. and KHARADLY, M.M.Z. Field behaviour near anisotropic and multidielectric edges. IEEE Transactions on Antennas and Propagation, vol. 25, pp 571-575, 1977.

BURROWS, M.L. Equivalence of the Rayleigh solution and the extended-boundary condition solution for scattering problems. Electr. Lett., vol. 5, pp 277-278, 1969.

BURROWS, M.L. Example of the generalised-function validity of the Rayleigh hypothesis. Electr. Lett., vol. 5, pp 694-695, 1969.

CABAYAN, H.S., MURPHY, R.C. and PAVLASEK, T.J.F. Numerical stability and near field reconstruction, IEEE Transactions on Antennas and Propagation, vol. 21, pp 346-351, 1973.

CARSLAW, H.S. Diffraction of waves by a wedge of any angle. Proc. Lond. Math. Soc., vol. 18, pp 291-306, 1920.

CHADHA, R. and GUPTA, K.C. Green's functions for circular sectors, annular rings and annualr sectors in planar microwave circuit. IEEE Transactions on Microwave Theory and Techniques, vol. 29, pp 68-71, 1981.

CHANM K.K. and FELSEN, L.B. The pulsed field due to an electric dipole in the presence of a perfectly conducting wedge. IEEE Transactions on Antennas and Propagation, vol. 25, pp 420-423, 1977.

CHU, T.S., KOUYOUMJIAN, R.G., KARAL, F.C., KARP, S.N. The diffraction of surface waves by a terminated structure in the form of a right-angle bend. IRE Transactions on Antennas and Propagation, vol. 10, pp 679-686, 1962.

CHU, T.S. and KOUYOUMJIAN, R.G. On the surface wave diffraction by a wedge. IEEE Transactions on Antennas and Propagation, vol. 13, pp 159-164, 1965.

CLARKOWSKI, A., BOERSMA J. and MITTRA, R. Plane-wave diffraction by a wedge - a spectral domain approach, IEEE Transactions on Antennas and Propagation, vol. 32, pp 20-29, 1984.

CLEMMOW, P.C., 'The plane wave spectrum representation of electromagnetic fields'. Peragmon Presa: Oxford, 1966.

COHOON, D.K. Reduction of the cost of solving an integral equation arising in electromagnetic scattering through the use of group theory, IEEE Transactions on Antennas and Propagation, vol. 28, pp 104-127, 1980.

COLLIN, R.E. Scattering by an infinite array of thin dielectric sheets. IRE Transactions on Antennas and Propagation, vol. 8, pp 62-67, 1960.

COLLIN, L. 'Mathematics of Profile Inversion', NASA TMX - 62, 150, NASA Technical Memorandum, 1972.

COLTON, D. and KRESS, R. The unique solvability of the null-field equations of acoustics. Q.J. Mech. Appl. Math., vol. 36, pp 87-95, 1983.

DAS, Y. and BOERNER, W.M. On radar target shape estimation using algorithms for reconstruction from projections. IEEE Transactions on Antennas and Propagation, vol. 26, pp 274-279, 1978.

DAVIES, J.B. and MUILWYK, C.A. Numerical solution of uniform hollow waveguides with boundaries of arbitrary shape. Proc. IEE. vol. 113, pp 277-284, 1966.

DAVIES, J.B. A least-squares boundary residual method for the numerical solution of scattering problems. IEEE Transactions on Microwave Theory and Techniques, vol. 21, pp 99-104, 1973.

DAVIES, L.C. Electrostatic edge modes of a dielectric wedge. Phys. Rev., vol. 14, pp 5523-5525, 1976.

DECKEN, J.G. Approximating conditional moments of the multivariate normal distribution. SIAM J. Sci. Stat. Comput., vol. 4, pp 720-732, 1983.

DESCHAMPS, G.A. and CABAYAN, H.S. Antenna synthesis and solution of inverse problems by regulatisation methods. IEEE Transactions on Antennas and Propagation, vol. 20, pp 268-274, 1972.

DEVANEY, A.J. and WOLF, E. Multipole expansions and plane wave representations of the electromagnetic field. J. Math. Phys., vol. 15, pp 234-244, 1974.

DEVANEY, A.J. and CHIDLAW, R. On the uniqueness question in the problem of phase retrival from intensity measurements. J. Opt. Soc. Am., vol. 68, pp 1352-1354, 1978.

DEVANEY, A.J. Inverse-scattering theory within the Rytov approximation. Optics Letters, vol. 6, pp 374-376, 1981.

DEVANEY, A.J. Inversion formula for inverse scattering within the Born approximation. Optics Letters, vol. 7, pp 111-112, 1982.

DEVANEY, A.J. and SHERMAN, G.C. Nonuniqueness in inverse source and scattering problems. IEEE Transactions on Antennas and Propagation, vol. 30, pp 1034-1042, 1982.

DOBRZYNSKI, L. and MARADUDIN, A.A. Electrostatic edge modes in a dielectric wedge. Phys. Rev. B, vol. 6, pp 3810-3815, 1972.

DUNLOP, G.R., BOERNER, W.M. and BATES, R.H.T. On an extended Rytov approximation and its comparison with the Born approximation. IEEE AP-S Int. Symp. Pub. pp 587-591, 1976.

EGUILUS, A. and MARADUDIN, A.A. Electrostatic edge modes along a parabolic wedge. Phys. Rev. B. vol. 14, pp 5526-5528, 1976,

EL-BEHERY, I.N. and MACPHIE, R.H. Maximum likelihood estimation of the number, directions and strength of point radio sources from baseline interferometer data. IEEE Transactions on Antennas and Propagation, vol. 26, pp 294-301, 1978.

FELSEN, L.B. Electromagnetic properties of wedges and cone surfaces with a linearly varying surface impedance. IEEE Transactions on Antennas and Propagation, vol. 7, pp 231-243, 1959.

FELSEN L.B. and MARCUVITZ, N. 'Radiation and scattering of waves'. Prentice-Hall: New Jersey, 1973.

FILIPPOV, A.F. Diffraction of an arbitrary acoustic wave by a wedge PMM, vol. 28, pp 305-318, 1964.

FOCK, V.A. Diffraction of radio waves on the earth's surface. J. Phys. of the USSR, vol. 9, pp 255-266, 1945.

GARDEN, K.L. An overview of computed tomography. Ph.D. thesis, University of Canterbury, 1984.

GAUTESEN, A.K. Integral representations for edge diffraction. J. Acoust. Soc. Am., vol. 72, pp 1942-1946, 1982,

GAUTESEN, A.K. Integral representations for elastodynamic edge diffraction. Wave Motion. vol. 5, pp 69-82, 1983.

GLISSON, A.W. and WILTON, D.R. Simple and efficient numerical methods for problems of electromagnetic radiation and scattering from surfaces. IEEE Transactions on Antennas and Propagation, vol. 28, pp 593-603, 1980.

GOSS, V.F. and HANCHEN, H. Ein never und fundamentaler versuch zur total-reflexion. Ann. Phys., vol. 1, pp 333-346, 1947.

GRADSHTEYN, I.S. and RYZHIK, I.M. Tables of integrals, series and products. Academic Press, NY, 1965,

GRZESIK, J. Field matching through volume suppression, Proc IEE part H. vol. 127, pp 20-26, 1980.

HADAMARD, J. Lectures on Cauchy's Problem in linear partial differential equations. Yale University Press. England, 1923.

HARRINGTONM R.F. 'Field computation by moment methods'. The Macmillian Co.: New York, 1968.

HASHIMOTO, M. and FUJISAWA, K. Consideration on matrix methods and estimation of their errors. IEEE Transactions on Microwave Theory and Techniques., vol. 18, pp 352-359, 1970.

HOENDERS, B.J. The exact calculation of the field generated by the scattering of a plane wave at a rectangular protrusion. Optik, vol. 62, pp 255-261, 1982.

HUDSON, J.A. The diffraction of an acoustic wave by an embodd quarter-space. IMA J. Appl. Math., vol. 28, pp 1-21, 1982.

HUNTER, J.D. and BATES, J.H.T. Secondary diffraction from close edges on perfectly conducting bodies. Int. J. Elect. vol. 32, pp 321-333, 1972.

HUNTER, J.D. Scattering by conducting notched and wedged circular cylinders. Int. J. Electr. vol. 36, pp. 375-381, 1974.

HURD, B.A. The edge condition in electromagnetic. IEEE Transactions on Antennas and Propagation, vol. 24, pp 70-73, 1976.

HURD, B.A. On Meixner's edge condition for dielectric wedges. Can. J. Phys., vol. 55, pp 1970-1971, 1977.

IKUNO, H. and YASUURA, K. Improved point-matching method with application to scattering from a periodic surface. IEEE Transactions on Antennas and propagation, vol. 21, pp 657-662, 1973.

ISKANDER, M.F., LAKHTAKIA, A. and DURNEY, C.H. A new iterative procedure to solve for scattering and absorption by dielectric objects. Proc. IEEE, vol. 70, pp 1361-1362, 1982.

ISKANDER, M.F., LAKHTAKIA, A and DURNEY, C.H. A new procedure for improving the solution stability and extending the frequency range of the EBCM. IEEE Transactions on Antennas and Propagation, vol. 31, pp 317-323, 1983.

IWATA, K. and NAGATA, R. Calculation of refractive index distribution from interferograms using the Born and Rytov's approximation. Japan J. Appl. Phys., vol. 14, suppl. 14-1, pp 379-383, 1975.

JACOBS, D. 'The state of the art in numerical analysis'. Academic Press: London, 1977.

JAMES, G.L. and KERDEMELIDIS, V. Reflector antenna radiation pattern analysis by equivalent edge currents, IEEE Transactions on Antennas and Propagation, vol. 21, pp 19-24, 1973.

JAMES, G.L. 'Geometrical theory of diffraction for electromagnetic waves.' Peter Peregrinus: England. 1976.

JAMES, G.L. Uniform diffraction coefficients for an impedance wedge, Electr. Lett., vol. 13, pp 403-404, 1977.

JAMES, J.R. and GALLETT, I.N.L. Point-matched solutions for propagating modes on arbitrarily-shaped dielectric rods. Radio Electr. Engr., vol. 42, pp 103-113, 1972.

JAMES, J.R. and GALLETT, I.N.L. Modal analysis of triangular-cored glass-fibre waveguide. Proc. IEE, part H, vol. 120, pp 1362-1370, 1973.

JAMWAL, K.K.S. and DAHR, A. Design of high directive gain polymer rectangular antennas in x-band. Indian J. Rad. and Space Phys., vol. 10, pp 115-117, 1981.

JAMWAL, K.K.S., DAHR, A. and VAKIL, R. Analysis, design and characteristics of X-band dielectric wedge waveguide antennas. Microwave J., vol. 25, pp 99-102, 1982.

JANNSON, T. and JANICKI, R. An eigenvalue formulation of inverse theory of scalar diffraction. Optik, vol. 56, pp 429-441, 1980.

JOHNSON, S.A. and TRACY, M.L. Inverse scattering solutions by a sinc basis multiple source moment method. Part I. Theory. Ultrasonic Imaging, vol. 5, pp 361-375, 1983.

JOHNSON, S.A. ZHOU, Y., TRACY, M.L., BERGGREN, N.J. and STENGER, F. Inverse scattering solutions by a sinc basis multiple source moment method. Part III, Fast algorithms. Ultrasonic Imaging, vol. 6, pp 103-116, 1984.

JONES, D.S. and PIDDUCK, F.B. Diffraction by a metal wedge at large angles. Q.J. Math., vol. 2, pp 229-237, 1950.

JONES, D.S. 'The theory of electromagnetism'. Pergamon Press: Oxford, 1964.

JONES, D.S. Double knife-edge diffraction and ray theory. Q.J. Mech. Appl. Math., vol. 26, pp 1-18, 1973.

JONES, D.S. 'Methods in electromagnetic wave propagation'. Clarendon Press: Oxford, 1979.

JONES, D.S. The Kontorowich-Lebedev Transform. J. Int. Maths. Applics. vol. 26, pp 133-141, 1980.

JOO, C.S., RA, J.W. and SHIN, S.Y. Edge diffraction by a right-angled dielectric wedge. Elect. Lett., vol. 16, pp 934-935, 1980.

JOO, C.S., RA, J.W. and SHIN, S.Y. Scattering by right angle dielectric wedge. IEEE Transactions on Antennas and Propagation, vol. 32, pp 61-69, 1984.

JORDAN, A.K. and AHN, S. Inverse scattering theory and profile reconstruction. Proc. IEE. vol. 126, pp 945-950, 1979.

KAMINETZKY, L. and KELLER, J.B. Diffraction coefficients fo higher order edges and vertexes. SIAM. J. Appl. Math., vol. 22, pp 109-134, 1972.

KAMINETZKY, L. and KELLER, J.B. Diffraction by edges and vertexes of interfaces. SIAM J. Appl. Math., vol. 28, pp 839-856, 1975.

KAPILEVICH, B.Y. and SIMIN, N.S. Reflection from a dielectric wedge in a rectangular waveguide. Radiophysics and Quantum Electronics, vol. 19, pp 93-96, 1976.

KAPUSTIANSKII, S.M. On an exact solution of the problem of elastic wave diffraction by a wedge. PMM, vol. 40, pp 190-192, 1976.

KARAL, F.C., KARP, S.N. Diffraction of a skew plane electromagnetic wave by an absorbing right angled wedge. Comm. Pure Appl. Math., vol. 11, pp 495-533, 1958.

KARAL, F.C., KARP, S.N., CHU, T.S. and KOUYOUMJIAN, R.G. Scattering of a surface wave by a discontinuity in the surface reactance on a right angled wedge. Comm. Pure Appl. Math., vol. 14, pp 35-48, 1961.

KARP, S.N. and KARAL, F.C. A new method for the determination of far fields with applications to the problem of radiation of a line source at the tip of an absorbing wedge. IEEE Transactions on Antennas and Propagation. vol. AP-S, pp 91-102, 1959.

KELLER, J.B. and BLANK, A. Diffraction and reflection of pulses by wedges and corners. Comm. Pure Appl. Math., vol. 4, pp 75-94, 1951.

KELLER, J.B. Geometrical theory of diffraction, JOSA, vol. 52, pp 116-130, 1962.

KILDAL, P. On the accuracy of physical optics. IEEE Transactions on Antennas and Propagation, vol. 30, pp 509-512, 1982.

KIM, S.Y., RA, J.W. and SHIN, S.Y. Edge diffraction by dielectric wedge of arbitrary angle. Electr. Lett., vol. 19, pp 851-853, 1983.

KIM, T.J. and THIELE, G.A. A hybrid diffraction technique - General theory and applications. IEEEE Transaction on Antennas and Propagation. vol. 30, pp 888-897, 1982.

KINBER, B. Ye. Diffraction of the open end of a sectoral horn. Electron. Phys. vol. 6, pp 1620-1623, 1962.

KING, R.J. and HUSTING, C.H. Microwave surface impedance measurements of a dielectric wedge on a perfect conductor. Can. J. Phys., vol. 49, pp 820-830, 1971.

KNOTT, E.F. and SENIOR, T.B.A. Comparison of three high frequency diffraction techniques. Proc. IEEE. vol. 62, pp 1468-1474, 1974.

KONTOROWICH, M.J. and LEBEDEV, W.M. On a method of solution of some problem in the diffraction theory. J. of Phys. of the USSR, vol. 1, pp 229-241, 1939.

KOST, A. Characteristic impedance of a double line in front of a dielectric wedge. Archiv fur Electrotechnik, vol. 60, pp 213-219, July 1978.

KOSTROV, B.V. Diffraction of a plane wave by a smooth rigid wedge in an unbounded elastic medium in absence of friction. PMM, vol. 30, pp 198-203, 1966.

KOUYOUMJIAN, R.G. Asymptotic high-frequency methods. Proc. IEEE. vol. 53, pp 864-876, 1985.

KRAUT, E.A. Diffraction of elastic waves by a rigid 90 wedge. Bull Sesi. Soc. Am. vol. 58, pp 1083-1115, 1968.

KRAUT, E.A. and LEHMAN, G.W. Diffraction of electromagnetic waves by a right-angle dielectric wedge. J. Math. Phys., vol. 10, pp 1340-1348, 1969.

KREYSZIG, E. 'Advanced engineering mathematics'. John Wiley and Sons, Inc,: New York, 1972.

KRISTENSSON G. and STROM, S. Electromagnetic scattering from geophysical targets by means of the T-matrix approach - A review of some recent results. Open symposium on Mathematical Models of Radio Propagation, URSI XXth General Assembly, Washington DC, 1981.

KRISTENSSON, G., RAMM, A.G. and STROM, S. Convergence of the T-matrix approach in scattering theory II. J. Math. Phys., vol. 24, 2619-2631, 1983.

KUMAR, A. Measurement of diffraction by a dielectric wedge. IEEE EEMTIC'81, Digest. pp 111-115, 1981.

KUNZ, K.S. and LEE, K.M. A three-dimensional finite-difference solution of the external response of an aircraft to a complex transient EM environment: Part I - The method and its implementation. Part II comparison of predictions and measurement, IEEE Transactions on Electromagnetic Compatibility, vol. 20, pp 328-341, 1978.

KUO, N.H. and PLONUS, M.A. A systematic technique in the solution of diffraction by a right-angled dielectric wedge. J. Math. Phys., vol. 46, pp 394-407, 1967.

KURIKO, V.I. Theory of the radiation Q factor of a dielectric resonator. Sov. Phys. vol. 13, pp 423-425, 1968.

LANDSTORFER, F.M. Nearfield measurements with dielectric antennas of new kind. IEEE Transactions on Antenna Propagation, vol. AP-S, pp 272-275, 1975.

LANG, K.C. Edge condition of a perfectly conducting wedge with its exterior region divided by a resistive sheet. IEEE Transactions on Antennas and Propagation, vol. 21, pp 237-238, 1973.

LARSEN, J. Diffraction of elastic waves by a rigid wedge. Proc. R. Soc. Lond. A. vol. 376, pp 409-617, 1980.

LATZ. N. Electromagnetic diffraction by imperfectly dielectric wedges. J. Math. Analy. and Applc., vol. 43, pp 373-387, 1973.

LEROY, M. On the convergence of numerical results in modal analysis. IEEE Transactions on Antennas and Propagation, vol. 31, pp 655-659, 1983.

LESSELIER, D. Optimization techniques and inverse problems: reconstruction of conductivity profiles in the time domain. IEEE Transactions on Antennas and Propagation, vol. 30, pp 59-65, 1982.

LEWIN, L. Wedge-diffraction functions and their use in quasi-optics. Proc. IEE. Vol. 116, pp 71-76, 1969.

LEWIN, L. On the inadequacy of discrete mode-matching techniques in some waveguide discontinuity problems. IEEE Transactions on Microwave Theory and Techniques, vol. 18, pp 364-372, 1970.

LEWIN, L. On the restricted validity of point-matching techniques. IEEE Transactions on Microwave Theory and Techniques, vol. 18, pp 1041-1047, 1970.

LWEIN, L. The near field of a locally illuminated diffracting edge. IEEE Transactions on Antennas and Propagation, vol. 19, pp 134-136, 1971.

LEWIN, L., and SREENIVASIAH, I. USRl Conference, Boulder, U.S.A. 1978.

LEWIS R.M. and BOERSMA, J. Uniform asymptotic theory of edge diffraction. J. Math. Phys. vol. 10, pp 2291-2305, 1969.

LWEIS, R.M. Physical optics inverse diffraction. IEEE Transactions on Antennas and Propagation, vol. 17, pp 308-314, 1969.

LEWIS, R.M. and MCKENNA, J. The field of a line charge near the tip of a dielectric wedge. BSTJ vol. 55, pp 355-342, 1976.

LUEBBERS, R.J. Finite conductivity uniform GTD versus knife edge diffraction in prediction of propagation path loss. IEEE Transactions of Antennas and Propagation, vol. 32, pp 70-76, 1984.

LUEBBERS, R.J. Propagation prediction for hilly terrain using GTD wedge diffraction. IEEE Transactions on Antennas and Propagation, vol. 32, pp 951-955, 1984.

LUKE, Y.L. 'Integrals of Bessel functions'. McGraw-Hill Book Co.: New York, 1982.

MACDONALD, H.M. The electrical distribution on a conductor bounded by two spherical surfaces cutting at an angle. Proc. Lond. Math. Soc., vol. 26, pp 156-172, 1895.

MAILLOUX, R.J. Radiation and near-field coupling between two colinear open-ended waveguides. IEEE Transactions on Antennas and Propagation, vol. 17, pp 49-55, 1969.

MARCUVITZ, N. 'Waveguide handbook' McGraw-Hill: New York, 1951.

MARTIN, P.A. On the null-field equations for the exterior problems of acoustics. Q.JL. Mech. Appl. Math., vol. 33, pt. 4. 1980.

MARTIN, P.A. Acoustic scattering and radiation problems, and the null-field method. Wave motion, vol. 4, pp 391-408, 1982.

MAURER, S.J. and FELSEN, L.B. Ray-optical techniques for guided waves. Proc. IEEE, vol. 55, pp 1718-1729, 1967.

MECKELBURG, H. Scatterer reconstruction from multistatic far-field data. Electr. Lett., vol. 18, p 341-343, 1982.

MEIXNER, J. The behaviour of electromagnetic fields at edges. IEEE Transactions on Antennas and Propagation, vol. 20, pp 442-446, 1972.

MICHAELI, A. Equivalent edge currents for arbitrary aspects of o bservation, IEEE Transactions on Antennas and Propagation, vol. 32, pp 252-258, 1984.

MILLAR, R.F. The location of singularities of two-dimensional harmonic functions I : Theory, II : Applications. SIAM J. Math. Ana. vol. 1, pp 333-353, 1970.

MILLAR, R.F. Singularities of two-dimensional exterior solutions of the Helmholtz equation, Proc. Camb. Phil. Soc. vol. 69, pp 175-188, 1971.

MILLAR, R.F. The Rayleigh hypotheses and a related least-square solution to scattering problems for periodic surfaces and other scatterers. Radio Science, vol. 8, pp 785-796, 1973.

MITTRA, R. Relative convergence of the solution of a doubly infinite set of equations. J. Res. NBS, vol. 67D, pp 245-254, 1963.

MITTRA, R. and LEE, S.W. 'Analytical techniques in the theory of guided waves'. Macmillan: New York, 1971.

MITTRA, R., ITOH, T. and LI, T.S. Analytical and numerical studies of the relative convergence phenomenon arising in the solution of an integral equation by the moment method. IEEE Transactions on Microwave Theory and Techniques, vol. 20, pp 96-104, 1972.

MITTRA, R. and TEW, M. Accuracy test for high-frequency asymptotic solutions. IEEE Transactions on Antennas and Propagation, vol. 27, pp 62-68, 1979.

MNYAMA, D. Measurement of cutoff frequencies of cylindrical cavities load with sharp-edged dielectrics. Third Professional Year Project Report, University of Canterbury, 1983.

MOHSEN, A. and HAMID, M.A.K. Diffraction by a conducting wedge in the near field. Proc. IEE. vol. 110, 301-304, 1971.

MOON, P. and SPENCER, D.E. 'Field theory handbook'. Springer-Verleg: Berlin 1971.

MORITA, N. Surface integral representations for electromagnetic scattering from dielectric cylinders. IEEE Transactions on Antennas and Propagation, vol. 26, pp 261-266, 1978.

MORITA, N. Another method of extending the boundary condition for the problem of scattering by dielectric cylinders. IEEE Transactions on Antennas and Propagation, vol. 27, pp 97-99, 1979.

MORRISON, J.A. Integral equations for electromagnetic scattering by perfect conductors with two-dimensional geometry. BSTJ vol. 58, pp 409-425, 1979.

MORSE, P.M. and FESHBACH, H. 'Methods of Theoretical Physics Vol. I and II'. McGraw-Hill: New York, 1953.

MUR, G. The modelling of singularities in the finite-difference approximation of the time-domain electromagnetic-field equations. IEEE Transactions on Microwave Theory and Techniques, vol. 29,. pp 1073-1077, 1981.

MUR, G. Absorbing boundary conditions for the finite-difference approximation of the time-domain electromagnetic-field equations. IEEE Transactions on Electromagnetic Compatibility, vol. 23, pp 377-382, 1981.

NEFEDOV, Y.I. and SIVOV, A.N. Geometri-optic solution of the problem of a dielectric wedge. Radio Eng. Electr. Phys., vol. 19, pp 121-123, 1974.

NEWTON, R.G. Inverse problems in physics. SIAM Review, vol. 12, pp 346-356, 1970.

NOBLE, B. 'Methods based on the Wiener-Hopf technique for solution of partial differential equations'. Pergamon Press: London, 1958.

OBERHETTINGER, F. Diffraction of waves by a wedge. Comm. Pure Appl. Math., vol. 7, pp 551-563, 1954.

OKUNO, Y. and YASUURA, K. Numerical algorithm based on the mode-matching method with a singular-smoothing procedure for analysing edge-type scattering problems. IEEE Transactions on Antennas and Propagation, vol. 30, pp 580-587, 1982.

PAPDOPOULOUS, M. Diffraction of elastic waves by a wedge with free boundaries. Proc. R. Soc. Lond. A. vol. 388, pp 335-352, 1983.

PARKET, R.L. Inverse theory with grossly inadequate data. Geophys. J. Roy. Astron. Soc. Vol. 29, pp. 123-138, 1972.

PARKET, R.L. Understanding inverse theory. Ann. Rev. Earth Plannet, Sci., vol. 3, pp 35-64, 1977.

PATHAK, P., WONG, N., BURNSIDE, W. and KOUYOUMJIAN, R.G. A uniform GTD solution for the radiation from sources on a convex surface. IEEE Transactions on Antennas and Propagation, vol. 29, pp 609-622, 1981.

PATTANAYAK, D.N. and WOLF, E. General form and a new interpretation of the Ewald-Oseen extinction theorem. Optics Comm., vol. 6, pp 217-220, 1972.

PETERSON, B. and STROM, S. T-matrix formulation of electromagnetic scattering from multilayed of Scatterers. Phys. Rev. D., vol. 10, pp 2670-2684, 1974.

PETIT, R. and CADILHAC, M. Form of the electromagnetic field in the groove region of a perfectly conducting echellete grating. JOSA, vol. 73, pp 963-965, 1983.

PIEFKE, G. Reflection at incidence of an Hmn-wave at junction of circular waveguide and circular horn. Electromagnetic Theory and Antennas, Part I. Jordan, E.C. ed. New York: Pergamon, pp 209-234, 1963.

POGORZELSKI, W.A. 'Integral equations and their applications' Pergamon Press: Oxford, 1966.

POINCARE, H. Sur la polarisation par diffraction. Acta Math., vol. 16, pp 297-339, 1892.

POINCARE, H. Sur la polarisation par diffraction. Acta Math., vol. 20, pp 313-355, 1897.

PERTER, R.P. and DEVANEY, A.I. Holography and the inverse source problem. J. Opt. Soc. Am., vol. 72, pp 327-330, 1982.

PORUCHIKOV, V.B. Diffraction of a spherical elastic wave by a wedge. PMM, vol. 40, pp 898-908, 1976.

RADLOW, J. Diffraction by a right-angled dielectric wedge. Int. J. Eng. Sci., vol. 2, pp 275-290, 1964.

RAMM, A.G. Justification of the T-matrix approach. IEEE AP-S symposium publication, pp 13-14, 1982.

RAMM, A.G. Convergence of the T-matrix approach to scattering theory, J. Math. Phys., vol. 23, pp 1123-1125, 1982.

RAMM, A.G. Convergence of the T-matrix in the potential scattering. J. Math. Phys. vol. 23, pp 2408-2409, 1982.

RAWLINS, A.D. Diffraction by a dielectric wedge. J. Inst. Math. Applics., vol. 19, pp 231-279, 1977a.

HAWLINS, A.D. Diffraction by an acoustically penetrable or an electromagnetically dielectric half-plane. Int. J. Eng. Sci., vol. 15, pp 569-578, 1977b.

RAYLEIGH, LORD (STRUTT, S.W.) 'The theory of sound vol. I and II', Dover Publication: New York, 1945.

ROGER, A. Newton-Kantorowich algorithm applied to an electromagnetic inverse problem, IEEE Transactions on Antennas and Propagation, vol. 29, pp 232-238, 1981.

ROSS, R.A. and HAMID, M.A.K. Scattering by a wedge with rounded edge. IEEE Transactions on Antennas and Propagation, vol. 19, pp 507-516, 1971.

RUDDUCK, R.C. and WU, D.C.F. Slope diffraction analysis of TEM parallel plate waveguides radiation patterns, IEEE Transactions on Antennas and Propagation, vol. 17, pp 797-799, 1969.

SABATIER, P.C. Spectral and scattering inverse problems. J. Math. Phys. vol. 19, pp 2410-2425, 1978.

SABATIER, P.C. Theoretical consideration for inverse scattering. Radio Science, vol. 18, pp 1-18, 1983.

SARKER , T., STARKIEWICS, K.R. and STRATTON, R.F. Survey of numerical methods for solution of large sytems of linear equations for electromagnetic field problems. IEEE Transactions on Antennas and Propagation, vol. 29, pp 847-856, 1981.

SCHIFF, L.I. 'Quantum mechanics', McGraw-Hill: New York, 1949.

SEAGAR, A.D., YEO, T.S. and BATES, R.H.T. Full-wave computed tomography Part 2: Resolution limits. Proc. IEE Part A, vol. 131, pp 616-622, 1984.

SHULEY, N.V. A note on relative convergence for moment-method solutions of integral equations of the first kind as applied to dichroic problems. To appear in Electr. Lett., 1985.

SILVER, S. 'Microwave antenna theory and design'. McGraw-Hill, New York, 1949.

SILVESTER, P. A general high-order finite-element waveguide analysis program. IEEE Transactions on Microwave Theory and Techniques. vol. 17, pp 204-209, 1969.

SINHA, B., GUHA, D. and GUPTA, J.P. Diffraction coefficients of a 90° straight dielectric wedge with TM illumination: a numerical approach. J. Int. Electr. Tele. Eng. (India), vol. 26, pp 500-502, 1980.

SLEEMAN, B.D. The inverse problem of acoustic scattering. IMA. J. Appl. Maths., vol. 29, pp 113-142, 1982.

SOMMERFELD, A. Mathematische theorie der diffraction. Math. Ann., vol. 47, pp 317-341, 1896.

STEVENS, W.N.R. and JOHNS, P.B. Imaging by numerical analysis of wave scattering in the time domain using tansmission - line modelling, signal processing and optimisation. IEE Proc. Part A, vol. 129, pp 190-197, 1982.

STRATTON, J.A. 'Electromagnetic theory'. McGraw-Hill Book Co.: New York, 1941.

STROM, S. T-matrix for electromagnetic scattering from an arbitrary number of scatterers with continuously varying electromagnetic properties. Phys. Rev. D, vol. 10. pp 2688-2690, 1974.

STROM, S. On the integral equations for electromagnetic scattering. An. J. Phys., vol. 43, pp 1060-1069, 1975.

SUCHER, M. and FOX, J. 'Handbook of microwave measurements vols. I, II and III'. New York Polytechnic Press: Brooklyn, 1963.

SUGIMOTO, S. and KOZAKI, S. New approach to calculation of electromagnetic scattering by a perfectly conducting rectangular cylinder. Electr. Letts. vol. 19, pp 861-862, 1983.

SYNGE, J.L. Th general problem of antenna radiation and the fundamental integral equation with application to an antenna of revolution - Part II. Quarterly appl. Math., vol. 6, pp 133-156, 1948.

TABBARA, W. On an inverse scattering method. IEEE Transactions on Antennas and Propagation, vol. 21, pp 245-246, 1973.

TAKENAKA, T. and FUKUMITSU, O. Accurate analysis of the abrupt discontinuity in a dielectric waveguide. Elect. Lett., vol. 19, pp 806-807, 1983.

TAN, K.P. A parallel-plate electromagnetic wave scattering range. Third Professional Year Project Report, University of Canterbury, 1984.

THIEL, D.V. Surface impedance and wave tilt interpretation over horizontally stratified media. J.E.E.E. Aust., vol. 2, pp 240-244, 1982.

THIELE, G.A. and NEWHOUSE, T.H. A hybrid technique for combining moment methods with the geometrical thory of diffraction. IEEE Transactions on Antennas and Propagation, vol. 23, pp 62-69, 1975.

TIBERIO, R. and KOUYOUMJIAN, R.G. A uniform GTD solution for the diffraction by strips illuminated at grazing incidence. Radio Science, vol. 14, pp 933-941, 1979.

TIBERIO, R. and KOUYOUMJIAN, R.G. An analysis of diffraction at edges illuminated by transition region fields. Radio Science, vol. 17, pp 323-336, 1982.

TRACY, M.L. and JOHNSON, S.A. Inverse scattering solutins by a sinc basis multiple source moment. Part II. Numerical evaluations. Ultrasonic Imaging, vol. 5, p 376-392, 1983.

TYRES, G. 'Radiation and propagation of electromagnetic waves'. Academic Press: New York, 1969.

UFIMTSEV, P. YA. Method of edge waves in the physical theory of diffration. Report No. FTD - HC - 23 - 259 - 71. Reproduced by National Technical Information Service, U.S.A., 1971.

VANDENBERGHE, F.H. and BOERNER, W.M. On the inverse problem of scattering from a perfectly conducting prolate spheroid. Canadian J. Phys., vol. 50, pp 754-759, 1972.

VANDENBERGHE, F.H. and BOERNER, W.M. On the inverse problem of scattering from a perfectly conducting elliptic cylinder. Canadian J. Phys., vol. 50, pp 1987-1992, 1972.

van der BERG, P.M. and FOKKEMA, J.T. The Rayleigh hypotheses in the theory of diffraction by a cylindrical obstacle. IEEE Transactions on Antennas and Propagation, vol. 27, pp 577-583, 1979a.

van der BERG, P.M. and FOKKEMA, J.K. The Rayleigh hypotheses in the theory of reflection by a grating. J. Opt. Soc. Am., vol. 69, pp 27-31, 1979b.

van der BERG, P.M. Transition matrix in acoustic scattering by a strip. J Acoust. Soc. Am., vol. 70, pp 615-619, 1981.

van der BERG, P.M. Reflection by a grating: Rayleigh method. J. Opt. Soc. Am., vol. 71, pp 1224-1229, 1982.

VARADAN, V.K. and VARADAN, V.V. 'Acoustic, electromagnetic and elastic wave scattering - forcus on the T-matrix approach'. Pergamon Press: New York, 1980.

VARADAN, V.V. and VARADAN, V.K. Configurations with finite numbers of scatterers - a self consistent T-matrix approach. J. Acoust. Soc. Am., vol. 70, pp 213-217, 1981.

VARADAN, V.V., WALL, D.J.N., TSAO, S.J. and VARADAN, V.K. Elastic wave scattering from surface breaking cylinder cracks: SH waves. J. Acoust. Soc. Am., vol. 71, pp 1384-1390, 1982.

VASIL'EV, E.N. and SOLODOUKHOV, V.V. Numerical solution of the problem of electromagnetic waves diffraction by a dielectric wedge. URSI Intel. Symp., pp 512-517, 1971.

VASIL'EV, E.N. and SOLODOUKHOV, V.V. Diffraction of electromagnetic waves by dielectric wedge. Radio Phys. Quant. Electr., vol. 17, pp 1161-1169, 1974.

VASSALLO, C. On a direct use of edge condition in modal analysis. IEEE Transactions on Microwave Theory and Techniques, vol. 24, pp 208-212, 1976.

VOGELZAN, G.E., YEVICK, D. and FERWERDA, H.A. A numerical procedure for solving the inverse scattering problem for stratified dielectric media. Optics Comm., vol. 45, pp 376-379, 1983.

VON HIPPEL, A. 'Dielectrics materials and applications'. The Technology Press of MIT: Cambridge, 1954.

WADE, G., MUELLER, R.K. and KAVCH, M. A survey of techniques for ultrasonics tomography, in RAVIV, J., GREENLEAF, J.F. and HERMAN, G.T. eds, 'Computer aided tomography and ultransonics in medicien'. North-Holland: Amsterdam, pp 165-214, 1979.

WAIT, J.R. 'Theory of electromagnetism', 1985.

WALL, D.J.N. Method of overcoming numerical instabilities associated with the T-matrix method, in VARADAN, V.K. and VARADAN, V.V. eds, 'Acoustic, electromagnetic and elastic wave scattering - forcus on the T-matrix approach', Pergamon Press: New York, 1980.

WALL, D.J.N. and O'BRIEN, D.M. Radiation from whip antenna mounted on a sphere. J. Phys. D: Appl. Phys., vol. 13, pp 2185-2215, 1980.

WALL, D.J.N., VARADAN, V.V. and VARADAN, V.K. Dynamic stress concentrations of cylindrical cavities with sharp and smooth boundaries: I. SH waves. Wave Motion, vol. 3, pp 203-213, 1981.

WALL, D.J.N. Private communication, 1984.

WANDINGER, L. and NALBANDIAN, V. Millimeter-wave power combiner using quasi-optical techniques. IEEE Transactions on Microwave Theory and Techniques, vol. 31, pp 189-193, 1983.

WANG. D.K. and LAYBOURN, P.J.R. Coupling between prism and rectangular optical waveguide. Proc. IEE Part H, vol. 130 pp 255-260, 1983.

WATERMAN, P.C. Matrix formulation of electromagnetic scattering. Proc. IEEE, pp 805-812, 1965.

WATERMAN, P.C. New formulation of acoustic scattering. J. Acoust. Soc. Am., vol. 45, pp 1417-1429, 1968.

WATERMAN, P.C. Symmetry, unitarity and geometry in electromagnetic scattering. Phys. Rev. D, vol. 3, pp 825-839, 1971.

WATERMAN, P.C. Scattering by periodic surface. J Acoust. Soc. Am., vol. 57, pp 791-802, 1975.

WATERMAN, P.C. Analytical consequences of the extended boundary condition. Wave Motion, vol. 5, pp 273-295, 1983.

WATSON, G.N. 'A treatise on the theory of Bessel functions'. Cambridge University Press: Cambridge, 1966.

WEAVER, R.L. and PAO, V.M. Application of the transition matrix to a ribbon-shaped scatterer. J. Acoust. Soc. Am., vol 66, pp 1199-1206, 1979.

WESIS, M.F. Inverse scattering in the geometric-optic limit. Jr. Opt. Soc. Am., vol. 58, pp 1524-1529, 1968.

WESTON, V.H. and BOERNER, W.M. An inverse scattering technique for electromagnetic bistatic scattering. Canadian J. Phys., vol. 47, pp 1177-1184, 1969.

WESTON, V.H. On the inverse problem for a hyperbolic dispersive partial differential equation. J. math. Phys., vol. 13, pp 1952-1956, 1972.

WESTON, V.H. and KRUEGER, R.J. On the inverse problem for a hyperbolic dispersive partial differential equations II. J. Math. Phys., vol. 14, pp 406-408, 1973.

WESTON, V.H. On inverse scattering. J. Math. Phys., vol. 15, pp 209-213, 1974.

WEXLER, A. Computation of electromagnetic fields. IEEE Transcations on the Microwave Theory and Techniques, vol. 17, pp 416-439, 1969.

WILTON, D.R. and MITTRA, R. A new numerical approach to the calculation of electromagnetic scattering properties of two-dimensional bodies of arbitrary cross section. IEEE Transactions on Antennas and Propagation, vol. 20, pp 310-317, 1972.

WIRGIN, A. and PETIT, P. Plane-wave expansions used to describe the field diffracted by a grating: comments. J. Opt. Soc. Am., vol. 72, pp 812-814, 1982.

WONG, C.T. Null-field treatment of antenna. Ph.D. thesis, University of Canterbury, 1972.

WU, T.K. and TSAI, L.L. Scattering by a dielectric wedge: a numerical solution. IEEE Transactions on Antennas and Propagation, vol. 25, pp 570-571, 1977.

YEE, H.Y. and FELSEN, L.B. Ray optics - a novel approach to scattering by discontinuities in a waveguide. IEEE Transactions on Microwave Theory and Techniques. vol. 17, pp 73-85, 1969.

YEE, K.S. Numerical solution of initial value problems involving Maxwell's equations in isotropic media. IEEE Transactions on Antennas and Propagation, vol. 14, pp 302-307, 1966.

YU, J.S. and RUDDICK, R.C. On higher-order diffraction concepts applied to a conducting strip. IEEE Transactions on Antennas and Propagation, vol. 15, pp 662-668, 1967.

ZABREYKO, P.P., KOSHELEV, A.I., KRASNOEL 'SKII, M.A., MIKHLIN, S.G., RAKOVSHCHIK, L.S. and STET'SENKO, V. YA. 'Integral equations - a reference test'. Noordhoff International Publishing: Leyden, 1975.

ZEMELL, S.H. Diffraction of elastic waves by a rigid-smooth wedge. SIAM J. Appl. Math. Vol. 29, pp 582-596, 1975.